Algorithmes semi-implicites pour des problèmes d'interaction fluide structure : approches procédures partagées et monolithiques

Soyibou Sy

UNIVERSITE DE HAUTE ALSACE

Faculté des Sciences et Technique
Laboratoire de Mathématiques, Informatique et Applications

Thèse

présentée par:

Soyibou SY

pour obtenir le grade de

Docteur de l'Université de Haute Alsace

Spécialité : Mathématiques Appliquées

Algorithmes semi-implicites pour des problèmes d'interaction fluide structure : approches procédures partagées et monolithiques

---

Sous la direction de Cornel Marius MUREA

Soutenue le 23 octobre 2009, devant le jury composé de

S. AKESBI	Université de Haute Alsace	HDR	Examinateur
B. BRIGHI	Université de Haute Alsace	Professeur	Examinateur
B. MAURY	Université Paris-Sud	Professeur	Rapporteur
C. M. MUREA	Université de Haute Alsace	HDR	Directeur de thèse
C. PRUD'HOMME	Université Grenoble 1	Professeur	Président du jury
M. TUCSNAK	Université Nancy 1	Professeur	Rapporteur

À ma femme et mon fils.
Au reste de ma famille.

Remerciements

Ma très sincère gratitude va d'abord à mon directeur de thèse Monsieur Cornel Marius MUREA, qui a été un encadreur fantastique. J'admire en lui sa grande culture scientifique et ses talents pédagogiques. Il m'en a fait profiter généreusement durant les trois années de préparation de ma thèse au sein du laboratoire LMIA[1] de l'Université de Haute Alsace de Mulhouse.

Je remercie chaleureusement le Professeur Christophe PRUD'HOMME, qui m'a fait l'honneur de présider mon jury de thèse.

Je tiens à remercier tout spécialement les deux rapporteurs de cette thèse, les Professeurs Marius TUCSNACK et Bertrand MAURY pour l'effort fourni dans la lecture du manuscrit et pour l'intêret qu'ils ont porté à mon travail.

Je présente toute ma reconnaissance à Monsieur Samir AKESBI et au Professeur Bernard BRIGHI pour avoir accepté d'examiner ma thèse et de faire partie de mon jury de thèse.

Mes remerciements vont aussi à tous les membres du laboratoire LMIA de l'Université de Haute Alsace pour l'accueil chaleureux qu'ils m'ont temoigné.

Mes parents, amis et surtout ma très chère épouse Aichétou SY, qui m'ont beaucoup encouragé et soutenu tout au long de ces trois longues années de thèse, ma reconnaissance leur est due pour toujours.

Je ne finirai pas sans remercier les Professeurs Mary Teuw Niane de l'UGB[2] de Saint-Louis Sénégal et Marie Françoise Véron de l'Université de Tours (France), qui m'ont offert des très bonnes bases sur la partie théorique des équations aux dérivées partielles. Ils trouveront ici avec un coeur plein de joie mes meilleures reconnaissances.

[1]Laboratoire de Mathématiques, Informatique et Applications.
[2]Université Gaston Berger de Saint-Louis Sénégal

Résumé

Le but de cette thèse est de développer des algorithmes “semi-implicites” procédures partagées (c’est-à-dire le fluide et la structure sont traités séparément) et “semi-implicites” monolithiques (c’est-à-dire le fluide et la structure sont traités dans un même bloc) pour simuler numériquement les problèmes d’interaction fluide structure bidimensionnels, observés dans les artères. Le fluide représente le sang et la structure la paroi de l’artère. Le mot “semi-implicite” signifie que la position de l’interface entre le fluide et la structure est déterminée de façon explicite tandis que la vitesse du fluide, la pression du fluide et les déplacements de la structure sont calculés de manière implicite.

Le fluide étant gouverné par les équations de Navier-Stokes posées sur un domaine en mouvement, une formulation ALE (Arbitrary Lagrangian, Eulerian) de ces équations a été introduite. La structure est gouvernée soit par les équations d’élasticité linéaire dans le cas des petits déplacements, soit par le modèle de Saint-Venant Kirchhoff non linéaire dans le cas des grands déplacements.

Dans le but de comparer la rapidité des algorithmes semi-implicites par rapport aux algorithmes implicites et celle des algorithmes monolithiques par rapport aux algorithmes procédures partagées, nous avons effectué un calcul des temps CPU pour chaque cas.

Le travail est reparti en trois chapitres:

Dans le premier chapitre, nous présentons un algorithme semi-implicite procé- dures partagées pour résoudre un problème non stationnaire d’interaction fluide structure. L’algorithme est obtenu en combinant un schéma d’Euler implicite avec une linéarisation du terme de convection pour les équations de Navier-Stokes et un θ-schéma d’ordre deux pour la structure. Deux cas de modèles pour la structure sont étudiés. Le modèle d’élasticité linéaire pour les petits déplacements de la structure et le modèle de Saint-Venant Kirchhoff non linéaire pour les grands déplacements. A chaque pas de temps, l’algorithme calcule explicitement la position de l’interface à partir d’une prédiction d’ordre deux des déplacements de la structure. Par conséquent un problème d’optimisation doit être résolu, de telle sorte que la continuité des vitesses et l’égalité des contraintes soient satisfaites à l’interface. Durant les itérations de l’algorithme de BFGS (Broyden, Fletcher, Goldforb, Shano) pour résoudre le problème d’optimisation, le maillage fluide reste fixe et la matrice fluide n’est factorisée qu’une seule fois, ce qui réduit considérablement l’effort de calcul. Les résultats numériques sont présentés. Pour résoudre le problème de la structure, nous avons employé la méthode de décomposition modale dans le cas linéaire et la méthode de Newton dans le cas non linéaire.

Dans le second chapitre, nous proposons un autre algorithme semi-implicite procédures partagées pour les problèmes d'interaction fluide structure avec des petits déplacements de la structure. Les mêmes schémas discrets en temps considérés dans le premier chapitre ont été employés. L'algorithme est basé sur un calcul explicite de la position de l'interface à partir de la vitesse du domaine fluide à l'instant précédent et un calcul implicite de la vitesse du fluide, de la pression du fluide et des déplacements de la structure. Un problème d'optimisation est alors résolu par BFGS pour satisfaire la continuité des vitesses et l'égalité des contraintes à l'interface. Durant les itérations de BFGS, le maillage fluide reste fixe et la matrice fluide n'est factorisée qu'une seule fois. Un résultat de stabilité inconditionnelle en temps de l'algorithme a été obtenu par le biais des estimations d'énergie. Les résultats numériques présentés montrent que la solution calculée est similaire à celle obtenue par l'algorithme implicite équivalent, mais le temps de calcul est réduit.

Les deux algorithmes présentés dans les chapitres I et II ont été combinés pour simuler numériquement le phénomène d'interaction fluide structure dans l'anévrisme cérébral, dans le but de comprendre ce phénomène et d'appliquer le second algorithme à une géométrie plus complexe que celle de l'artère.

Enfin, dans le troisième chapitre, nous mettons au point un algorithme semi-implicite monolithique pour résoudre un problème d'interaction fluide structure avec des petits déplacements de la structure. L'algorithme utilise un maillage global mobile pour le domaine fluide structure, obtenu comme union des maillages fluide et structure choisis compatibles à l'interface. Un seul champ de vitesse a été introduit pour satisfaire automatiquement la condition de continuité des vitesses à l'interface. Par le principe d'action et de réaction, la condition d'égalité des contraintes n'apparaît pas explicitement dans la formulation faible du problème. A chaque pas de temps, un système linéaire d'inconnues vitesse et pression, définies sur le domaine global est résolu par l'algorithme de GMRES. Les résultats numériques sont présentés.

Mots clés

Interaction fluide structure, algorithmes semi-implicites, différences finies, éléments finis, ALE, fluide dans un domaine en mouvement, approche procédures partagées, approche monolithique, fonctions caractéristiques.

Contents

Introduction

Dans les problèmes d'interaction fluide structure, d'une part les contraintes imposées par le fluide déplacent la structure et d'autre part le domaine fluide dépend des déplacements de la structure. A l'interface, la continuité des vitesses et l'égalité des contraintes sont imposées. On peut citer un très grand nombre d'exemples d'interaction fluide structure, par exemple en biomécanique : écoulement du sang dans une artère. Le champ d'écoulement du sang déforme la paroi de l'artère et les déformations de celle-ci modifient le champ d'écoulement du sang. Ou encore en hydroélasticité, où le fluide est en phase liquide, écoulement liquide à l'intérieur des conduites, mouvement de liquide dans un réservoir, etc. Mais aussi en aéroélasticité, où le fluide est en phase gazeuse, écoulements de l'air autour des véhicules aériens et terrestres (avions et automobiles etc).

Deux principales approches sont en général utilisées pour simuler numériquement le phénomène d'interaction fluide structure : approche procédures partagées, c'est-à-dire le fluide et la structure sont traités séparément et approche monolithique, le fluide et la structure sont traités dans un même bloc. Dans le cadre des procédures partagées, différents algorithmes ont été développés : explicites, implicites et tout récemment "semi-implicites"

Dans les algorithmes explicites, les deux conditions de couplage ne sont pas simultanément vérifiées, par exemple, à chaque pas de temps la condition de continuité des vitesses a lieu mais celle de l'égalité des contraintes est violée à l'interface, ou inversement. Ces algorithmes ont été employés avec succès en aérodynamique (voir [8]). Cependant, ils sont instables quand la structure est flexible et sa densité est comparable à celle du fluide, de telles situations apparaîssent en biomécanique. Par exemple, les résultats numériques présentés dans [26] montrent un algorithme explicite basé sur le schéma saute-mouton (Leap-Frog) pour la structure et sur le schéma d'Euler implicite pour le fluide, qui est instable pour la simulation numérique de l'écoulement du sang dans les grandes artères. Cette instabilité est indépendante du pas de temps mais dépend des densités du fluide et de la structure et de sa géométrie. Les résultats théoriques présentés dans [4] le confirment. Dans [9], il est montré que les algorithmes explicites basés sur α-méthode généralisée pour la structure et un schéma aux différences finies implicite à trois pas pour le fluide sont instables quand le rapport des densités massiques du fluide et de la structure est plus grand qu'un certain nombre.

Les algorithmes implicites sont connus pour être stables, mais très coûteux en temps de calcul. Dans le cas d'interaction fluide structure, à chaque pas de temps le domaine fluide, la vitesse du fluide et la pression du fluide ainsi que les déplacements de la structure doivent être déterminés de manière implicite par des méthodes itératives. De plus, le domaine fluide change à chaque pas de temps à l'intérieur de la boucle où les autres inconnues du problème sont calculées. Des algorithmes implicites basés sur la stratégie du point fixe sont présentés dans [20], [26], [10] et d'autres utilisant des techniques de transpiration, où la convergence peut être accélérée sont proposés dans [11], [7]. D'autres algorithmes implicites rapides sont obtenus quand la dérivation est employée, un algorithme de Newton par bloc a été utilisé dans [29], quand la dérivée de l'opérateur est approchée par différences finies. La méthode Newton a été utilisée dans [14], où la dérivée de l'opérateur est remplacée par un simple opérateur et dans [12], où le gradient est calculé analytiquement. De plus la méthode de Newton incorporant la linéarisation du modèle discret global a été décrit dans [5] et les techniques éléments finis espace-temps pour les problèmes d'interaction fluide structure sont présentées dans [33]. Par ailleurs, d'autres algorithmes implicites utilisant l'approche contrôle optimal sont présentés dans [21], [22] pour les problèmes d'interaction fluide structure stationnaires. La même technique peut être utilisée dans le cas évolutif, seulement à chaque pas de temps on doit résoudre un problème d'optimisation. Le gradient de la fonction coût est approchée par différences finies dans [23], où il est montré la supériorité de la méthode de BFGS (Broyden, Fletcher, Goldforb, Shano) comparée à celle de Newton modifiée, quand un pas de temps modéré est utilisé. La formule analytique du gradient de la fonction coût est présentée dans [24].

Du fait que les algorithmes implicites sont très coûteux en temps de calcul, un algorithme "semi-implicite" basé sur le schéma de projection de Chorin-Temam a été introduit dans [15] pour un problème d'interaction fluide structure mono-dimensionnel. Une analyse de la stabilité de cet algorithme est effectuée quand le domaine du fluide est fixe. L'idée des algorithmes "semi-implicites" est de calculer explicitement le domaine fluide à l'extérieur de la boucle où sont calculés la vitesse du fluide, la pression du fluide et les déplacements de la structure. Par conséquent un maillage fluide fixe est utilisé durant les itérations de l'algorithme jusqu'à que les conditions de couplage à l'interface soient satisfaites. Un algorithme semi-implicite est présenté dans [27], où les équations de la structure sont injectées dans celles du fluide et dans [25], où le problème de couplage fluide structure est résolu par la méthode du Lagrangien augmenté. Une analyse de la stabilité des algorithmes semi-implicites peut être trouvée par exemple dans [26, Sec. 4.10, p. 138], où l'auteur présente un algorithme semi-implicite basé sur le schéma saute-mouton (Leap-Frog) pour la structure et un schéma d'Euler implicite pour le fluide. Dans le but de linéariser le terme de convection dans les équations de Navier-Stokes, un problème supplémentaire fluide doit être résolu. La stabilité de l'algorithme est prouvée sous une condition dépendante du pas de temps. De plus l'auteur montre à la page 140 que cette condition peut être trop restreinte dans les applications hémodynamiques. Une étude de la stabilité d'un algorithme semi-implicite avec un schéma d'ordre un en temps pour le problème d'interaction fluide structure peut être trouvée dans [3] et [32]. Dans le cas d'une interaction entre un fluide et une structure rigide, on peut consulter [30]. Les résultats numériques montrent que le temps de calcul est réduit quand un algorithme semi-implicite est employé à la place d'un algorithme implicite. L'avantage des algorithmes semi-implicites par rapport aux algorithmes implicites, sont leur moindre coût et qu'ils permettent de faire disparaître la non linéarité de la géométrie.

Nous présentons dans le premier chapitre de ce document un algorithme semi-implicite, basé sur une prédiction explicite des déplacements de la structure pour déterminer la position de l'interface et un calcul implicite de la vitesse du fluide, de la pression du fluide et des déplacements de la structure. Nous avons employé la méthode de décomposition modale pour résoudre le problème de la structure dans le cas des petits déplacements et la méthode de Newton dans le cas des grands déplacements.
Dans le second chapitre, on introduit un autre algorithme semi-implicite, basé sur un calcul explicite de la position de l'interface à partir de la vitesse du fluide à l'instant précédent et un calcul implicite de la vitesse du fluide, de la pression du fluide et des déplacements de la structure. La stabilité inconditionnelle en temps de l'algorithme a été établie via la méthode des estimations d'énergie.

Dans le cadre monolithique, plusieurs algorithmes ont été proposés, monolithique implicites et monolithiques semi-implicites.

Des algorithmes monolithiques implicites peuvent être trouvés dans [16], [18], [19]. Plus précisément dans [16], l'algorithme présenté, utilise la même discrétisation en temps pour le fluide et la structure, et le système non linéaire résultant est résolu par la méthode de Newton. La technique des éléments finis espace-temps est aussi présentée dans [19] et [33]. Un algorithme implicite monolithique basé sur la méthode Level set pour les problèmes d'interaction fluide structure avec un domaine fluide fixe est proposé dans [6]. Dans cet algorithme, la position de l'interface est déterminée à chaque itération par la méthode Level set.

Un algorithme monolithique semi-implicite basé sur le schéma de projection de Chorin-Temam a été introduit dans [13], où l'idée principale était de découpler le calcul de la vitesse fluide du système couplé fluide structure, qui ne fait intervenir que la pression du fluide et la vitesse de la structure comme inconnues. D'autres algorithmes monolithiques semi-implicites basés sur des méthodes algébriques et employant l'approche procédures partagées quand les vitesses et pressions sont calculés, sont proposés dans [1], [2], [31].

Nous avons adopté l'approche monolithique dans le dernier chapitre de ce document, en proposant un algorithme semi-implicite monolithique pour un problème d'interaction fluide structure avec des petits déplacements de la structure. Un maillage global fluide structure, obtenu comme union des maillages fluide et structure a été introduit. La condition de continuité des vitesses est satisfaite automatiquement par l'utilisation d'un seul champ de vitesse et la condition d'égalité des contraintes est éliminée à partir de la formulation faible du problème. L'utilisation des fonctions caractérisques nous a permis d'avoir une liberté sur le choix des schémas discrets des équations.

Nous sommes motivés par des applications hémodynamiques, telles que l'écoulement du sang dans les artères et le phénomène d'interaction fluide structure dans les anévrismes cérébraux.

L'anévrisme cérébral résulte d'une dilatation anormale de la paroi artérielle sous différents facteurs, excès du tabac, d'alcool etc. Il se crée par conséquent une poche où le sang s'accumule. L'anévrisme cérébral est fréquemment découvert entre 35 et 60 ans sur 2% à 3% de la population. La rupture de l'anévrisme cérébral cause une hémorragie mortelle. Cette rupture est généralement associée aux forces de contraintes produites par la paroi de l'anévrisme. Il existe une littérature abondante sur l'étude d'interaction fluide structure dans les anévrismes cérébraux, on peut consulter sur ce sujet, par exemple [34] et [35]. De manière plus précise, dans [35], les auteurs décrivent un phénomène d'interaction entre le sang et la paroi de l'artère d'un anévrisme en phase terminale, de plus ils calculent les tenseurs des contraintes de la paroi, la pression, les tenseurs effectifs et les déformations.

Tout au long de ce document, nous admettons que le fluide est Newtonien, incompressible, visqueux et modélisé par les équations de Navier-Stokes posées sur un domaine en mouvement. La formulation ALE de ces équations a été introduite. La structure est gouvernée, dans le cas des petits déplacements par les équations d'élasticité linéaire et dans le cas des grands déplacements par le modèle de Saint-Venant Kirchhoff non linéaire. Le couplage entre le fluide et la structure est réalisé à partir de deux conditions à l'interface : la continuité des vitesses et l'égalité des contraintes.
La discrétisation en temps des équations du fluide est obtenue en combinant un schéma d'Euler implicite avec une linéarisation du terme de convection et celle de la structure est faite soit à l'aide d'un θ-schéma d'ordre deux, soit en utilisant le schéma de Newmark d'ordre deux. Pour la discrétisation en espace, nous avons employé des éléments finis du type $\mathbb{P}_1$ + *bubble* pour les vitesses, $\mathbb{P}_1$ pour les pressions et les déplacements et $\mathbb{P}_0$ pour les fonctions caractéristiques. Les tests numériques sont effectués en FreeFem++, voir [17].

Modèles mathématiques

Nous nous intéressons à des problèmes d'interactions fluide structure bidimensionels.

Nous notons Ω^S le domaine non déformé de la structure et nous admettons que son bord $\partial\Omega^S$ se décompose en $\partial\Omega^S = \Gamma_D \cup \Gamma_N \cup \Gamma_0$, avec $\Gamma_D = [AB] \cup [CD]$ et $\Gamma_N = [AD]$. Nous notons Ω_0^F le domaine initial du fluide, borné par Σ_1 la section d'entrée du fluide, Σ_2 le bord inférieur, Σ_3 la section de sortie du fluide et Γ_0 le bord supérieur. La section Γ_0 représente l'interface commune entre le fluide et la structure (voir Figure 1 à gauche).

Sous l'action des contraintes exercées par le fluide sur la structure, le domaine occupé par la structure se déforme. A l'instant t, le fluide occupera le domaine Ω_t^F borné par l'interface mobile Γ_t et le bord rigide $\Sigma = \Sigma_1 \cup \Sigma_2 \cup \Sigma_3$ (voir Figure 1 à droite).

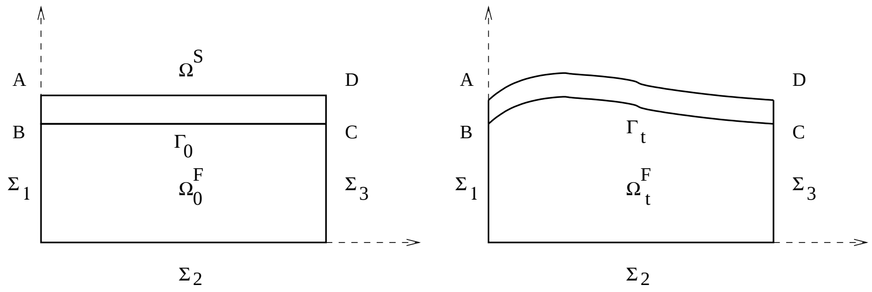

Figure 1: Configuration initiale (à gauche) et configuration intermédiaire (à droite).

Equations de Navier-Stokes

$$
\begin{aligned}
\rho^F\left(\frac{\partial \mathbf{v}}{\partial t}+(\mathbf{v}\cdot\nabla)\mathbf{v}\right)-\nabla\cdot\sigma^F &= \mathbf{f}^F, \quad \forall t\in(0,T],\forall \mathbf{x}\in\Omega_t^F & (1)\\
\nabla\cdot\mathbf{v} &= 0, \quad \forall t\in(0,T],\forall \mathbf{x}\in\Omega_t^F & (2)\\
\epsilon^F(\mathbf{v}) &= \frac{1}{2}\Big(\nabla\mathbf{v}+(\nabla\mathbf{v})^T\Big) & (3)\\
\sigma^F &= -p\mathbb{I}_2+2\mu^F\epsilon^F(\mathbf{v}) & (4)\\
\sigma^F\mathbf{n}^F &= \mathbf{h}_{in}, \quad \text{sur } \Sigma_1\times(0,T] & (5)\\
\sigma^F\mathbf{n}^F &= \mathbf{h}_{out}, \quad \text{sur } \Sigma_3\times(0,T] & (6)\\
\mathbf{v} &= 0, \quad \text{sur } \Sigma_2\times(0,T], & (7)
\end{aligned}
$$

où $\rho^F > 0$ et $\mu^F > 0$ sont la densité massique et la viscosité du fluide, $\mathbf{f}^F = (f_1^F, f_2^F)$ sont les forces volumiques appliquées, qui sont en général des forces gravitationnelles, $h_{in} : \Sigma_1 \times (0,T) \to \mathbb{R}^2$ et $h_{out} : \Sigma_3 \times (0,T) \to \mathbb{R}^2$ sont les forces de contraintes prescrites au bord et $\mathbf{n}^F$ est la normale extérieure au bord $\partial\Omega_t^F$. L'interface Γ_t est obtenue comme image du bord Γ_0 par l'application

$$\mathbb{T}(\mathbf{X}) = \mathbf{X} + \mathbf{u}(\mathbf{X}, t). \tag{8}$$

Formulation ALE des équations de Navier-Stokes

La formulation ALE est une formulation intermédiaire entre la formulation Lagrangienne et la formulation Eulérienne. Elle permet dans le système (1) - (7) de remplacer la dérivée en temps, qui est écrite par rapport à un domaine en mouvement Ω_t par une dérivée en temps écrite par rapport un domaine de référence fixe. Cette formulation induit une correction dans le terme de transport $(\mathbf{v}\cdot\nabla)\mathbf{v}$, en retranchant la vitesse du domaine à la vitesse du transport $\mathbf{v}$. Pour plus de détails voir par exemple [28].
Soit $\widehat{\Omega}^F$ le domaine de référence du fluide et $\mathcal{A}_t, t \in [0,T]$ une famille d'homéomorphismes telle que

$$\mathcal{A}_t(\widehat{\mathbf{x}}) = \mathbf{x},\ \forall\,\widehat{\mathbf{x}} \in \widehat{\Omega}^F,\ \mathcal{A}_t(\widehat{\Omega}^F) = \Omega_t^F,$$

où $\widehat{\mathbf{x}} = (\widehat{x}_1, \widehat{x}_2)^T \in \widehat{\Omega}^F$ sont les coordonnées ALE et $\mathbf{x} = (x_1, x_2)^T \in \Omega_t^F$ les coordonnées Eulériennes.
Soit $\mathbf{v}$ la vitesse du fluide en coordonnées Eulériennes. On note $\widehat{\mathbf{v}} : \widehat{\Omega}^F \longrightarrow \mathbb{R}^2$ la fonction correspondante en coordonnées ALE, définie par

$$\widehat{\mathbf{v}}(\widehat{\mathbf{x}}, t) = \mathbf{v}(\mathcal{A}_t(\widehat{\mathbf{x}}), t) = \mathbf{v}(\mathbf{x}, t).$$

Nous définissons la vitesse du domaine fluide $\boldsymbol{\vartheta}$ par

$$\boldsymbol{\vartheta}(\mathbf{x}, t) = \frac{\partial \mathcal{A}_t}{\partial t}(\widehat{\mathbf{x}}) = \frac{\partial \mathcal{A}_t}{\partial t}\left(\mathcal{A}_t^{-1}(\mathbf{x})\right)$$

et la dérivée ALE en temps de la vitesse du fluide par

$$\left.\frac{\partial \mathbf{v}}{\partial t}\right|_{\widehat{\mathbf{x}}}(\mathbf{x}, t) = \frac{\partial \widehat{\mathbf{v}}}{\partial t}(\widehat{\mathbf{x}}, t).$$

En utilisant la relation suivante, qui lie la dérivée Eulérienne à la dérivée ALE

$$\left.\frac{\partial \mathbf{v}}{\partial t}\right|_{\widehat{\mathbf{x}}} = \frac{\partial \mathbf{v}}{\partial t} + (\boldsymbol{\vartheta} \cdot \nabla)\mathbf{v}.$$

Le système gouvernant le fluide devient par conséquent

Equations de Navier-Stokes dans le cadre ALE

$$\begin{aligned}
\rho^F \left(\left.\frac{\partial \mathbf{v}}{\partial t}\right|_{\widehat{\mathbf{x}}} + \left((\mathbf{v} - \boldsymbol{\vartheta}) \cdot \nabla\right) \mathbf{v} \right) - 2\mu^F \nabla \cdot \epsilon\,(\mathbf{v}) + \nabla p &= \mathbf{f}^F,\ \Omega_t^F \times (0, T] && (9)\\
\nabla \cdot \mathbf{v} &= 0,\ \Omega_t^F \times [0, T] && (10)\\
\sigma^F \mathbf{n}^F &= \mathbf{h}_{in},\ \Sigma_1 \times (0, T] && (11)\\
\sigma^F \mathbf{n}^F &= \mathbf{h}_{out},\ \Sigma_3 \times (0, T] && (12)\\
\mathbf{v} &= 0,\ \Sigma_2 \times (0, T] && (13)\\
\mathbf{v}(\mathbf{X}, 0) &= \mathbf{v}^0(\mathbf{X}),\ \Omega_0^F. && (14)
\end{aligned}$$

Modèles mathématiques pour la structure

Dans le cas des petits déplacements de la structure, le modèle utilisé pour la structure est celui de l'élasticité linéaire.

Equations de l'élasticité linéaire

$$
\begin{aligned}
\rho^S \frac{\partial^2 \mathbf{u}}{\partial t^2} - \nabla \cdot \sigma^S &= \mathbf{f}^S, \quad \text{dans } \Omega^S \times (0,T] && (15)\\
\mathbf{u} &= 0, \quad \text{sur } \Gamma_D \times (0,T] && (16)\\
\epsilon^S(\mathbf{u}) &= \frac{1}{2}\Big(\nabla \mathbf{u} + (\nabla \mathbf{u})^T\Big) && (17)\\
\sigma^S &= \lambda^S (\nabla \cdot \mathbf{u}) \mathbb{I}_2 + 2\mu^S \epsilon^S(\mathbf{u}) && (18)\\
\sigma^S \mathbf{n}^S &= 0, \quad \text{sur } \Gamma_N \times (0,T] && (19)\\
\mathbf{u}(\mathbf{X},0) &= \mathbf{u}^0(\mathbf{X}), \quad \text{dans } \Omega^S && (20)\\
\frac{\partial \mathbf{u}}{\partial t}(\mathbf{X},0) &= \dot{\mathbf{u}}^0(\mathbf{X}), \quad \text{dans } \Omega^S, && (21)
\end{aligned}
$$

où $\rho^S > 0$ est la densité massique de la structure, $\lambda^S > 0$ et $\mu^S > 0$ sont les constantes de Lamé, $\mathbf{f}^S : \Omega^S \times (0,T) \rightarrow \mathbb{R}^2$ sont les forces volumiques appliquées par unité de surface, $\epsilon(\mathbf{u})$ est le tenseur des déformations linéarisé, $\mathbf{u}^0$ est le déplacement initial, $\dot{\mathbf{u}}^0$ est la vitesse initiale et $\mathbf{n}^S$ est le vecteur normal unitaire le long du bord $\partial\Omega^S$.
Dans le cas des grands déplacements de la structure, on substitue au modèle linéaire de la structure le modèle de Saint-Venant Kirchhhoff, obtenu en remplaçant dans (15) et (19) σ^S par

$$
\big(\mathbb{I}_2 + \nabla \mathbf{u}\big)\Sigma^S, \tag{22}
$$

où

$$
\Sigma^S = \big[\lambda^S \left(E_{11}(\mathbf{u}) + E_{22}(\mathbf{u})\right) \mathbb{I}_2 + 2\mu^S \mathbb{E}(\mathbf{u})\,\big]
$$

et

$$
\mathbb{E}(\mathbf{u}) = \frac{1}{2}\left(\nabla \mathbf{u} + (\nabla \mathbf{u})^T + (\nabla \mathbf{u})^T \nabla \mathbf{u}\right).
$$

Nous admettons que l'interaction fluide structure est gouvernée par les systèmes (9) - (14) et (15) - (21) (en tenant compte de (22) pour les grands déplacements de la structure) couplés à l'interface par les conditions suivantes

Conditions de couplage

Continuité des vitesses

$$
\mathbf{v}(\mathbf{X} + \mathbf{u}(\mathbf{X},t), t) = \frac{\partial \mathbf{u}}{\partial t}(\mathbf{X},t), \quad \text{sur } \Gamma_0 \times (0,T], \tag{23}
$$

Egalité des contraintes, cas des petits déplacements

$$
(\sigma^F \mathbf{n}^F)_{(\mathbf{X}+\mathbf{u}(\mathbf{X},t),t)} = -(\sigma^S \mathbf{n}^S)_{(\mathbf{X},t)}, \quad \text{sur } \Gamma_0 \times (0,T]. \tag{24}
$$

Egalité des contraintes, cas des grands déplacements

$$
(\sigma^F \mathbf{n}^F)_{(\mathbf{X}+\mathbf{u}(\mathbf{X},t),t)}\, \omega(\mathbf{X},t) = -(\big(\mathbb{I}_2 + \nabla \mathbf{u}\big)\Sigma^S \mathbf{n}^S)_{(\mathbf{X},t)}, \quad \text{sur } \Gamma_0 \times (0,T] \tag{25}
$$

où $\omega(\mathbf{X},t) = \|\mathrm{cof}(\nabla \mathbb{T})\mathbf{n}^S\|_{\mathbb{R}^2}$ et l'application $\mathbb{T}$ est donnée par (8).

Synthèse du chapitre I

Dans cette section, on suppose que l'interaction fluide structure est gouvernée, dans le cas des petits déplacements de la structure par (9)–(21), couplés à l'interface par (23), (24) et dans le cas des grands déplacements par le même modèle fluide et le modèle de Saint-Venant Kirchhoff pour la structure, couplés à l'interface par (23), (25).

Nous proposons ici un algorithme semi-implicite procédures partagées, qui à chaque pas de temps prédit la position de l'interface de manière explicite. Par conséquent un problème d'optimisation, où le gradient de la fonction coût est approché par différences finis est résolu, afin d'identifier les contraintes à l'interface. La condition de continuité de vitesses est utilisée comme condition au bord à l'interface dans le problème fluide. L'algorithme de BFGS a été employé pour résoudre le problème d'optimisation, car moins sensible par rapport au point de départ que celui de Newton. Durant les itérations de BFGS, le maillage fluide reste fixe et la matrice fluide n'est factorisée qu'une seule fois, ce qui réduit de façon considérable le temps de calcul. Une comparaison des temps CPU a permis de montrer que cet algorithme est plus rapide que l'algorithme implicite équivalent. La méthode de décomposition modale a été employée pour la structure dans le cas des petits déplacements et celle de Newton dans le cas des grands déplacements.

Méthodes numériques pour la structure

Formulation faible

Nous introduisons pour le problème de la structure, l'espace des fonctions test suivant

$$\mathbf{W}^S = \left\{ \mathbf{w}^S \in \left(H^1\left(\Omega^S\right)\right)^2;\ \mathbf{w}^S = 0 \text{ sur } \Gamma_D \right\}.$$

Si on multiplie l'équation (15) par la fonction test $\mathbf{w}^S \in \mathbf{W}^S$, par la formule de Green, on obtient la formulation faible suivante

Trouver $\mathbf{u} \in \mathbf{W}^S$ tel que

$$\int_{\Omega^S} \rho^S \frac{\partial^2 \mathbf{u}}{\partial t^2} \cdot \mathbf{w}^S d\mathbf{X} + a_S\left(\mathbf{u}, \mathbf{w}^S\right) = \int_{\Omega^S} \mathbf{f}^S \cdot \mathbf{w}^S d\mathbf{X} + \int_{\Gamma_0} \left(\sigma^S \mathbf{n}^S\right) \cdot \mathbf{w}^S d\,s, \quad \forall \mathbf{w}^S \in \mathbf{W}^S, \tag{26}$$

où

$$a_S\left(\mathbf{u}, \mathbf{w}^S\right) = \int_{\Omega^S} \lambda^S \left(\nabla \cdot \mathbf{u}\right)\left(\nabla \cdot \mathbf{w}^S\right) d\mathbf{X} + \int_{\Omega^S} 2\mu^S \epsilon\left(\mathbf{u}\right) : \epsilon\left(\mathbf{w}^S\right) d\mathbf{X}$$

dans le cas linéaire et

$$a_S\left(\mathbf{u}, \mathbf{w}^S\right) = \int_{\Omega^S} \left(\mathbb{I}_2 + \nabla \mathbf{u}\right)\left(\lambda^S \left(E_{11}\left(\mathbf{u}\right) + E_{22}\left(\mathbf{u}\right)\right)\mathbb{I}_2 + 2\mu^S \mathbb{E}\left(\mathbf{u}\right)\right) : \left(\nabla \mathbf{w}^S\right) d\mathbf{X}$$

dans le cas non linéaire.

Méthode de décomposition modale pour le modèle linéaire

Pour chaque $i \in \mathbb{N}^*$, il existe une unique valeur propre $\lambda_i > 0$ et un unique vecteur propre $\boldsymbol{\phi}^i \in \mathbf{W}^S$, solution de

$$a_S\left(\boldsymbol{\phi}^i, \mathbf{w}^S\right) = \lambda_i \int_{\Omega^S} \rho^S \boldsymbol{\phi}^i \cdot \mathbf{w}^S d\mathbf{X}, \quad \forall \mathbf{w}^S \in \mathbf{W}^S \tag{27}$$

tels que

$$\int_{\Omega^S} \rho^S \boldsymbol{\phi}^i \cdot \boldsymbol{\phi}^j d\mathbf{X} = \delta_{ij}. \tag{28}$$

La résolution en éléments finis du problème (27)–(28) est équivalente à la résolution du problème généralisé aux modes propres suivant

$$K_h \boldsymbol{\Phi}_h^i = \lambda_{i,h} M_h \boldsymbol{\Phi}_h^i, \quad \left(\boldsymbol{\Phi}_h^j\right)^T M_h \boldsymbol{\Phi}_h^i = \mathbb{I}_2.$$

Notons $\alpha_i(t) = \displaystyle\int_{\Gamma_0} \left(\sigma^S \mathbf{n}^S\right)(t) \cdot \boldsymbol{\phi}^i d\,s$. La solution de (26) peut être écrite sous la forme

$$\mathbf{u}(t) = \sum_{i \geq 1} q_i(t) \boldsymbol{\phi}^i,$$

où les coefficients q_i sont solutions de l'équation différentielle de second ordre suivante

$$q_i''(t) + \lambda_i q_i(t) = \int_{\Omega^S} \mathbf{f}^S(t) \cdot \boldsymbol{\phi}^i d\mathbf{X} + \alpha_i(t), \quad t \in (0, T) \tag{29}$$

$$q_i(0) = \int_{\Omega^S} \rho^S \mathbf{u}^0 \cdot \boldsymbol{\phi}^i d\mathbf{X} \tag{30}$$

$$q_i'(0) = \int_{\Omega^S} \rho^S \dot{\mathbf{u}}^0 \cdot \boldsymbol{\phi}^i d\mathbf{X}. \tag{31}$$

De plus les fonctions $\boldsymbol{\phi}^i$ forment une base orthonormale de $L^2(\Omega^S)$ et si λ_i est assez grand, l'influence des $q_i(t)$ sur $\mathbf{u}(t)$ diminue. Ainsi en pratique seuls les m premières valeurs propres seront considérées

$$0 < \lambda_1 \leq \lambda_2 \leq \cdots \leq \lambda_m.$$

Pour l'approximation en temps du problème (29) - (30) - (31), nous utilisons un θ-schéma centré d'ordre deux. Soit $N \in \mathbb{N}^*$ le nombre de pas de temps et $\Delta t = T/N$ le pas de temps. On pose $t_n = n\Delta t$ pour $n = 0, 1, \ldots, N$. On note respectivement α_i^n, $\mathbf{u}^n$, $\mathbf{f}^n$ et q_i^n les approximations $\alpha_i(t_n)$, $\mathbf{u}(t_n)$, $\mathbf{f}(t_n)$ et de $q_i(t_n)$. Le problème (29) est approché par le schéma suivant

Connaissant q_i^{n-1} et q_i^n, trouver q_i^{n+1} tel que

$$\frac{\left(q_i^{n+1} - 2q_i^n + q_i^{n-1}\right)}{(\Delta t)^2} + \lambda_{i,h}\left(\theta q_i^{n+1} + (1-2\theta) q_i^n + \theta q_i^{n-1}\right)$$
$$= \int_{\Omega^S} \left(\theta \mathbf{f}^{S,n+1} + (1-2\theta)\mathbf{f}^{S,n} + \theta \mathbf{f}^{S,n-1}\right) \cdot \boldsymbol{\phi}^i d\mathbf{X} + \theta \alpha_i^{n+1} + (1-2\theta)\alpha_i^n + \theta \alpha_i^{n-1}, \quad (32)$$

où $\theta \in \left(0, \dfrac{1}{2}\right)$ et $\mathbf{f}^{S,n} = \mathbf{f}^S(t_n)$.

Ce schéma est inconditionnellement stable si $\theta \in \left[\dfrac{1}{4}, \dfrac{1}{2}\right]$.

On note m le nombre de modes propres de l'opérateur considéré dans (27). Le déplacement de la structure à l'instant t_n sera alors approché par

$$\mathbf{u}_h^n(\mathbf{X}) = \sum_{i=1}^{m} q_i^n \boldsymbol{\phi}_h^i(\mathbf{X}), \quad \forall \mathbf{X} \in \Omega^S.$$

Méthode de Newton pour le modèle non linéaire

On considère le schéma d'ordre deux en temps ci-dessous pour le problème (26), dans le cas non linéaire

Trouver $\mathbf{u}^{n+1} \in \mathbf{W}^S$ une approximation de $\mathbf{u}(t_{n+1})$ telle que

$$\int_{\Omega^S} \rho^S \frac{(\mathbf{u}^{n+1} - 2\mathbf{u}^n + \mathbf{u}^{n-1})}{(\Delta t)^2} \cdot \mathbf{w}^S d\mathbf{X}$$
$$+\theta a_S\left(\mathbf{u}^{n+1}, \mathbf{w}^S\right) + (1-2\theta) a_S\left(\mathbf{u}^n, \mathbf{w}^S\right) + \theta a_S\left(\mathbf{u}^{n-1}, \mathbf{w}^S\right)$$
$$= \int_{\Omega^S} \left(\theta \mathbf{f}^{S,n+1} + (1-2\theta)\mathbf{f}^{S,n} + \theta \mathbf{f}^{S,n-1}\right) \cdot \mathbf{w}^S d\mathbf{X}$$
$$+ \int_{\Gamma_0} \left(\theta \mathbf{F}^{S,n+1} + (1-2\theta)\mathbf{F}^{S,n} + \theta \mathbf{F}^{S,n-1}\right) \cdot \mathbf{w}^S d\, s, \quad \forall \mathbf{w}^S \in \mathbf{W}^S, \quad (33)$$

où $\mathbf{f}^{S,n} = \mathbf{f}^S(t_n)$, $\mathbf{F}^{S,n} = \left(\sigma^S \mathbf{n}^S\right)(t_n)$ et θ un paramètre réel appartenant à $\left(0, \dfrac{1}{2}\right)$.

Les composantes du tenseur de Saint-Venant Kirchhoff peuvent être obtenues à partir de (22). De plus, l'application $\mathbf{u} \to \mathbb{E}(\mathbf{u})$ étant non linéaire, nous utiliserons la méthode de Newton pour déterminer la solution $\mathbf{u}^{n+1}$ de (33).

Connaissant les dérivées des composantes du tenseur des déformations de Green-Saint Venant $\mathbb{E}(\mathbf{u})$ et celles de $(\mathbb{I}_2 + \nabla \mathbf{u})$ par rapport à $\mathbf{u}$ pour un $\mathbf{h} = (h_1, h_2)$ arbitraire dans $\mathbf{W}^S$, on calcule facilement

$$\frac{d\, a_S}{d\, \mathbf{u}}\left(\mathbf{u}, \mathbf{w}^S\right) \mathbf{h} = \sum_{i,j=1}^{2} \int_{\Omega^S} \frac{d\, \sigma_{ij}^S}{d\, \mathbf{u}} (\mathbf{u})\, \mathbf{h}\, \frac{\partial w_i^S}{\partial x_j} d\mathbf{X}.$$

Algorithme de Newton pour le problème (33)

Etape 0. Initialisation. On pose $k=0$ et $\mathbf{u}^{n+1,0}=\mathbf{u}^n$. Nous générerons $\mathbf{u}^{n+1,k}$ pour $k=1,2,\ldots$

Etape 1. Trouver $\mathbf{h}^k$ solution du système linéaire

$$\begin{aligned}
&\int_{\Omega^S} \rho^S \frac{\mathbf{h}^k}{(\Delta t)^2}\cdot \mathbf{w}^S d\mathbf{X} + \frac{d\,a_S}{d\,\mathbf{u}}\left(\mathbf{u}^{n+1,k},\mathbf{w}^S\right)\mathbf{h}^k \\
&= \int_{\Omega^S} \rho^S \frac{\left(\mathbf{u}^{n+1,k}-2\mathbf{u}^n+\mathbf{u}^{n-1}\right)}{(\Delta t)^2}\cdot \mathbf{w}^S d\mathbf{X} \\
&+\theta a_S\left(\mathbf{u}^{n+1,k},\mathbf{w}^S\right)+(1-2\theta)a_S\left(\mathbf{u}^n,\mathbf{w}^S\right)+\theta a_S\left(\mathbf{u}^{n-1},\mathbf{w}^S\right) \\
&-\int_{\Omega^S}\left(\theta \mathbf{f}^{S,n+1}+(1-2\theta)\mathbf{f}^{S,n}+\theta\mathbf{f}^{S,n-1}\right)\cdot \mathbf{w}^S d\mathbf{X} \\
&-\int_{\Gamma_0}\left(\theta \mathbf{F}^{S,n+1}+(1-2\theta)\mathbf{F}^{S,n}+\theta\mathbf{F}^{S,n-1}\right)\cdot \mathbf{w}^S d\,s, \quad \forall \mathbf{w}^S\in \mathbf{W}^S. \qquad (34)
\end{aligned}$$

Etape 2. Si $\mathbf{h}^k$ est petit, alors on arrête.

Etape 3. On pose $\mathbf{u}^{n+1,k+1}=\mathbf{u}^{n+1,k}-\mathbf{h}^k$; $k\leftarrow k+1$; aller à **Etape 1.**

Remarque 1 *Le problème variationnel* (34) *est résolu par la méthode des éléments finis et on note* $\mathbf{u}_h^{n+1}$ *le déplacement de la structure à l'instant* t_{n+1}.

Approximation en temps des équations du fluide en cadre ALE

Formulation faible discrète en temps

On introduit les espaces des fonctions test suivants

$$\mathbf{W}^F=\left\{\mathbf{w}^F\in\left(H^1\left(\Omega_t^F\right)\right)^2;\ \mathbf{w}^F=0 \text{ sur } \Sigma_2\cup\Gamma_t\right\},\quad Q=L^2(\Omega_t^F).$$

Multiplions l'équation (9) par $\mathbf{w}^F\in\mathbf{W}^F$ et l'équation (10) par $q\in Q$ et en utilisant la formule de Green, on obtient

$$\begin{aligned}
&\int_{\Omega_t^F}\rho^F \left.\frac{\partial \mathbf{v}}{\partial t}\right|_{\widehat{\mathbf{x}}}\cdot \mathbf{w}^F d\mathbf{x} + \int_{\Omega_t^F}\rho^F\left(\left(\left(\mathbf{v}-\boldsymbol{\vartheta}\right)\cdot\nabla\right)\mathbf{v}\right)\cdot\mathbf{w}^F d\mathbf{x} \\
&\qquad + a_F\left(\mathbf{v},\mathbf{w}^F\right)+b_F\left(\mathbf{w}^F,p\right)=\ell_F\left(\mathbf{w}^F\right),\ \forall \mathbf{w}^F\in\mathbf{W}^F, \\
&b_F(\mathbf{v},q)=0,\quad \forall q\in Q,
\end{aligned}$$

où

$$a_F\left(\mathbf{v},\mathbf{w}^F\right)=\int_{\Omega_t^F}2\mu^F\epsilon(\mathbf{v}):\epsilon\left(\mathbf{w}^F\right)d\mathbf{x},\quad b_F\left(\mathbf{w}^F,q\right)=-\int_{\Omega_t^F}\left(\nabla\cdot\mathbf{w}^F\right)q\,d\mathbf{x},$$

$$\ell_F\left(\mathbf{w}^F\right)=\int_{\Omega_t^F}\mathbf{f}^F\cdot\mathbf{w}^F d\mathbf{x}+\int_{\Sigma_1}\mathbf{h}_{in}\cdot\mathbf{w}^F d\,s+\int_{\Sigma_3}\mathbf{h}_{out}\cdot\mathbf{w}^F d\,s.$$

Pour la discrétisation en temps, on note Δt le pas de temps et $t_n = n\Delta t$ les points de $[0,T]$. Les approximations de $\mathbf{h}_{in}(t_n)$, $\mathbf{h}_{out}(t_n)$, $\mathbf{v}(t_n)$, $p(t_n)$ et $\mathbf{f}^F(t_n)$ sont respectivement notées $\mathbf{h}_{in}^n$, $\mathbf{h}_{out}^n$, $\mathbf{v}^n$, p^n et $\mathbf{f}^{F,n}$. Ensuite, on utilise un algorithme d'intégration basé sur le schéma d'Euler implicite et une linéarisation du terme de convection, pour obtenir

Connaissant Ω_n^F, Ω_{n+1}^F, $\mathbf{V}^n$, $\boldsymbol{\vartheta}^{n+1}$, trouver $\mathbf{v}^{n+1}$ et p^{n+1} telles que

$$\mathbf{v}^{n+1}\left(\mathbf{X}+\mathbf{u}_h^{n+1}(\mathbf{X})\right)=\sum_{i=1}^{m}\frac{q_i^{n+1}-q_i^n}{\Delta t}\boldsymbol{\phi}_h^i(\mathbf{X}),\quad \forall \mathbf{X}\in\Gamma_0, \tag{35}$$

$$\begin{aligned}&\int_{\Omega_{n+1}^F}\rho^F\left(\frac{\mathbf{v}^{n+1}-\mathbf{V}^n}{\Delta t}\right)\cdot\mathbf{w}^F d\mathbf{x}+\int_{\Omega_{n+1}^F}\rho^F\left(\left(\left(\mathbf{V}^n-\boldsymbol{\vartheta}^{n+1}\right)\cdot\nabla\right)\mathbf{v}^{n+1}\right)\cdot\mathbf{w}^F d\mathbf{x}\\&+\int_{\Omega_{n+1}^F}2\mu^F\epsilon\left(\mathbf{v}^{n+1}\right):\epsilon\left(\mathbf{w}^F\right)d\mathbf{x}-\int_{\Omega_{n+1}^F}\left(\nabla\cdot\mathbf{w}^F\right)p^{n+1}d\mathbf{x}\\&=\int_{\Omega_{n+1}^F}\mathbf{f}^F\cdot\mathbf{w}^F d\mathbf{x}+\int_{\Sigma_1}\mathbf{h}_{in}^{n+1}\cdot\mathbf{w}^F d\,s\\&+\int_{\Sigma_3}\mathbf{h}_{out}^{n+1}\cdot\mathbf{w}^F d\,s,\ \forall\mathbf{w}^F=0 \text{ sur } \Sigma_2\cup\Gamma_{n+1},\end{aligned}\tag{36}$$

$$-\int_{\Omega_{n+1}^F}\left(\nabla\cdot\mathbf{v}^{n+1}\right)q\,d\mathbf{x}=0,\quad\forall q, \tag{37}$$

où

$$\mathbf{V}^n(\mathbf{x})=\mathbf{v}^n\left(\mathcal{A}_{t_n}\circ\mathcal{A}_{t_{n+1}}^{-1}(\mathbf{x})\right)$$

et

$$\boldsymbol{\vartheta}^{n+1}(\mathbf{x})=\frac{\mathcal{A}_{t_{n+1}}(\widehat{\mathbf{x}})-\mathcal{A}_{t_n}(\widehat{\mathbf{x}})}{\Delta t}=\frac{\mathbf{x}-\mathcal{A}_{t_n}\circ\mathcal{A}_{t_{n+1}}^{-1}(\mathbf{x})}{\Delta t}.$$

Nous avons besoin de l'application ALE discrète pour calculer explicitement le domaine fluide à l'instant $n+1$ et la vitesse du domaine fluide $\boldsymbol{\vartheta}^{n+1}$, afin de résoudre le problème (35) - (37).

Construction de l'application ALE discrète

On note $\mathcal{T}_h^0$ le maillage en éléments finis triangulaires du domaine de référence fluide $\widehat{\Omega}^F=\Omega_0^F$. Connaissant le déplacement de la structure $\widetilde{\mathbf{u}}_h^{n+1}:\Omega^S\to\mathbb{R}^2$, on peut calculer le déplacement du domaine fluide $\widetilde{\mathbf{d}}^{n+1}:\Omega_0^F\to\mathbb{R}^2$ à partir du problème aux limites suivant

$$\begin{aligned}\Delta\widetilde{\mathbf{d}}^{n+1}&=0,\quad \text{sur } \Omega_0^F, &(38)\\ \widetilde{\mathbf{d}}^{n+1}&=\widetilde{\mathbf{u}}_h^{n+1},\quad \text{sur } \Gamma_0, &(39)\\ \widetilde{\mathbf{d}}^{n+1}&=0,\quad \text{sur } \Sigma_1\cup\Sigma_2\cup\Sigma_3. &(40)\end{aligned}$$

On construit ensuite l'application ALE discrète comme suit

$$\mathcal{A}_{h,n+1}\left(\widehat{\mathbf{x}}\right) = \widehat{\mathbf{x}} + \widetilde{\mathbf{d}}^{n+1}(\widehat{\mathbf{x}})$$

et le maillage du domaine Ω^F_{n+1} peut être obtenu par

$$\widetilde{\mathcal{T}}_h^{n+1} = \mathcal{A}_{h,n+1}\left(\mathcal{T}_h^0\right). \tag{41}$$

Remarque 2 *Dans le cas d'un domaine non convexe, l'application ALE obtenue par extension harmonique inverse les triangles du maillage du domaine de référence et produit alors un maillage non valide. Une autre technique alternative est de minimiser l'énergie du système mécanique de l'ensemble des arêtes qui relient les noeuds du maillage. Un terme de pénalisation pourrait assurer la non inversion des triangles.*

La vitesse du domaine fluide est calculée par la formule de différences finies suivante

$$\widetilde{\boldsymbol{\vartheta}}^{n+1}(\mathbf{x}) = \frac{\widetilde{\mathbf{d}}^{n+1}(\widehat{\mathbf{x}}) - \widetilde{\mathbf{d}}^{n}(\widehat{\mathbf{x}})}{\Delta t}. \tag{42}$$

Si on prédit de manière explicite le déplacement de la structure à l'aide de la formule

$$\widetilde{\mathbf{u}}_h^{n+1} = 2\mathbf{u}_h^n - \mathbf{u}_h^{n-1},$$

nous pouvons obtenir directement la vitesse du domaine fluide comme solution de

$$\begin{aligned}
\Delta\widetilde{\boldsymbol{\vartheta}}^{n+1} &= 0, \quad \text{dans } \Omega_0^F, \\
\widetilde{\boldsymbol{\vartheta}}^{n+1} &= \frac{2\mathbf{u}_h^n - 3\mathbf{u}_h^{n-1} + \mathbf{u}_h^{n-2}}{\Delta t}, \quad \text{sur } \Gamma_0, \\
\widetilde{\boldsymbol{\vartheta}}^{n+1} &= 0, \quad \text{sur } \Sigma_1 \cup \Sigma_2 \cup \Sigma_3.
\end{aligned}$$

Algorithmes semi-implicites pour le problème couplé

Les composantes normales des forces de contraintes $(\sigma^S \mathbf{n}^S)(t)$ à l'interface fluide structure ne sont pas connues. Nous utiliserons les méthodes suivantes pour les approcher.

Cas d'un modèle linéaire de la structure

La condition d'égalité des contraintes à l'interface permet d'écrire

$$\int_{\Gamma_0} \left(\sigma^S \mathbf{n}^S\right)(t) \cdot \boldsymbol{\phi}^i d\,s = -\int_{\Gamma_0} \left(\sigma^F \mathbf{n}^F\right)_{(\mathbf{X}+\mathbf{u}(\mathbf{X},t),t)} \cdot \boldsymbol{\phi}^i d\,s,$$

donc en posant

$$\beta_i(t) = -\int_{\Gamma_0} \left(\sigma^F \mathbf{n}^F\right)_{(\mathbf{X}+\mathbf{u}(\mathbf{X},t),t)} \cdot \boldsymbol{\phi}^i d\,s, \tag{43}$$

et $\alpha_i(t) = \displaystyle\int_{\Gamma_0} \left(\sigma^S \mathbf{n}^S\right)(t) \cdot \boldsymbol{\phi}^i d\, s$, on obtient

$$\alpha_i(t) = \beta_i(t), \quad \forall\, i \geq 1,\ \forall\, t \in [0, T].$$

Cependant, après discrétisation totale du système, l'égalité ci-dessus n'est plus vérifiée. On utilise alors la méthode des moindres carrés pour traiter le problème. On approche les composantes β_i, des contraintes venant du fluide à l'aide des deux méthodes suivantes

1. On approche d'abord les β_i donnés par (43), en utilisant l'application définie dans (8) par
$$-\int_{\Gamma_t} \left(\sigma_h^F \mathbf{n}_h^F\right) \cdot \boldsymbol{\phi}_h^i \left(\mathbb{T}^{-1}\right) d\, s.$$
2. Ensuite, on introduit les tenseurs des contraintes définis sur le domaine de référence $\widehat{\Omega}^F$, de composantes
$$\widehat{\Sigma}_{ij}^F = -\widehat{p}\, \delta_{ij} + \mu^F \left(\frac{\partial \widehat{v}_i}{\partial \widehat{x}_j} + \frac{\partial \widehat{v}_j}{\partial \widehat{x}_i}\right)$$
et on approche enfin $\beta_i(t)$ par
$$-\int_{\Gamma_0} \left(\widehat{\Sigma}^F \widehat{\mathbf{n}}^F\right) \cdot \boldsymbol{\phi}^i d\, s.$$

Cas d'un modèle non linéaire de la structure

Les forces de contraintes à l'interface $\mathbf{F}^{S,n+1} = \left(\sigma^S \mathbf{n}^S\right)(t_{n+1})$ dans le problème (33) sont inconnues. Nous les approchons à l'instant t_{n+1} par

$$\sum_{i=1}^{m} \xi_i^{n+1} \boldsymbol{\psi}^i,$$

où les ξ_i^{n+1} doivent être identifiés et $\boldsymbol{\psi}^i \in \left(L^2(\Gamma_0)\right)^2$ sont les fonctions de base. Ces fonctions de base ne sont pas forcément compatibles avec les fonctions de base éléments finis du fluide ou de la structure. Il est possible de choisir les fonctions $\boldsymbol{\psi}^i$ comme des fonctions polynômiales, ou des fonctions de base éléments finis. Dans ce document, nous adoptons les fonctions $\boldsymbol{\psi}^i$ solutions de

$$a_S\left(\boldsymbol{\psi}^i, \mathbf{w}^S\right) = \mu_i \int_{\Gamma_0} \boldsymbol{\psi}^i \cdot \mathbf{w}^S d\mathbf{X},\ \forall\, \mathbf{w}^S \in \mathbf{W}^S, \qquad \int_{\Gamma_0} \boldsymbol{\psi}^i \cdot \boldsymbol{\psi}^j d\mathbf{X} = \delta_{ij}.$$

On peut noter par ailleurs, contrairement aux fonctions propres $\boldsymbol{\phi}^i$, que les traces des $\boldsymbol{\psi}^i$ sont orthonormales pour le produit scalaire de $L^2(\Gamma_0)$.

Nous présentons à présent l'algorithme semi-implicite dans le cas d'un modèle linéaire de la structure. Dans le cas non linéaire, l'algorithme reste valable, mis à part le fait qu'il faut remplacer l'étape 6 de l'algorithme ci-dessous par la remarque qui suit.

Algorithme

Etape 1. Prédiction explicite. On pose $\widetilde{\mathbf{u}}_h^{n+1} = 2\mathbf{u}_h^n - \mathbf{u}_h^{n-1}$.

Etape 2. Extension harmonique. Résoudre $\Delta\widetilde{\mathbf{d}}^{n+1} = 0$ dans Ω_0^F, $\widetilde{\mathbf{d}}^{n+1} = \widetilde{\mathbf{u}}^{n+1}$ sur Γ_0, $\widetilde{\mathbf{d}}^{n+1} = 0$ sur $\Sigma_1 \cup \Sigma_2 \cup \Sigma_3$.

Etape 3. Construction du maillage. On pose $\mathcal{A}_{h,n+1}(\widehat{\mathbf{x}}) = \widehat{\mathbf{x}} + \widetilde{\mathbf{d}}^{n+1}(\widehat{\mathbf{x}})$. Le maillage du domaine fluide à l'instant $n+1$ est donné par

$$\widetilde{\mathcal{T}}_h^{n+1} = \mathcal{A}_{h,n+1}\left(\mathcal{T}_h^0\right).$$

Etape 4. On définit la vitesse du domaine fluide par $\widetilde{\boldsymbol{\vartheta}}^{n+1}(\mathbf{x}) = \dfrac{\widetilde{\mathbf{d}}^{n+1}(\widehat{\mathbf{x}}) - \widetilde{\mathbf{d}}^{n}(\widehat{\mathbf{x}})}{\Delta t}$.

Etape 5. Assemblage des éléments finis de la matrice du problème fluide (36)–(37). Pour obtenir une factorisation LU de cette matrice.

Etape 6. Résoudre le problème fluide structure sur le maillage fixe $\widetilde{\mathcal{T}}_h^{n+1}$ par l'algorithme de BFGS , en partant du point $\boldsymbol{\alpha}^n$

$$\boldsymbol{\alpha}^{n+1} \in \arg\min_{\boldsymbol{\alpha}\in\mathbb{R}^m} J(\boldsymbol{\alpha}),$$

où la fonction coût est calculée comme suit

i) Résoudre le problème de la structure. Pour obtenir $\mathbf{q}^{n+1}$ à partir de (32), où $\boldsymbol{\alpha}^{n+1}$ a été remplacé par $\boldsymbol{\alpha}$. On obtient le déplacement de la structure, en posant $\mathbf{u} = \sum_{i=1}^m q_i^{n+1}\boldsymbol{\phi}^i$.

ii) Résoudre le problème fluide (36)–(37) sur le maillage $\widetilde{\mathcal{T}}_h^{n+1}$, en imposant la condition d'égalité des vitesses (35) comme condition au bord à l'interface. Pour obtenir la vitesse $\mathbf{v}$ et la pression p du fluide.

iii) Calculer β_i à partir de (43) pour $i = 1, \ldots, m$.

iv) On pose la fonction coût

$$J(\boldsymbol{\alpha}) = \frac{1}{2}\|\boldsymbol{\alpha} - \boldsymbol{\beta}\|_{\mathbb{R}^m}^2.$$

Le gradient de cette fonction est approché par différences finies.

Etape 7. Mises à jour $\mathbf{q}^{n-1} \leftarrow \mathbf{q}^n$, $\mathbf{q}^n \leftarrow \mathbf{q}^{n+1}$, $\boldsymbol{\alpha}^{n-1} \leftarrow \boldsymbol{\alpha}^n$, $\boldsymbol{\alpha}^n \leftarrow \boldsymbol{\alpha}^{n+1}$, etc.

Remarque 3 *Dans le cas où la structure est gouvernée par le modèle non linéaire, on remplace l'étape 6 dans l'algorithme par*

Résoudre par BFGS le problème d'optimisation

$$\boldsymbol{\xi}^{n+1} \in \arg\min_{\boldsymbol{\xi}\in\mathbb{R}^m} J(\boldsymbol{\xi}),$$

où la fonction coût est calculée comme suit

i) Résoudre le problème de la structure (33) *par la méthode de Newton avec les forces à l'interface*

$$\mathbf{F}^{S,n+1} = \sum_{i=1}^{m} \xi_i \boldsymbol{\psi}^i,$$

pour obtenir le déplacement de la structure $\mathbf{u}$*.*

ii) Résoudre le problème fluide $(36)-(37)$ *sur le maillage* $\widetilde{\mathcal{T}}_h^{n+1}$ *avec la condition au bord vitesse du fluide égale à* $\dfrac{\mathbf{u}-\mathbf{u}^n}{\Delta t}$ *à l'interface. Pour obtenir la vitesse* $\mathbf{v}$ *et la pression* p *du fluide.*

iii) Calculer

$$\alpha_i = \int_{\Gamma_0} \left(\sum_{j=1}^{m} \xi_j \boldsymbol{\psi}^j \right) \cdot \boldsymbol{\psi}^i d\, s, \quad \beta_i = -\int_{\Gamma_0} \left(\sigma^F \mathbf{n}^F \right)_{(\mathbf{X}+\tilde{\mathbf{u}}(\mathbf{X},t),t)} \cdot \boldsymbol{\psi}^i d\, s, \quad i = 1, \ldots, m.$$

iv) On définit la fonction coût

$$J(\boldsymbol{\alpha}) = \frac{1}{2} \|\boldsymbol{\alpha} - \boldsymbol{\beta}\|^2_{\mathbb{R}^m}.$$

Résultats numériques

Paramètres physiques et numériques

Le domaine fluide considéré est de longueur $L = 6\ cm$ et de hauteur $H = 1\ cm$. On prend comme viscosité du fluide $\mu = 0.035\ \frac{g}{cm\cdot s}$, sa densité $\rho^F = 1\ \frac{g}{cm^3}$. L'épaisseur du domaine élastique est $h^S = 0.1\ cm$, on prend comme module de Young $E = 3\cdot 10^6\ \frac{g}{cm\cdot s^2}$, la constante de Poisson $\nu = 0.3$, la densité de la structure $\rho^S = 1.1\ \frac{g}{cm^3}$. Les constantes de Lamé sont obtenues à partir de

$$\lambda^S = \frac{\nu^S E}{(1-2\nu^S)(1+\nu^S)}, \quad \mu^S = \frac{E}{2(1+\nu^S)}.$$

Les forces volumiques dans le fluide et la structure sont $\mathbf{f}^F = (0,0)^T$ et $\mathbf{f}^S = (0,0)^T$. Les contraintes imposées à la section d'entrée du fluide sont

$$\mathbf{h}_{in}(\mathbf{x},t) = \begin{cases} \left(10^3(1-\cos(2\pi t/0.025)),\ 0\right)^T, & \mathbf{x} \in \Sigma_1, 0 \leq t \leq 0.025 \\ (0,\ 0)^T, & \mathbf{x} \in \Sigma_1, 0.025 \leq t \leq T \end{cases}$$

et celles imposées à la section de sortie sont $\mathbf{h}_{out} = (0,\ 0)^T$.

Les tests numériques ont été réalisés à partir du logiciel *FreeFem++* (voir [17]). Nous avons utilisé les éléments finis $\mathbb{P}_1 + bubble$ pour les vitesses et $\mathbb{P}_1$ pour la pression et les déplacements. De plus on a fixé $\theta = 0.25$ dans les tests numériques.

Cas d'un modèle linéaire pour la structure

Maillage

Nous avons utilisé dans le cas où les extrémités gauche et droite de la structure sont fixés, un maillage de référence pour la structure de 60 triangles et 62 sommets et un maillage de référence pour le fluide de 1250 triangles et 696 sommets.

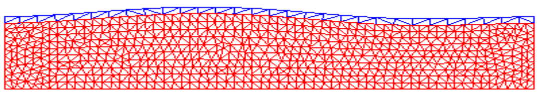

Figure 2: Les maillages fluide et structure à l'instant $t = 0.035$.

La simulation a été effectuée en supposant que la composante horizontale du déplacement de la structure de la section droite est nulle et la composante verticale est libre. Dans ce cas, on a remplacé la condition au bord sur Σ_3 dans le problème (38)-(40) par

$$\widetilde{\mathbf{d}}^{n+1}(L,x_2) = \left(0,\ \frac{x_2\, \widetilde{u}_{h,2}(L,H)}{H}\right), \quad \forall x_2 \in (0,H).$$

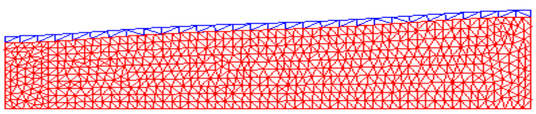

Figure 3: Les maillages fluide et structure à l'instant $t = 0.100$.

Critère d'arrêt de BFGS et nombre d'appel de la fonction coût

La simulation numérique est faite avec une durée de temps $T = 0.1\,s$, un pas de temps de $\Delta t = 0.001\,s$ et un nombre d'itérations en temps $N = 100$. La valeur finale de la fonction coût est inférieure à $4.5.10^{-10}$. De plus la simulation a été effectuée pour différents pas de temps et la valeur finale de la fonction coût reste inférieure à 8.10^{-10}, voir la figure 4.

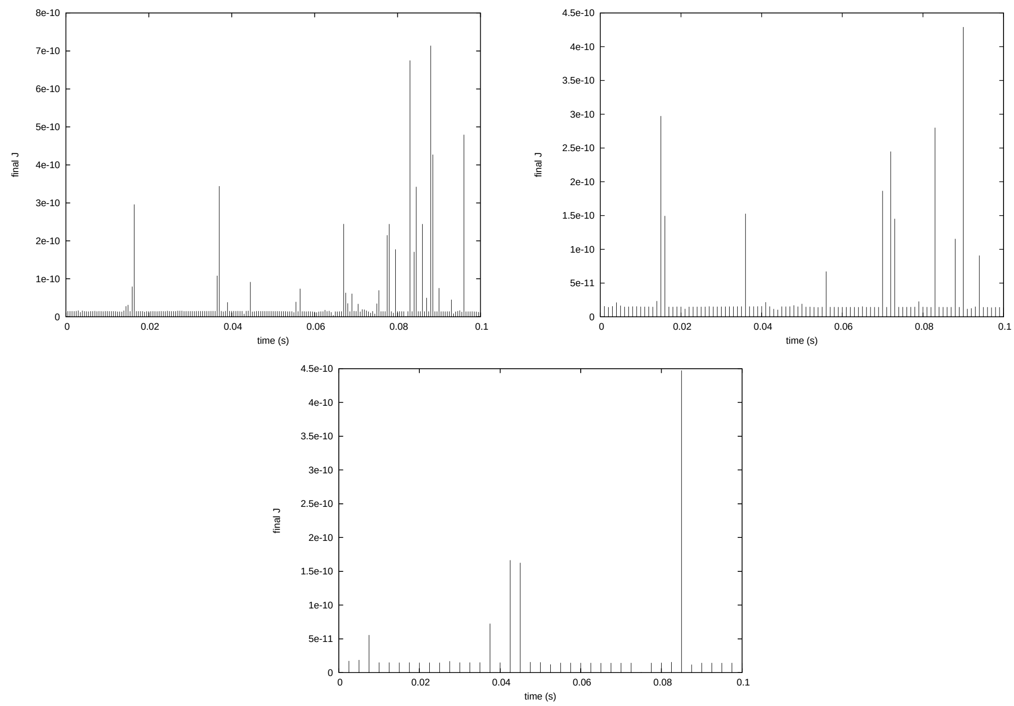

Figure 4: Les valeurs finales de la fonction coût obtenues par la méthode de BFGS pour $\Delta t = 0.0005$ (en haut à gauche), $\Delta t = 0.001$ (en haut à droit), $\Delta t = 0.0025$ (en bas).

L'algorithme de BFGS, pour le problème d'optimisation utilise le critère d'arrêt $\|\nabla J\| < \epsilon$, ou bien quand le nombre d'itérations atteint une valeur maximale *nbiter*. On a pris $\epsilon = 10^{-4}$ et *nbiter* $= 10$. Pour la recherche en ligne, le nombre maximal d'itérations est supposé égal à 5. A chaque pas de temps, BFGS effectue en moyenne 6.08 itérations et à chaque itération de BFGS, 2.6 évaluations de la fonction coût sont nécessaires en moyenne pour la recherche en ligne et un appel du gradient. Ce dernier est approché ici par le schéma de différences finies suivant

$$\frac{\partial J}{\partial \alpha_k}(\boldsymbol{\alpha}) \approx \frac{J(\boldsymbol{\alpha} + \Delta\alpha_k \mathbf{e_k}) - J(\boldsymbol{\alpha})}{\Delta\alpha_k}, \quad \text{où } \Delta\alpha_k = 10^{-6}.$$

Ainsi $m+1 = 4$ appels de la fonction coût sont indispensables pour le calcul du gradient.

Comportement des solutions

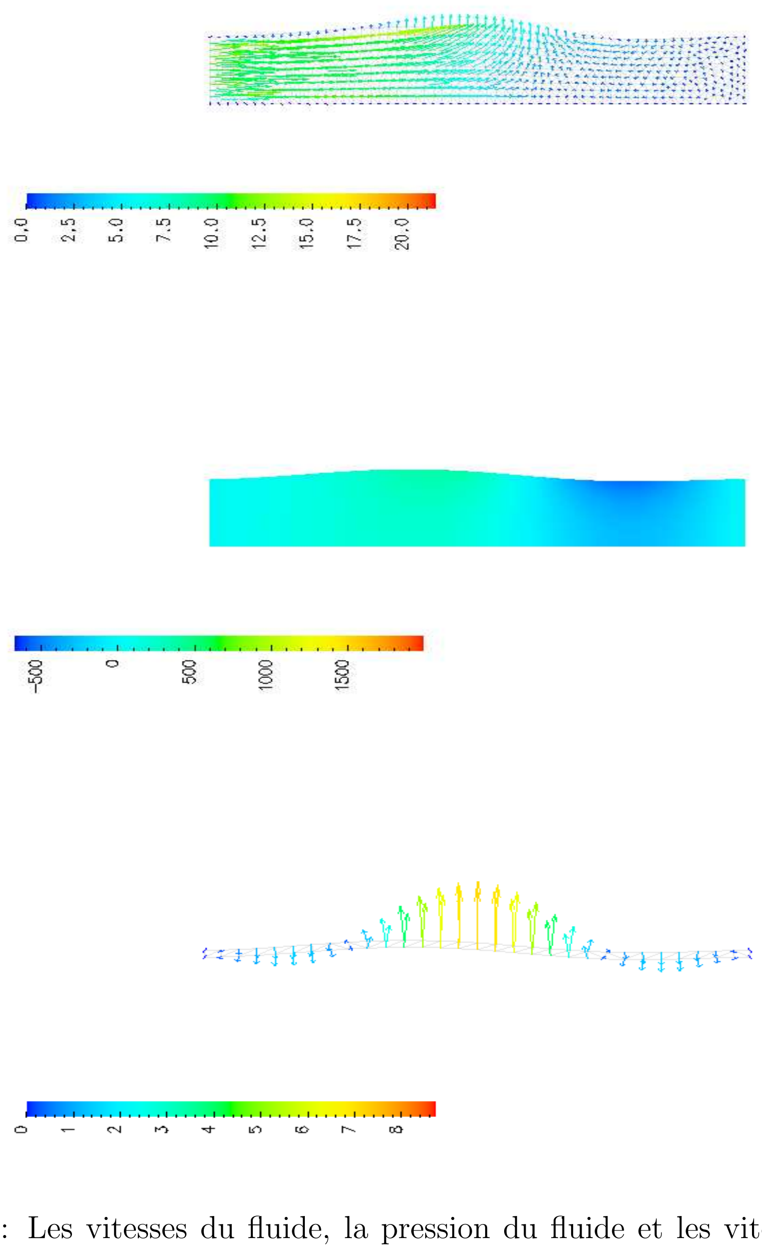

Figure 5: Les vitesses du fluide, la pression du fluide et les vitesses de la structure à l'instant $t = 0.035$.

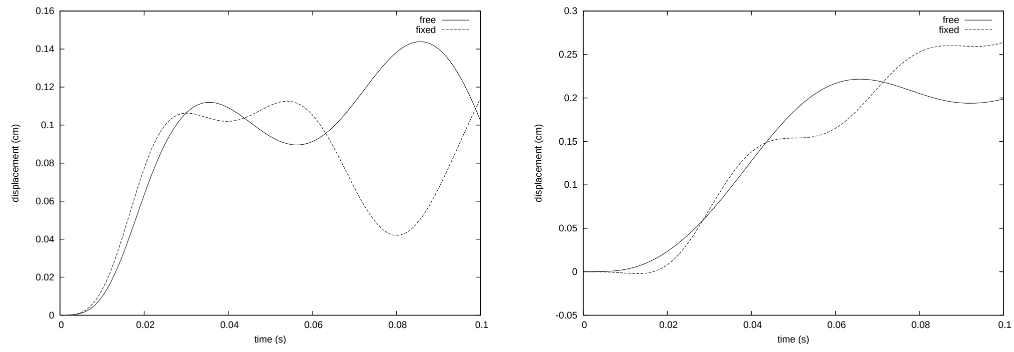

Figure 6: Déplacements verticaux aux points $x_1 = L/4$ (en haut à gauche), $x_2 = L/2$ (en haut à droite) de l'interface, quand l'extrémité gauche de la structure est libre ou fixée.

Temps CPU

La simulation dure 6 minutes et 14 secondes sur un ordinateur avec deux processeurs de 3.6 GHz de fréquence pour $\Delta t = 0.001\, s$ et $N = 100$. Une comparaison de performance entre cet algorithme et l'algorithme implicite (qui diffère de l'algorithme semi-implicite, par le calcul de la fonction coût) est réalisée (voir chapitre 1, pour plus de détails). On montre que l'algorithme semi-implicite est **11.34** fois plus rapide. La simulation a été faite d'abord pour un maillage de 1632 sommets et 3052 triangles et le temps CPU est 13 minutes 53 secondes pour le semi-implicite et 173 minutes 52 secondes pour l'implicite. Ensuite pour un nombre de modes propres fixés à $m = 7$, avec un maillage de 1250 triangles et 696 sommets, le temps CPU pour le semi-implicite est 14 minutes 30 secondes et le rapport des CPU entre le semi-implicite et l'implicite est **13.31**.

Cas d'un modèle non linéaire pour la structure

La simulation est faite avec un maillage similaire à celui du cas linéaire. Le problème de la structure est résolu par la méthode de Newton à chaque appel de la fonction coût. Le temps CPU est 17 minutes 13 secondes pour $\Delta t = 0.001\, s$ et $N = 100$ sur une machine de fréquence 306 GHz. Dans ce cas, l'algorithme semi-implicite est **5.94** fois plus rapide que l'implicite.
La figure 7 montre une similarité entre les déplacements verticaux en deux différents points de l'interface calculés par les algorithmes semi-implicite et implicite. La simulation a été effectuée quand les contraintes à l'entrée sont multipliées par 3. Le déplacement maximal de la structure est alors environ $0.6\, cm$. La figure 8 donne le comportement des vitesses du fluide.

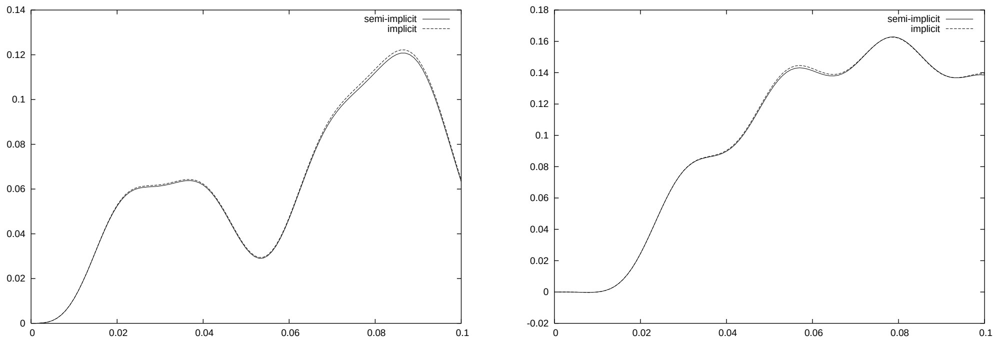

Figure 7: Déplacements verticaux aux points de coordonnées $x_1 = L/4$ (à gauche), $x_2 = L/2$ (à droite) de l'interface obtenus par les algorithmes semi-implicite et implicite.

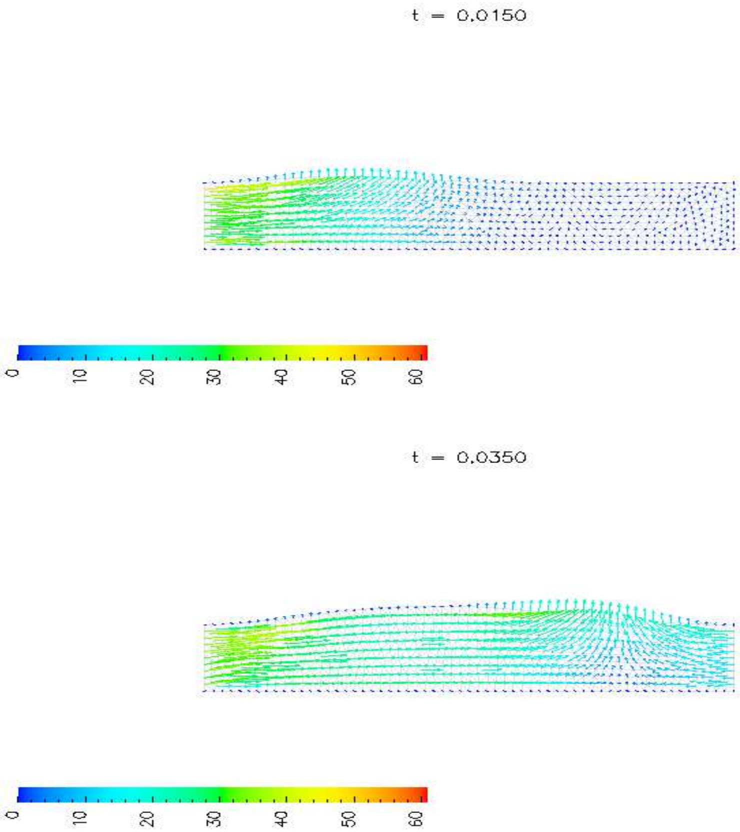

Figure 8: Vitesses du fluide à l'instant $t = 0.015\,s$ (en haut) et à $t = 0.035\,s$ (en bas).

Synthèse du chapitre II

Nous proposons dans cette section un algorithme semi-implicite procédures partagées pour résoudre le problème d'interaction fluide structure avec des petits déplacements de la structure et nous prouvons la stabilité inconditionnelle en temps de l'algorithme via les estimations d'énergie. L'algorithme est basé sur un calcul explicite de la position de l'interface à partir de la vitesse du domaine fluide à l'instant précédent et sur une résolution d'un problème d'optimisation par l'algorithme de BFGS pour identifier les contraintes à l'interface. La condition de continuité des vitesses est imposée comme condition au bord à l'interface, dans le problème fluide. L'algorithme utilise un maillage fluide fixe et une seule factorisation de la matrice fluide durant les itérations de BFGS. Un calcul des temps CPU pour différents paramètres a été effectué pour montrer la rapidité de cet algorithme par rapport à l'algorithme implicite équivalent. Ici, contrairement au premier chapitre, le domaine de calcul pour le fluide est le domaine connu Ω_n^F.

Discrétisation en temps et formulation faible des équations

On suppose que l'interaction fluide structure est gouvernée par les systèmes (9) - (14) et (15) -(21), couplés à l'interface par les conditions (23) et (24).

Les équations du fluide (9) - (14) sont discrétisées en temps à l'aide d'un schéma d'Euler implicite pour la dérivée en temps et une linéarisation du terme de convection. Les équations de la structure (15) -(21) sont traitées avec un θ-schéma d'ordre deux en temps.
On note $N \in \mathbb{N}^*$ le nombre de pas de temps, $\Delta t = T/N$ le pas de temps et $t_n = n\Delta t$ pour $n = 0, \dots, N$, les points de la subdivision de $[0, T]$. De plus on note respectivement $\mathbf{f}^n$, $\mathbf{h}_{in}^n$, $\mathbf{h}_{out}^n$, $\mathbf{g}^n$ $\mathbf{v}^n$ et $\mathbf{u}^n$ les approximations de $\mathbf{f}^F(n\Delta t)$, $\mathbf{h}_{in}(n\Delta t)$, $\mathbf{h}_{out}(n\Delta t)$, $\mathbf{f}^S(n\Delta t)$, $\mathbf{v}(n\Delta t)$ et de $\mathbf{u}(n\Delta t)$.

L'application discrète ALE est construite comme suit, on pose $\widehat{\Omega}^F = \Omega_n^F$ le domaine référence du fluide et on définit $\boldsymbol{\vartheta}^n = (\vartheta_1^n, \vartheta_2^n)^T$ la vitesse du domaine fluide comme solution de

$$\left\{\begin{array}{lcll} \Delta_{\widehat{\mathbf{x}}} \boldsymbol{\vartheta}^n & = & 0, & \text{dans } \Omega_n^F \\ \boldsymbol{\vartheta}^n & = & 0, & \text{sur } \partial\Omega_n^F \setminus \Gamma_n \\ \boldsymbol{\vartheta}^n & = & \mathbf{v}^n, & \text{sur } \Gamma_n, \end{array}\right. \tag{44}$$

avec $\mathbf{v}^n$ la vitesse du fluide à l'instant n.
Pour tout $n = 0, \cdots, N-1$, on note $\mathcal{A}_{t_{n+1}}$ l'application définie par

$$\begin{array}{rcl} \mathcal{A}_{t_{n+1}}(\widehat{x}_1, \widehat{x}_2) : \overline{\Omega}_n^F & \longrightarrow & \mathbb{R}^2 \\ (\widehat{x}_1, \widehat{x}_2) & \mapsto & (\widehat{x}_1 + \Delta t \vartheta_1^n, \widehat{x}_2 + \Delta t \vartheta_2^n). \end{array}$$

On pose
$$\Omega^F_{n+1} = \mathcal{A}_{t_{n+1}}(\Omega^F_n) \quad \text{et} \quad \Gamma_{n+1} = \mathcal{A}_{t_{n+1}}(\Gamma_n).$$
De plus on définit l'application
$$\mathbb{T} = \mathcal{A}_{t_n} \circ \mathcal{A}_{t_{n-1}} \cdots \circ \mathcal{A}_{t_1}.$$
On obtient ainsi l'interface Γ_n en fonction de l'interface initiale Γ_0 :
$$\Gamma_n = \mathbb{T}(\Gamma_0).$$
Par ailleurs, le Jacobien de $\mathcal{A}_{t_{n+1}}$ est donné par
$$1 + \Delta t(\nabla_{\widehat{\mathbf{x}}} \cdot \boldsymbol{\vartheta}^n) + (\Delta t)^2\Big(\frac{\partial \vartheta_1^n}{\partial \widehat{x}_1} \cdot \frac{\partial \vartheta_2^n}{\partial \widehat{x}_2} - \frac{\partial \vartheta_2^n}{\partial \widehat{x}_1} \cdot \frac{\partial \vartheta_1^n}{\partial \widehat{x}_2}\Big).$$
Nous introduisons maintenant les espaces des fonctions test suivants
$$\begin{array}{rcl} \widehat{W}^F_n &=& \{\widehat{\mathbf{w}}^F \in (H^1(\Omega^F_n))^2;\ \widehat{\mathbf{w}}^F = 0 \text{ sur } \Sigma_2\}, \quad \widehat{Q}^F_n = L^2(\Omega^F_n), \\ W^S &=& \{\mathbf{w}^S \in (H^1(\Omega^S))^2;\ \mathbf{w}^S = 0 \text{ sur } \Gamma_D\}. \end{array}$$
Après discrétisation en temps des équations du fluide et de la structure par les schémas cités ci-dessus, on effectue la formulation variationnelle de ces équations pour aboutir à l'algorithme suivant

On suppose qu'on connaît Ω^F_n, $\mathbf{v}^n \in (L^2(\Omega^F_n))^2$, $\mathbf{u}^{n-1}, \mathbf{u}^n \in \big(L^2(\Omega^S)\big)^2$.

Etape 1. Trouver $\boldsymbol{\vartheta}^n \in (H^1(\Omega^F_n))^2$ solution de (44).

Etape 2. Trouver $(\widehat{\mathbf{v}}^{n+1}, \widehat{p}^{n+1}, \mathbf{u}^{n+1}) \in \widehat{W}^F_n \times \widehat{Q}^F_n \times W^S;\ \widehat{\mathbf{v}}^{n+1} \circ \mathbb{T} = \dfrac{\mathbf{u}^{n+1} - \mathbf{u}^{n-1}}{2\Delta t}$ sur Γ_0, tels que
$$\begin{aligned} &\rho^F \int_{\Omega^F_n} \frac{(\widehat{\mathbf{v}}^{n+1} - \mathbf{v}^n)}{\Delta t} \cdot \widehat{\mathbf{w}}^F + \rho^F \int_{\Omega^F_n} (((\mathbf{v}^n - \boldsymbol{\vartheta}^n) \cdot \nabla_{\widehat{\mathbf{x}}})\widehat{\mathbf{v}}^{n+1}) \cdot \widehat{\mathbf{w}}^F \\ &+ \frac{\rho^F}{2} \int_{\Omega^F_n} \delta(\widehat{\mathbf{x}})\widehat{\mathbf{v}}^{n+1} \cdot \widehat{\mathbf{w}}^F + 2\mu^F \int_{\Omega^F_n} \epsilon_{\widehat{\mathbf{x}}}(\widehat{\mathbf{v}}^{n+1}) : \epsilon_{\widehat{\mathbf{x}}}(\widehat{\mathbf{w}}^F) \\ &- \int_{\Omega^F_n} \widehat{p}^{n+1}(\nabla_{\widehat{\mathbf{x}}} \cdot \widehat{\mathbf{w}}^F) - \int_{\Omega^F_n} \widehat{q}(\nabla_{\widehat{\mathbf{x}}} \cdot \widehat{\mathbf{v}}^{n+1}) \\ &+ \rho^S \int_{\Omega^S} \Big(\frac{\mathbf{u}^{n+1} - 2\mathbf{u}^n + \mathbf{u}^{n-1}}{\Delta t^2}\Big) \cdot \mathbf{w}^S + a_S(\theta \mathbf{u}^{n+1} + (1-2\theta)\mathbf{u}^n + \theta \mathbf{u}^{n-1}, \mathbf{w}^S) \\ &= \int_{\Omega^F_n} \widehat{\mathbf{f}}^{n+1} \cdot \widehat{\mathbf{w}}^F + \int_{\Omega^S} \bar{\mathbf{g}}^{n+1} \cdot \mathbf{w}^S + \int_{\Sigma_1} \mathbf{h}^{n+1}_{in} \cdot \widehat{\mathbf{w}}^F + \int_{\Sigma_3} \mathbf{h}^{n+1}_{out} \cdot \widehat{\mathbf{w}}^F, \end{aligned} \tag{45}$$

pour tous $\widehat{\mathbf{w}}^F \in \widehat{W}_n,\ \widehat{q} \in \widehat{Q}_n^F,\ \mathbf{w}^S \in W^S$ avec $\mathbf{w}^S = \widehat{\mathbf{w}}^F \circ \mathbb{T}$ sur Γ_0, où

$$\widehat{\mathbf{f}}^{n+1} = \mathbf{f}^{n+1} \circ \mathcal{A}_{t_{n+1}}, \quad \bar{\mathbf{g}}^{n+1} = \theta \mathbf{g}^{n+1} + (1-2\theta)\mathbf{g}^n + \theta \mathbf{g}^{n-1}$$

et

$$\delta(\widehat{\mathbf{x}}) = \Delta t \Big(\frac{\partial \vartheta_1^n}{\partial \widehat{x}_1} \cdot \frac{\partial \vartheta_2^n}{\partial \widehat{x}_2} - \frac{\partial \vartheta_2^n}{\partial \widehat{x}_1} \cdot \frac{\partial \vartheta_1^n}{\partial \widehat{x}_2} \Big).$$

Stabilité

Soit θ un nombre réel, on note

$$X^n = \theta a_S(\mathbf{u}^n, \mathbf{u}^n) + (1-2\theta) a_S(\mathbf{u}^n, \mathbf{u}^{n-1}) + \theta a_S(\mathbf{u}^{n-1}, \mathbf{u}^{n-1}) \tag{46}$$

et on définit la vitesse du fluide $\mathbf{v}^{n+1}$ à l'instant $n+1$ sur Ω_{n+1}^F par

$$\mathbf{v}^{n+1}(\mathbf{x}) = \widehat{\mathbf{v}}^{n+1}(\widehat{\mathbf{x}}), \quad \forall\ \forall\, \widehat{\mathbf{x}} \in \Omega_n^F,\ \text{et } \mathbf{x} = \mathcal{A}_{t_{n+1}}(\widehat{\mathbf{x}}) \in \Omega_{n+1}^F,$$

où $\widehat{\mathbf{v}}^{n+1}$ est la vitesse du fluide à l'instant $n+1$ sur $\widehat{\Omega}_n^F$.

Théorème 1 (Théorème de stabilité) *Soit Ω_n^F un domaine borné de $\mathbb{R}^2$. On suppose que $\displaystyle\int_{\Sigma_1 \cup \Sigma_3} (\mathbf{v}^n \cdot \mathbf{n}^F) |\widehat{\mathbf{v}}^{n+1}|^2 \geq 0$. Si $\theta \in \Big[\frac{1}{4}, \frac{1}{2}\Big]$, alors l'estimation*

$$\begin{aligned}
&\rho^F \|\mathbf{v}^{n+1}\|^2_{L^2(\Omega^F_{n+1})} + 2\mu^F \Delta t \|\epsilon_{\widehat{\mathbf{x}}}(\widehat{\mathbf{v}}^{n+1})\|^2_{L^2(\Omega^F_n)} + \rho^S \Big\| \frac{\mathbf{u}^{n+1} - \mathbf{u}^n}{\Delta t} \Big\|^2_{L^2(\Omega^S)} \\
&+ X^{n+1} \leq \exp(T) \Big[\rho^F \|\mathbf{v}^1\|^2_{L^2(\Omega^F_1)} + 2\mu^F \Delta t \|\epsilon_{\widehat{\mathbf{x}}}(\widehat{\mathbf{v}}^1)\|^2_{L^2(\Omega^F_0)} \\
&+ \rho^S \Big\| \frac{\mathbf{u}^1 - \mathbf{u}^0}{\Delta t} \Big\|^2_{L^2(\Omega^S)} + X^1 + C \Big(\max_{t \in [0,T]} \|\mathbf{f}^F(t)\|^2_{L^2(\Omega^F_t)} \\
&+ \max_{t \in [0,T]} \|\mathbf{f}^S(t)\|^2_{L^2(\Omega^S)} + \max_{t \in [0,T]} \|\mathbf{h}_{in}(t)\|^2_{L^2(\Sigma_1)} + \max_{t \in [0,T]} \|\mathbf{h}_{out}(t)\|^2_{L^2(\Sigma_3)} \Big) \Big]
\end{aligned}$$

est satisfaite.

Avec $C > 0$ une constante indépendante de Δt. De plus les quantités

$$\|\mathbf{v}^{n+1}\|_{L^2(\Omega^F_{n+1})}, \quad \Delta t \|\epsilon_{\widehat{\mathbf{x}}}(\widehat{\mathbf{v}}^{n+1})\|_{L^2(\Omega^F_n)}, \quad \Big\| \frac{\mathbf{u}^{n+1} - \mathbf{u}^n}{\Delta t} \Big\|_{L^2(\Omega^S)}, \ X^{n+1}$$

sont bornées.

Algorithme semi-implicite pour le problème couplé

La méthode de décomposition modale est employée pour la structure, avec un nombre fini de modes propres, noté m comme dans le problème (32). On suit les étapes suivantes pour implémenter l'algorithme précédent.

Algorithme

On suppose qu'on connaît Ω_n^F, $\mathbf{v}^n \in (L^2(\Omega_n^F))^2$, $\mathbf{u}^{n-1}, \mathbf{u}^n \in \left(L^2(\Omega^S)\right)^2$.

Etape 1. Calculer la vitesse du domaine fluide $\boldsymbol{\vartheta}^n$ à partir de (44).

Etape 2. Assembler la matrice du problème fluide donné par (45), en utilisant le maillage $\mathcal{T}^n$ obtenu à l'étape précédente. Obtenir une factorisation LU de la matrice.

Etape 3. Résoudre par BFGS le problème d'optimisation sur le maillage fixe $\mathcal{T}^n$

$$\boldsymbol{\alpha}^{n+1} \in \arg \min_{\boldsymbol{\alpha} \in \mathbb{R}^m} J(\boldsymbol{\alpha}),$$

où la fonction coût est calculée comme suit

- Soit $\sum_{i=1}^m \alpha_i \boldsymbol{\phi}^i$ les forces de contraintes à l'interface.
- Résoudre le problème de la structure avec les forces contraintes à l'interface $\sum_{i=1}^m \alpha_i \boldsymbol{\phi}^i$, pour obtenir le déplacement $\mathbf{u}$.
- Résoudre le problème fluide sur le maillage $\mathcal{T}^n$ avec condition d'égalité des vitesses à l'interface, pour obtenir la vitesse $\mathbf{v}$ et la pression p du fluide.
- Calculer
$$\beta_i = -\int_{\Gamma_0} \left(\sigma^F(\mathbf{v}, p)\, \mathbf{n}^F\right) \cdot \boldsymbol{\phi}^i(\mathbf{X})\, \omega(\mathbf{X}, t), \quad \forall\, i = 1, \ldots, m.$$
- On pose la fonction coût
$$J(\boldsymbol{\alpha}) = \frac{1}{2} \|\boldsymbol{\alpha} - \boldsymbol{\beta}\|^2_{\mathbb{R}^m}.$$

Etape 4. Construire le maillage fluide $\mathcal{T}^{n+1}$, obtenu comme image de $\mathcal{T}^n$ par l'application $\widehat{x} \mapsto \widehat{x} + \Delta t \boldsymbol{\vartheta}^n(\widehat{x})$ et sauver le maillage $\mathcal{T}^{n+1}$, la vitesse du fluide $\mathbf{v}^{n+1}(\mathbf{x}) = \widehat{\mathbf{v}}^{n+1}(\widehat{\mathbf{x}})$, etc.

Remarque 4 *Contrairement à l'algorithme implicite, où le maillage du domaine fluide change à chaque appel de la fonction coût durant le processus de minimisation, le semi-implicite utilise un maillage fluide fixe et une seule factorisation de la matrice fluide durant les itérations de BFGS. Ce qui réduit l'effort de calcul.*

Résultats numériques

On a utilisé les mêmes paramètres physiques et numériques et les mêmes maillages de référence comme dans le chapitre I, où le modèle de la structure est celui de l'élasticité linéaire. Cependant ici, on fixe $\theta = 0.3$. Le nombre des modes propres est fixé à $m = 3$ et les trois premières valeurs propres correspondantes sont $\lambda_{1,h} = 7018.91$, $\lambda_{2,h} = 50500$ et $\lambda_{3,h} = 193418$.

Maillage

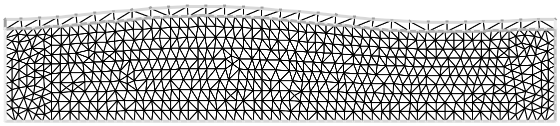

Figure 9: Les maillages fluide et structure à l'instant $t = 0.035$.

Critère d'arrêt de BFGS et nombre d'appel de la fonction coût

Le critère d'arrêt utilisé par BFGS est $\|\nabla J\| \leq \epsilon$ ou quand le nombre itérations atteint une valeur maximale *nbiter*. La simulation est faite avec $\epsilon = 10^{-4}$ et $nbiter = 10$. La valeur finale de la fonction coût est inférieure à 6.10^{-12}. En d'autres termes, la continuité des vitesses est vérifiée à chaque pas de temps et l'erreur entre les valeurs des forces de contraintes est inférieure à 6.10^{-12}. Donc $\|\Delta q_i^{n+1}\|$ est inférieur à 10^{-13}. Le gradient de la fonction est aussi approché par différences finies.

Comportements des solutions

La simulation est effectuée avec une durée de temps $T = 0.1\,s$, un pas de temps $\Delta t = 0.001\,s$ et un nombre d'itérations $N = 100$. Dans la figure 10, on compare les solutions calculées par l'algorithme semi-implicite et celles calculées par l'implicite. A la figure 11, on montre que la stabilité de l'algorithme ne dépend pas du pas de temps et la figure 12 donne le comportement des vitesses et de la pression du fluide à $t = 0.035\,s$.

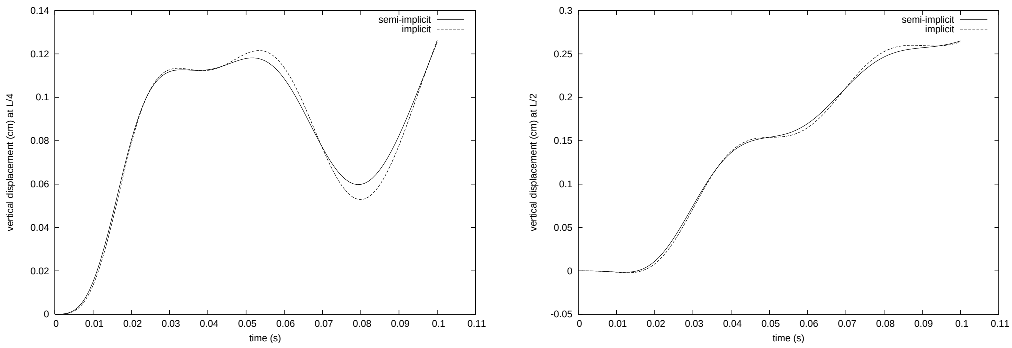

Figure 10: Déplacements verticaux pour $\Delta t = 0.001s$ aux points $x_1 = L/4$, (à gauche) $x_2 = L/2$, (à droite) de l'interface, pour les algorithmes semi-implicite et implicite.

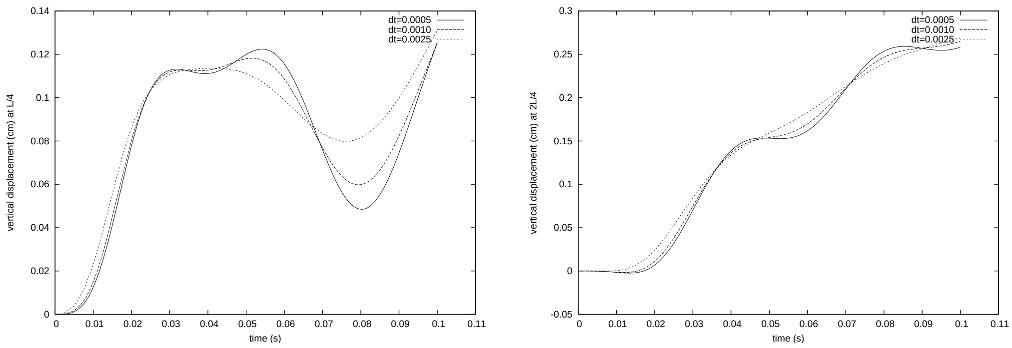

Figure 11: Déplacements verticaux pour $\Delta t = 0.001s$, $\Delta t = 0.0005s$, $\Delta t = 0.0025s$ aux points $x_1 = L/4$ (à gauche), $x_1 = L/2$ (à droit) de l'interface dans le cas de l'algorithme semi-implicite.

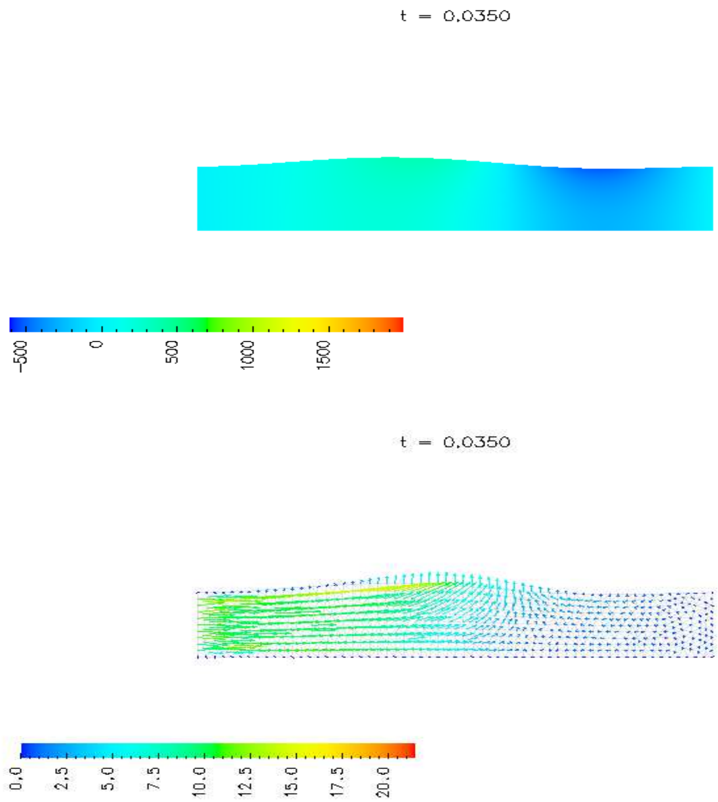

Figure 12: La pression $[\frac{dynes}{cm^2}]$ et les vitesses du fluide $[cm/s]$ à l'instant $t = 0.035$.

Temps CPU

Les calculs numériques sont faits sur un ordinateur avec un processeur de 1.66 GHz de fréquence et de 2 Gb de RAM. Les tableaux ci-dessous nous fournissent les rapports des temps CPU entre l'algorithme semi-implicite (présenté ici) et l'implicite (qui diffère du semi-implicite par le calcul de la fonction coût) pour différentes valeurs de Δt, de m et des paramètres du maillage. Nous notons nv, le nombre des sommets et nt, le nombre des triangles du maillage fluide.

1. CPU en fonction de Δt, quand $m = 3$, $nv = 696$ et $nt = 1250$

Δt	N	CPU-semi-implicite	CPU-implicite	$\frac{\text{CPU-implicite}}{\text{CPU-semi-implicite}}$
0.0005	200	14 mn 48 s	187 mn 47 s	12.95
0.0010	100	8 mn 30 s	92 mn 30 s	11.12
0.0025	40	3 mn 27 s	36 mn 24 s	11.08

2. CPU en fonction de m, quand $\Delta t = 0.001\,s$, $N = 100$, $nv = 696$ et $nt = 1250$

m	CPU-semi-implicite	CPU-implicite	$\frac{\text{CPU-implicite}}{\text{CPU-semi-implicite}}$
3	8 mn 30 s	92 mn 30 s	11.12
7	21 mn 44 s	227 mn 53 s	10.62
10	29 mn 54 s	304 mn 22 s	10.30

3. CPU en fonction du pas du maillage, quand $\Delta t = 0.001\,s$, $N = 100$ et $m = 3$.

nv	nt	h	CPU-semi-implicite	CPU-implicite	$\frac{\text{CPU-implicite}}{\text{CPU-semi-implicite}}$
696	1250	0.16	8 mn 30 s	92 mn 30 s	11.12
1632	3052	0.11	19mn 48 s	226 mn 42 s	11.62
2664	5046	0.08	33 mn 50 s	415 mn 23 s	12.39

Synthèse du chapitre III

Nous présentons dans cette section un algorithme semi-implicite monolithique pour les problèmes d'interaction fluide structure, avec des petits déplacements de la structure. L'algorithme utilise un maillage global pour le domaine fluide structure, obtenu comme union des maillages fluide et structure, choisis compatibles à l'interface. Le problème de la structure est reformulé en cadre Eulérien et une pression définie sur le domaine global a été introduite. Un seul champ de vitesses a été aussi introduit, afin de satisfaire de manière automatique la condition de continuité des vitesses à l'interface. La condition d'égalité des contraintes à l'interface est éliminée à partir de la formulation faible du problème fluide structure. Un système linéaire monolithique d'inconnues vitesse et pression est par conséquent résolu par l'algorithme de GMRES. L'utilisation des fonctions caractéristiques fluide et structure nous a permis de choisir de manière indépendante les schémas discrets pour les équations du fluide et de la structure.

On suppose dans cette partie que l'interaction fluide structure est modélisée par les systèmes (9) - (14) et (15) - (21), couplés à l'interface par (23), (24).
Sans risque de confusion nous adoptons les notations suivantes. Nous notons ∇ l'opérateur gradient par rapport aux coordonnées Lagrangiennes $\mathbf{X}$ ou Eulériennes $\mathbf{x}$. On utilise la même convention pour les opérateurs divergence et laplacien.

Discrétisation en temps des équations

La discrétisation en temps des équations du fluide (9) - (14) est basée sur un schéma d'Euler implicite et une linéarisation du terme de convection. Celle des équations de la structure (15) - (21) est faite à l'aide d'un schéma de Newmark d'ordre deux en temps. Nous notons N le nombre de pas de temps, Δt le pas de temps et $t_n = n\Delta t$ les points de la subdivision de l'intervalle $[0, T]$.
Pour la structure, nous notons respectivement $\mathbf{u}^{S,n}$, $\dot{\mathbf{u}}^{S,n}$, $\ddot{\mathbf{u}}^{S,n}$, $\mathbf{f}^{S,n+1}$ les approximations de $\mathbf{u}^S(t_n)$, $\dfrac{\partial \mathbf{u}^S}{\partial t}(t_n)$, $\dfrac{\partial^2 \mathbf{u}^S}{\partial t^2}(t_n)$, $\mathbf{f}^S(t_{n+1})$ et pour le fluide, on note respectivement $\mathbf{f}^{F,n}$, $\mathbf{h}^n_{in}$, $\mathbf{h}^n_{out}$, $\mathbf{v}^{F,n}$, $p^{F,n}$ les approximations de $\mathbf{f}^F(t_n)$, $\mathbf{h}_{in}(t_n)$, $\mathbf{h}_{out}(t_n)$, $\mathbf{v}^F(t_n)$, $p^F(t_n)$.

La vitesse du domaine fluide $\boldsymbol{\vartheta}^n = (\vartheta^n_1, \vartheta^n_2)^T$ est obtenue de la même façon que dans le chapitre II. On introduit ensuite les vitesses du fluide $\widehat{\mathbf{v}}^{F,n+1} : \Omega^F_n \to \mathbb{R}^2$ (respectivement la pression du fluide $\widehat{p}^{F,n+1} : \Omega^F_n \to \mathbb{R}$) à l'instant $n+1$ sur Ω^F_n comme suit

$$\begin{aligned}
&\widehat{\mathbf{v}}^{F,n+1}(\widehat{\mathbf{x}}) = \mathbf{v}^{F,n+1}(\mathbf{x}), \text{ et } \widehat{p}^{F,n+1}(\widehat{\mathbf{x}}) = p^{F,n+1}(\mathbf{x}), \\
&\forall\, \widehat{\mathbf{x}} \in \Omega^F_n,\ \mathbf{x} = \mathcal{A}_{t_{n+1}}(\widehat{\mathbf{x}}) \in \Omega^F_{n+1}.
\end{aligned}$$

où $\mathbf{v}^{F,n+1}$ et $p^{F,n+1}$ sont les vitesses et la pression du fluide à l'instant $n+1$ sur Ω^F_{n+1}.

Le système discret correspondant à (9)-(24) est donné par

Equations discrètes du fluide

Trouver $\widehat{\mathbf{v}}^{F,n+1} : \Omega_n^F \to \mathbb{R}^2$ et $\widehat{p}^{F,n+1} : \Omega_n^F \to \mathbb{R}$ tel que

$$\begin{aligned}
&\rho^F \left(\frac{\widehat{\mathbf{v}}^{F,n+1} - \mathbf{v}^{F,n}}{\Delta t} + \left(\left(\mathbf{v}^{F,n} - \boldsymbol{\vartheta}^n \right) \cdot \nabla \right) \widehat{\mathbf{v}}^{F,n+1} \right) \\
&-2\mu^F \nabla \cdot \epsilon \left(\widehat{\mathbf{v}}^{F,n+1} \right) + \nabla \widehat{p}^{F,n+1} = \widehat{\mathbf{f}}^{F,n+1}, \text{ dans } \Omega_n^F && (47) \\
&\nabla \cdot \widehat{\mathbf{v}}^{F,n+1} = 0, \text{ dans } \Omega_n^F && (48) \\
&\sigma^F(\widehat{\mathbf{v}}^{F,n+1}, \widehat{p}^{F,n+1}) \cdot \mathbf{n}^F = \mathbf{h}_{in}^{n+1}, \text{ sur } \Sigma_1 && (49) \\
&\sigma^F(\widehat{\mathbf{v}}^{F,n+1}, \widehat{p}^{F,n+1}) \cdot \mathbf{n}^F = \mathbf{h}_{out}^{n+1}, \text{ sur } \Sigma_3 && (50) \\
&\widehat{\mathbf{v}}^{F,n+1} = 0, \text{ sur } \Sigma_2 && (51) \\
&\mathbf{v}^F(\mathbf{X}, 0) = \mathbf{v}^0(\mathbf{X}), \text{ dans } \Omega_0^F. && (52)
\end{aligned}$$

Equations discrètes de la structure

Trouver $\mathbf{u}^{S,n+1}$, $\dot{\mathbf{u}}^{S,n+1}$, $\ddot{\mathbf{u}}^{S,n+1} : \Omega_0^S \to \mathbb{R}^2$ tel que

$$\begin{aligned}
&\rho^S \ddot{\mathbf{u}}^{S,n+1} - \nabla \cdot \sigma^S(\mathbf{u}^{S,n+1}) = \mathbf{f}^{S,n+1}, \quad \text{dans } \Omega_0^S && (53) \\
&\mathbf{u}^{S,n+1} = 0, \quad \text{sur } \Gamma_D && (54) \\
&\sigma^S(\mathbf{u}^{S,n+1})\mathbf{n}^S = 0, \quad \text{sur } \Gamma_N && (55) \\
&\mathbf{u}^S(\mathbf{X}, 0) = \mathbf{u}^0(\mathbf{X}), \quad \text{dans } \Omega_0^S && (56)
\end{aligned}$$

$$\begin{aligned}
\dot{\mathbf{u}}^{S,n+1} &= \dot{\mathbf{u}}^{S,n} + \Delta t \Big[(1-\delta) \ddot{\mathbf{u}}^{S,n} + \delta \ddot{\mathbf{u}}^{S,n+1} \Big] && (57) \\
\mathbf{u}^{S,n+1} &= \mathbf{u}^n + \Delta t \dot{\mathbf{u}}^{S,n} \\
&\quad + (\Delta t)^2 \Big[\Big(\frac{1}{2} - \theta \Big) \ddot{\mathbf{u}}^{S,n} + \theta \ddot{\mathbf{u}}^{n+1} \Big]. && (58)
\end{aligned}$$

Pour $\delta = \dfrac{1}{2}$, le schéma de Newmark est d'ordre deux en temps.

Conditions de continuité des vitesses à l'interface

$$\widehat{\mathbf{v}}^{F,n+1} \circ \mathbb{T} = \dot{\mathbf{u}}^{S,n+1}, \quad \text{sur } \Gamma_0 \times (0, T] \tag{59}$$

Condition d'égalité des contraintes à l'interface

$$(\sigma^F(\widehat{\mathbf{v}}^{F,n+1}, \widehat{p}^{F,n+1})\mathbf{n}^F) \circ \mathbb{T} = -\sigma^S(\mathbf{u}^{S,n+1})\mathbf{n}^S, \quad \text{sur } \Gamma_0 \times (0, T]. \tag{60}$$

Formulation variationnelle des problèmes

On introduit les espaces des fonctions test pour le fluide

$$\widehat{W}_n^F = \left\{ \widehat{\mathbf{w}}^F \in (H^1(\Omega_n^F))^2;\ \ \widehat{\mathbf{w}}^F = 0 \ \text{ sur } \ \Sigma_2 \right\}, \quad \widehat{Q}_n^F = L^2(\Omega_n^F).$$

On montre aisément que la formulation faible correspondante au système discret fluide (47) - (52) est donnée par

Trouver $\widehat{\mathbf{v}}^{F,n+1} \in \widehat{W}_n^F$ et $\widehat{p}^{F,n+1} \in \widehat{Q}_n^F$ tel que

$$\begin{aligned}
&\int_{\Omega_n^F} \rho^F \frac{\widehat{\mathbf{v}}^{F,n+1}}{\Delta t} \cdot \widehat{\mathbf{w}}^F + \int_{\Omega_n^F} \rho^F \left(\left(\left(\mathbf{v}^{F,n} - \boldsymbol{\vartheta}^n \right) \cdot \nabla \right) \widehat{\mathbf{v}}^{F,n+1} \right) \cdot \widehat{\mathbf{w}}^F \\
&- \int_{\Omega_n^F} \left(\nabla \cdot \widehat{\mathbf{w}}^F \right) \widehat{p}^{F,n+1} + \int_{\Omega_n^F} 2\mu^F \epsilon \left(\widehat{\mathbf{v}}^{F,n+1} \right) : \epsilon \left(\widehat{\mathbf{w}}^F \right) \\
&- \int_{\Gamma_n} \left(\sigma^F \mathbf{n}^F \right) \cdot \widehat{\mathbf{w}}^F = \mathcal{L}_F(\widehat{\mathbf{w}}^F), \quad \forall\, \widehat{\mathbf{w}}^F \in \widehat{W}_n^F
\end{aligned} \tag{61}$$

$$\int_{\Omega_n^F} \widehat{q} (\nabla \cdot \widehat{\mathbf{v}}^{F,n+1}) = 0, \quad \forall\, \widehat{q} \in \widehat{Q}_n^F \tag{62}$$

où

$$\mathcal{L}_F(\widehat{\mathbf{w}}^F) = \int_{\Omega_n^F} \rho^F \frac{\widehat{\mathbf{v}}^{F,n}}{\Delta t} \cdot \widehat{\mathbf{w}}^F + \int_{\Omega_n^F} \widehat{\mathbf{f}}^{n+1,F} \cdot \widehat{\mathbf{w}}^F + \int_{\Sigma_1} \widehat{\mathbf{h}}_{in}^{n+1} \cdot \widehat{\mathbf{w}}^F + \int_{\Sigma_3} \widehat{\mathbf{h}}_{out}^{n+1} \cdot \widehat{\mathbf{w}}^F.$$

On introduit ensuite pour la structure, l'espace des fonctions test suivant

$$W^S = \left\{ \mathbf{w}^S \in (H^1(\Omega_0^S))^2;\ \ \mathbf{w}^S = 0 \ \text{ sur } \Gamma_D \right\}.$$

En se servant des identités (57) et (58), on peut exprimer le système (53) - (56) en fonction seulement de la vitesse $\dot{\mathbf{u}}^{S,n+1}$. Après formulation faible, on aboutit à

Trouver $\dot{\mathbf{u}}^{S,n+1} \in W^S$ tel que

$$\begin{aligned}
&\int_{\Omega_0^S} \frac{2\rho^S}{\Delta t} \dot{\mathbf{u}}^{S,n+1} \cdot \mathbf{w}^S + 2\theta \Delta t a_S(\dot{\mathbf{u}}^{S,n+1}, \mathbf{w}^S) \\
&- \int_{\Gamma_0} (\sigma^S \mathbf{n}^S) \cdot \mathbf{w}^S = \mathcal{L}_S(\mathbf{w}^S), \quad \forall \mathbf{w}^S \in W^S,
\end{aligned} \tag{63}$$

où

$$a_S(\mathbf{u}, \mathbf{w}) = \int_{\Omega_0^S} \left[\lambda^S (\nabla \cdot \mathbf{u})(\nabla \cdot \mathbf{w}) + 2\mu^S \epsilon(\mathbf{u}) : \epsilon(\mathbf{w}) \right]$$

et

$$\begin{aligned}
\mathcal{L}_S(\mathbf{w}^S) = &\int_{\Omega_0^S} f^S \cdot \mathbf{w}^S + \int_{\Omega_0^S} \frac{2\rho^S}{\Delta t} \dot{\mathbf{u}}^{S,n} \cdot \mathbf{w}^S + \int_{\Omega_0^S} \rho^S \ddot{\mathbf{u}}^{S,n} \cdot \mathbf{w}^S - a_S(\mathbf{u}^{S,n}, \mathbf{w}^S) \\
&- \Delta t (1 - 2\theta) a_S(\dot{\mathbf{u}}^{S,n}, \mathbf{w}^S) - (\Delta t)^2 \Big(\frac{1}{2} - 2\theta \Big) a_S(\ddot{\mathbf{u}}^{S,n}, \mathbf{w}^S).
\end{aligned}$$

Formulation monolithique

Dans cette sous-section, l'objectif est de mettre le système (61) - (63) sous une forme monolithique en vitesse et pression. Pour cela nous avons besoin d'introduire un domaine global fluide structure, un seul champ de vitesse pour le fluide et la structure, une pression définie sur le domaine global et enfin une vitesse du domaine global.
En se référant à la Figure 1, on note $\Omega_0 = \Omega_0^F \cup \Omega_0^S \cup \Gamma_0$ le domaine initial fluide structure et le domaine global à l'instant t sera noté $\Omega_t = \Omega_t^F \cup \Omega_t^S \cup \Gamma_t$. Nous avons ajouté l'interface Γ_0 pour obtenir un domaine connexe.
Nous notons respectivement la vitesse, le déplacement et l'accélération fluide structure $\mathbf{v} = (v_1, v_2)^T : \Omega_t \to \mathbb{R}^2$, $\mathbf{u} = (u_1, u_2)^T : \Omega_t \to \mathbb{R}^2$ et $\ddot{\mathbf{u}} = (\ddot{u}_1, \ddot{u}_2)^T : \Omega_t \to \mathbb{R}^2$. De plus on note leurs approximations en $t_n = n\Delta t$

$$\mathbf{v}^n : \Omega_n \to \mathbb{R}^2, \quad \mathbf{u}^n : \Omega_n \to \mathbb{R}^2, \quad \ddot{\mathbf{u}}^n : \Omega_n \to \mathbb{R}^2.$$

Nous introduisons ensuite les fonctions caractéristiques $\chi_{\Omega_t^F} : \overline{\Omega}_t \to \mathbb{R}$ relative au domaine fluide et $\chi_{\Omega_t^S} : \overline{\Omega}_t \to \mathbb{R}$ relative au domaine structure comme suit

$$\chi_{\Omega_t^S} = \begin{cases} 1, \text{ sur } \overline{\Omega}_t^S \\ 0, \text{ ailleurs} \end{cases} \qquad \text{et} \qquad \chi_{\Omega_t^F} = 1 - \chi_{\Omega_t^S}. \tag{64}$$

La vitesse $\tilde{\boldsymbol{\vartheta}}^n = (\tilde{\vartheta}_1^n, \tilde{\vartheta}_2^n)$ du domaine global fluide structure est définie comme extension de la vitesse du domaine fluide au domaine Ω_n, par

$$\begin{cases} -\triangle \tilde{\boldsymbol{\vartheta}}^n &= 0, \quad \text{dans } \Omega_n \\ \tilde{\boldsymbol{\vartheta}}^n &= 0 \quad \text{sur } \partial\Omega_n \\ \tilde{\boldsymbol{\vartheta}}^n &= \mathbf{v}^n, \quad \text{sur } \Gamma_n. \end{cases} \tag{65}$$

Remarque 5 *Le problème (65) est bien posé, car Γ_n est une courbe qui sépare Ω_n^F et Ω_n^S.*

Nous introduisons la pression globale fluide structure $p : \Omega_t \longrightarrow \mathbb{R}$, qui coïncide avec la pression du fluide p^F sur le domaine fluide Ω_t^F. La valeur de p sur le domaine de la structure Ω_t^S n'a pas de signification physique. Nous retournerons plus tard sur ce point. On note $\widehat{p}^{n+1}$ l'approximation en temps de p sur Ω_n au point $t_{n+1} = (n+1)\Delta t$.

Pour obtenir la formulation faible du système monolithique, nous définissons les espaces des fonctions test vitesses et pression suivants

$$\widehat{W}_n = \left\{ \widehat{\mathbf{w}} \in (H^1(\Omega_n))^2; \quad \widehat{\mathbf{w}} = 0 \text{ sur } \Gamma_D \cup \Sigma_2 \right\}, \quad \widehat{Q}_n = L^2(\Omega_n).$$

Remarque 6 *1. L'utilisation d'un seul champ de vitesse permet de vérifier automatiquement la condition (59).*

2. A partir de (60), nous avons

$$\int_{\Gamma_n} (\sigma^S \mathbf{n}^S) \cdot \widehat{\mathbf{w}} + \int_{\Gamma_n} \left(\sigma^F \mathbf{n}^F\right) \cdot \widehat{\mathbf{w}} = 0, \quad \forall \widehat{\mathbf{w}} \in \widehat{W}_n. \tag{66}$$

Si on réécrit les intégrales (61), (62) et (63) sur Ω_n, en utilisant les fonctions caractéristiques définies dans (64) et l'identité (66), nous obtenons la formulation faible monolithique fluide structure suivante

Trouver $(\widehat{\mathbf{v}}^{n+1}, \widehat{p}^{n+1}) \in \widehat{W}_n \times \widehat{Q}_n$ telles que

$$\begin{aligned}
&\int_{\Omega_n} \chi_{\Omega_n^F}\, \rho^F \frac{\widehat{\mathbf{v}}^{n+1}}{\Delta t} \cdot \widehat{\mathbf{w}} + \int_{\Omega_n} \chi_{\Omega_n^F}\, \rho^F \left(\left(\left(\mathbf{v}^n - \tilde{\boldsymbol{\vartheta}}^n \right) \cdot \nabla \right) \widehat{\mathbf{v}}^{n+1} \right) \cdot \widehat{\mathbf{w}} \\
&- \int_{\Omega_n} \chi_{\Omega_n^F} \left(\nabla \cdot \widehat{\mathbf{w}} \right) \widehat{p}^{n+1} + \int_{\Omega_n} \chi_{\Omega_n^F}\, 2\mu^F \epsilon \left(\widehat{\mathbf{v}}^{n+1} \right) : \epsilon \left(\widehat{\mathbf{w}} \right) \\
&+ \int_{\Omega_n} \chi_{\Omega_n^S} \frac{2\rho^S}{\Delta t} \widehat{\mathbf{v}}^{n+1} \cdot \widehat{\mathbf{w}} + 2\theta \Delta t \tilde{a}_S(\widehat{\mathbf{v}}^{n+1}, \widehat{\mathbf{w}}) \\
&= \mathcal{L}_F(\widehat{\mathbf{w}}) + \tilde{\mathcal{L}}_S(\widehat{\mathbf{w}}), \quad \forall\, \widehat{\mathbf{w}} \in \widehat{W}_n
\end{aligned} \tag{67}$$

$$\int_{\Omega_n} \chi_{\Omega_n^F}\, \widehat{q}(\nabla \cdot \widehat{\mathbf{v}}^{n+1}) = 0, \quad \forall\, \widehat{q} \in \widehat{Q}_n. \tag{68}$$

où

$$\mathcal{L}_F(\widehat{\mathbf{w}}) = \int_{\Omega_n} \chi_{\Omega_n^F} \rho^F \frac{\widehat{\mathbf{v}}^n}{\Delta t} \cdot \widehat{\mathbf{w}} + \int_{\Omega_n} \chi_{\Omega_n^F} \widehat{\mathbf{f}}^{n+1,F} \cdot \widehat{\mathbf{w}} + \int_{\Sigma_1} \widehat{\mathbf{h}}_{in}^{n+1} \cdot \widehat{\mathbf{w}} + \int_{\Sigma_3} \widehat{\mathbf{h}}_{out}^{n+1} \cdot \widehat{\mathbf{w}},$$

$$\tilde{a}_S(\mathbf{u}, \mathbf{w}) = \int_{\Omega_n} \chi_{\Omega_n^S} \Big[\lambda^S (\nabla \cdot \mathbf{u})(\nabla \cdot \mathbf{w}) + 2\mu^S \epsilon(\mathbf{u}) : \epsilon(\mathbf{w}) \Big]$$

et

$$\begin{aligned}
\tilde{\mathcal{L}}_S(\widehat{\mathbf{w}}) = &\int_{\Omega_n} \chi_{\Omega_n^S} f^S \cdot \widehat{\mathbf{w}} + \int_{\Omega_n} \chi_{\Omega_n} \frac{2\rho^S}{\Delta t} \mathbf{v}^n \cdot \widehat{\mathbf{w}} + \int_{\Omega_n} \chi_{\Omega_n^S} \rho^S \ddot{\mathbf{u}}^n \cdot \widehat{\mathbf{w}} \\
&- \tilde{a}_S(\mathbf{u}^n, \widehat{\mathbf{w}}) - \Delta t(1 - 2\theta) \tilde{a}_S(\mathbf{v}^n, \widehat{\mathbf{w}}) - (\Delta t)^2 \Big(\frac{1}{2} - 2\theta \Big) \tilde{a}_S(\ddot{\mathbf{u}}^n, \widehat{\mathbf{w}}).
\end{aligned}$$

Le système (67) et (68) peut se mettre sous la forme matricielle suivante

$$\begin{bmatrix} A & B^T & 0 \\ B & 0 & 0 \\ 0 & 0 & 0 \end{bmatrix} \begin{bmatrix} \mathbf{v} \\ p^F \\ p^S \end{bmatrix} = \begin{bmatrix} \mathcal{L} \\ 0 \\ 0 \end{bmatrix}, \tag{69}$$

où $\mathbf{v}$ est la vitesse globale, p^F la pression du fluide et p^S la pression de la structure. On note $\mathcal{L} = \tilde{\mathcal{L}}_F(\phi_i) + \tilde{\mathcal{L}}_S(\phi_i)$, avec ϕ_i et π_i les fonctions de base éléments finis pour la vitesse et la pression. Les matrices ci-dessus sont données par

$$A_{i,j} = \int_{\Omega_n} \chi_{\Omega_n^F} \rho^F \frac{\phi_j}{\Delta t} \cdot \phi_i + \int_{\Omega_n} \chi_{\Omega_n^F} \rho^F \left(\left(\left(\mathbf{v}^n - \tilde{\boldsymbol{\vartheta}}^n \right) \cdot \nabla \right) \phi_j \right) \cdot \phi_i$$
$$+ \int_{\Omega_n} \chi_{\Omega_n^F} 2\mu^F \epsilon(\phi_j) : \epsilon(\phi_i) + \int_{\Omega_n} \chi_{\Omega_n^S} \frac{2\rho^S}{\Delta t} \phi_j \cdot \phi_i + 2\theta \Delta t \, \tilde{a}_S(\phi_j, \phi_i)$$

et

$$B_{i,j} = -\int_{\Omega_n} \chi_{\Omega_n^F} \left(\nabla \cdot \phi_j \right) \pi_i,$$

On peut constater que le système (69) admet plusieurs solutions. Ceci est dû au fait que la pression p^S de la structure peut prendre n'importe quelles valeurs. Pour obtenir $p^S = 0$ sur le domaine Ω_n^S nous avons ajouté le terme $\epsilon \int_{\Omega_n} \widehat{p}^{n+1} \widehat{q}$ dans la formulation faible globale ci-dessus, et la forme matricielle finale devient

$$\begin{bmatrix} A & B^T & 0 \\ B & \epsilon M^F & 0 \\ 0 & 0 & \epsilon M^S \end{bmatrix} \begin{bmatrix} \mathbf{v} \\ p^F \\ p^S \end{bmatrix} = \begin{bmatrix} \mathcal{L} \\ 0 \\ 0 \end{bmatrix}, \tag{70}$$

où $\epsilon = 10^{-6}$ $\begin{bmatrix} \epsilon M^F & 0 \\ 0 & \epsilon M^S \end{bmatrix} = \left(\epsilon \int_{\Omega_n} \pi_j \pi_i \right)_{1 \le i,j \le nv}$, $\epsilon = 10^{-6}$. et nv le nombre des sommets du maillage global.

Remark 0.1 *Si on approche la pression globale par des fonctions de type éléments finis globalement continues, on obtient une pression $p^S = 0$ sur les sommets des triangles de $\Omega_t^S \setminus \Gamma_t$ et la pression du fluide p^F sur le domaine $\Omega_t^F \cup \Gamma_t$.*

Les déplacements et accélérations à l'instant $n+1$ sur Ω_n sont obtenus à partir de (57) et (58) par

$$\widehat{\mathbf{u}}^{n+1} = \mathbf{u}^n + (\Delta t)^2 \left(\frac{1}{2} - 2\theta \right) \ddot{\mathbf{u}}^n + \Delta t (1 - 2\theta) \mathbf{v}^n + 2\theta \Delta t \, \widehat{\mathbf{v}}^{n+1} \tag{71}$$

$$\widehat{\ddot{\mathbf{u}}}^{n+1} = \frac{2}{\Delta t} \left(\widehat{\mathbf{v}}^{n+1} - \mathbf{v}^n \right) - \ddot{\mathbf{u}}^n. \tag{72}$$

Pour obtenir la vitesse $\mathbf{v}^{n+1} : \Omega_{n+1} \to \mathbb{R}^2$, le déplacement $\mathbf{u}^{n+1} : \Omega_{n+1} \to \mathbb{R}^2$ et l'accélération $\ddot{\mathbf{u}}^{n+1} : \Omega_{n+1} \to \mathbb{R}^2$ à l'instant $n+1$ sur Ω_{n+1}, on introduit l'application $\mathbb{T}_n : \overline{\Omega}_n \to \mathbb{R}^2$ définie par

$$\mathbb{T}_n(\widehat{\mathbf{x}}) = \widehat{\mathbf{x}} + \Delta t \tilde{\boldsymbol{\vartheta}}^n(\widehat{\mathbf{x}}) \chi_{\Omega_n^F}(\widehat{\mathbf{x}}) + (\widehat{\mathbf{u}}^{n+1}(\widehat{\mathbf{x}}) - \mathbf{u}^n(\widehat{\mathbf{x}})) \chi_{\Omega_n^S}(\widehat{\mathbf{x}}). \tag{73}$$

et on pose

$$\Omega_{n+1} = \mathbb{T}_n(\Omega_n), \quad \Gamma_{n+1} = \mathbb{T}_n(\Gamma_n).$$

On définit alors

$$\mathbf{v}^{n+1}(\mathbf{x}) = \widehat{\mathbf{v}}^{n+1}(\widehat{\mathbf{x}}), \quad p^{n+1}(\mathbf{x}) = \widehat{p}^{n+1}(\widehat{\mathbf{x}}), \quad \forall\, \widehat{\mathbf{x}} \in \Omega_n \text{ et } \mathbf{x} = \mathbb{T}_n(\widehat{\mathbf{x}})$$
$$\mathbf{u}^{n+1}(\mathbf{x}) = \widehat{\mathbf{v}}^{n+1}(\widehat{\mathbf{x}}), \quad \ddot{\mathbf{u}}^{n+1}(\mathbf{x}) = \widehat{\ddot{\mathbf{u}}}^{n+1}(\widehat{\mathbf{x}}), \quad \forall\, \widehat{\mathbf{x}} \in \Omega_n \text{ et } \mathbf{x} = \mathbb{T}_n(\widehat{\mathbf{x}}).$$

Algorithme

On suppose qu'on connaît Ω_n, $\mathbf{v}^n$, $\mathbf{u}^n$, $\ddot{\mathbf{u}}^n$.
ETape 1. Calculer $\tilde{\boldsymbol{\vartheta}}^n$ à partir de (65).

Etape 2. Résoudre (67), (68) par GMRES sur le maillage $\mathcal{T}_h^n$ de Ω_n. Pour obtenir la vitesse $\widehat{\mathbf{v}}^{n+1}$ et la pression $\widehat{p}^{n+1}$.

Etape 3. Calculer $\widehat{\mathbf{u}}^{n+1}$ à partir de (71) et $\widehat{\ddot{\mathbf{u}}}^{n+1}$ à partir de (72).

Etape 4. Construire le maillage $\mathcal{T}_h^{n+1}$ comme image de $\mathcal{T}_h^n$ par l'application définie par la formule (73) et sauver $\mathcal{T}_h^{n+1}$, $\mathbf{v}^{n+1}$, p^{n+1}, $\mathbf{u}^{n+1}$ et $\ddot{\mathbf{u}}^{n+1}$.

Résultats numériques

Paramètres physiques et numériques

Les mêmes paramètres physiques comme dans la synthèse du chapitre I ont été considérés. On choisit $\delta = 0.5$ et $\theta = 0.3$ dans le schéma de Newmark. On pose $\Delta t = 0.001\, s$ et $N = 100$. Les calculs numériques sont effectués en FreeFem++ (voir [17]) avec un ordinateur de 3.6 GHz de fréquence.

Temps CPU

1. *Temps CPU pour l'algorithme monolithique*

   On note $nsFS$ le nombre de segments sur l'interface. nous avons utilisé un maillage de $nt = 2426$ triangles et $nv = 1305$ sommets. Les éléments finis $\mathbb{P}_1$ + *bubble* ont été employés pour les vitesses, $\mathbb{P}_1$ pour les pressions et $\mathbb{P}_0$ pour les fonctions caractéristiques Nous avons effectué un calcul des temps CPU pour différentes valeurs de $nsFS$. Les degrés de liberté Dof sont calculés à partir de la formule

   $$Dof = 2(nv + nt) + nv = 3nv + 2nt,$$

   où $2(nv + nt)$ est considéré pour les vitesses et nv pour les pressions.

$nsFS$	nt	nv	global Dof	CPU_{mono}
80	2426	1305	8767	5 mn 25 s
100	3916	2070	14042	7 mn 18 s
120	5039	2649	18016	11 mn 34 s

Table 1: Temps CPU pour l'algorithme monolithique.

2. *Temps CPU pour l'algorithme semi-implicite procédures partagées*

   Dans cet algorithme, quelques itérations sont nécessaires pour résoudre le problème d'optimisation (voir synthèse chapitre I) afin de satisfaire les conditions à l'interface. Les éléments finis $\mathbb{P}_1 + bubble$ ont été utilisés pour les vitesses du fluide et $\mathbb{P}_1$ pour la pression du fluide et les déplacements de la structure. Les degrés de liberté du fluide sont donnés par $DofF = 3nvF + 2ntF$, avec $2(nvF + ntF)$ pour la vitesse et nvF pour la pression. Ceux de la structure sont donnés par $DofS = 2nvS$.

$nsSF$	ntF	nvF	ntS	nvS	DofF	DofS	CPU_{pp}	CPU_{pp}/CPU_{mono}
80	2106	1144	320	242	7644	484	10 mn 49 s	1.99
100	3538	1880	378	291	12716	582	15 mn 57 s	2.18
120	4582	2422	452	348	16430	696	21 mn 06 s	1.82

Table 2: Algorithme semi-implicite procédures partagées pour $m = 3$.

3. Dans le tableau ci-dessous, nous comparons les temps CPU entre les deux algorithmes cités ci-dessus pour différentes valeurs du nombre des modes propres m.

m	CPU_{pp}	CPU_{pp}/CPU_{mono}
3	10 m 49 s	1.99
7	27 m 47 s	5.12
10	41 m 07 s	7.59

Table 3: Rapport des CPUs en temps pour $nsFS = 80$.

Maillages

On montre dans la figure 13 ci-dessous, le maillage global fluide structure (en haut) et séparément les maillages fluide et structure (en bas). Le maillage global est l'union des maillages fluide et structure, qui sont compatibles à l'interface. Cette compatibilité de maillages peut être vérifiée par : $nv = nvF + nvS - (nsFS + 1)$, et $nt = ntF + ntS$.

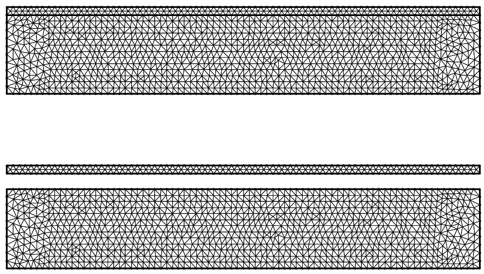

Figure 13: Maillage global (en haut) et maillages fluide et structure (en bas).

Comportements des solutions

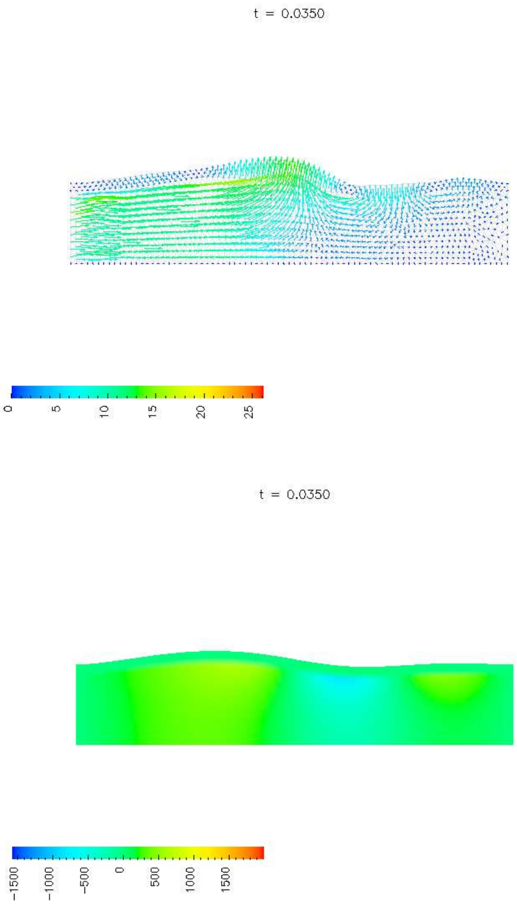

Figure 14: Vitesses (en haut) et pression (en bas) fluide structure à l'instant $t = 0.035$.

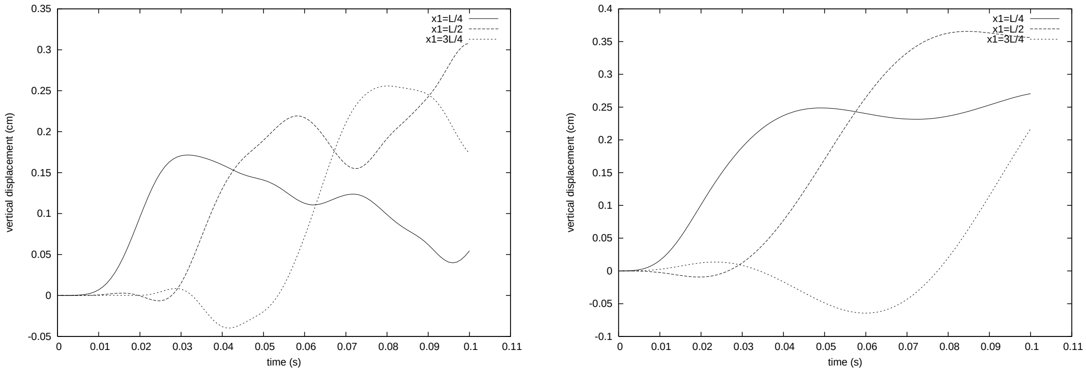

Figure 15: Déplacements verticaux en $x_1 = L/4$, $x_2 = L/2$ et $x_3 = 3L/4$ de l'interface, dans le cas monolithique (à gauche) et dans le cas procédures partagées (à droite).

Remark 0.2 *Nous pouvons remarquer à partir de la Figure 15 que les déplacements verticaux calculés par les algorithmes monolithique et procédures partagées sont différents. Cette différence peut s'expliquer par le fait que le problème de la structure est écrit en cadre Lagrangien dans le cas des procédures partagées et en cadre Eulérien dans le cas monolithique. De plus cette différence s'explique par le fait que le problème de la structure est résolu par la méthode de décomposition modale dans le cas des procédures partagées.*

Conclusion et perspectives

Nous avons présenté dans les chapitres I et II deux algorithmes semi-implicites procédures partagées pour des problèmes d'interaction fluide structure bidimensionnels. Le premier algorithme est mis au point pour les cas des petits et des grands déplacements de la structure. Cet algorithme détermine à chaque pas de temps la position de l'interface de manière explicite à partir d'une prédiction des déplacements de la structure, tandis que la vitesse du fluide, la pression du fluide et les déplacements de la structure sont calculés de façon implicite. Le second algorithme proposé dans le cas des petits déplacements de la structure, est basé sur un calcul explicite de la position de l'interface à partir de la vitesse du domaine fluide à l'instant précédent et sur un calcul implicite de la vitesse du fluide, de la pression du fluide et des déplacements de la structure. L'algorithme utilise le domaine connu Ω_n^F comme domaine de calcul pour le fluide. Une analyse de la stabilité de l'algorithme a été effectuée par le biais des estimations d'énergie. Dans les deux algorithmes ci-dessus, un problème d'optimisation est résolu par BFGS pour satisfaire les conditions de continuité des vitesses et d'égalité des contraintes à l'interface. Durant ce processus de minimisation, le maillage fluide reste fixe et la matrice fluide n'est factorisée qu'une seule fois, ce qui réduit considérablement l'effort de calcul.

Dans le chapitre III, un algorithme semi-implicite monolithique pour un problème d'interaction fluide structure avec des petits déplacements de la structure est proposé. Cet algorithme utilise un maillage global fluide structure, obtenu comme union des maillages fluide et structure, choisis compatibles à l'interface. Les fonctions caractéristiques employées ont permis de choisir de manière indépendante les schémas discrets des problèmes. La condition de continuité des vitesses est satisfaite automatiquement par l'utilisation d'un seul champ de vitesse fluide structure. Celle de l'égalité des contraintes a été éliminée à partir de la formulation faible. Le problème fluide structure est par conséquent mis sous la forme d'un système linéaire, résolu par l'algorithme de GMRES. Un calcul des temps CPU a permis de montrer que le temps de calcul est réduit quand l'approche monolithique est utilisée à la place des procédures partagées particulières.

Dans le futur, nous adopterons l'approche proposée dans le chapitre III, avec un modèle non linéaire pour la structure et nous analyserons la stabilité de l'algorithme obtenu. A présent, nous travaillons sur une approche monolithique, qui consiste à rajouter une équation supplémentaire dans le système global pour traiter la condition d'égalité des vitesses à l'interface.

Bibliography

[1] S. Badia, A. Quaini, A. Quarteroni, *Splitting methods based on algebraic factorization for fluid-structure interaction.* SIAM J. Sci. Comput. **30** (2008), no. 4, 1778–1805.

[2] S. Badia, A. Quaini, A. Quarteroni, *Modular vs. non-modular preconditioners for fluid-structure systems with large added-mass effect.* Comput. Methods Appl. Mech. Engrg. **197** (2008), no. 49-50, 4216–4232.

[3] L. Baffico, *A characteristic-ALE formulation for a fluid-membrane interaction problem,* Communications in Numerical Methods in Engineering 2005; **21** : 723–734.

[4] P. Causin, J.F. Gerbeau, F. Nobile, *Added-mass effect in the design of partitioned algorithms for fluid-structure problems*, Comput. Methods Appl. Mech. Engrg.**194** (2005) 4506–4527.

[5] W. Dettmer, D. Perić, *A computational framework for fluid-structure interaction : Finite element formulation and applications*, Comput. Methods Appl. Mech. Engrg. **195** (2006) 5754-5779.

[6] T. Dunne, *An Eulerian approach to fluid-structure interaction and goal-oriented mesh adaptation.* Inter. J. Num. Meth. Fluids, **51** (2006), pp. 1017-1039.

[7] S. Deparis, M. A. Fernández, L. Formaggia, *Acceleration of a fixed point algorithm for fluid-structure interaction using transpiration conditions*, Mathematical Modelling and Numerical Analysis 2003; **37**(4) : 601-616.

[8] C. Farhat, M. Lesoinne, *Two efficient staggered algorithms for the serial and parallel solution of three-dimensional nonlinear transient aeroelastic problems.* Computer Methods in Applied Mechanics and Engineering 2000; **182**(3-4) : 499–515.

[9] C. Forster, WA. Wall, E. Ramm, *Artificial added mass instabilities in sequential staggered coupling of nonlinear structures and incompressible viscous flows*, Computer Methods in Applied Mechanics and Engineering 2007; **196**(7) : 1278–1293.

[10] L. Formaggia, J. F. Gerbeau, F. Nobile, A. Quarteroni, *On the coupling of 3D and 1D Navier-Stokes equations for flow problems in compliant vessels*, Computer Methods in Applied Mechanics and Engineering 2001; **191**(6-7) : 561–582.

[11] M. A. Fernandez, P. Le Tallec, *Linear fluid-structure stability analysis with transpiration. Part I: formulation and mathematical analysis*, Computer Methods in Applied Mechanics and Engineering 2003; **192** : 4805-4835.

[12] M. A. Fernandez, M. Moubachir, *A Newton method using exact jacobians for solving fluid-structure coupling*, Computers & Structures 2005; **83**(2-3) : 127-142.

[13] M. A. Fernandez, J. F. Gerbeau, C. Grandmont, *A projection semi-implicit scheme for the coupling of elastic structure with an incompressible fluid*, Inter. J. for Num. Methods in Eng. 2007; **69**(4) : 794–821.

[14] J. F. Gerbeau, M. Vidrascu, *A quasi-Newton algorithm on a reduced model for fluid-structure interaction problems in blood flows*, Mathematical Modelling and Numerical Analysis 2003; **37**(4) : 631-648.

[15] C. Grandmont, V. Guimet, Y. Maday, *Numerical analysis of some decoupling techniques for the approximation of the unsteady fluid structure interaction*, Math. Models Methods Appl. Sci. 11 (2001), no. 8, 1349–1377.

[16] J. Hron, S. Turek, *A monolithic FEM/multigrid solver for an ALE formulation of fluid-structure interaction with applications in biomechanics*, Fluid-structure interaction. 146–170, Lect. Notes Comput. Sci. Eng., **53**, Springer, Berlin, 2006.

[17] F. Hecht, O. Pironneau, *A finite element software for PDE: FreeFem++*, http://www.freefem.org.

[18] M. Heil, A. L. Hazed, J. Boyle, *Solvers for large-displacement fluid-structure interaction problems: segregated versus monolithic approaches.* Cumput. Mech (2008), DOI 10.1007/s00466-008-0270-6.

[19] B. Hubner, E. Walhorn, D. Dinkler, *A monolithic approach to fluid-structure interaction using space-time finite elements.* Comput. Meth. Appl. Mech. Eng., **193** (2004), pp. 2087-2104.

[20] P. Le Tallec, J. Mouro, *Fluid-structure interaction with large structural displacements*, Computer Methods in Applied Mechanics and Engineering 2001; **190**(24-25) : 3039–3067.

[21] C. M. Murea, C. Vazquez, *Sensitivity and approximation of coupled fluid-structure equations by virtual control method*, Applied Mathematics and Optimization 2005; **52**(2) : 183–218.

[22] C. M. Murea, *The BFGS algorithm for a nonlinear least squares problem arising from blood flow in arteries*, Computer & Mathematics with Applications 2005; **49** : 171–186.

[23] C. M. Murea, *Numerical simulation of a pulsatile flow through a flexible channel*, ESAIM: Mathematical Modelling and Numerical Analysis 2006; **40**(6) : 1101-1125.

[24] I. Mbaye, C. M. Murea, *Numerical procedure with analytic derivative for unsteady fluid-structure interaction*, Communications in Numerical Methods in Engineering, published online 13 Jul 2007, DOI : 10.1002/cnm.1031.

[25] C. M. Murea, *A semi-implicit algorithm based on the Augmented Lagragian Method for fluid-structure interface*, in: K. Kunish, G. Of, O. Steinbach (eds.) Numerical Mathematics and Advanced Applications, Proceedings of ENUMAT 2007, the 7th Euopean Conference on Numerical Mathematics and Advanced Applications, Graz, Austria, Steptember 2007. Springer, pp. 555-562.

[26] F. Nobile, *Numerical approximation of fluid-structure interaction problems with application to haemodynamics*, Ph.D. Thesis, EPFL, Switzerland, 2001.

[27] F. Nobile, C. Vergara, *An effective fluid-structure interaction formulation for vascular dynamics by generalized Robin conditions* MOX Report 01/2007.

[28] A. Quarteroni, L. Formaggia, *Mathematical modelling and numerical simulation of the cardiovascular system*, in P.G. Ciarlet (Ed.), Handbook of numerical analysis, Vol. XII, North-Holland, Amsterdam, 2004, 3–127.

[29] J. Steindorf, HG. Matthies, *Partioned but strongly coupled iteration schemes for nonlinear fluid-structure interaction*, Computers & Structures 2002; **80** : 1991–1999.

[30] J. San Martin, J. F. Scheid, T. Takahashi, M. Tucsnak, *Convergence of the Lagrange-Galerkin method for the Equations Modelling the Motion of a Fluid-Rigid System*, SIAM J. Numerical Analysis **43** (2005), 1536-1571; **80** : 1991–1999.

[31] A. Quaini, A. Quarteroni, *A semi-implicit approach for fluid-structure interaction based on an algebraic fractional step method.* Math. Models Methods Appl. Sci. **17** (2007), no. 6, 957–983.

[32] EW. Swim, P. Seshaiyer, *A nonconforming finite element method for fluid-structure interaction problems*, Computer Methods in Applied Mechanics and Engineering 2006; **195** : 2088–2099.

[33] TE. Tezduyar, S. Sathe, R. Keedy, K. Stein, *Space-time finite element techniques for computation of fluid-structure interactions*, Computer Methods in Applied Mechanics and Engineering 2006; **195** : 2002–2027.

[34] R. Torii,M. Oshima, T. Kobayashi, K. Takagi and E. T. Tezduyar, *Fluid-structure interaction modeling of aneurysmal condition with high and normal blood pressure*, Mech, 38 : 482-490, 2006.

[35] A. Valencia and F. Solis, *Blood flow dynamics and arterial wall interaction in a saccular aneurysm model of the basilar artery*, Comput. Struct, 84:1326-1337, 2006.

Chapter 1

A fast method for solving fluid-structure interaction problems numerically

This chapter is based on the paper:

C.M. Murea, S. Sy, *A fast method for solving fluid-structure interaction problems numerically*, Inter. J. Num. Method in Fluids, DOI: 10.1002/fld.1931, published online: October, 23, 2008.

Abstract. We present a semi-implicit algorithm for solving an unsteady fluid-structure interaction problem. The algorithm for solving numerically the fluid-structure interaction problems was obtained by combining the backward Euler scheme with a semi-implicit treatment of the convection term for the Navier-Stokes equations and an implicit centered scheme for the structure equations. The structure is governed either by the linear elasticity or by the non-linear St Venant-Kirchhoff elasticity models. At each time step, the position of the interface is predicted in an explicit way. Then, an optimization problem must be solved, such that the continuity of the velocity as well as the continuity of the stress hold at the interface. During the Broyden, Fletcher, Goldforb, Shano (BFGS) iterations for solving the optimization problem, the fluid mesh does not move, which reduces the computational effort. The term "semi-implicit" used for the fully algorithm means that the interface position is computed explicitly, while the displacement of the structure, velocity and the pressure of the fluid are computed implicitly. Numerical results are presented.

1.1 Introduction

We consider an unsteady incompressible flow through a channel with elastic wall. This kind of fluid-structure interaction problem is of considerable interest in bio-mechanics.

A family of explicit algorithms known also as staggered was successfully employed for the aeroelastic applications [1]. The numerical results presented in [2] show that an explicit algorithm based on the leap-frog scheme for the structure and on the backward Euler scheme for the fluid is unstable for simulation of blood flow in large arteries. The instability does not depend on the time step but on the mass densities of fluid and structure and on the geometry. The theoretical result presented in [3] confirms that. In [4], explicit algorithms based on the generalized α method for the structure and three backward differencing schemes for the fluid will get unstable when the mass density ratio of fluid and structure is greater than a certain threshold.

Implicit algorithms have been developed based on fixed point strategies [5], [2], [6]. Using the transpiration technique [7], [8], the convergence can be accelerated. Faster algorithms are obtained when the derivative is employed. A block Newton algorithm was used in [9], where the derivative of the operators are approached by finite differences. The Newton method was employed in [10], where the derivative of the operator was replaced by a simpler operator and in [11] where the gradient was computed analytically. The Newton method which incorporate the linearization of the fully discretized model was described in [12]. Space-time finite element techniques for fluid-structure interactions problems are presented in [13].

Other implicit algorithms based on optimal control model was investigated in [14], [15] in the steady case.We can use the same strategy for the unsteady fluid-structure interaction problems and at each time step, we have to solve an optimization problem. The gradient of the cost function is approached by finite differences in [16] where it is proved the superiority of the Broyden, Fletcher, Goldforb, Shano (BFGS) method in comparison to the modified Newton method (Newton with line search), when moderate time step is used. The analytic formula of the gradient of the cost function is presented in [17].

Since the implicit algorithms are very expensive in computational time, a semi-implicit strategy based on the Chorin-Temam projection scheme for incompressible flows is introduced in [18]. The term semi-implicit means that the interface position is computed explicitly, while the displacement of the structure, velocity and the pressure of the fluid are computed implicitly. A related semi-implicit algorithm is presented in [19], where the structure equation is embedded into the fluid equations.

The aim of this chapter is to present a semi-implicit algorithm based on the optimal control idea. The numerical results prove that the computational effort is reduced in comparison to the implicit algorithm, while the computed solutions obtained by the two methods are almost the same.

1.2 Statement of the problem

Let us denote by Ω^S the undeformed structure domain. We shall assume that its boundary admits the decomposition $\partial\Omega^S = \Gamma_D \cup \Gamma_N \cup \Gamma_0$ On Γ_D the displacement will be prescribed and on Γ_N the stress is known. The initial fluid domain Ω_0^F is bounded by: Σ_1 the inlet section, Σ_2 the bottom boundary Σ_3 the outlet section and Γ_0 the top boundary (see Figure 1.1, at the left). The boundary Γ_0 is common of both domains and it represents the initial position of the fluid-structure interface. Under the action of the fluid stress, the structure will be deformed. At the time instant t, the fluid occupies the domain Ω_t^F bounded by the moving interface Γ_t and by the rigid boundary $\Sigma = \Sigma_1 \cup \Sigma_2 \cup \Sigma_3$ (see Figure 1.1, at the right).

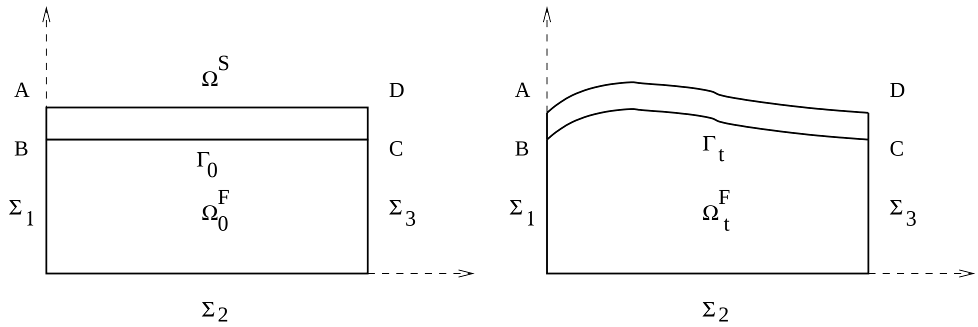

Figure 1.1: Initial (left) and intermediate (right) geometrical configuration.

We have assumed that the fluid is governed by the Navier-Stokes equations, while either linear elasticity or non-linear St Venant-Kirchhoff elasticity models have been employed for the structure. At each time instant $t \in [0, T]$, we are interested to know: the structure displacement $\mathbf{u} = (u_1, u_2)^T : \Omega^S \times [0, T] \to \mathbb{R}^2$, the fluid domain Ω_t^F, the fluid velocity $\mathbf{v}(t) = (v_1(t), v_2(t))^T : \Omega_t^F \to \mathbb{R}^2$ and the fluid pressure $p(t) : \Omega_t^F \to \mathbb{R}$.

Linear elasticity equations

$$\begin{aligned}
\rho^S \frac{\partial^2 \mathbf{u}}{\partial t^2} - \nabla \cdot \sigma^S &= \mathbf{f}^S, \quad \text{in } \Omega^S \times (0, T) && (1.1)\\
\sigma^S &= \lambda^S (\nabla \cdot \mathbf{u}) \mathbb{I}_2 + 2\mu^S \epsilon(\mathbf{u}) && (1.2)\\
\epsilon(\mathbf{u}) &= \frac{1}{2}\left(\nabla \mathbf{u} + (\nabla \mathbf{u})^T\right) && (1.3)\\
\mathbf{u} &= 0, \quad \text{on } \Gamma_D \times (0, T) && (1.4)\\
\sigma^S \mathbf{n}^S &= 0, \quad \text{on } \Gamma_N \times (0, T), && (1.5)
\end{aligned}$$

where $\rho^S > 0$ is the mass density of the structure, $\lambda^S > 0$ and $\mu^S > 0$ are the Lamé parameters, $\mathbf{f}^S : \Omega^S \times (0, T) \to \mathbb{R}^2$ is the applied volume force per unit area, $\epsilon(\mathbf{u})$ is the linearized strain tensor, $\mathbb{I}_2$ is the identity matrix, $\mathbf{n}^S$ is the unit outer normal vector along the boundary $\partial\Omega^S$.

Navier-Stokes equations

$$\begin{aligned}
\rho^F\left(\frac{\partial \mathbf{v}}{\partial t}+(\mathbf{v}\cdot\nabla)\mathbf{v}\right)-\nabla\cdot\sigma^F &= \mathbf{f}^F, \quad \forall t\in(0,T),\forall \mathbf{x}\in\Omega_t^F && (1.6)\\
\nabla\cdot\mathbf{v} &= 0, \quad \forall t\in(0,T),\forall \mathbf{x}\in\Omega_t^F && (1.7)\\
\sigma^F &= -p\mathbb{I}_2+2\mu^F\epsilon(\mathbf{v}) && (1.8)\\
\sigma^F\mathbf{n}^F &= \mathbf{h}_{in}, \quad \text{on } \Sigma_1\times(0,T) && (1.9)\\
\sigma^F\mathbf{n}^F &= \mathbf{h}_{out}, \quad \text{on } \Sigma_3\times(0,T) && (1.10)\\
\mathbf{v} &= 0, \quad \text{on } \Sigma_2\times(0,T), && (1.11)
\end{aligned}$$

where $\rho^F>0,\ \mu^F>0$ are the mass density and the viscosity of the fluid, $\mathbf{f}^F=(f_1^F,f_2^F)$ are the applied volume forces, in general the gravity forces, $h_{in}:\Sigma_1\times(0,T)\to\mathbb{R}^2$ and $h_{out}:\Sigma_3\times(0,T)\to\mathbb{R}^2$ are prescribed boundary stress, $\mathbf{n}^F$ is the unit outer normal vector along the boundary $\partial\Omega_t^F$. The interface Γ_t is the image of the boundary Γ_0 by the map:

$$\mathbb{T}(\mathbf{X})=\mathbf{X}+\mathbf{u}(\mathbf{X},t).$$

Interface conditions

$$\begin{aligned}
\mathbf{v}(\mathbf{X}+\mathbf{u}(\mathbf{X},t),t) &= \frac{\partial\mathbf{u}}{\partial t}(\mathbf{X},t),\ \forall(\mathbf{X},t)\in\Gamma_0\times(0,T) && (1.12)\\
\left(\sigma^F\mathbf{n}^F\right)_{(\mathbf{X}+\mathbf{u}(\mathbf{X},t),t)} &= -\left(\sigma^S\mathbf{n}^S\right)_{(\mathbf{X},t)},\ \forall(\mathbf{X},t)\in\Gamma_0\times(0,T). && (1.13)
\end{aligned}$$

The equations (1.12) and (1.13) represent the continuity of velocity and of stress at the interface, respectively.

Initial conditions

$$\begin{aligned}
\mathbf{u}(\mathbf{X},t=0) &= \mathbf{u}^0(\mathbf{X}),\ \text{in } \Omega^S && (1.14)\\
\frac{\partial\mathbf{u}}{\partial t}(\mathbf{X},t=0) &= \dot{\mathbf{u}}^0(\mathbf{X}),\ \text{in } \Omega^S && (1.15)\\
\mathbf{v}(\mathbf{x},t=0) &= \mathbf{v}^0(\mathbf{x}),\ \text{in } \Omega_0^F, && (1.16)
\end{aligned}$$

where $\mathbf{u}^0$ is the initial structure displacement, $\dot{\mathbf{u}}^0$ is the initial structure velocity and $\mathbf{v}^0$ is the initial fluid velocity.

The governing equations for fluid-structure interaction problem are (1.1)–(1.16). The above fluid and structure models could be considered unbalanced: on the one hand, the structure is governed by a linear elastic constitutive law adapted for small displacements and, on the other hand, the fluid equations are written in a moving domain. In the real life, the displacement of a segment of human artery (6 cm length, 0.1 cm thickness, 1 cm diameter) is about 0.1 cm, therefore a linear mathematical model for the structure could be sufficient for this particular application. Contrary to the elastic solids, the fluids are very sensitive to a moving boundary. This is probably due to weak intermolecular forces and even a small displacement of a boundary produces important modifications in a fluid flow. For this reason, it is necessary to write the fluid equations in a moving domain. Coupling Navier-Stokes equations with a linear model for the structure was used in [2], [6], [20] where the structure is governed by the independent rings model, by Navier equation [21] or by a linear membrane [22], [23].

Non-linear elasticity equations: In applications with large displacement of the structure, non-linear models have to be used as in [5], [10], [13], [18] (shells), in [24] (beams), or in [25] (membrane). In this chapter, we include also the study of interaction of the Navier-Stokes equations with a non-linear St Venant-Kirchhoff elasticity model (see [26]). We just replace the equations (1.2)-(1.3) and (1.13) by

$$\sigma^S = \left(\mathbb{I}_2 + \nabla \mathbf{u}\right)\left[\lambda^S \left(E_{11}(\mathbf{u}) + E_{22}(\mathbf{u})\right)\mathbb{I}_2 + 2\mu^S \mathbb{E}(\mathbf{u})\right] \tag{1.17}$$

$$\mathbb{E}(\mathbf{u}) = \frac{1}{2}\left(\nabla \mathbf{u} + (\nabla \mathbf{u})^T + (\nabla \mathbf{u})^T \nabla \mathbf{u}\right), \tag{1.18}$$

where $\mathbb{E}(\mathbf{u}) = \left(E_{ij}(\mathbf{u})\right)_{i,j=1,2}$, is the Green-St Venant strain tensor. The non-linear St Venant-Kirchhoff elasticity model could be used for large displacements but small strains of the structure.

In the nonlinear case, we have to multiply the left side of (1.13) by $\omega(\mathbf{X}, t)$ where $\omega(\mathbf{X}, t) = \|\mathrm{cof}(\nabla \mathbb{T})\mathbf{n}^S\|_{\mathbb{R}^2}$.

1.3 Structure approximation by centred time advancing scheme

We introduce the following Hilbert space:

$$\mathbf{W}^S = \left\{\mathbf{w}^S \in \left(H^1\left(\Omega^S\right)\right)^2;\ \mathbf{w}^S = 0 \text{ on } \Gamma_D\right\}.$$

The habitual regularity of a weak solution of the linear elasticity model is

$$u \in L^2\left(0, T;\, \mathbf{W}^S\right) \text{ and } \frac{du}{dt} \in L^2\left(0, T;\, \left(H^1\left(\Omega^S\right)\right)^2\right)(\text{see } [27, Chap. XVIII]),$$

but for fluid-structure interaction problem, more regularity is required (see [28]). For example, the condition (1.12) makes sense if the structure velocity $\frac{du}{dt}(t)$ is at least in $\left(H^1\left(\Omega^S\right)\right)^2$.

Multiplying equation (1.1) by $\mathbf{w}^S \in \mathbf{W}^S$ and from the Green formula, we obtain

$$\int_{\Omega^S} \rho^S \frac{\partial^2 \mathbf{u}}{\partial t^2} \cdot \mathbf{w}^S d\mathbf{X} + a_S\left(\mathbf{u}, \mathbf{w}^S\right) = \int_{\Omega^S} \mathbf{f}^S \cdot \mathbf{w}^S d\mathbf{X} + \int_{\Gamma_0} \left(\sigma^S \mathbf{n}^S\right) \cdot \mathbf{w}^S d\, s, \quad \forall \mathbf{w}^S \in \mathbf{W}^S, \tag{1.19}$$

where

$$a_S\left(\mathbf{u}, \mathbf{w}^S\right) = \int_{\Omega^S} \lambda^S \left(\nabla \cdot \mathbf{u}\right)\left(\nabla \cdot \mathbf{w}^S\right) d\mathbf{X} + \int_{\Omega^S} 2\mu^S \epsilon\left(\mathbf{u}\right) : \epsilon\left(\mathbf{w}^S\right) d\mathbf{X}$$

in the linear case and

$$a_S\left(\mathbf{u}, \mathbf{w}^S\right) = \int_{\Omega^S} \left(\mathbb{I}_2 + \nabla \mathbf{u}\right)\left(\lambda^S \left(E_{11}\left(\mathbf{u}\right) + E_{22}\left(\mathbf{u}\right)\right)\mathbb{I}_2 + 2\mu^S \mathbb{E}\left(\mathbf{u}\right)\right) : \left(\nabla \mathbf{w}^S\right) d\mathbf{X}$$

in the non-linear case.

1.3.1 Modal decomposition of the linear model

For each $i \in \mathbb{N}^*$, there exists an unique eigenvalue $\lambda_i > 0$ and an unique eigenfunction $\boldsymbol{\phi}^i \in \mathbf{W}^S$, solution of

$$a_S\left(\boldsymbol{\phi}^i, \mathbf{w}^S\right) = \lambda_i \int_{\Omega^S} \rho^S \boldsymbol{\phi}^i \cdot \mathbf{w}^S d\mathbf{X}, \quad \forall \mathbf{w}^S \in \mathbf{W}^S \tag{1.20}$$

such that

$$\int_{\Omega^S} \rho^S \boldsymbol{\phi}^i \cdot \boldsymbol{\phi}^j d\mathbf{X} = \delta_{ij}. \tag{1.21}$$

Let us denote by $\alpha_i(t) = \displaystyle\int_{\Gamma_0} \left(\sigma^S \mathbf{n}^S\right)(t) \cdot \boldsymbol{\phi}^i d\, s$. The problem (1.19) has a solution of the form

$$\mathbf{u}(t) = \sum_{i \geq 1} q_i(t) \boldsymbol{\phi}^i,$$

where q_i is the solution of the second order differential equation

$$q_i''(t) + \lambda_i q_i(t) = \int_{\Omega^S} \mathbf{f}^S(t) \cdot \boldsymbol{\phi}^i d\mathbf{X} + \alpha_i(t), \quad t \in (0, T) \tag{1.22}$$

$$q_i(0) = \int_{\Omega^S} \rho^S \mathbf{u}^0 \cdot \boldsymbol{\phi}^i d\mathbf{X} \tag{1.23}$$

$$q_i'(0) = \int_{\Omega^S} \rho^S \dot{\mathbf{u}}^0 \cdot \boldsymbol{\phi}^i d\mathbf{X}. \tag{1.24}$$

The solution of the problem (1.20)–(1.21) can be approached by using the finite element method. We have to solve in this case a generalized eigenproblem of the form

$$K_h \boldsymbol{\Phi}_h^i = \lambda_{i,h} M_h \boldsymbol{\Phi}_h^i, \quad \left(\boldsymbol{\Phi}_h^j\right)^T M_h \boldsymbol{\Phi}_h^i = \mathbb{I}_2.$$

Remark 1.1 *Following [29, p. 572], when the initial displacement and velocity are zero, the solution of (1.22) is given by*

$$q_i(t) = \frac{1}{\sqrt{\lambda_i}} \int_0^t f_i(s) \sin\left(\sqrt{\lambda_i}(t-s)\right) d\,s,$$

where $f_i(t) = \displaystyle\int_{\Omega^S} \mathbf{f}^S(t) \cdot \boldsymbol{\phi}^i d\mathbf{X} + \alpha_i(t)$. *If* λ_i *is very large, the influence of* $q_i(t)$ *in* $\mathbf{u}(t)$ *diminishes, therefore in practical calculation, only the first* m *eigenvalues will be considered*

$$0 < \lambda_{1,h} \leq \lambda_{2,h} \leq \cdots \leq \lambda_{m,h}.$$

Let $N \in \mathbb{N}^*$ be the number of time steps and $\Delta t = T/N$ the time step. We set $t_n = n\Delta t$ for $n = 0, 1, \ldots, N$. We denote $\alpha_i^n = \alpha_i(t_n)$ and let q_i^n be approximation of $q_i(t_n)$. The equation (1.22) will be approached by the following centered scheme: knowing q_i^{n-1} and q_i^n, find q_i^{n+1} such that

$$\begin{aligned}
&\frac{\left(q_i^{n+1} - 2q_i^n + q_i^{n-1}\right)}{(\Delta t)^2} + \lambda_{i,h}\left(\theta q_i^{n+1} + (1-2\theta) q_i^n + \theta q_i^{n-1}\right) \\
&= \int_{\Omega^S} \left(\theta \mathbf{f}^{S,n+1} + (1-2\theta)\mathbf{f}^{S,n} + \theta \mathbf{f}^{S,n-1}\right) \cdot \boldsymbol{\phi}^i d\mathbf{X} + \theta\alpha_i^{n+1} + (1-2\theta)\alpha_i^n + \theta\alpha_i^{n-1}, \quad (1.25)
\end{aligned}$$

where θ is a real parameter in $\left(0, \frac{1}{2}\right)$ and $\mathbf{f}^{S,n} = \mathbf{f}^S(t_n)$ are the volume forces. This scheme is of second order in time and if $\theta \in \left[\frac{1}{4}, \frac{1}{2}\right]$, then it is unconditionally stable.

The structure displacement at time instant t_n will be approached by

$$\mathbf{u}_h^n(\mathbf{X}) = \sum_{i=1}^m q_i^n \boldsymbol{\phi}_h^i(\mathbf{X}), \quad \forall \mathbf{X} \in \Omega^S.$$

1.3.2 Newton's method for the non-linear model

A second order time advancing scheme for (1.19) is: find $\mathbf{u}^{n+1} \in \mathbf{W}^S$ an approximation of $\mathbf{u}(t_{n+1})$ such that

$$\begin{aligned}
&\int_{\Omega^S} \rho^S \frac{(\mathbf{u}^{n+1} - 2\mathbf{u}^n + \mathbf{u}^{n-1})}{(\Delta t)^2} \cdot \mathbf{w}^S d\mathbf{X} \\
&+\theta a_S\left(\mathbf{u}^{n+1}, \mathbf{w}^S\right) + (1-2\theta) a_S\left(\mathbf{u}^n, \mathbf{w}^S\right) + \theta a_S\left(\mathbf{u}^{n-1}, \mathbf{w}^S\right) \\
&= \int_{\Omega^S} \left(\theta \mathbf{f}^{S,n+1} + (1-2\theta)\mathbf{f}^{S,n} + \theta\mathbf{f}^{S,n-1}\right) \cdot \mathbf{w}^S d\mathbf{X} \\
&+ \int_{\Gamma_0} \left(\theta \mathbf{F}^{S,n+1} + (1-2\theta)\mathbf{F}^{S,n} + \theta\mathbf{F}^{S,n-1}\right) \cdot \mathbf{w}^S d\,s, \quad \forall \mathbf{w}^S \in \mathbf{W}^S, \qquad (1.26)
\end{aligned}$$

where $\mathbf{f}^{S,n} = \mathbf{f}^S(t_n)$ are the volume forces, $\mathbf{F}^{S,n} = \left(\sigma^S \mathbf{n}^S\right)(t_n)$ are the surface forces acting on the interface and θ is a real parameter in $\left(0, \frac{1}{2}\right)$.

We recall that the components of the St Venant-Kirchhoff stress tensor are

$$\sigma_{ij}^S(\mathbf{u}) = \lambda^S\left(E_{11}(\mathbf{u}) + E_{22}(\mathbf{u})\right)\delta_{ij} + 2\mu^S E_{ij}(\mathbf{u}),$$

where the Green-St Venant strain tensor $\mathbb{E}(\mathbf{u})$ is given by (1.18). The map $\mathbf{u} \to \mathbb{E}(\mathbf{u})$ is non-linear and we will use the Newton's method in order to obtain $\mathbf{u}^{n+1}$ the solution of (1.26).

Knowing the derivative with respect to $\mathbf{u}$ of the components of the Green-St Venant strain tensor and of $(\mathbb{I}_2 + \nabla\mathbf{u})$ for an arbitrary $\mathbf{h} = (h_1, h_2)$ in $\mathbf{W}^S$:

$$\begin{aligned}
\frac{d\,E_{11}}{d\,\mathbf{u}}(\mathbf{u})\,\mathbf{h} &= \frac{1}{2}\left(2\frac{\partial h_1}{\partial x_1} + 2\frac{\partial u_1}{\partial x_1}\frac{\partial h_1}{\partial x_1} + 2\frac{\partial u_1}{\partial x_2}\frac{\partial h_1}{\partial x_2}\right)\\
\frac{d\,E_{22}}{d\,\mathbf{u}}(\mathbf{u})\,\mathbf{h} &= \frac{1}{2}\left(2\frac{\partial h_2}{\partial x_2} + 2\frac{\partial u_2}{\partial x_1}\frac{\partial h_2}{\partial x_1} + 2\frac{\partial u_2}{\partial x_2}\frac{\partial h_2}{\partial x_2}\right)\\
\frac{d\,E_{12}}{d\,\mathbf{u}}(\mathbf{u})\,\mathbf{h} &= \frac{1}{2}\left(\frac{\partial h_1}{\partial x_2} + \frac{\partial h_2}{\partial x_1} + \frac{\partial u_2}{\partial x_1}\frac{\partial h_1}{\partial x_1} + \frac{\partial u_2}{\partial x_2}\frac{\partial h_1}{\partial x_2} + \frac{\partial u_1}{\partial x_1}\frac{\partial h_2}{\partial x_1} + \frac{\partial u_1}{\partial x_2}\frac{\partial h_2}{\partial x_2}\right)\\
\frac{d\,E_{21}}{d\,\mathbf{u}}(\mathbf{u})\,\mathbf{h} &= \frac{d\,E_{12}}{d\,\mathbf{u}}(\mathbf{u})\,\mathbf{h}\\
\frac{d\left(\mathbb{I}_2 + \nabla\mathbf{u}\right)}{d\,\mathbf{u}}\mathbf{h} &= \nabla\mathbf{h},
\end{aligned}$$

we can compute easily

$$\frac{d\,a_S}{d\,\mathbf{u}}\left(\mathbf{u}, \mathbf{w}^S\right)\mathbf{h} = \sum_{i,j=1}^{2}\int_{\Omega^S}\frac{d\,\sigma_{ij}^S}{d\,\mathbf{u}}(\mathbf{u})\,\mathbf{h}\,\frac{\partial w_i^S}{\partial x_j}d\mathbf{X}.$$

Newton's method for solving (1.26)

Step 0. Initialization. Set $k = 0$ and $\mathbf{u}^{n+1,0} = \mathbf{u}^n$. We will generate $\mathbf{u}^{n+1,k}$ for $k = 1, 2, \ldots$

Step 1. Find $\mathbf{h}^k$ the solution of the linear system

$$\begin{aligned}
&\int_{\Omega^S}\rho^S\frac{\mathbf{h}^k}{(\Delta t)^2}\cdot\mathbf{w}^S d\mathbf{X} + \frac{d\,a_S}{d\,\mathbf{u}}\left(\mathbf{u}^{n+1,k}, \mathbf{w}^S\right)\mathbf{h}^k\\
&= \int_{\Omega^S}\rho^S\frac{\left(\mathbf{u}^{n+1,k} - 2\mathbf{u}^n + \mathbf{u}^{n-1}\right)}{(\Delta t)^2}\cdot\mathbf{w}^S d\mathbf{X}\\
&+\theta a_S\left(\mathbf{u}^{n+1,k}, \mathbf{w}^S\right) + (1-2\theta)a_S\left(\mathbf{u}^n, \mathbf{w}^S\right) + \theta a_S\left(\mathbf{u}^{n-1}, \mathbf{w}^S\right)\\
&-\int_{\Omega^S}\left(\theta\mathbf{f}^{S,n+1} + (1-2\theta)\mathbf{f}^{S,n} + \theta\mathbf{f}^{S,n-1}\right)\cdot\mathbf{w}^S d\mathbf{X}\\
&-\int_{\Gamma_0}\left(\theta\mathbf{F}^{S,n+1} + (1-2\theta)\mathbf{F}^{S,n} + \theta\mathbf{F}^{S,n-1}\right)\cdot\mathbf{w}^S d\,s, \quad \forall\mathbf{w}^S \in \mathbf{W}^S.
\end{aligned} \tag{1.27}$$

Step 2. If $\mathbf{h}^k$ is small, then stop.

Step 3. Set $\mathbf{u}^{n+1,k+1} = \mathbf{u}^{n+1,k} - \mathbf{h}^k$; $k \leftarrow k+1$; go to **Step 1.**

The variational equation (1.27) will be solved by the finite element method. We denote by $\mathbf{u}_h^{n+1}$ the displacement of the structure at the time instant t_{n+1}.

1.4 Arbitrary Lagrangian Eulerian (ALE) Framework for approximation of fluid equations

Let $\widehat{\Omega}^F$ be a reference fixed domain. Let $\mathcal{A}_t$, $t \in [0,T]$ be a family of transformations such that

$$\mathcal{A}_t\left(\widehat{\mathbf{x}}\right) = \widehat{\mathbf{x}}, \quad \forall\, \widehat{\mathbf{x}} \in \Sigma_1 \cup \Sigma_2 \cup \Sigma_3, \quad \mathcal{A}_t\left(\Gamma_0\right) = \Gamma_t, \quad \mathcal{A}_t\left(\widehat{\Omega}^F\right) = \Omega_t^F,$$

where $\widehat{\mathbf{x}} = \left(\widehat{x}_1, \widehat{x}_2\right)^T \in \widehat{\Omega}^F$ represent the ALE coordinates and $\mathbf{x} = \left(x_1, x_2\right)^T = \mathcal{A}_t\left(\widehat{\mathbf{x}}\right)$ the Eulerian coordinates.

Let $\mathbf{v}$ be the velocity of the fluid in the Eulerian coordinates. The corresponding function in the ALE framework $\widehat{\mathbf{v}} : \widehat{\Omega}^F \times [0,T] \to \mathbb{R}^2$ is defined by

$$\widehat{\mathbf{v}}\left(\widehat{\mathbf{x}}, t\right) = \mathbf{v}\left(\mathcal{A}_t\left(\widehat{\mathbf{x}}\right), t\right) = \mathbf{v}\left(\mathbf{x}, t\right).$$

We denote the ALE time derivative by

$$\left.\frac{\partial \mathbf{v}}{\partial t}\right|_{\widehat{\mathbf{x}}} \left(\mathbf{x}, t\right) = \frac{\partial \widehat{\mathbf{v}}}{\partial t}\left(\widehat{\mathbf{x}}, t\right)$$

and the domain velocity by

$$\boldsymbol{\vartheta}(\mathbf{x}, t) = \frac{\partial \mathcal{A}_t}{\partial t}(\widehat{\mathbf{x}}).$$

In order to obtain the existence of a weak solution of the Navier-Stokes equations in moving domain, we assume that $\mathbf{v}(t) \in \left(H^1\left(\Omega_t^F\right)\right)^2$, $p(t) \in L^2\left(\Omega_t^F\right)$ and $\mathcal{A}_t$ is $\mathcal{C}^1$-diffeomorphism for each t, but for fluid-structure interaction problem, the existence is obtained in some particular Sobolev spaces (see [28]).

The Navier-Stokes equations in the ALE framework give: find the fluid velocity $\mathbf{v}$ verifying (1.12) and the fluid pressure p such that

$$\begin{aligned} \rho^F \left(\left.\frac{\partial \mathbf{v}}{\partial t}\right|_{\widehat{\mathbf{x}}} + \left(\left(\mathbf{v} - \boldsymbol{\vartheta}\right) \cdot \nabla\right) \mathbf{v} \right) - 2\mu^F \nabla \cdot \epsilon\left(\mathbf{v}\right) + \nabla p &= \mathbf{f}^F, \quad \forall t \in (0,T), \forall \mathbf{x} \in \Omega_t^F, \\ \nabla \cdot \mathbf{v} &= 0, \quad \forall t \in (0,T), \forall \mathbf{x} \in \Omega_t^F. \end{aligned}$$

Multiplying the above equations by $\mathbf{w}^F$ and q respectively and using the Green formula, we have

$$\begin{aligned}
\int_{\Omega_t^F} \rho^F \left.\frac{\partial \mathbf{v}}{\partial t}\right|_{\widehat{\mathbf{x}}} \cdot \mathbf{w}^F d\mathbf{x} \quad &+ \quad \int_{\Omega_t^F} \rho^F \left(\left(\left(\mathbf{v}-\boldsymbol{\vartheta}\right)\cdot\nabla\right)\mathbf{v}\right)\cdot \mathbf{w}^F d\mathbf{x} \\
&+ \quad a_F\left(\mathbf{v},\mathbf{w}^F\right) + b_F\left(\mathbf{w}^F, p\right) = \ell_F\left(\mathbf{w}^F\right), \ \forall \mathbf{w}^F = 0 \text{ on } \Sigma_2 \cup \Gamma_t, \\
b_F\left(\mathbf{v}, q\right) = 0, \quad \forall q, &
\end{aligned}$$

where

$$\begin{aligned}
a_F\left(\mathbf{v},\mathbf{w}^F\right) &= \int_{\Omega_t^F} 2\mu^F \epsilon\left(\mathbf{v}\right) : \epsilon\left(\mathbf{w}^F\right) d\mathbf{x}, \\
b_F\left(\mathbf{w}^F, q\right) &= -\int_{\Omega_t^F} \left(\nabla\cdot\mathbf{w}^F\right) q \, d\mathbf{x}, \\
\ell_F\left(\mathbf{w}^F\right) &= \int_{\Omega_t^F} \mathbf{f}^F \cdot \mathbf{w}^F d\mathbf{x} + \int_{\Sigma_1} \mathbf{h}_{in}\cdot\mathbf{w}^F d\, s + \int_{\Sigma_3} \mathbf{h}_{out}\cdot\mathbf{w}^F d\, s.
\end{aligned}$$

For the approximation of fluid equations, we employ a time integration algorithm based on the backward Euler scheme and a semi-implicit treatment of the convection term. In the case of a fixed domain, this scheme has been analyzed in [30], where the unconditional stability is proved. For the fully discrete problem in a fixed domain, a stability bound on $\dfrac{\Delta t}{h^\alpha}$ is required, where $\alpha > 0$. This condition is less restrictive than the condition necessary for the explicit algorithm.

Knowing Ω_n^F, Ω_{n+1}^F, $\mathbf{V}^n$, $\boldsymbol{\vartheta}^{n+1}$, find $\mathbf{v}^{n+1}$ and p^{n+1} such that

$$\mathbf{v}^{n+1}\left(\mathbf{X}+\mathbf{u}_h^{n+1}(\mathbf{X})\right) = \sum_{i=1}^m \frac{q_i^{n+1}-q_i^n}{\Delta t}\boldsymbol{\phi}_h^i(\mathbf{X}), \quad \forall \mathbf{X}\in\Gamma_0, \tag{1.28}$$

$$\begin{aligned}
&\int_{\Omega_{n+1}^F} \rho^F \left(\frac{\mathbf{v}^{n+1}-\mathbf{V}^n}{\Delta t}\right)\cdot\mathbf{w}^F d\mathbf{x} + \int_{\Omega_{n+1}^F} \rho^F \left(\left(\left(\mathbf{V}^n - \boldsymbol{\vartheta}^{n+1}\right)\cdot\nabla\right)\mathbf{v}^{n+1}\right)\cdot\mathbf{w}^F d\mathbf{x} \\
&+ \int_{\Omega_{n+1}^F} 2\mu^F \epsilon\left(\mathbf{v}^{n+1}\right) : \epsilon\left(\mathbf{w}^F\right) d\mathbf{x} - \int_{\Omega_{n+1}^F} \left(\nabla\cdot\mathbf{w}^F\right) p^{n+1} d\mathbf{x} \\
&= \int_{\Omega_{n+1}^F} \mathbf{f}^F\cdot\mathbf{w}^F d\mathbf{x} + \int_{\Sigma_1} \mathbf{h}_{in}^{n+1}\cdot\mathbf{w}^F d\, s \\
&+ \int_{\Sigma_3} \mathbf{h}_{out}^{n+1}\cdot\mathbf{w}^F d\, s, \ \forall\mathbf{w}^F = 0 \text{ on } \Sigma_2\cup\Gamma_{n+1},
\end{aligned} \tag{1.29}$$

$$-\int_{\Omega_{n+1}^F} \left(\nabla\cdot\mathbf{v}^{n+1}\right) q \, d\mathbf{x} = 0, \quad \forall q, \tag{1.30}$$

where $\mathbf{V}^n(\mathbf{x}) = \mathbf{v}^n\left(\mathcal{A}_{t_n} \circ \mathcal{A}^{-1}_{t_{n+1}}(\mathbf{x})\right)$ and

$$\boldsymbol{\vartheta}^{n+1}(\mathbf{x}) = \frac{\mathcal{A}_{t_{n+1}}(\widehat{\mathbf{x}}) - \mathcal{A}_{t_n}(\widehat{\mathbf{x}})}{\Delta t} = \frac{\mathbf{x} - \mathcal{A}_{t_n} \circ \mathcal{A}^{-1}_{t_{n+1}}(\mathbf{x})}{\Delta t}.$$

The condition (1.28) is the discrete version of the continuity of the velocity at the interface (1.12).

Building the discrete ALE map

Let $\mathcal{T}_h^0$ be a mesh of triangular finite elements for the reference domain $\widehat{\Omega}^F = \Omega_0^F$. If we know the displacement of the structure $\widetilde{\mathbf{u}}_h^{n+1} : \Omega^S \to \mathbb{R}^2$, we can compute $\widetilde{\mathbf{d}}^{n+1} : \Omega_0^F \to \mathbb{R}^2$ from the following boundary value problem:

$$\begin{aligned} \Delta\widetilde{\mathbf{d}}^{n+1} &= 0, \quad \text{on } \Omega_0^F, &(1.31)\\ \widetilde{\mathbf{d}}^{n+1} &= \widetilde{\mathbf{u}}_h^{n+1}, \quad \text{on } \Gamma_0, &(1.32)\\ \widetilde{\mathbf{d}}^{n+1} &= 0, \quad \text{on } \Sigma_1 \cup \Sigma_2 \cup \Sigma_3. &(1.33)\end{aligned}$$

We can set the discrete ALE map as follows $\mathcal{A}_{h,n+1}(\widehat{\mathbf{x}}) = \widehat{\mathbf{x}} + \widetilde{\mathbf{d}}^{n+1}(\widehat{\mathbf{x}})$ and the mesh for the domain at time instant t_{n+1} can be obtained by

$$\widetilde{\mathcal{T}}_h^{n+1} = \mathcal{A}_{h,n+1}\left(\mathcal{T}_h^0\right). \tag{1.34}$$

Sometimes, especially for non-convex domains, the ALE map obtained by harmonic extension reverses the triangles of the reference domain and produces non-valid mesh. An alternative technique is to minimize the energy of a mechanical system formed by a set of springs that joins the mesh nodes. A penalty term could ensures that the triangles are not reversed.

The mesh velocity is computed by the finite difference formula

$$\widetilde{\boldsymbol{\vartheta}}^{n+1}(\mathbf{x}) = \frac{\widetilde{\mathbf{d}}^{n+1}(\widehat{\mathbf{x}}) - \widetilde{\mathbf{d}}^{n}(\widehat{\mathbf{x}})}{\Delta t}. \tag{1.35}$$

If we predict explicitly the structure displacement by the formula $\widetilde{\mathbf{u}}_h^{n+1} = 2\mathbf{u}_h^n - \mathbf{u}_h^{n-1}$, we can obtain directly the mesh velocity as the solution of

$$\begin{aligned} \Delta\widetilde{\boldsymbol{\vartheta}}^{n+1} &= 0, \quad \text{on } \Omega_0^F,\\ \widetilde{\boldsymbol{\vartheta}}^{n+1} &= \frac{2\mathbf{u}_h^n - 3\mathbf{u}_h^{n-1} + \mathbf{u}_h^{n-2}}{\Delta t}, \quad \text{on } \Gamma_0,\\ \widetilde{\boldsymbol{\vartheta}}^{n+1} &= 0, \quad \text{on } \Sigma_1 \cup \Sigma_2 \cup \Sigma_3.\end{aligned}$$

Now, the right side part of the boundary condition on Γ_0 depends on the displacements of the structure obtained after solving the coupled problem at previous time steps. Other possibility used in [18] is to prescribe the mesh velocity at the interface to be $\dfrac{3\dot{\mathbf{u}}_h^n - \dot{\mathbf{u}}_h^{n-1}}{2}$ which is Adams-Bashforth formula. We have denoted by $\dot{\mathbf{u}}_h^n$ an approximation of the structure velocity at time instant t_n. Also, we can use higher order multi-step backward extrapolating schemes.

1.5 Implicit and Semi-implicit time integration schemes

The method that we use here to solve the coupled problem uses partitioned procedure (the fluid and structure equations are solved separately), which is very often used technique to solve fluid-structure interaction problems. In this way, the exiting solvers for each problem can be employed. Alternatively, the fluid-structure interaction problems could be solved by monolithic algorithms [31].

At each time step, an optimization problem of the form

$$\inf_{\boldsymbol{\alpha}\in\mathbb{R}^m} J(\boldsymbol{\alpha})$$

has to be solved. This technique was successful employed in [16], [17], where implicit algorithms are presented. We will use the same least square method based on the Broyden, Fletcher, Goldford, Shano (BFGS) method in order to impose the continuity of the stress at the interface. Details on the BFGS algorithm can be found in [32].

1.5.1 The structure is governed by a linear model and solved by modal decomposition

In a previous section, we have denoted by

$$\alpha_i(t) = \int_{\Gamma_0} \left(\sigma^S \mathbf{n}^S\right)(t) \cdot \boldsymbol{\phi}^i d\,s.$$

The stress at the fluid-structure interface $\left(\sigma^S \mathbf{n}^S\right)(t)$ is not known. Since the stress is continuous across the interface, we obtain that

$$\int_{\Gamma_0} \left(\sigma^S \mathbf{n}^S\right)(t) \cdot \boldsymbol{\phi}^i d\,s = -\int_{\Gamma_0} \left(\sigma^F \mathbf{n}^F\right)_{(\mathbf{X}+\mathbf{u}(\mathbf{X},t),t)} \cdot \boldsymbol{\phi}^i d\,s.$$

Consequently, if we set

$$\beta_i(t) = -\int_{\Gamma_0} \left(\sigma^F \mathbf{n}^F\right)_{(\mathbf{X}+\mathbf{u}(\mathbf{X},t),t)} \cdot \boldsymbol{\phi}^i d\,s, \tag{1.36}$$

we get

$$\alpha_i(t) = \beta_i(t), \quad \forall\, i \geq 1,\ \forall\, t \in [0,T].$$

After the full discretization, this equality does not hold and it will be treated by the least squares method.

How the stress at the fluid-structure interface is computed:

Method 1. The integral (1.36) mixes functions defined on different domains: the fluid stress tensor defined in the fluid domain, the unit outer normal vector defined on the interface and an eigenfunction defined in the structure domain. If $\mathbf{v}_h$ and p_h are finite element approximations of fluid velocity and pressure, respectively, we can define σ_h^F the $\mathbb{P}_1$ interpolation of $-p_h\mathbb{I}_2 + 2\mu^F\epsilon\,(\mathbf{v}_h)$. On every segment of the interface, we can compute the normal $\mathbf{n}_h^F$. Let us define

$$\mathbf{g}_h = \sigma_h^F \mathbf{n}_h^F$$

which is a piecewise linear function on the interface, but not continuous. Without supplementary computations, we set

$$\widehat{\mathbf{g}}_h(\mathbf{X},t) = \mathbf{g}_h\left(\mathbf{X} + \mathbf{u}_h\left(\mathbf{X},t\right),t\right).$$

More precisely, in a node $\mathbf{P}$ of the mesh of Γ_0, the finite element function $\widehat{\mathbf{g}}_h$ takes the same value as $\mathbf{g}_h$ in the node $\mathbf{P}+\mathbf{u}_h\left(\mathbf{P},t\right)$ of the mesh of Γ_t. Though both finite element functions $\widehat{\mathbf{g}}_h$ and $\boldsymbol{\phi}_h^i$ are defined on Γ_0, the first one use a grid derived from the fluid mesh and the other use the structure mesh which are not necessarily compatible at the interface. Finally, we compute

$$\beta_i(t) = -\int_{\Gamma_0} \widehat{\mathbf{g}}_h \cdot \boldsymbol{\phi}_h^i d\, s.$$

Method 2. Alternatively, we can approach $\beta_i(t)$ by

$$-\int_{\Gamma_t} \left(\sigma_h^F \mathbf{n}_h^F\right) \cdot \boldsymbol{\phi}_h^i \left(\mathbb{T}^{-1}\right) d\, s.$$

Method 3. Let us introduce the fluid stress tensor defined on the reference domain $\widehat{\Omega}^F$ of components

$$\widehat{\Sigma}_{ij}^F = -\widehat{p}\,\delta_{ij} + \mu^F\left(\frac{\partial \widehat{v}_i}{\partial \widehat{x}_j} + \frac{\partial \widehat{v}_j}{\partial \widehat{x}_i}\right).$$

We can approach $\beta_i(t)$ by

$$-\int_{\Gamma_0} \left(\widehat{\Sigma}^F \widehat{\mathbf{n}}^F\right) \cdot \boldsymbol{\phi}^i d\, s.$$

Contrary to the first two methods, where $\mathbf{n}^F$ have to be computed on the moving interface, the third one requires the computation of $\widehat{\mathbf{n}}^F$ on the reference interface.

Method 4. In [33] was introduced a technique which is popular because the computation of the normal vector to the interface is not necessary. The structure load is computed as the residual of the first fluid equation.

We have employed for the numerical simulation the second and the third methods which are more adapted to our computational environment.

Implicit time advancing algorithm

Suppose that at the previous time steps we know: $\boldsymbol{\alpha}^{n-1}, \boldsymbol{\alpha}^n \in \mathbb{R}^m$ and $\mathbf{q}^{n-1}, \mathbf{q}^n \in \mathbb{R}^m$.

Step 1. Solve by BFGS method starting from the point $\boldsymbol{\alpha}^n$ the optimization problem

$$\boldsymbol{\alpha}^{n+1} \in \arg \min_{\boldsymbol{\alpha} \in \mathbb{R}^m} J(\boldsymbol{\alpha}),$$

where the cost function is computed as following:

i) Solve the structure problem. We obtain $\mathbf{q}^{n+1}$ from (1.25), where $\boldsymbol{\alpha}^{n+1}$ was replaced by $\boldsymbol{\alpha}$. Then set the displacement of the structure $\mathbf{u} = \sum_{i=1}^m q_i^{n+1} \boldsymbol{\phi}^i$.

ii) Build a fluid mesh $\mathcal{T}$ depending on the displacement $\mathbf{u}$.

iii) Solve the fluid problem on the mesh $\mathcal{T}$ under prescribed velocity at the fluid-structure interface in order to get the fluid velocity $\mathbf{v}$ and pressure p.

iv) Compute β_i from (1.36) for $i = 1, \ldots, m$.

v) Set the cost function
$$J(\boldsymbol{\alpha}) = \frac{1}{2} \|\boldsymbol{\alpha} - \boldsymbol{\beta}\|^2_{\mathbb{R}^m}.$$

Step 2. Save the mesh $\mathcal{T}^{n+1}$, the structure displacement $\mathbf{u}^{n+1}$, the fluid velocity $\mathbf{v}^{n+1}$, the fluid pressure p^{n+1} obtained at the last iteration of the BFGS algorithm at **Step 1**.

Remark 1.2 *We emphasize that in the implicit strategy, the fluid mesh changes at each call of the cost function during the minimization process. Consequently, the fluid matrix at the step iii) have to be assembled and factorized at every cost function call.*

Now, let us introduce the semi-implicit algorithm. The term "semi-implicit" means that the interface position is computed explicitly, while the displacement of the structure, velocity and the pressure of the fluid are computed implicitly. This kind of algorithm was introduced in [18]. Our algorithm propose a different strategy based on the least squares method in order to get the continuity of the stress at the fluid-structure interface. Also, the continuity of the velocity at the interface holds at each time step.

Semi-implicit time advancing algorithm

Step 1. Explicit prediction. Set $\widetilde{\mathbf{u}}_h^{n+1} = 2\mathbf{u}_h^n - \mathbf{u}_h^{n-1}$.

Step 2. Harmonic extension. Solve $\Delta\widetilde{\mathbf{d}}^{n+1} = 0$ in Ω_0^F, $\widetilde{\mathbf{d}}^{n+1} = \widetilde{\mathbf{u}}^{n+1}$ on Γ_0, $\widetilde{\mathbf{d}}^{n+1} = 0$ on $\Sigma_1 \cup \Sigma_2 \cup \Sigma_3$.

Step 3. Build mesh. Set $\mathcal{A}_{h,n+1}(\widehat{\mathbf{x}}) = \widehat{\mathbf{x}} + \widetilde{\mathbf{d}}^{n+1}(\widehat{\mathbf{x}})$. The mesh for the fluid domain at time instant t_{n+1} can be obtained by $\widetilde{\mathcal{T}}_h^{n+1} = \mathcal{A}_{h,n+1}(\mathcal{T}_h^0)$.

Step 4. Set the mesh velocity $\widetilde{\boldsymbol{\vartheta}}^{n+1}(\mathbf{x}) = \dfrac{\widetilde{\mathbf{d}}^{n+1}(\widehat{\mathbf{x}}) - \widetilde{\mathbf{d}}^{n}(\widehat{\mathbf{x}})}{\Delta t}$.

Step 5. Assembling the finite element matrix of fluid problem (1.29)–(1.30). Get a *LU* factorization of this matrix.

Step 6. Solve fluid-structure coupled problem in the fixed mesh $\widetilde{\mathcal{T}}_h^{n+1}$ by BFGS algorithm starting from the point $\boldsymbol{\alpha}^n$

$$\boldsymbol{\alpha}^{n+1} \in \arg\min_{\boldsymbol{\alpha}\in\mathbb{R}^m} J(\boldsymbol{\alpha}),$$

where the cost function is computed as following:

i) Solve the structure problem. We obtain $\mathbf{q}^{n+1}$ from (1.25), where $\boldsymbol{\alpha}^{n+1}$ was replaced by $\boldsymbol{\alpha}$. Then set the displacement of the structure $\mathbf{u} = \sum_{i=1}^m q_i^{n+1}\boldsymbol{\phi}^i$.

ii) Solve the fluid problem (1.29)–(1.30) on the mesh $\widetilde{\mathcal{T}}_h^{n+1}$ under prescribed velocity at the fluid-structure interface (1.28) in order to get the fluid velocity $\mathbf{v}$ and pressure p.

iii) Compute β_i from (1.36) for $i = 1, \ldots, m$.

iv) Set the cost function

$$J(\boldsymbol{\alpha}) = \frac{1}{2}\|\boldsymbol{\alpha} - \boldsymbol{\beta}\|_{\mathbb{R}^m}^2.$$

The gradient of the cost function is computed by finite differences.

Step 7. Update $\mathbf{q}^{n-1} \leftarrow \mathbf{q}^n$, $\mathbf{q}^n \leftarrow \mathbf{q}^{n+1}$, $\boldsymbol{\alpha}^{n-1} \leftarrow \boldsymbol{\alpha}^n$, $\boldsymbol{\alpha}^n \leftarrow \boldsymbol{\alpha}^{n+1}$, etc.

Remark 1.3 *The major advantage of this implementation consists in using during* ***Step 6****, the same factorized matrix of the fluid problem obtained at* ***Step 5****. This was possible because the fluid mesh and the left side of the equations (1.29)–(1.30) do not depend on* $\boldsymbol{\alpha}$*. Only the right side of equation (1.28) contains data (*$\mathbf{q}^{n+1}$*) which depends on* $\boldsymbol{\alpha}$*.*

1.5.2 The structure is governed by a non-linear model and solved by Newton's method

The stress at the interface $\mathbf{F}^{S,n+1} = \left(\sigma^S \mathbf{n}^S\right)(t_{n+1})$ in the θ-scheme (1.26) is unknown. We approach the stress at the interface at the time instant t_{n+1} by

$$\sum_{i=1}^{m} \xi_i^{n+1} \boldsymbol{\psi}^i,$$

where ξ_i^{n+1} have to be identified and $\boldsymbol{\psi}^i \in \left(L^2\left(\Gamma_0\right)\right)^2$ are shape functions. The shape functions $\boldsymbol{\psi}^i$ are not necessary compatible with the structure or fluid finite element functions. Possible choices for $\boldsymbol{\psi}^i$ are polynomial functions [15], finite element like functions [34]. In this chapter we have adopted $\boldsymbol{\psi}^i$ the solution of

$$a_S\left(\boldsymbol{\psi}^i, \mathbf{w}^S\right) = \mu_i \int_{\Gamma_0} \boldsymbol{\psi}^i \cdot \mathbf{w}^S d\mathbf{X},\ \forall\, \mathbf{w}^S \in \mathbf{W}^S, \qquad \int_{\Gamma_0} \boldsymbol{\psi}^i \cdot \boldsymbol{\psi}^j d\mathbf{X} = \delta_{ij}.$$

Let us emphasize that, contrary to the eigenfunction $\boldsymbol{\phi}^i$, the traces of $\boldsymbol{\psi}^i$ are orthonormal for the scalar product of $L^2\left(\Gamma_0\right)$.

The implicit and semi-implicit time advancing algorithms when the structure is governed by a non-linear model are the same as for the linear model, excepting the definition of the cost function.

The **Step 1** in the implicit algorithm becomes: solve the optimization problem by BFGS method starting from the point $\boldsymbol{\xi}^n$,

$$\boldsymbol{\xi}^{n+1} \in \arg\min_{\boldsymbol{\xi}\in\mathbb{R}^m} J(\boldsymbol{\xi}),$$

where the cost function is computed as following:

i) Solve the structure problem (1.26) by Newton's method under the load

$$\mathbf{F}^{S,n+1} = \sum_{i=1}^{m} \xi_i \boldsymbol{\psi}^i$$

and get the structure displacement $\mathbf{u}$. We recall that $a_S(\cdot,\cdot)$ is non-linear in the first argument.

ii) Build a fluid mesh $\mathcal{T}$ depending on the displacement $\mathbf{u}$.

iii) Solve the fluid problem on the mesh $\mathcal{T}$ under prescribed velocity at the fluid-structure interface in order to get the fluid velocity $\mathbf{v}$ and pressure p.

iv) Compute

$$\alpha_i = \int_{\Gamma_0} \left(\sum_{j=1}^{m} \xi_j \boldsymbol{\psi}^j \right) \cdot \boldsymbol{\psi}^i d\, s, \quad \beta_i = -\int_{\Gamma_0} \left(\sigma^F \mathbf{n}^F \right)_{(\mathbf{X}+\tilde{\mathbf{u}}(\mathbf{X},t),t)} \cdot \boldsymbol{\psi}^i d\, s, \quad i = 1, \dots, m.$$

vi) Set the cost function

$$J(\boldsymbol{\alpha}) = \frac{1}{2} \|\boldsymbol{\alpha} - \boldsymbol{\beta}\|^2_{\mathbb{R}^m}.$$

Similarly, the **Step 6** in the semi-implicit algorithm becomes: solve by BFGS the optimization problem

$$\boldsymbol{\xi}^{n+1} \in \arg \min_{\boldsymbol{\xi} \in \mathbb{R}^m} J(\boldsymbol{\xi}),$$

where the cost function is computed as following:

i) Solve the structure problem (1.26) by Newton's method under the load

$$\mathbf{F}^{S,n+1} = \sum_{i=1}^{m} \xi_i \boldsymbol{\psi}^i$$

and get the structure displacement $\mathbf{u}$. We recall that $a_S(\cdot,\cdot)$ is non-linear in the first argument.

ii) Solve the fluid problem (1.29)–(1.30) on the mesh $\widetilde{\mathcal{T}}_h^{n+1}$ under prescribed velocity at the fluid-structure interface $\dfrac{\mathbf{u} - \mathbf{u}^n}{\Delta t}$ in order to get the fluid velocity $\mathbf{v}$ and pressure p.

iii) Compute

$$\alpha_i = \int_{\Gamma_0} \left(\sum_{j=1}^{m} \xi_j \boldsymbol{\psi}^j \right) \cdot \boldsymbol{\psi}^i d\, s, \quad \beta_i = -\int_{\Gamma_0} \left(\sigma^F \mathbf{n}^F \right)_{(\mathbf{X}+\tilde{\mathbf{u}}(\mathbf{X},t),t)} \cdot \boldsymbol{\psi}^i d\, s, \quad i = 1, \dots, m.$$

iv) Set the cost function

$$J(\boldsymbol{\alpha}) = \frac{1}{2} \|\boldsymbol{\alpha} - \boldsymbol{\beta}\|^2_{\mathbb{R}^m}.$$

1.6 Numerical results

The numerical tests have been produced using *FreeFem++* (see [35]).

The computation has been made in a domain of length $L = 6\ cm$ and height $H = 1\ cm$. The viscosity of the fluid was taken to be $\mu = 0.035\ \frac{g}{cm \cdot s}$, its density $\rho^F = 1\ \frac{g}{cm^3}$. The thickness of the elastic wall is $h^S = 0.1\ cm$, the Young modulus $E = 3 \cdot 10^6\ \frac{g}{cm \cdot s^2}$, the Poisson ratio $\nu = 0.3$, the density $\rho^S = 1.1\ \frac{g}{cm^3}$. The Lamé parameters are computed by the formulas:

$$\lambda^S = \frac{\nu^S E}{(1 - 2\nu^S)(1 + \nu^S)}, \quad \mu^S = \frac{E}{2(1 + \nu^S)}.$$

The volume force in fluid and structure are $\mathbf{f}^F = (0, 0)^T$ and $\mathbf{f}^S = (0, 0)^T$. The prescribed boundary stress at the inlet is

$$\mathbf{h}_{in}(\mathbf{x}, t) = \begin{cases} (10^3(1 - \cos(2\pi t/0.025)),\ 0)^T, & \mathbf{x} \in \Sigma_1, 0 \leq t \leq 0.025 \\ (0,\ 0)^T, & \mathbf{x} \in \Sigma_1, 0.025 \leq t \leq T \end{cases}$$

and $\mathbf{h}_{out} = (0,\ 0)^T$ at the outlet.

Remark 1.4 *The above physical parameters correspond to the human blood flow in large arteries. Similar data were used in [2] and [3] where the structure is governed by the generalized string model. The explicit algorithm based on the leap-frog scheme for the structure and on the backward Euler scheme for the fluid fails for this particular application (see [2]). Moreover, an implicit algorithm based on a classical fixed point iteration is unstable. A small relaxation parameter is necessary in order to get the stability of the fixed point iterations (see[3]). The same problem as in the present chapter has been solved in [17], where the continuity of the velocity was treated by a Lagrange multiplier. The numerical results presented in [17] show that the continuity of the velocity is not very well respected and a small time step is necessary.*

1.6.1 Linear elasticity. The structure is fixed at the left and at the right sides

We have used for the structure a reference mesh of 60 triangles and 62 vertices and for the fluid a reference mesh of 1250 triangles and 696 vertices. The meshes are not necessary compatible at the interface (see Figure 1.2). The structure is fixed at the left and at the right sides.

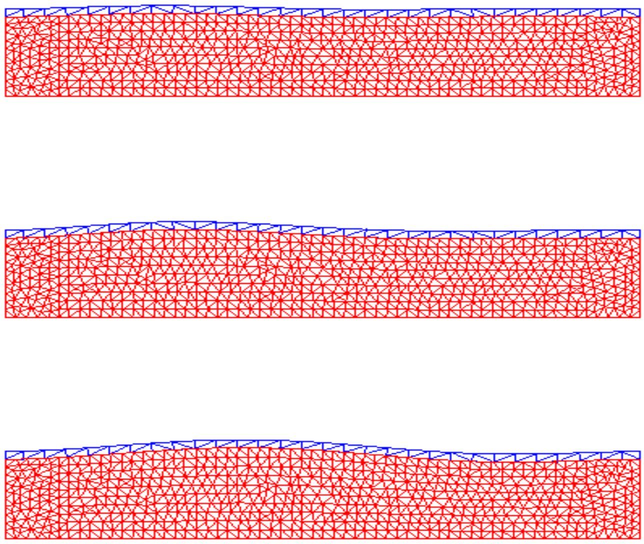

Figure 1.2: Linear elasticity. Fluid and structure meshes at time instant $t = 0.015$ (top), $t = 0.025$ (middle), $t = 0.035$ (bottom).

For the approximation of the fluid velocity and pressure we have employed the triangular finite elements $\mathbb{P}_1$+*bubble* and $\mathbb{P}_1$ respectively. The finite element $\mathbb{P}_1$ was used in order to solve the eigenproblem of the structure.

The first eigenvalues are: $\lambda_{1,h} = 7018.91$, $\lambda_{2,h} = 50500$, $\lambda_{3,h} = 193418$, $\lambda_{4,h} = 529809$, $\lambda_{5,h} = 832389$, $\lambda_{6,h} = 1.13276e^{06}$, $\lambda_{7,h} = 2.12627e^{06}$. For the physical parameters above and in view of the Remark 1.1, only the first $m = 3$ modes have been considered for instant. More modes do not quantitatively change the value of the structure displacement.

The real parameter in the centered scheme (1.25) was chosen to be $\theta = 0.25$.

Stopping criteria and the mean number of cost function calls

We have performed the simulation for a time duration $T = 0.1$ s, with the time step $\Delta t = 0.001$ s and $N = 100$ time iterations.

At each time step, the optimization problem have been solved by the BFGS algorithm. The final values of the cost function are less than $4.5 \cdot 10^{-10}$ (see Figure 1.3, top right).

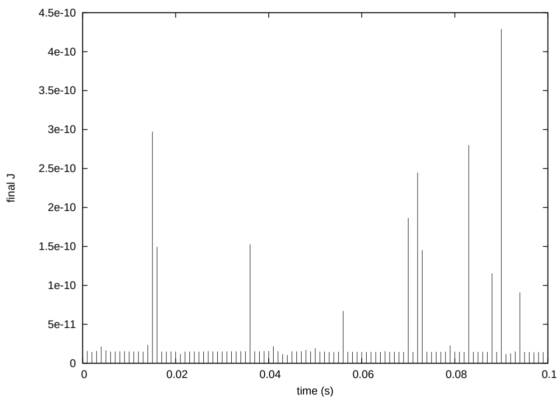

Figure 1.3: Linear elasticity. Time history of the final values of the cost function obtained by the BFGS method for $\Delta t = 0.001$.

We have employed the *FreeFem++* implementation of the BFGS algorithm which use the stopping criteria: $\|\nabla J\| < \epsilon$ or the number of iterations reaches a maximal value $nbiter$. We have performed the computations with $\epsilon = 10^{-4}$ and $nbiter = 10$. We set to 5 the maximal number of the iterations for the line search.

At each time step, the BFGS performs in average 6.08 iterations in the semi-implicit case and 6.24 iterations in the implicit case. At each BFGS iteration, 2.6 evaluations of the cost function are necessary in average for the line search and one call of the gradient. In this chapter, we compute $\nabla J(\boldsymbol{\alpha})$ by the finite differences scheme

$$\frac{\partial J}{\partial \alpha_k}(\boldsymbol{\alpha}) \approx \frac{J(\boldsymbol{\alpha} + \Delta\alpha_k \mathbf{e_k}) - J(\boldsymbol{\alpha})}{\Delta\alpha_k}$$

where $\mathbf{e_k}$ is the k-th vector of the canonical base of $\mathbb{R}^m$ and $\Delta\alpha_k = 10^{-6}$ is the grid spacing.

Consequently, $m+1 = 4$ calls of the cost function are needed in order to compute the gradient. To sum up, at each time step, the BFGS performs in average 40.24 evaluations of the cost function in the semi-implicit case and 41.61 iterations in the implicit case.

CPU time

The CPU time is 6 minutes and 14 seconds for $\Delta t = 0.001\ s$ and $N = 100$ time iterations on a computer with two processors of 3.6 GHz frequency.

In order to prove the superiority of the semi-implicit time advancing algorithm, we will compare to the CPU time obtained using implicit time advancing algorithm hich is of 71 minutes and 6 seconds. So the semi-implicit strategy is **11.34** times faster than the implicit one.

In the case of implicit strategy, at each evaluation of the cost function we have to solve one structure problem, to update the fluid mesh, to assembling the finite element matrix, to factorize it and to solve the fluid problem. We recall that, in the case of the semi-implicit time advancing algorithm, the evaluation of the cost function needs to solve a linear system, but what is of great practical importance consist in knowing a LU factorization of the matrix obtained at the **Step 5**.

Computational gain on a finer fluid mesh

Also, we have performed the computations for a fluid mesh of 1632 vertices and 3052 triangles. In this case, the CPU time is 13 minutes and 53 seconds when the semi-implicit strategy is employed and 173 minutes and 52 seconds in the case of the implicit strategy, which gives that the first one is **12.52** faster than the second.

Computational reduction when the number of eigenfunctions is $m = 7$

The CPU times is 193 minutes and 35 seconds in the case of the implicit strategy on fluid mesh of 1250 triangles and 696 vertices, when $m = 7$. The semi-implicit scheme takes 14 minutes and 30 seconds, therefore we get a reduction of factor **13.31**.

Stability

We have performed the simulation for time steps: $\Delta t = 0.0005\ s$, $\Delta t = 0.001\ s$, $\Delta t = 0.0025\ s$. The final values of the cost function are less than $8 \cdot 10^{-10}$ (see Figure 1.4).

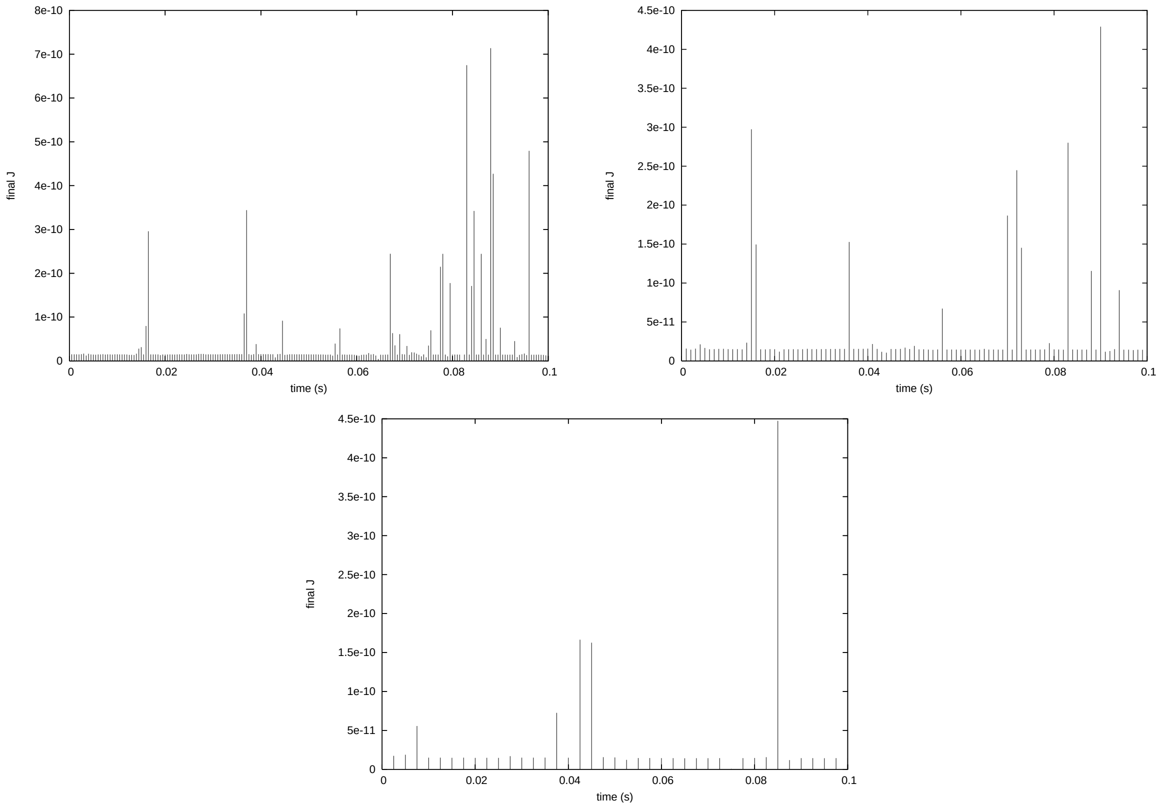

Figure 1.4: Linear elasticity. Time history of the final values of the cost function obtained by the BFGS method for $\Delta t = 0.0005$ (top, left), $\Delta t = 0.001$ (top, right), $\Delta t = 0.0025$ (bottom).

The semi-implicit algorithm has good stability properties, because the computed solution for moderate time steps are similar to the solution obtained by implicit method.

Behavior of the computed solution

The behavior of the fluid-structure interaction problem at different time instants is presented in Figures 1.2, 1.5, 1.6, and 1.7. A wave starts from the left side of the structure and it will be reflected at the right side. Movies with these simulations can be find at the address `http://www.edp.lmia.uha.fr/murea/`

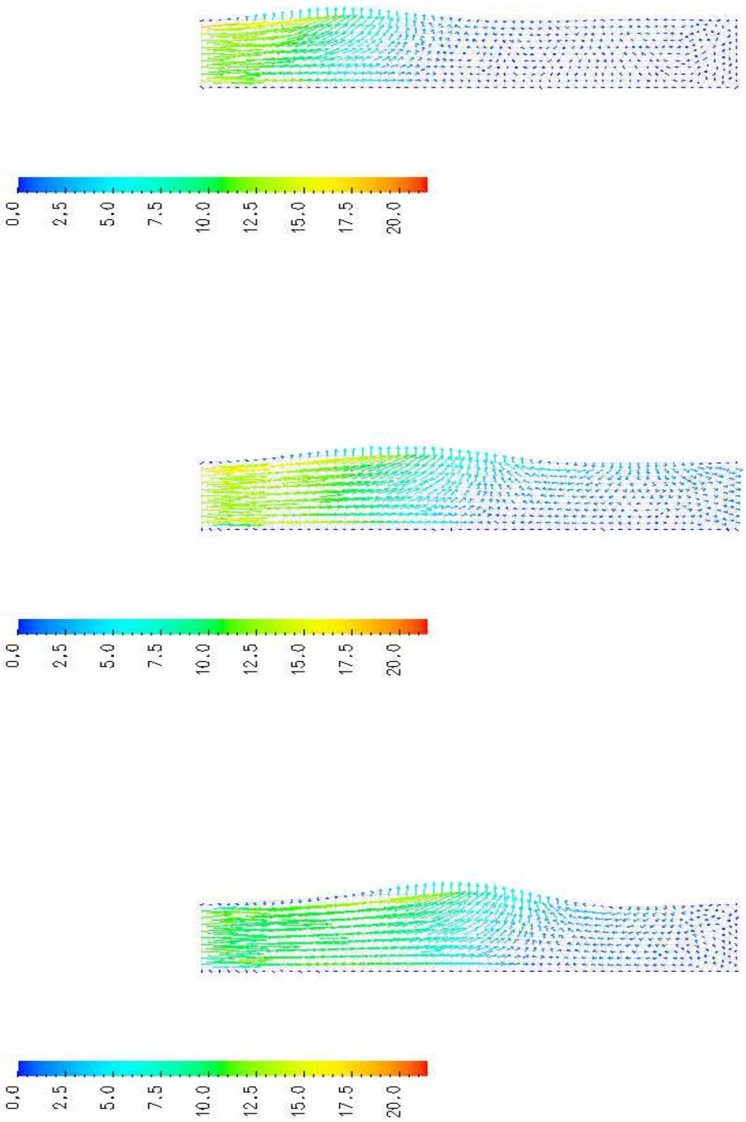

Figure 1.5: Linear elasticity. Fluid velocity $[cm/s]$ at time instant $t = 0.015$ (top), $t = 0.025$ (middle), $t = 0.035$ (bottom).

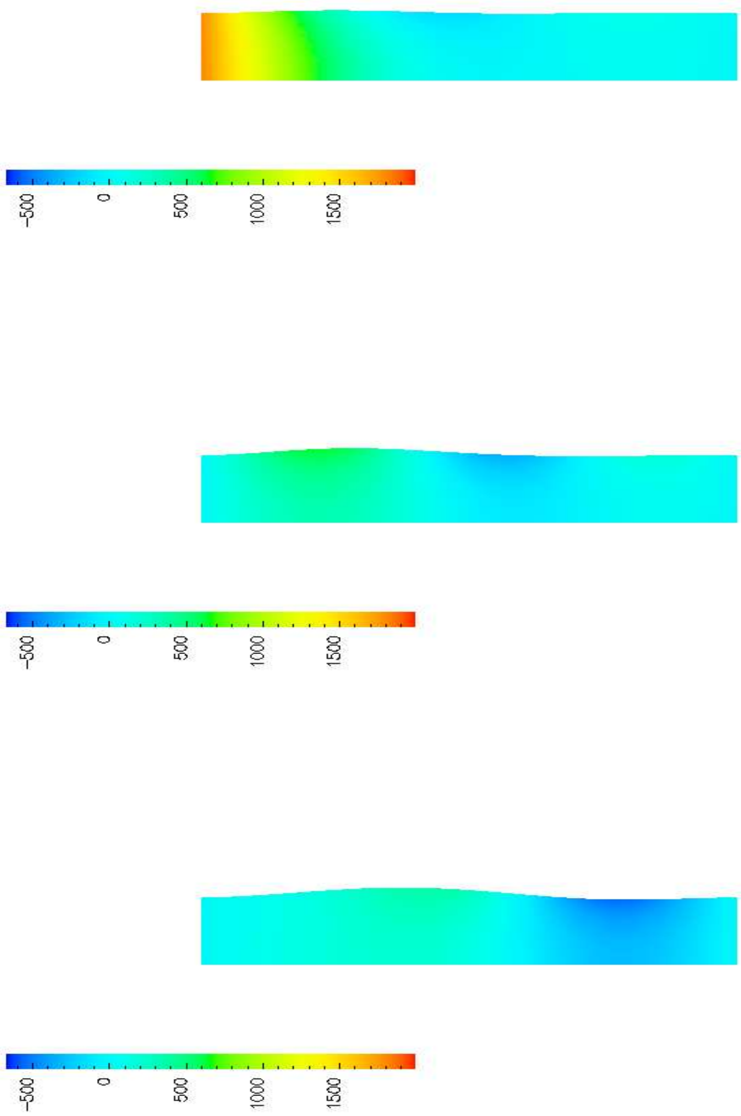

Figure 1.6: Linear elasticity. Fluid pressure $[\frac{dynes}{cm^2}]$ at time instant $t = 0.015$ (top), $t = 0.025$ (middle), $t = 0.035$ (bottom).

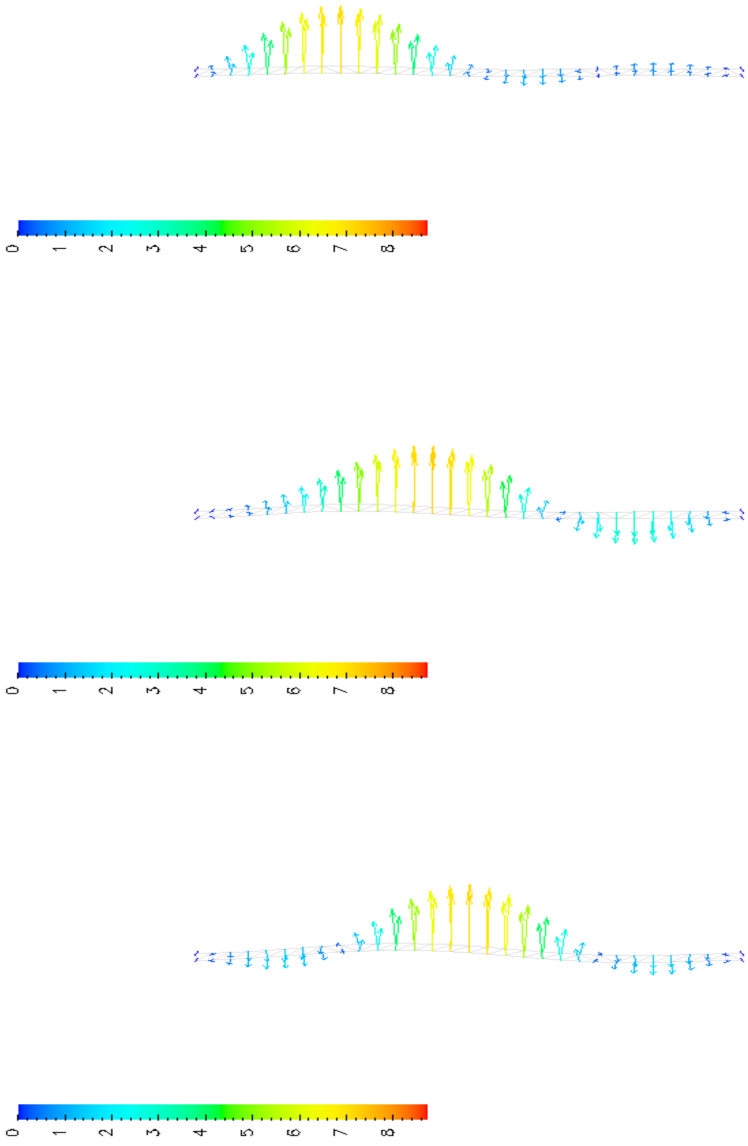

Figure 1.7: Linear elasticity. Structure velocity $[cm/s]$ at time instant $t = 0.015$ (top), $t = 0.025$ (middle), $t = 0.035$ (bottom).

1.6.2 Linear elasticity. The structure is fixed at the left and free at the right

In addition, we have performed simulation in the case when the horizontal displacement of the structure at the right side is supposed to be zero but the vertical displacement is free. In this case, when we build the discrete ALE map, the boundary condition on Σ_3 in problem (1.31)–(1.31) was replaced by

$$\widetilde{\mathbf{d}}^{n+1}(L, x_2) = \left(0,\ \frac{x_2\, \widetilde{u}_{h,2}(L, H)}{H}\right), \quad \forall x_2 \in (0, H).$$

Fluid and structure meshes at different time instants are shown in Figure 1.8.

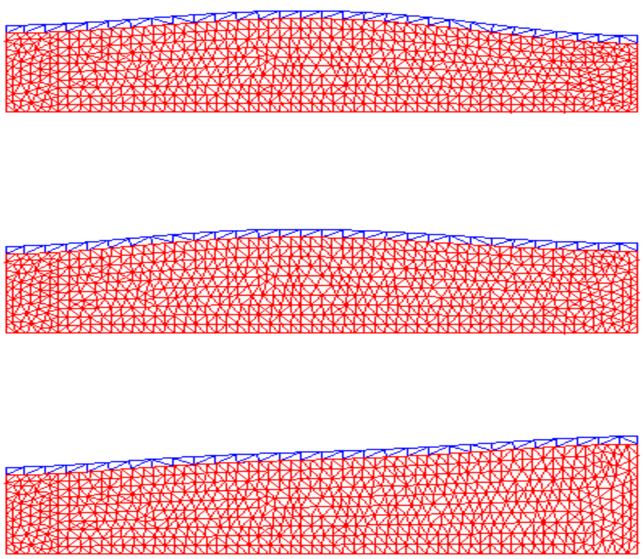

Figure 1.8: Linear elasticity and the left side of the structure is free. Fluid and structure meshes at time instant $t = 0.050$ (top), $t = 0.075$ (middle), $t = 0.100$ (bottom).

We have investigated the vertical displacement of three points on the interface of coordinates $x_1 = \dfrac{L}{4}$, $x_2 = \dfrac{L}{2}$, $x_3 = \dfrac{3L}{4}$, respectively (see Figure 1.9). We recall that L denotes the length of the undeformed interface.

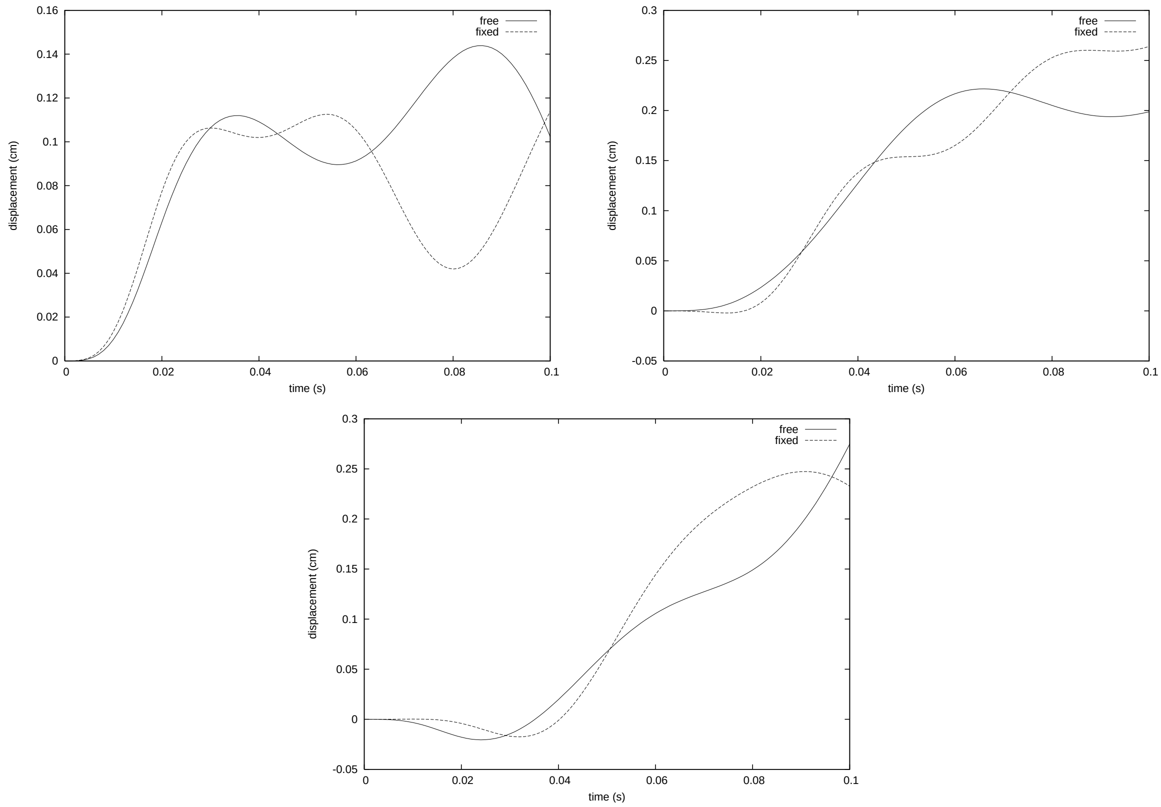

Figure 1.9: Linear elasticity. Time history of the vertical displacement of three points on the interface when the left side of the structure is fixed or free. Points of horizontal coordinate $x_1 = \dfrac{L}{4}$ (top, left), $x_2 = \dfrac{L}{2}$ (top, right), $x_3 = \dfrac{3L}{4}$ (bottom).

1.6.3 Non-linear elasticity. The structure is fixed at the left and at the right sides

We have used for the structure a reference mesh of 60 triangles and 62 vertices and for the fluid a reference mesh of 1250 triangles and 696 vertices. We use the same physical and numerical parameters as in the linear case. This time, at every cost function call, the structure problem is solved by the Newton's method. The finite element $\mathbb{P}_1$ was used in order to solve the linear system (1.27) at each Newton iteration.

The CPU time is 17 minutes and 13 seconds for $\Delta t = 0.001\ s$ and $N = 100$ time iterations on a computer with two processors of 3.6 GHz frequency. The CPU time obtained using implicit time advancing algorithm which is of 102 minutes and 26 seconds. So the semi-implicit strategy is **5.94** times faster than the implicit one.

At each time step, the BFGS performs in average 7.11 iterations in the semi-implicit case and 7.34 iterations in the implicit case. At each BFGS iteration, 2.62 evaluations of the cost function are necessary in average for the line search in the semi-implicit case and 2.60 iterations in the implicit case. One call of the gradient is necessary at each BFGS iteration for the both semi-implicit and implicit strategies. At each time step, the BFGS performs in average 47.10 evaluations of the cost function in the semi-implicit case and 48.48 iterations in the implicit case. Newton's method performs in average 2 iterations at every cost function call for the both semi-implicit and implicit strategies.

Figure 1.10 shows a good agreement between the solutions computed by the semi-implicit and implicit algorithm. In addition, we have performed simulation when the prescribed boundary stress at the inlet was magnified by a factor of 3. The maximal vertical displacement of the structure is about 0.6 cm.

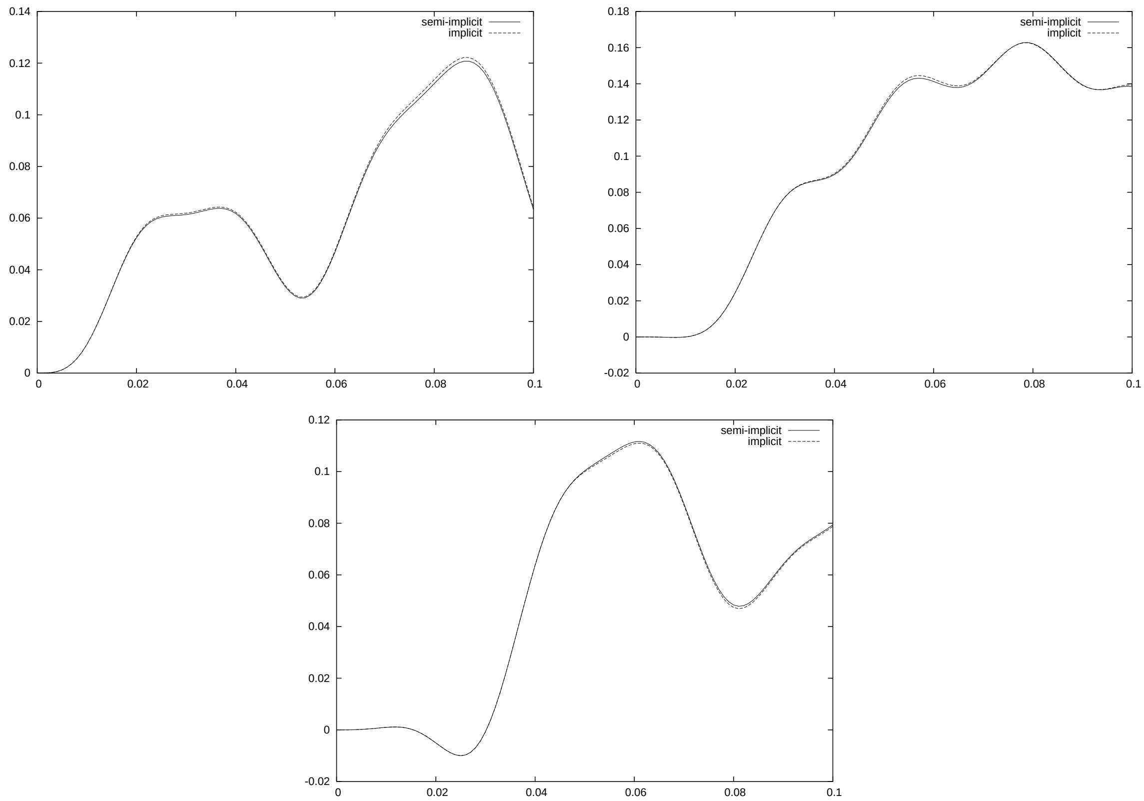

Figure 1.10: Non-linear elasticity. Time history of the vertical displacement of three points on the interface when the left side of the structure is fixed. Points of horizontal coordinate $x_1 = \dfrac{L}{4}$ (top, left), $x_2 = \dfrac{L}{2}$ (top, right), $x_3 = \dfrac{3L}{4}$ (bottom). We observe a good agreement between the curves obtained by the implicit and semi-implicit algorithms.

The fluid velocity is plotted in Figure 1.11.

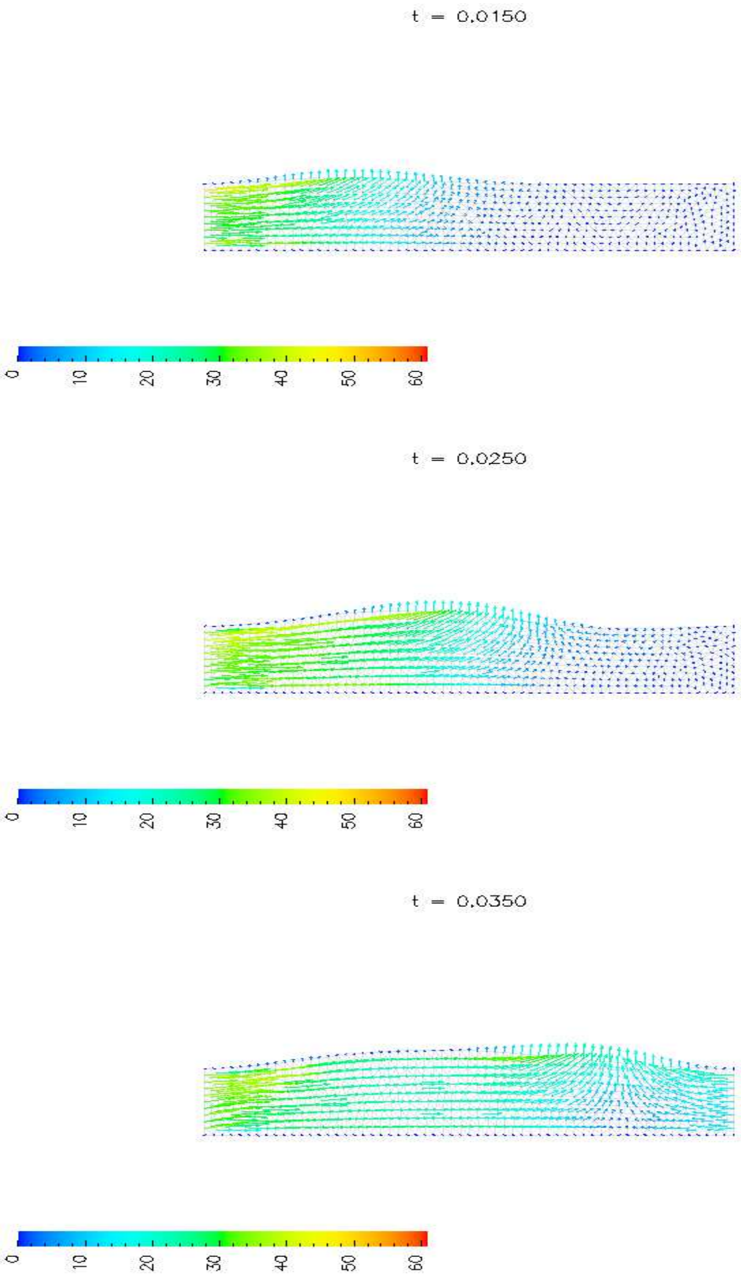

Figure 1.11: Non-linear elasticity. Fluid velocity $[cm/s]$ at time instant $t = 0.015$ (top), $t = 0.025$ (middle), $t = 0.035$ (bottom).

1.6.4 Discussions

The CPU time ratio of implicit and semi-implicit algorithms is **11.34** when the structure is governed by linear elasticity model and solved by modal decomposition, while the same ratio is **5.94** when the structure is non-linear and solved by Newton's method. In average, we have

$$\begin{aligned}
&\text{total CPU time ratio} = \frac{N \times \text{CPU time for one time step (implicit)}}{N \times \text{CPU time for one time step (semi-implicit)}} \\
&= \frac{\text{number of } J \text{ calls (implicit)}}{\text{number of } J \text{ calls (semi-implicit)}} \times \frac{\text{CPU time for one call of } J \text{ (implicit)}}{\text{CPU time for one call of } J \text{ (semi-implicit)}}.
\end{aligned}$$

In the linear case, we have

$$\begin{aligned}
11.34 &= \frac{41.61}{40.24} \times \frac{\text{CPU time for one call of } J \text{ (implicit)}}{\text{CPU time for one call of } J \text{ (semi-implicit)}} \\
&= \frac{41.61}{40.24} \\
&\times \frac{\text{CPU time fluid (implicit)} + \text{CPU time structure} + \text{CPU time other}}{\text{CPU time fluid (semi-implicit)} + \text{CPU time structure} + \text{CPU time other}}
\end{aligned}$$

and in the non-linear case, we have

$$\begin{aligned}
5.94 &= \frac{48.48}{47.10} \\
&\times \frac{\text{CPU time fluid (implicit)} + \text{CPU time structure} + \text{CPU time other}}{\text{CPU time fluid (semi-implicit)} + \text{CPU time structure} + \text{CPU time other}}.
\end{aligned}$$

Since the CPU time fluid (implicit) is greater that the CPU time fluid (semi-implicit), the function

$$x \longrightarrow \frac{\text{CPU time fluid (implicit)} + \text{x} + \text{CPU time other}}{\text{CPU time fluid (semi-implicit)} + \text{x} + \text{CPU time other}}$$

is decreasing for $x > 0$. This explains why in our application the ratio of the total CPU time decreases when the CPU time structure is longer, for example in the non linear case.

The ratio of the total CPU time depends also on the ratio of the number of the cost functions calls. In our application, we have employed the same BFGS method in order to solve the coupled fluid-structure problem at every time step. The ratio of the number of the cost functions calls is $\frac{41.61}{40.24}$ for a linear structure and $\frac{48.48}{47.10}$ in the non-linear case. But, if we employ a better method for solving the coupled fluid-structure problem in the semi-implicit algorithm, the denominators of the previous ratios decrease and then the ratio of the total CPU time increases.

A straightforward calculation leads to

$$\begin{aligned}
& \frac{\text{CPU time fluid (implicit)}}{\text{CPU time fluid (semi-implicit)}} \\
> \; & \frac{\text{CPU time fluid (implicit)} + \text{CPU time structure} + \text{CPU time other}}{\text{CPU time fluid (semi-implicit)} + \text{CPU time structure} + \text{CPU time other}} \\
= \; & 11.34 \times \frac{40.24}{41.61} = 11.06
\end{aligned}$$

which proves that the CPU time fluid is considerable reduced when the semi-implicit strategy is adopted to solve our particular application.

1.7 Conclusion

A semi-implicit algorithm for solving numerically an unsteady fluid-structure interaction problem was presented. At each time step, the position of the interface is predicted in an explicit way. The displacement of the structure, velocity and the pressure of the fluid are computed implicitly by solving at each time step an optimization problem such that the continuity of the velocity as well as the continuity of the stress hold at the interface. During the optimization process, the fluid mesh does not move, which reduces the computational effort. The semi-implicit algorithm has good stability properties even if the interface was computed explicitly.

Bibliography

[1] Farhat C, Lesoinne M. *Two efficient staggered algorithms for the serial and parallel solution of three-dimensional nonlinear transient aeroelastic problems*, Computer Methods in Applied Mechanics and Engineering 2000; **182**(3-4):499–515.

[2] Nobile F, *Numerical approximation of fluid-structure interaction problems with application to haemodynamics*, Ph.D. Thesis, EPFL, Switzerland, 2001.

[3] Causin P, Gerbeau JF, Nobile N, *Added-mass effect in the design of partitioned algorithms for fluid-structure problems*, Computer Methods in Applied Mechanics and Engineering 2005; **194**:4506–4527.

[4] Forster C, Wall WA, Ramm E, *Artificial added mass instabilities in sequential staggered coupling of nonlinear structures and incompressible viscous flows*, Computer Methods in Applied Mechanics and Engineering 2007; **196**(7):1278–1293.

[5] Le Tallec P, Mouro J, *Fluid-structure interaction with large structural displacements*, Computer Methods in Applied Mechanics and Engineering 2001; **190**(24-25):3039–3067.

[6] Formaggia L, Gerbeau GF, Nobile F, Quarteroni A, *On the coupling of 3D and 1D Navier-Stokes equations for flow problems in compliant vessels*, Computer Methods in Applied Mechanics and Engineering 2001; **191**(6-7):561–582.

[7] Fernandez MA, Le Tallec P, *Linear fluid-structure stability analysis with transpiration. Part I: formulation and mathematical analysis*, Computer Methods in Applied Mechanics and Engineering 2003; **192**:4805-4835.

[8] Deparis S, Fernández MA, Formaggia L, *Acceleration of a fixed point algorithm for fluid-structure interaction using transpiration conditions*, Mathematical Modelling and Numerical Analysis 2003; **37**(4):601-616.

[9] Steindorf J, Matthies HG, *Partioned but strongly coupled iteration schemes for nonlinear fluid-structure interaction*, Computers & Structures 2002; **80**:1991–1999.

[10] Gerbeau JF, Vidrascu M, *A quasi-Newton algorithm on a reduced model for fluid-structure interaction problems in blood flows*, Mathematical Modelling and Numerical Analysis 2003; **37**(4):631-648.

[11] Fernandez MA, Moubachir M, *A Newton method using exact jacobians for solving fluid-structure coupling*, Computers & Structures 2005; **83**(2-3):127-142.

[12] Dettmer W, Perić D, *A computational framework for fluid-structure interaction: Finite element formulation and applications*, Computer Methods in Applied Mechanics and Engineering 2006; **195**(41-43):5754-5779.

[13] Tezduyar TE, Sathe S, Keedy R, Stein K, *Space-time finite element techniques for computation of fluid-structure interactions*, Computer Methods in Applied Mechanics and Engineering 2006; **195**:2002–2027.

[14] Murea CM, Vazquez C, *Sensitivity and approximation of coupled fluid-structure equations by virtual control method*, Applied Mathematics and Optimization 2005; **52**(2):183–218.

[15] Murea CM, *The BFGS algorithm for a nonlinear least squares problem arising from blood flow in arteries*, Computer & Mathematics with Applications 2005; **49**:171–186.

[16] Murea CM, *Numerical simulation of a pulsatile flow through a flexible channel*, ESAIM: Mathematical Modelling and Numerical Analysis 2006; **40**(6):1101-1125.

[17] Mbaye I, Murea CM, *Numerical procedure with analytic derivative for unsteady fluid-structure interaction*, Communications in Numerical Methods in Engineering, published online 13 Jul 2007, DOI: 10.1002/cnm.1031.

[18] Fernandez MA, Gerbeau JF, Grandmont C, *A projection semi-implicit scheme for the coupling of elastic structure with an incompressible fluid*, International Journal for Numerical Methods in Engineering 2007; **69**(4):794–821.

[19] Nobile F, Vergara C, *An effective fluid-structure interaction formulation for vascular dynamics by generalized Robin conditions*, MOX Report 01/2007.

[20] Quarteroni A, Formaggia L, *Mathematical modelling and numerical simulation of the cardiovascular system*, in P.G. Ciarlet (Ed.), Handbook of numerical analysis, Vol. XII, North-Holland, Amsterdam, 2004, 3–127.

[21] Chen H, Sheu T, *Finite-element simulation of incompressible fluid flow in an elastic vessel*, International Journal for Numerical Methods in Fluids 2003; **42**:131–146.

[22] Baffico L, *A characteristic-ALE formulation for a fluid-membrane interaction problem*, Communications in Numerical Methods in Engineering 2005; **21**:723–734.

[23] Swim EW, Seshaiyer P, *A nonconforming finite element method for fluid-structure interaction problems*, Computer Methods in Applied Mechanics and Engineering 2006; **195**:2088–2099.

[24] Cai ZX, Luo XY, *A fluid-beam model for flow in collapsible channel*, Journal of Fluids and Structures 2003; **17**:125–146.

[25] Heil M, *An efficient solver for the fully coupled solution of large-displacement fluid-structure interaction problems*, Computer Methods in Applied Mechanics and Engineering 2004; **193**(1-2):1–23.

[26] Ciarlet PG, *Elasticité tridimensionnelle*, (French) Research in Applied Mathematics, 1. Masson, Paris, 1986.

[27] Dautray R, Lions JL, *Analyse mathématique et calcul numérique pour les sciences et les techniques*, Vol. 8, Paris, Masson, 1988.

[28] Chambolle A, Desjardins B, Esteban M, Grandmont C, *Existence of weak solutions for the unsteady interaction of a viscous fluid with an elastic plate*, Journal of Mathematical Fluid Mechanics 2005; **7**(3):368–404.

[29] Hughes Th, *The Finite Element Method: Linear Static and Dynamic Finite Element Analysis*, Dover, 2000.

[30] Temam R, *Navier-Stokes equations*, North-Holland, Amsterdam, 1979.

[31] Hron J, Turek S, *A monolithic FEM/multigrid solver for an ALE formulation of fluid-structure interaction with applications in biomechanics*, Fluid-structure interaction. 146–170, Lect. Notes Comput. Sci. Eng., **53**, Springer, Berlin, 2006.

[32] Dennis Jr. JE, Schnabel RB, *Numerical methods for unconstrained optimization and nonlinear equations*, Classics in Applied Mathematics, 16. Society for Industrial and Applied Mathematics, Philadelphia, PA, 1996.

[33] Farhat C, Lesoinne M, Le Tallec P, *Load and motion transfer algorithms for fluid/structure interaction problems with non-matching discrete interfaces: momentum and energy conservation, optimal discretization and application to aeroelasticity*, Computer Methods in Applied Mechanics and Engineering 1998; **21**:95–114.

[34] Mbaye I, Murea CM, *Approximation par la méthode des moindres carrés d'un problème bidimensionnel stationnaire d'interaction fluide-structure*, Proceedings of Euro-Mediterranean Conference on Bio-mathematics, Cairo, June 26-28, 2007.

[35] Hecht F, Pironneau O, *A finite element software for PDE: FreeFem++*, http://www.freefem.org.

[36] Murea CM, *A semi-implicit algorithm based on the Augmented Lagragian Method for fluid-structure interface*, in: K. Kunish, G. Of, O. Steinbach (eds.) Numerical Mathematics and Advanced Applications, Proceedings of ENUMAT 2007, the 7th Euopean Conference on Numerical Mathematics and Advanced Applications, Graz, Austria, Steptember 2007. Springer, pp. 555-562.

Chapter 2

A stable time advancing scheme for solving fluid-structure interaction problem at small structural displacements

This chapter is based on the paper:

S. Sy, C.M. Murea, *A Stable time advancing scheme for solving fluid-structure interaction problem at small structural displacements*, Comput. Methods Appl. Mech. Eng, **198** (2008), pp. 210-222, DOI: 10.1016/j.cma. 2008. 07. 010/ Published online: August, 3, 2008.

Abstract. A semi-implicit time advancing scheme for transient fluid-structure interaction problem is presented. At every time step, a least squares problem is solved by partitioned procedures, such that the continuity of the velocity as well as the continuity of the stress hold at the interface. During the iterative method for solving the optimization problem, the fluid mesh does not move, which reduces the computational effort. The stability of the algorithm is derived. The numerical results presented in this chapter show that the computed solution is similar to the one obtained by the implicit algorithm, but the computational time is reduced.

2.1 Introduction

In fluid-structure interaction problems, on the one hand, the stresses from the fluid move the structure and on the other hand, the fluid domain depends on the displacement of the structure. At the fluid-structure interface, the continuity of the stress and of the velocity are imposed. The flow inside a compliant vessel or the displacement of high buildings under the action of the wind are examples of fluid-structure interaction. We are interested in the haemodynamics applications such that the blood flow in large arteries.

Different time advancing algorithms have been developed for unsteady fluid-structure interaction: explicit, implicit and, recently, semi-implicit. In the explicit algorithms, the two coupling conditions are not verified simultaneously. For example, at a time step the continuity of the velocity holds, but the continuity of the stress across the interface is violated or inversely. Explicit algorithms have been successfully employed in aero-elasticity [8]. But, these algorithms are unstable when the structure is light and its density is comparable to that of the fluid [16], [4], [12]. Such situations appear in the bio-mechanics applications, for example.

At every time step of the implicit algorithms, the fluid domain as well as the displacement of the structure, velocity and the pressure of the fluid have to be determined by iterative methods. This can be done using fixed point strategies [21], [11], Newton or quasi-Newton methods [25], [14], [1], [9], [27], [6], [5]. Optimal control approaches have been employed in [19], [17] where, at each time step, an optimization problem must be solved. Contrary to Newton or fixed point iterations, the optimization approach is less sensitive to the starting point, which permits to use moderate time step. Numerical results presented in [19] suggest to use Modified Newton Method for small time step, while the optimization approach is preferable for moderate time step.

In the case of implicit algorithms, we emphasize that at a time instant, the fluid domain is changed in the interior of the loop where the structure displacement, the velocity and the pressure of the fluid are computed iteratively. The idea of semi-implicit algorithms is to compute explicitly the fluid domain out of the loop, then a frozen fluid mesh is used during the iterative algorithm until both coupling conditions at the interface hold. This strategy reduces the computational time.

A semi-implicit algorithm for a mono-dimensional simplified fluid-structure interaction problem is introduced in [13] and the stability in time is proved. In [21, Sec. 4.10, p. 138] a semi-implicit algorithm based on the Leap-Frog discretization for the structure and on the implicit Euler discretization for the fluid is presented. In order to linearize the convection term of Navier-Stokes equation, a supplementary fluid problem has to be solved. The stability is proved under a condition on the time step governed only by the structure. The author remarks at p. 140 that this condition might to be too restrictive in haemodynamics applications. The stability analysis of semi-implicit algorithms of first order in time for fluid-structure interaction problems can be found in [2] and [26]. In [10], a semi-implicit algorithm based on the Chorin-Temam projection scheme for incompressible flows is proposed. The stability has been proved when the fluid domain is fixed. The numerical results show that the computational time is reduced when the semi-implicit strategy is employed in place of the implicit one. Other semi-implicit algorithms are presented in [22], where the structure equation is embedded into the fluid equations and in [20], where the fluid-structure coupled problem is solved by the Augmented Lagrangian Method.

The aim of this chapter is to introduce a different semi-implicit algorithm for transient fluid-structure interaction problems. The main differences between our method and the ones proposed in [21], [2], [26] are: we use a centered scheme of order two in time for the structure and more general boundary conditions for the fluid. The unconditional stability of the algorithm is derived. Moreover, the numerical results presented in this chapter show that the computed solution is similar to the one obtained by the implicit algorithm, but the computational time is reduced.

2.2 Mathematical model and stability analysis

2.2.1 The mathematical model

We are interested in fluid-structure interaction problem in two dimensions. Let us denote by Ω^S the undeformed structure domain and we suppose that its boundary $\partial\Omega^S$ admits decomposition $\partial\Omega^S = \Gamma_D \cup \Gamma_N \cup \Gamma_0$, with $\Gamma_D = [AB] \cup [CD]$ and $\Gamma_N = [AD]$ (see Figure 2.1 on the left). We denote by Ω_0^F the initial fluid domain bounded by: Σ_1 the inflow section, Σ_2 the bottom boundary, Σ_3 the outflow section and Γ_0 the top boundary. The boundary Γ_0 is common to both domains and it represents the fluid-structure interface. Under the action of the fluid stress, the structure will be deformed. At the time instant t, the fluid occupies the domain Ω_t^F bounded by the moving interface Γ_t and by the rigid boundary $\Sigma = \Sigma_1 \cup \Sigma_2 \cup \Sigma_3$ (see Figure 2.1 at the right).

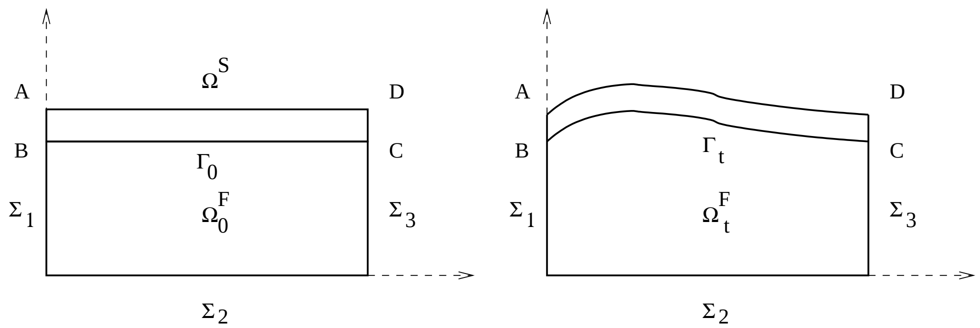

Figure 2.1: Initial configuration (left) and intermediate configuration (right).

We assume that the fluid is viscous, Newtonian and incompressible and it is governed by the Navier-Stokes equations. We also assume that the structure is governed by the linear elasticity equations. The coupling between the fluid and the structure is realized through two boundary conditions at the interface, namely, the continuity of the velocity and the equality of the stress. At each time $t \in [0, T]$, we are interested to know: the fluid velocity $\mathbf{v}(t) = (v_1(t), v_2(t))^T : \Omega_t^F \longrightarrow \mathbb{R}^2$, the fluid pressure $p(t) : \Omega_t^F \longrightarrow \mathbb{R}$ and the structure displacement $\mathbf{u}(t) = (u_1(t), u_2(t))^T : \Omega^S \longrightarrow \mathbb{R}^2$.

We are going to use the ALE (Arbitrary Lagrangian Eulerian) coordinates for the fluid equations, see for example [23]. Let $\widehat{\Omega}^F$ be the reference fixed domain and let $\mathcal{A}_t, t \in [0,T]$ be a family of transformations such that:

$$\mathcal{A}_t(\widehat{\mathbf{x}}) = \mathbf{x},\ \forall\, \widehat{\mathbf{x}} \in \widehat{\Omega}^F,\ \mathcal{A}_t(\widehat{\Omega}^F) = \Omega_t^F,$$

where $\widehat{\mathbf{x}} = (\widehat{x}_1, \widehat{x}_2)^T \in \widehat{\Omega}^F$ are the ALE coordinates and $\mathbf{x} = (x_1, x_2)^T \in \Omega_t^F$ are the Eulerian coordinates.
Let $\mathbf{v}$ be the fluid velocity in the Eulerian coordinates. We denote by $\widehat{\mathbf{v}} : \widehat{\Omega}^F \longrightarrow \mathbb{R}^2$ the corresponding function in the ALE coordinates, which is defined by:

$$\widehat{\mathbf{v}}(\widehat{\mathbf{x}}, t) = \mathbf{v}(\mathcal{A}_t(\widehat{\mathbf{x}}), t) = \mathbf{v}(\mathbf{x}, t).$$

We denote the domain velocity by:

$$\boldsymbol{\vartheta}(\mathbf{x}, t) = \frac{\partial \mathcal{A}_t}{\partial t}(\widehat{\mathbf{x}}) = \frac{\partial \mathcal{A}_t}{\partial t}\left(\mathcal{A}_t^{-1}(\mathbf{x})\right)$$

and the ALE time derivative of the fluid velocity by:

$$\left.\frac{\partial \mathbf{v}}{\partial t}\right|_{\widehat{\mathbf{x}}}(\mathbf{x}, t) = \frac{\partial \widehat{\mathbf{v}}}{\partial t}(\widehat{\mathbf{x}}, t).$$

We assume that the fluid-structure interaction is governed by the following equations:

Navier-Stokes

$$\begin{aligned}
\rho^F \left(\left.\frac{\partial \mathbf{v}}{\partial t}\right|_{\widehat{\mathbf{x}}} + ((\mathbf{v} - \boldsymbol{\vartheta}) \cdot \nabla)\, \mathbf{v} \right) - 2\mu^F \nabla \cdot \epsilon\,(\mathbf{v}) + \nabla p &= \mathbf{f}^F,\ \Omega_t^F \times (0,T] && (2.1)\\
\nabla \cdot \mathbf{v} &= 0,\ \Omega_t^F \times [0,T] && (2.2)\\
\sigma^F \mathbf{n}^F &= \mathbf{h}_{in},\ \Sigma_1 \times (0,T] && (2.3)\\
\sigma^F \mathbf{n}^F &= \mathbf{h}_{out},\ \Sigma_3 \times (0,T] && (2.4)\\
\mathbf{v} &= 0,\ \Sigma_2 \times (0,T] && (2.5)\\
\mathbf{v}(\mathbf{X}, 0) &= \mathbf{v}^0(\mathbf{X}),\ \Omega_0^F. && (2.6)
\end{aligned}$$

Linear elasticity

$$\begin{aligned}
\rho^S \frac{\partial^2 \mathbf{u}}{\partial t^2} - \nabla \cdot \sigma^S &= \mathbf{f}^S, \quad \text{in } \Omega^S \times (0,T] && (2.7)\\
\mathbf{u} &= 0, \quad \text{on } \Gamma_D \times (0,T] && (2.8)\\
\sigma^S \mathbf{n}^S &= 0, \quad \text{on } \Gamma_N \times (0,T] && (2.9)\\
\mathbf{u}(\mathbf{X}, 0) &= \mathbf{u}^0(\mathbf{X}), \quad \text{in } \Omega^S && (2.10)\\
\frac{\partial \mathbf{u}}{\partial t}(\mathbf{X}, 0) &= \dot{\mathbf{u}}^0(\mathbf{X}), \quad \text{in } \Omega^S. && (2.11)
\end{aligned}$$

Interface conditions

$$\begin{aligned} \mathbf{v}(\mathbf{X}+\mathbf{u}(\mathbf{X},t),t) &= \frac{\partial \mathbf{u}}{\partial t}(\mathbf{X},t), \quad \text{on } \Gamma_0 \times (0,T], & (2.12)\\ (\sigma^F \mathbf{n}^F)_{(\mathbf{X}+\mathbf{u}(\mathbf{X},t),t)} &= -(\sigma^S \mathbf{n}^S)_{(\mathbf{X},t)}, \quad \text{on } \Gamma_0 \times (0,T]. & (2.13) \end{aligned}$$

We have used the following notations:

$$\epsilon(\mathbf{v}) = \frac{1}{2}\Big(\nabla \mathbf{v} + (\nabla \mathbf{v})^T\Big), \quad \sigma^F = -p\mathbb{I}_2 + 2\mu^F \epsilon(\mathbf{v}), \quad \sigma^S = \lambda^S (\nabla \cdot \mathbf{u})\mathbb{I}_2 + 2\mu^S \epsilon(\mathbf{u}),$$

$\rho^F > 0$ is the mass density of the fluid (respectively $\rho^S > 0$ is the mass density of the structure), μ^F is the viscosity of the fluid (respectively μ^S and λ^S are the Lamé coefficients), $\mathbf{f}^F = (f_1^F, f_2^F)$ are the applied volume forces of the fluid, in general the gravity forces, (respectively $\mathbf{f}^S = (f_1^S, f_2^S)$ are the applied volume forces on the structure), $\mathbf{h}_{in}$ (respectively $\mathbf{h}_{out}$) is the prescribed boundary stress on Σ_1 (respectively on Σ_3). $\mathbf{n}^S = (n_1^S, n_2^S)$ and $\mathbf{n}^F = (n_1^F, n_2^F)$ are the unit outer normal vectors to $\partial\Omega_t^F$ and $\partial\Omega^S$ respectively. The interface Γ_t is the image of the boundary Γ_0 by the map:

$$\mathbb{T}_{\mathbf{u}}(\mathbf{X}) = \mathbf{X} + \mathbf{u}(\mathbf{X},t).$$

Remark 2.1 *In the system (2.1)–(2.13), the fluid and the structure are treated differently: on the one hand, the structure is governed by a linear elastic constitutive law adapted for small deformations and, on the other hand, the fluid equations are written in a moving domain. We are motivated by haemodynamics applications and for instance we study numerically the blood flow in a segment of artery of 6 cm length, 0.1 cm thickness and 1 cm diameter. In the real life, the deformation of the artery is about 0.1 cm and a linear mathematical model for the structure could be sufficient. Contrary to the elastic solids, the fluids are very sensitive to a moving boundary. This is probably due to weak intermolecular forces and even a small deformation of a boundary produces important modifications in a fluid flow. For this reason, it is necessary to write the fluid equations in a moving domain. Coupling Navier-Stokes equations with a linear model for the structure was used in [21], [11], [23], [2], [26] where the structure is governed by the independent rings or linear membrane model. In applications with large deformations of the structure, non-linear structure models have to be used as in [16], [14], [27], [10] (shells) or in [3] (beams). In a future work, we intend to replace the linear elasticity equations by a non-linear hyper-elastic model.*

2.2.2 Weak formulation of the model

Let $\mathbf{w}^F$ be a test function defined on Ω_t^F, such that $\mathbf{w}^F = 0$ on Σ_2. Let us multiply the equation (2.1) by $\mathbf{w}^F$ and using the Green's formula, we get:

$$\begin{aligned}
&\int_{\Omega_t^F} \rho^F \left.\frac{\partial \mathbf{v}}{\partial t}\right|_{\widehat{\mathbf{x}}} \cdot \mathbf{w}^F + \int_{\Omega_t^F} \rho^F \left(\left(\left(\mathbf{v}-\boldsymbol{\vartheta}\right)\cdot\nabla\right)\mathbf{v}\right)\cdot \mathbf{w}^F \\
&+ \int_{\Omega_t^F} 2\mu^F \epsilon\left(\mathbf{v}\right) : \epsilon\left(\mathbf{w}^F\right) - \int_{\Omega_t^F} \left(\nabla\cdot\mathbf{w}^F\right) p = \int_{\Omega_t^F} \mathbf{f}^F \cdot \mathbf{w}^F \\
&+ \int_{\Gamma_t} \left(\sigma^F \mathbf{n}^F\right)\cdot\mathbf{w}^F + \int_{\Sigma_1} \mathbf{h}_{in}\cdot\mathbf{w}^F + \int_{\Sigma_3} \mathbf{h}_{out}\cdot\mathbf{w}^F. \qquad (2.14)
\end{aligned}$$

Also, when we multiply the equation (2.7) by $\mathbf{w}^S : \Omega^S \longrightarrow \mathbb{R}^2$ such that $\mathbf{w}^S = 0$ on Γ_D, using again the Green's formula, we obtain:

$$\int_{\Omega^S} \rho^S \frac{\partial^2 \mathbf{u}}{\partial t^2}\cdot \mathbf{w}^S + a_S\left(\mathbf{u},\mathbf{w}^S\right) = \int_{\Omega^S} \mathbf{f}^S\cdot\mathbf{w}^S + \int_{\Gamma_0}\left(\sigma^S\mathbf{n}^S\right)\cdot\mathbf{w}^S, \qquad (2.15)$$

where

$$a_S\left(\mathbf{u},\mathbf{w}^S\right) = \int_{\Omega^S}\lambda^S\left(\nabla\cdot\mathbf{u}\right)\left(\nabla\cdot\mathbf{w}^S\right) + \int_{\Omega^S} 2\mu^S\epsilon\left(\mathbf{u}\right) : \epsilon\left(\mathbf{w}^S\right).$$

If $\mathbf{w}^S = \mathbf{w}^F \circ \mathbb{T}_{\mathbf{u}}$ at the interface Γ_0 and from the equation (2.13), we have :

$$\int_{\Gamma_0}\left(\sigma^S\mathbf{n}^S\right)\cdot\mathbf{w}^S + \int_{\Gamma_t}\left(\sigma^F\mathbf{n}^F\right)\cdot\mathbf{w}^F = 0. \qquad (2.16)$$

Now, if we multiply the equation (2.2) by $q \in L^2(\Omega_t^F)$, taking the sum with the precedent equations (2.14), (2.15) and referring to (2.16), we get the following weak formulation of (2.1)-(2.13):

Find $\mathbf{v} \in (H^1(\Omega_t^F))^2$; $\mathbf{v} = 0$ on $\Sigma_2 \times [0,T]$, $p \in L^2(\Omega_t^F)$ and $\mathbf{u} \in (H^1(\Omega^S))^2$; $\mathbf{u} = 0$ on Γ_D with $\mathbf{v}(\mathbf{X}+\mathbf{u}(\mathbf{X},t),t) = \dfrac{\partial \mathbf{u}}{\partial t}(\mathbf{X},t)$ on $\Gamma_0 \times [0,T]$ solving:

$$\begin{aligned}
&\int_{\Omega_t^F} \rho^F \left.\frac{\partial \mathbf{v}}{\partial t}\right|_{\widehat{\mathbf{x}}} \cdot \mathbf{w}^F + \int_{\Omega_t^F} \rho^F \left(\left(\left(\mathbf{v}-\boldsymbol{\vartheta}\right)\cdot\nabla\right)\mathbf{v}\right)\cdot \mathbf{w}^F \\
&+ \int_{\Omega_t^F} 2\mu^F \epsilon\left(\mathbf{v}\right) : \epsilon\left(\mathbf{w}^F\right) - \int_{\Omega_t^F} \left(\nabla\cdot\mathbf{w}^F\right) p - \int_{\Omega_t^F}\left(\nabla\cdot\mathbf{v}\right) q \\
&+ \int_{\Omega^S} \rho^S \frac{\partial^2 \mathbf{u}}{\partial t^2}\cdot\mathbf{w}^S + a_S\left(\mathbf{u},\mathbf{w}^S\right) = \int_{\Omega_t^F}\mathbf{f}^F\cdot\mathbf{w}^F + \int_{\Omega^S}\mathbf{f}^S\cdot\mathbf{w}^S \\
&+ \int_{\Sigma_1} \mathbf{h}_{in}\cdot\mathbf{w}^F + \int_{\Sigma_3} \mathbf{h}_{out}\cdot\mathbf{w}^F, \qquad (2.17)
\end{aligned}$$

for any $\mathbf{w}^F \in (H^1(\Omega_t^F))^2$; $\mathbf{w}^F = 0$ on $\Sigma_2 \times [0,T]$, $\mathbf{w}^S \in (H^1(\Omega^S))^2$; $\mathbf{w}^S = 0$ on Γ_D with $\mathbf{w}^F(\mathbf{X}+\mathbf{u}(\mathbf{X},t),t) = \mathbf{w}^S(\mathbf{X},t)$ on $\Gamma_0 \times [0,T]$ and for any $q \in L^2(\Omega_t^F)$.

2.2.3 Time discretization

Let $N \in \mathbb{N}^*$ be the number of time steps and we denote by $\Delta t = \dfrac{T}{N}$ the step time. We set $t_n = n\Delta t$ for $n = 0, \dots, N$ the subdivision points of $[0,T]$. We suppose that $\mathbf{f}^F : [0,T] \longrightarrow (L^2(\Omega_t^F))^2$, $\mathbf{h}_{in} : [0,T] \longrightarrow (L^2(\Sigma_1))^2$, $\mathbf{h}_{out} : [0,T] \longrightarrow (L^2(\Sigma_3))^2$ and $\mathbf{f}^S : [0,T] \longrightarrow (L^2(\Omega^S))^2$ are continuous maps and we set $\mathbf{f}^n = \mathbf{f}^F(n\Delta t)$, $\mathbf{h}_{in}^n = \mathbf{h}_{in}(n\Delta t)$, $\mathbf{h}_{out}^n = \mathbf{h}_{out}(n\Delta t)$ and $\mathbf{g}^n = \mathbf{f}^S(n\Delta t)$. We define $\mathbf{u}^n$ the approximation of $\mathbf{u}(n\Delta t)$.

For the fluid equations, we consider an implicit Euler scheme for the time derivative and a linearization of the convection term. For the structure, we employ a θ-centered scheme of second-order in time. We set $\widehat{\Omega}^F = \Omega_n^F$ and we define $\boldsymbol{\vartheta}^n = (\vartheta_1^n, \vartheta_2^n)^T$ the velocity of the fluid domain as solution of:

$$\left\{\begin{array}{lcll} \Delta_{\widehat{\mathbf{x}}}\boldsymbol{\vartheta}^n & = & 0, & \Omega_n^F \\ \boldsymbol{\vartheta}^n & = & 0, & \partial\Omega_n^F \setminus \Gamma_n \\ \boldsymbol{\vartheta}^n & = & \mathbf{v}^n, & \Gamma_n, \end{array}\right. \tag{2.18}$$

where $\mathbf{v}^n$ is the fluid velocity at time n on Ω_n^F. Under the assumption that Ω_n^F is Lipschitz, we have $\boldsymbol{\vartheta}^n \in (H^1(\Omega_n^F))^2$.

For all $n = 0, \cdots, N-1$, we denote by $\mathcal{A}_{t_{n+1}}$ the map from $\overline{\Omega}_n^F$ in $\mathbb{R}^2$ defined by:

$$\begin{array}{rcl} \mathcal{A}_{t_{n+1}}(\widehat{x}_1, \widehat{x}_2) : \overline{\Omega}_n^F & \longrightarrow & \mathbb{R}^2 \\ (\widehat{x}_1, \widehat{x}_2) & \mapsto & (\widehat{x}_1 + \Delta t \vartheta_1^n, \widehat{x}_2 + \Delta t \vartheta_2^n). \end{array}$$

We set $\Omega_{n+1}^F = \mathcal{A}_{t_{n+1}}(\Omega_n^F)$ and $\Gamma_{n+1} = \mathcal{A}_{t_{n+1}}(\Gamma_n)$. We define the map:

$$\mathbb{T} = \mathcal{A}_{t_n} \circ \mathcal{A}_{t_{n-1}} \cdots \circ \mathcal{A}_{t_1}$$

and we may observe that

$$\Gamma_n = \mathbb{T}(\Gamma_0).$$

The Jacobian of $\mathcal{A}_{t_{n+1}}$ is obtained by:

$$1 + \Delta t(\nabla_{\widehat{\mathbf{x}}} \cdot \boldsymbol{\vartheta}^n) + (\Delta t)^2\Big(\frac{\partial \vartheta_1^n}{\partial \widehat{x}_1} \cdot \frac{\partial \vartheta_2^n}{\partial \widehat{x}_2} - \frac{\partial \vartheta_2^n}{\partial \widehat{x}_1} \cdot \frac{\partial \vartheta_1^n}{\partial \widehat{x}_2}\Big).$$

We define the following spaces of test functions :

$$\begin{array}{rcl} \widehat{W}_n^F & = & \{\widehat{\mathbf{w}}^F \in (H^1(\Omega_n^F))^2;\ \widehat{\mathbf{w}}^F = 0 \text{ on } \Sigma_2\}, \\ \widehat{Q}_n^F & = & L^2(\Omega_n^F), \\ W^S & = & \{\mathbf{w}^S \in (H^1(\Omega^S))^2;\ \mathbf{w}^S = 0 \text{ on } \Gamma_D\}. \end{array}$$

We assume that we know Ω_n^F, $\mathbf{v}^n \in (L^2(\Omega_n^F))^2$, $\mathbf{u}^{n-1}, \mathbf{u}^n \in \big(L^2(\Omega^S)\big)^2$.

Step 1: Find $\boldsymbol{\vartheta}^n \in (H^1(\Omega_n^F))^2$ solution of the system (2.18).

Step 2: Find $\widehat{\mathbf{v}}^{n+1} \in \widehat{W}_n^F$, $\widehat{p}^{n+1} \in \widehat{Q}_n^F$, $\mathbf{u}^{n+1} \in W^S$ with $\widehat{\mathbf{v}}^{n+1} \circ \mathbb{T} = \dfrac{\mathbf{u}^{n+1} - \mathbf{u}^{n-1}}{2\Delta t}$ on Γ_0, such that:

$$\begin{aligned}
&\rho^F \int_{\Omega_n^F} \frac{(\widehat{\mathbf{v}}^{n+1} - \mathbf{v}^n)}{\Delta t} \cdot \widehat{\mathbf{w}}^F + \rho^F \int_{\Omega_n^F} (((\mathbf{v}^n - \boldsymbol{\vartheta}^n) \cdot \nabla_{\widehat{\mathbf{x}}})\widehat{\mathbf{v}}^{n+1}) \cdot \widehat{\mathbf{w}}^F \\
&+ \frac{\rho^F}{2} \int_{\Omega_n^F} \delta(\widehat{\mathbf{x}})\widehat{\mathbf{v}}^{n+1} \cdot \widehat{\mathbf{w}}^F + 2\mu^F \int_{\Omega_n^F} \epsilon_{\widehat{\mathbf{x}}}(\widehat{\mathbf{v}}^{n+1}) : \epsilon_{\widehat{\mathbf{x}}}(\widehat{\mathbf{w}}^F) \\
&- \int_{\Omega_n^F} \widehat{p}^{n+1}(\nabla_{\widehat{\mathbf{x}}} \cdot \widehat{\mathbf{w}}^F) - \int_{\Omega_n^F} \widehat{q}(\nabla_{\widehat{\mathbf{x}}} \cdot \widehat{\mathbf{v}}^{n+1}) \\
&+ \rho^S \int_{\Omega^S} \Big(\frac{\mathbf{u}^{n+1} - 2\mathbf{u}^n + \mathbf{u}^{n-1}}{\Delta t^2}\Big) \cdot \mathbf{w}^S + a_S(\theta \mathbf{u}^{n+1} + (1-2\theta)\mathbf{u}^n + \theta \mathbf{u}^{n-1}, \mathbf{w}^S) \\
&= \int_{\Omega_n^F} \widehat{\mathbf{f}}^{n+1} \cdot \widehat{\mathbf{w}}^F + \int_{\Omega^S} \bar{\mathbf{g}}^{n+1} \cdot \mathbf{w}^S + \int_{\Sigma_1} \mathbf{h}_{in}^{n+1} \cdot \widehat{\mathbf{w}}^F + \int_{\Sigma_3} \mathbf{h}_{out}^{n+1} \cdot \widehat{\mathbf{w}}^F,
\end{aligned} \tag{2.19}$$

for any $\widehat{\mathbf{w}}^F \in \widehat{W}_n$, $\widehat{q} \in \widehat{Q}_n^F$, $\mathbf{w}^S \in W^S$ with $\mathbf{w}^S = \widehat{\mathbf{w}}^F \circ \mathbb{T}$ on Γ_0, where

$$\widehat{\mathbf{f}}^{n+1} = \mathbf{f}^{n+1} \circ \mathcal{A}_{t_{n+1}} \text{ et } \bar{\mathbf{g}}^{n+1} = \theta \mathbf{g}^{n+1} + (1-2\theta)\mathbf{g}^n + \theta \mathbf{g}^{n-1}$$

and

$$\delta(\widehat{\mathbf{x}}) = \Delta t\Big(\frac{\partial \vartheta_1^n}{\partial \widehat{x}_1} \cdot \frac{\partial \vartheta_2^n}{\partial \widehat{x}_2} - \frac{\partial \vartheta_2^n}{\partial \widehat{x}_1} \cdot \frac{\partial \vartheta_1^n}{\partial \widehat{x}_2}\Big).$$

Remark 2.2 *Let us explain why the first term of the second line in (2.19) was added. First, this term contains Δt, therefore the scheme does not lose consistency after adding this term. The term containing $\delta(\widehat{\mathbf{x}})$ was added in order to obtain the stability without supplementary condition on the mesh velocity. We will see in the next section where the stability is proved that, adding the term containing $\delta(\widehat{\mathbf{x}})$ allows us to obtain the exact expression of the Jacobian of the map $\mathcal{A}_{t_{n+1}}$ and then, the integral over Ω_n^F of the terms containing the mesh velocity can be rewritten as an integral over Ω_{n+1}^F. In this way, the mesh velocity will be eliminated from the a-priori estimate. In fact, the mesh velocity is hidden in the definition of Ω_{n+1}^F.*

The system (2.19) can be reformulated as following :

$$\rho^F \int_{\Omega_n^F} \Big[\frac{\widehat{\mathbf{v}}^{n+1}}{\Delta t} + ((\mathbf{v}^n - \boldsymbol{\vartheta}^n)\cdot\nabla_{\widehat{\mathbf{x}}})\widehat{\mathbf{v}}^{n+1} + \frac{1}{2}\delta(\widehat{\mathbf{x}})\widehat{\mathbf{v}}^{n+1}\Big]\cdot\widehat{\mathbf{w}}^F$$
$$+a_F(\widehat{\mathbf{v}}^{n+1},\widehat{\mathbf{w}}^F) + b_F(\widehat{\mathbf{w}}^F,\widehat{p}^{n+1}) + b_F(\widehat{\mathbf{v}}^{n+1},\widehat{q})$$
$$+\rho^S\int_{\Omega^S}\Big(\frac{\mathbf{u}^{n+1}-2\mathbf{u}^n+\mathbf{u}^{n-1}}{\Delta t^2}\Big)\cdot\mathbf{w}^S$$
$$+a_S(\theta\mathbf{u}^{n+1}+(1-2\theta)\mathbf{u}^n+\theta\mathbf{u}^{n-1},\mathbf{w}^S) = \rho^F\int_{\Omega_n^F}\frac{\mathbf{v}^n}{\Delta t}\cdot\widehat{\mathbf{w}}^F$$
$$+\int_{\Omega_n^F}\widehat{\mathbf{f}}^{n+1}\cdot\widehat{\mathbf{w}}^F + \int_{\Omega^S}\overline{\mathbf{g}}^{n+1}\cdot\mathbf{w}^S + \int_{\Sigma_1}\mathbf{h}_{in}^{n+1}\cdot\widehat{\mathbf{w}}^F + \int_{\Sigma_3}\mathbf{h}_{out}^{n+1}\cdot\widehat{\mathbf{w}}^F, \quad (2.20)$$

for all $\widehat{\mathbf{w}}^F \in \widehat{W}_n^F$, $\mathbf{w}^S \in W^S$ with $\mathbf{w}^S = \widehat{\mathbf{w}}^F \circ \mathbb{T}$ on Γ_0 and $\widehat{q} \in \widehat{Q}_n^F$, where

$$a_F(\widehat{\mathbf{v}},\widehat{\mathbf{w}}^F) = 2\mu^F\int_{\Omega_n^F}\epsilon(\widehat{\mathbf{v}}):\epsilon(\widehat{\mathbf{w}}^F) \quad \text{and} \quad b_F(\widehat{\mathbf{w}}^F,\widehat{q}) = -\int_{\Omega_n^F}\widehat{q}(\nabla\cdot\widehat{\mathbf{w}}^F).$$

2.2.4 Stability

Let θ be a real. We denote by

$$X^n = \theta a_S(\mathbf{u}^n,\mathbf{u}^n) + (1-2\theta)a_S(\mathbf{u}^n,\mathbf{u}^{n-1}) + \theta a_S(\mathbf{u}^{n-1},\mathbf{u}^{n-1}) \quad (2.21)$$

and we define $\mathbf{v}^{n+1} : \Omega_{n+1}^F \longrightarrow \mathbb{R}^2$ the fluid velocity at time t_{n+1} on Ω_{n+1}^F by:

$$\mathbf{v}^{n+1}(\mathbf{x}) = \widehat{\mathbf{v}}^{n+1}(\widehat{\mathbf{x}}), \quad \forall\,\widehat{\mathbf{x}}\in\Omega_n^F, \text{ and } \mathbf{x} = \mathcal{A}_{t_{n+1}}(\widehat{\mathbf{x}}) \in \Omega_{n+1}^F.$$

We have the following stability result:

Theorem 2.1 *Let Ω_n^F be a bounded domain of $\mathbb{R}^2$ and assume that $\int_{\Sigma_1\cup\Sigma_3}(\mathbf{v}^n\cdot\mathbf{n}^F)|\widehat{\mathbf{v}}^{n+1}|^2$ is positive. If $\theta \in \Big[\frac{1}{4},\frac{1}{2}\Big]$, then the following energy estimation holds:*

$$\rho^F\|\mathbf{v}^{n+1}\|^2_{L^2(\Omega^F_{n+1})} + 2\mu^F\Delta t\|\epsilon_{\widehat{\mathbf{x}}}(\widehat{\mathbf{v}}^{n+1})\|^2_{L^2(\Omega_n^F)} + \rho^S\Big\|\frac{\mathbf{u}^{n+1}-\mathbf{u}^n}{\Delta t}\Big\|^2_{L^2(\Omega^S)}$$
$$+X^{n+1} \leq \exp(T)\Big[\rho^F\|\mathbf{v}^1\|^2_{L^2(\Omega_1^F)} + 2\mu^F\Delta t\|\epsilon_{\widehat{\mathbf{x}}}(\widehat{\mathbf{v}}^1)\|^2_{L^2(\Omega_0^F)}$$
$$+\rho^S\Big\|\frac{\mathbf{u}^1-\mathbf{u}^0}{\Delta t}\Big\|^2_{L^2(\Omega^S)} + X^1 + C\Big(\max_{t\in[0,T]}\|\mathbf{f}^F(t)\|^2_{L^2(\Omega_t^F)}$$
$$+\max_{t\in[0,T]}\|\mathbf{f}^S(t)\|^2_{L^2(\Omega^S)} + \max_{t\in[0,T]}\|\mathbf{h}_{in}(t)\|^2_{L^2(\Sigma_1)} + \max_{t\in[0,T]}\|\mathbf{h}_{out}(t)\|^2_{L^2(\Sigma_3)}\Big)\Big],$$

where $C > 0$ is independent of Δt.
Furthermore, we have

$$\|\mathbf{v}^{n+1}\|_{L^2(\Omega^F_{n+1})}, \quad \Delta t\|\epsilon_{\widehat{\mathbf{x}}}(\widehat{\mathbf{v}}^{n+1})\|_{L^2(\Omega^F_n)}, \quad \left\|\frac{\mathbf{u}^{n+1}-\mathbf{u}^n}{\Delta t}\right\|_{L^2(\Omega^S)} \text{ and } X^{n+1}$$

are bounded.

Before starting the proof of the stability theorem, we need to show some lemmas. We denote by

$$c_F(\widehat{\mathbf{v}}^{n+1}, \widehat{\mathbf{w}}^F) = \rho^F \int_{\Omega^F_n} \left[\frac{\widehat{\mathbf{v}}^{n+1}}{\Delta t} + ((\mathbf{v}^n - \boldsymbol{\vartheta}^n)\cdot\nabla_{\widehat{\mathbf{x}}})\widehat{\mathbf{v}}^{n+1} + \frac{1}{2}\delta(\widehat{\mathbf{x}})\widehat{\mathbf{v}}^{n+1}\right]\cdot\widehat{\mathbf{w}}^F.$$

Lemma 2.1 *The following inequality holds*

$$2\Delta t c_F(\widehat{\mathbf{v}}^{n+1}, \widehat{\mathbf{v}}^{n+1}) \geq \rho^F\|\widehat{\mathbf{v}}^{n+1}\|^2_{L^2(\Omega^F_n)} + \rho^F\|\mathbf{v}^{n+1}\|^2_{L^2(\Omega^F_{n+1})}.$$

Proof. Let us set $|\widehat{\mathbf{v}}^{n+1}|^2 = (\widehat{\mathrm{v}}^{n+1}_1)^2 + (\widehat{\mathrm{v}}^{n+1}_2)^2$, then we have:

$$\begin{aligned}
&2\Delta t c_F(\widehat{\mathbf{v}}^{n+1}, \widehat{\mathbf{v}}^{n+1})\\
&= 2\Delta t\rho^F \int_{\Omega^F_n} \left[\frac{\widehat{\mathbf{v}}^{n+1}}{\Delta t} + ((\mathbf{v}^n - \boldsymbol{\vartheta}^n)\cdot\nabla_{\widehat{\mathbf{x}}})\widehat{\mathbf{v}}^{n+1} + \frac{1}{2}\delta(\widehat{\mathbf{x}})\widehat{\mathbf{v}}^{n+1}\right]\cdot\widehat{\mathbf{v}}^{n+1}\\
&= 2\rho^F\int_{\Omega^F_n}|\widehat{\mathbf{v}}^{n+1}|^2 + 2\Delta t\rho^F\int_{\Omega^F_n}\left[((\mathbf{v}^n - \boldsymbol{\vartheta}^n)\cdot\nabla_{\widehat{\mathbf{x}}})\widehat{\mathbf{v}}^{n+1}\right]\cdot\widehat{\mathbf{v}}^{n+1}\\
&+\rho^F\Delta t\int_{\Omega^F_n}\delta(\widehat{\mathbf{x}})|\widehat{\mathbf{v}}^{n+1}|^2.
\end{aligned}$$

The middle term of the previous expression can be written as

$$2\Delta t\rho^F\int_{\Omega^F_n}\left[((\mathbf{v}^n - \boldsymbol{\vartheta}^n)\cdot\nabla_{\widehat{\mathbf{x}}})\widehat{\mathbf{v}}^{n+1}\right]\cdot\widehat{\mathbf{v}}^{n+1} = \rho^F\Delta t\int_{\Omega^F_n}(\mathbf{v}^n - \boldsymbol{\vartheta}^n)\cdot\nabla_{\widehat{\mathbf{x}}}(|\widehat{\mathbf{v}}^{n+1}|^2).$$

Now, when we integrate it by part we obtain :

$$\begin{aligned}
&\rho^F\Delta t\int_{\Omega^F_n}(\mathbf{v}^n - \boldsymbol{\vartheta}^n)\cdot\nabla_{\widehat{\mathbf{x}}}(|\widehat{\mathbf{v}}^{n+1}|^2) = -\rho^F\Delta t\int_{\Omega^F_n}\nabla_{\widehat{\mathbf{x}}}\cdot(\mathbf{v}^n - \boldsymbol{\vartheta}^n)|\widehat{\mathbf{v}}^{n+1}|^2\\
&+\rho^F\Delta t\int_{\partial\Omega^F_n}\Big((\mathbf{v}^n - \boldsymbol{\vartheta}^n)\cdot\mathbf{n}^F\Big)|\widehat{\mathbf{v}}^{n+1}|^2.
\end{aligned}$$

About the boundary term, we have

$$\rho^F\Delta t\int_{\partial\Omega^F_n}\Big((\mathbf{v}^n - \boldsymbol{\vartheta}^n)\cdot\mathbf{n}^F\Big)|\widehat{\mathbf{v}}^{n+1}|^2 \geq 0.$$

In fact this term vanishes on Γ_n since $\mathbf{v}^n = \boldsymbol{\vartheta}^n$, it vanishes again on Σ_2 since $\widehat{\mathbf{v}}^{n+1} = 0$. On $\Sigma_1 \cup \Sigma_3$, we have $\boldsymbol{\vartheta}^n = 0$ and $\displaystyle\int_{\Sigma_1 \cup \Sigma_3} (\mathbf{v}^n \cdot \mathbf{n}^F)|\widehat{\mathbf{v}}^{n+1}|^2$ is supposed to be positive.

Using now the assumption that $\nabla_{\widehat{\mathbf{x}}} \cdot \mathbf{v}^n = 0$, we get

$$-\rho^F \Delta t \int_{\Omega_n^F} \nabla_{\widehat{\mathbf{x}}} \cdot (\mathbf{v}^n - \boldsymbol{\vartheta}^n)|\widehat{\mathbf{v}}^{n+1}|^2 = \rho^F \Delta t \int_{\Omega_n^F} (\nabla_{\widehat{\mathbf{x}}} \cdot \boldsymbol{\vartheta}^n)|\widehat{\mathbf{v}}^{n+1}|^2.$$

This implies that

$$\begin{aligned} 2\rho^F \Delta t c_F(\widehat{\mathbf{v}}^{n+1}, \widehat{\mathbf{v}}^{n+1}) \;&\geq\; 2\rho^F \|\widehat{\mathbf{v}}^{n+1}\|^2_{L^2(\Omega_n^F)} \\ &+\; \rho^F \int_{\Omega_n^F} \Big(\Delta t(\nabla_{\widehat{\mathbf{x}}} \cdot \boldsymbol{\vartheta}^n) + \delta(\widehat{\mathbf{x}})\Delta t\Big)|\widehat{\mathbf{v}}^{n+1}|^2. \end{aligned}$$

If we add and we subtract the term $\rho^F \displaystyle\int_{\Omega_n^F} |\widehat{\mathbf{v}}^{n+1}|^2$ to the second member of the above inequality, we have:

$$\begin{aligned} 2\rho^F \Delta t c_F(\widehat{\mathbf{v}}^{n+1}, \widehat{\mathbf{v}}^{n+1}) \;&\geq\; \rho^F \|\widehat{\mathbf{v}}^{n+1}\|^2_{L^2(\Omega_n^F)} \\ &+\; \rho^F \int_{\Omega_n^F} \Big(1 + \Delta t(\nabla_{\widehat{\mathbf{x}}} \cdot \boldsymbol{\vartheta}^n) + \delta(\widehat{\mathbf{x}})\Delta t\Big)|\widehat{\mathbf{v}}^{n+1}|^2. \end{aligned}$$

We recalled at the beginning that $\Big(1 + \Delta t(\nabla_{\widehat{\mathbf{x}}} \cdot \boldsymbol{\vartheta}^n) + \Delta t\delta(\widehat{\mathbf{x}})\Big)$ is the Jacobian of $\mathcal{A}_{t_{n+1}}$ and by changing the domain, under the assumption that $\mathbf{v}^{n+1} \in (L^2(\Omega_{n+1}^F))^2$, we have:

$$\rho^F \int_{\Omega_n^F} \Big(1 + \Delta t(\nabla_{\widehat{\mathbf{x}}} \cdot \boldsymbol{\vartheta}^n) + \delta(\widehat{\mathbf{x}})\Delta t\Big)|\widehat{\mathbf{v}}^{n+1}|^2 = \rho^F \int_{\Omega_{n+1}^F} |\mathbf{v}^{n+1}|^2.$$

Finally, we get:

$$2\rho^F \Delta t c_F(\widehat{\mathbf{v}}^{n+1}, \widehat{\mathbf{v}}^{n+1}) \geq \rho^F \|\widehat{\mathbf{v}}^{n+1}\|^2_{L^2(\Omega_n^F)} + \rho^F \|\mathbf{v}^{n+1}\|^2_{L^2(\Omega_{n+1}^F)}.$$

This concludes the proof of the lemma. ∎

Remark 2.3 The following equality holds:

$$a_F(\widehat{\mathbf{v}}^{n+1}, 2\Delta t\widehat{\mathbf{v}}^{n+1}) = 4\mu^F \Delta t \|\epsilon_{\widehat{\mathbf{x}}}(\widehat{\mathbf{v}}^{n+1})\|^2_{L^2(\Omega_n^F)}.$$

In fact, by definition of $a_F(\cdot,\ \cdot)$ we have

$$\begin{aligned} &a_F(\widehat{\mathbf{v}}^{n+1}, 2\Delta t\widehat{\mathbf{v}}^{n+1}) = 4\mu^F \Delta t \int_{\Omega_n^F} \epsilon_{\widehat{\mathbf{x}}}(\widehat{\mathbf{v}}^{n+1}) : \epsilon_{\widehat{\mathbf{x}}}(\widehat{\mathbf{v}}^{n+1}) \\ &= 4\mu^F \Delta t \|\epsilon_{\widehat{\mathbf{x}}}(\widehat{\mathbf{v}}^{n+1})\|^2_{L^2(\Omega_n^F)}. \end{aligned}$$

Remark 2.4 To compute the terms $b_F(\cdot,\ \cdot)$ in the system (2.20), we set $\widehat{\mathbf{w}}^F = 2\Delta t\widehat{\mathbf{v}}^{n+1}$ and $\widehat{q} = -2\Delta t\widehat{p}^{n+1}$, we get therefore :

$$b_F(\widehat{\mathbf{v}}^{n+1}, \widehat{q}) + b_F(\widehat{\mathbf{w}}^F, \widehat{p}^{n+1}) = 2\Delta t\Big(- b_F(\widehat{\mathbf{v}}^{n+1}, \widehat{p}^{n+1}) + b_F(\widehat{\mathrm{v}}^{n+1}, \widehat{p}^{n+1})\Big) = 0.$$

Lemma 2.2 *The following equality holds*

$$\rho^S \int_{\Omega^S} \Big(\frac{\mathbf{u}^{n+1} - 2\mathbf{u}^n + \mathbf{u}^{n-1}}{(\Delta t)^2}\Big) \cdot (\mathbf{u}^{n+1} - \mathbf{u}^{n-1}) = \rho^S \Big\|\frac{\mathbf{u}^{n+1} - \mathbf{u}^n}{\Delta t}\Big\|^2_{L^2(\Omega^S)}$$
$$-\rho^S \Big\|\frac{\mathbf{u}^n - \mathbf{u}^{n-1}}{\Delta t}\Big\|^2_{L^2(\Omega^S)}.$$

Proof. Adding and subtracting $\mathbf{u}^n$ to the term $(\mathbf{u}^{n+1} - \mathbf{u}^{n-1})$, we have :

$$\rho^S \int_{\Omega^S} \Big(\frac{\mathbf{u}^{n+1} - 2\mathbf{u}^n + \mathbf{u}^{n-1}}{(\Delta t)^2}\Big) \cdot (\mathbf{u}^{n+1} - \mathbf{u}^{n-1})$$
$$= \rho^S \int_{\Omega^S} \Big(\frac{(\mathbf{u}^{n+1} - \mathbf{u}^n) - (\mathbf{u}^n - \mathbf{u}^{n-1})}{(\Delta t)^2}\Big) \cdot \Big((\mathbf{u}^{n+1} - \mathbf{u}^n) + (\mathbf{u}^n - \mathbf{u}^{n-1})\Big).$$

Let us remark that the above expression can be identified as $(a+b)(a-b)$, thus

$$\rho^S \int_{\Omega^S} \Big(\frac{\mathbf{u}^{n+1} - 2\mathbf{u}^n + \mathbf{u}^{n-1}}{(\Delta t)^2}\Big) \cdot (\mathbf{u}^{n+1} - \mathbf{u}^{n-1}) = \rho^S \Big\|\frac{\mathbf{u}^{n+1} - \mathbf{u}^n}{\Delta t}\Big\|^2_{L^2(\Omega^S)}$$
$$-\rho^S \Big\|\frac{\mathbf{u}^n - \mathbf{u}^{n-1}}{\Delta t}\Big\|^2_{L^2(\Omega^S)}.$$

This achieves the proof of the lemma. ■

Lemma 2.3 *We have*

$$a_S(\theta\mathbf{u}^{n+1} + (1-2\theta)\mathbf{u}^n + \theta\mathbf{u}^{n-1}, \mathbf{u}^{n+1} - \mathbf{u}^{n-1}) = X^{n+1} - X^n.$$

Proof. By bilinearity of $a_S(\cdot,\ \cdot)$, we get

$$a_S(\theta\mathbf{u}^{n+1} + (1-2\theta)\mathbf{u}^n + \theta\mathbf{u}^{n-1}, \mathbf{u}^{n+1} - \mathbf{u}^{n-1})$$
$$= a_S(\theta\mathbf{u}^{n+1} + (1-2\theta)\mathbf{u}^n + \theta\mathbf{u}^{n-1}, \mathbf{u}^{n+1})$$
$$-a_S(\theta\mathbf{u}^{n+1} + (1-2\theta)\mathbf{u}^n + \theta\mathbf{u}^{n-1}, \mathbf{u}^{n-1})$$
$$= \theta a_S(\mathbf{u}^{n+1}, \mathbf{u}^{n+1}) + (1-2\theta)a_S(\mathbf{u}^n, \mathbf{u}^{n+1}) + \theta a_S(\mathbf{u}^{n-1}, \mathbf{u}^{n+1})$$
$$-\theta a_S(\mathbf{u}^{n+1}, \mathbf{u}^{n-1}) - (1-2\theta)a_S(\mathbf{u}^n, \mathbf{u}^{n-1}) - \theta a_S(\mathbf{u}^{n-1}, \mathbf{u}^{n-1}).$$

Since $a_S(\cdot,\ \cdot)$ is symmetric, therefore

$$\theta a_S(\mathbf{u}^{n-1}, \mathbf{u}^{n+1}) - \theta a_S(\mathbf{u}^{n+1}, \mathbf{u}^{n-1}) = 0.$$

Moreover when we add and we subtract the term $\theta a_S(\mathbf{u}^n, \mathbf{u}^n)$ in the above final expression, we obtain:

$$\begin{aligned}
&a_S(\theta \mathbf{u}^{n+1} + (1-2\theta)\mathbf{u}^n + \theta \mathbf{u}^{n-1}, \mathbf{u}^{n+1} - \mathbf{u}^{n-1}) \\
&= \theta a_S(\mathbf{u}^{n+1}, \mathbf{u}^{n+1}) + (1-2\theta) a_S(\mathbf{u}^{n+1}, \mathbf{u}^n) + \theta a_S(\mathbf{u}^n, \mathbf{u}^n) \\
&-\theta a_S(\mathbf{u}^n, \mathbf{u}^n) - (1-2\theta) a_S(\mathbf{u}^n, \mathbf{u}^{n-1}) - \theta a_S(\mathbf{u}^{n-1}, \mathbf{u}^{n-1}).
\end{aligned}$$

Hence, we have

$$a_S(\theta \mathbf{u}^{n+1} + (1-2\theta)\mathbf{u}^n + \theta \mathbf{u}^{n-1}, \mathbf{u}^{n+1} - \mathbf{u}^{n-1}) = X^{n+1} - X^n.$$

This concludes the proof. ■

Lemma 2.4 *There exist two constants $C_2 > 0$ and $C' > 0$ such that :*

$$\begin{aligned}
&\int_{\Omega_n^F} \widehat{\mathbf{f}}^{n+1} \cdot (2\Delta t \widehat{\mathbf{v}}^{n+1}) + \int_{\Sigma_1} \mathbf{h}_{in}^{n+1} \cdot (2\Delta t \widehat{\mathbf{v}}^{n+1}) + \int_{\Sigma_3} \mathbf{h}_{out}^{n+1} \cdot (2\Delta t \widehat{\mathbf{v}}^{n+1}) \\
&\leq \Delta t \Big(C_2 \|\widehat{\mathbf{f}}^{n+1}\|^2_{L^2(\Omega_n^F)} + C' \|\mathbf{h}_{int}^{n+1}\|^2_{L^2(\Sigma_1)} + C' \|\mathbf{h}_{out}^{n+1}\|^2_{L^2(\Sigma_3)} \Big) \\
&+2\mu^F \Delta t \|\epsilon_{\widehat{\mathbf{x}}}(\widehat{\mathbf{v}}^{n+1})\|^2_{L^2(\Omega_n^F)}.
\end{aligned}$$

Before starting the proof of the Lemma 2.4, we recall two functional analysis lemmas.

Lemma 2.5 (Korn lemma, see [7], page 123.) *Let Ω be a convex and bounded open subset of $\mathbb{R}^n$. We denote by V the subspace of $(H^1(\Omega))^n$ defined by*

$$V = \big\{ v \in (H^1(\Omega))^n;\ \ v\big|_\Gamma = 0 \big\},$$

where Γ is a part of the boundary $\partial\Omega$ with $mes(\Gamma) > 0$. Then, there exists a constant C_Ω such that:

$$\|v\|^2_{L^2(\Omega)} \leq C_\Omega \|\epsilon(v)\|^2_{L^2(\Omega)}, \quad \forall\ \ v \in V.$$

Lemma 2.6 (Trace theorem, see [24], page 10.) *Let Ω be a bounded open subset of $\mathbb{R}^n$, with Lipschitz continuous boundary $\partial\Omega$. We define the trace map by:*

$$\begin{aligned}
\gamma_0 :\ H^1(\Omega) \cap C(\overline{\Omega}) &\longrightarrow L^2(\partial\Omega) \cap C(\overline{\partial\Omega}) \\
v &\mapsto \gamma_0(v) = v\big|_{\partial\Omega}.
\end{aligned}$$

This map γ_0 can be extended by continuity to the linear continuous map from $H^1(\Omega)$ to $L^2(\partial\Omega)$, also called γ_0. In particular there exists a constant $C_{\gamma_0} > 0$ such that for all $v \in H^1(\Omega)$

$$\|v\|_{L^2(\partial\Omega)} \leq C_{\gamma_0} \|v\|_{H^1(\Omega)}.$$

Proof. (Lemma 2.4) Firstly, let us set $A = \displaystyle\int_{\Omega_n^F} \widehat{\mathbf{f}}^{n+1} \cdot (2\Delta t)\widehat{\mathrm{v}}^{n+1}$ and by the Cauchy-Schwarz' inequality, we get

$$A \leq 2\Delta t \|\widehat{\mathbf{f}}^{n+1}\|_{L^2(\Omega_n^F)} \|\widehat{\mathbf{v}}^{n+1}\|_{L^2(\Omega_n^F)}.$$

We have from the lemma 2.5, there exists a constant $C_{\Omega_n^F} > 0$ (after taking $C_1 = 2\sqrt{C_{\Omega_n^F}}$) such that:

$$A \leq C_1 \Delta t \|\widehat{\mathbf{f}}^{n+1}\|_{L^2(\Omega_n^F)} \|\epsilon_{\widehat{\mathbf{x}}}(\widehat{\mathbf{v}}^{n+1})\|_{L^2(\Omega_n^F)}.$$

Setting

$$a = \frac{C_1 \|\widehat{\mathbf{f}}^{n+1}\|_{L^2(\Omega_n^F)}}{\sqrt{2\mu^F}}, \quad b = \sqrt{2\mu^F} \|\epsilon_{\widehat{\mathbf{x}}}(\widehat{\mathbf{v}}^{n+1})\|_{L^2(\Omega_n^F)}$$

and using the following Young's inequality:

$$ab \leq \frac{a^2}{2} + \frac{b^2}{2}, \quad \forall\, a, b \geq 0, \tag{2.22}$$

we finally obtain that there exists a constant $C_2 = \dfrac{C_1^2}{4\mu^F} > 0$ such that:

$$A \;\; \leq \;\; C_2 \Delta t \|\widehat{\mathbf{f}}^{n+1}\|^2_{L^2(\Omega_n^F)} + \mu^F \Delta t \|\epsilon_{\widehat{\mathbf{x}}}(\widehat{\mathbf{v}}^{n+1})\|^2_{L^2(\Omega_n^F)}.$$

Secondly, let us set

$$B = \int_{\Sigma_1} \mathbf{h}_{in}^{n+1} \cdot (2\Delta t)\mathbf{v}^{n+1} + \int_{\Sigma_3} \mathbf{h}_{out}^{n+1} \cdot (2\Delta t)\mathbf{v}^{n+1}.$$

From Cauchy-Schwarz' inequality, we have

$$B \leq 2\Delta t \Big(\|\mathbf{h}_{in}^{n+1}\|_{L^2(\Sigma_1)} + \|\mathbf{h}_{out}^{n+1}\|_{L^2(\Sigma_3)} \Big) \|\gamma_0(\widehat{\mathbf{v}}^{n+1})\|_{L^2(\partial\Omega_n^F)}$$

and referring to the lemma 2.6, there exists a constant $C_{\gamma_0} > 0$ (we after take $C_3 = 2C_{\gamma_0}$) such that

$$B \leq \Delta t C_3 \Big(\|\mathbf{h}_{in}^{n+1}\|_{L^2(\Sigma_1)} + \|\mathbf{h}_{out}^{n+1}\|_{L^2(\Sigma_3)} \Big) \|\widehat{\mathbf{v}}^{n+1}\|_{H^1(\Omega_n^F)}.$$

We set

$$a = C_3 \sqrt{\frac{1 + C_{\Omega_n^F}}{2\mu^F}} \Big(\|\mathbf{h}_{in}^{n+1}\|_{L^2(\Sigma_1)} + \|\mathbf{h}_{out}^{n+1}\|_{L^2(\Sigma_3)} \Big)$$

and

$$b = \sqrt{\frac{2\mu^F}{1 + C_{\Omega_n^F}}} \|\widehat{\mathbf{v}}^{n+1}\|_{H^1(\Omega_n^F)}.$$

Using (22) and the lemma 2.5 (ie, $\|\widehat{\mathbf{v}}^{n+1}\|^2_{H^1(\Omega^F_n)} \leq (1+C_{\Omega^F_n})\|\epsilon_{\widehat{x}}(\widehat{\mathbf{v}}^{n+1})\|^2_{L(\Omega^F_n)}$), we get

$$B \leq C_4\Delta t\Big(\|\mathbf{h}^{n+1}_{in}\|_{L^2(\Sigma_1)} + \|\mathbf{h}^{n+1}_{out}\|_{L^2(\Sigma_3)}\Big)^2 + \mu^F\Delta t\|\epsilon_{\widehat{x}}(\widehat{\mathbf{v}}^{n+1})\|^2_{L(\Omega^F_n)}.$$

By the inequality

$$(a+b)^2 \leq 2(a^2+b^2),$$

there exists a constant $C' = 2C_4$ such that

$$B \leq \Delta t C'\Big(\|\mathbf{h}^{n+1}_{in}\|^2_{L^2(\Sigma_1)} + \|\mathbf{h}^{n+1}_{out}\|^2_{L^2(\Sigma_3)}\Big) + \mu^F\Delta t\|\epsilon_{\widehat{x}}(\widehat{\mathbf{v}}^{n+1})\|^2_{L(\Omega^F_n)}$$

Finally, taking the sum of A and B we get the lemma. ■

Lemma 2.7 *The following inequality holds*

$$\rho^F\int_{\Omega^F_n}\frac{\mathbf{v}^n}{\Delta t}\cdot(2\Delta t\widehat{\mathbf{v}}^{n+1}) \leq \rho^F\|\mathbf{v}^n\|^2_{L^2(\Omega^F_n)} + \rho^F\|\widehat{\mathbf{v}}^{n+1}\|^2_{L^2(\Omega^F_n)}.$$

Proof. We have

$$\rho^F\int_{\Omega^F_n}\frac{\mathbf{v}^n}{\Delta t}\cdot(2\Delta t\widehat{\mathbf{v}}^{n+1}) = 2\rho^F\int_{\Omega^F_n}\mathbf{v}^n\cdot\widehat{\mathbf{v}}^{n+1} \leq 2\rho^F\|\mathbf{v}^n\|_{L^2(\Omega^F_n)}\|\widehat{\mathbf{v}}^{n+1}\|_{L^2(\Omega^F_n)},$$

and from (2.22) (with $a = \|\mathbf{v}^n\|_{L^2(\Omega^F_n)}$ and $b = \|\widehat{\mathbf{v}}^{n+1}\|_{L^2(\Omega^F_n)}$), we obtain:

$$\rho^F\int_{\Omega^F_n}\frac{\mathbf{v}^n}{\Delta t}\cdot(2\Delta t\widehat{\mathbf{v}}^{n+1}) \leq \rho^F\|\mathbf{v}^n\|^2_{L^2(\Omega^F_n)} + \rho^F\|\widehat{\mathbf{v}}^{n+1}\|^2_{L^2(\Omega^F_n)}.$$

That gives the waited inequality. ■

Lemma 2.8 *The inequality below holds*

$$\int_{\Omega^S}\bar{\mathbf{g}}^{n+1}\cdot(\mathbf{u}^{n+1}-\mathbf{u}^{n-1}) \leq \frac{\Delta t}{\rho^S}\|\bar{\mathbf{g}}^{n+1}\|^2_{L^2(\Omega^S)} + \frac{\rho^S\Delta t}{2}\Big\|\frac{\mathbf{u}^{n+1}-\mathbf{u}^n}{\Delta t}\Big\|^2_{L^2(\Omega^S)}$$
$$+\frac{\rho^S\Delta t}{2}\Big\|\frac{\mathbf{u}^n-\mathbf{u}^{n-1}}{\Delta t}\Big\|^2_{L^2(\Omega^S)}.$$

Proof. Multiplying and dividing the term

$$\int_{\Omega^S}\bar{\mathbf{g}}^{n+1}\cdot(\mathbf{u}^{n+1}-\mathbf{u}^{n-1})$$

by Δt, using Cauchy-Schwarz' inequality and triangular inequality, we obtain

$$\Delta t\int_{\Omega^S}\bar{\mathbf{g}}^{n+1}\cdot\frac{(\mathbf{u}^{n+1}-\mathbf{u}^{n-1})}{\Delta t} \leq \Delta t\sqrt{\frac{2}{\rho^S}}\|\bar{\mathbf{g}}^{n+1}\|_{L^2(\Omega^S)}\sqrt{\frac{\rho^S}{2}}\Big\|\frac{\mathbf{u}^{n+1}-\mathbf{u}^{n-1}}{\Delta t}\Big\|_{L^2(\Omega^S)}$$
$$\leq \Delta t\sqrt{\frac{2}{\rho^S}}\|\bar{\mathbf{g}}^{n+1}\|_{L^2(\Omega^S)}\sqrt{\frac{\rho^S}{2}}\Big(\Big\|\frac{\mathbf{u}^{n+1}-\mathbf{u}^n}{\Delta t}\Big\|_{L^2(\Omega^S)} + \Big\|\frac{\mathbf{u}^n-\mathbf{u}^{n-1}}{\Delta t}\Big\|_{L^2(\Omega^S)}\Big).$$

From (2.22), we infer that

$$\int_{\Omega^S} \bar{\mathbf{g}}^{n+1}\cdot(\mathbf{u}^{n+1}-\mathbf{u}^{n-1}) \le \frac{\rho^S\Delta t}{4}\Big(\Big\|\frac{\mathbf{u}^{n+1}-\mathbf{u}^n}{\Delta t}\Big\|_{L^2(\Omega^S)} + \Big\|\frac{\mathbf{u}^{n}-\mathbf{u}^{n-1}}{\Delta t}\Big\|_{L^2(\Omega^S)}\Big)^2$$
$$+\frac{\Delta t}{\rho^S}\|\bar{\mathbf{g}}^{n+1}\|^2_{L^2(\Omega^S)}.$$

Using the inequality

$$(\alpha+\beta)^2 \le 2(\alpha^2+\beta^2),$$

we get

$$\begin{aligned}\int_{\Omega^S} \bar{\mathbf{g}}^{n+1}\cdot(\mathbf{u}^{n+1}-\mathbf{u}^{n-1}) \quad \le \quad & \frac{\rho^S\Delta t}{2}\Big\|\frac{\mathbf{u}^{n+1}-\mathbf{u}^n}{\Delta t}\Big\|^2_{L^2(\Omega^S)} \\ & +\frac{\rho^S\Delta t}{2}\Big\|\frac{\mathbf{u}^{n}-\mathbf{u}^{n-1}}{\Delta t}\Big\|^2_{L^2(\Omega^S)} + \frac{\Delta t}{\rho^S}\|\bar{\mathbf{g}}^{n+1}\|^2_{L^2(\Omega^S)}.\end{aligned}$$

This achieves the proof of the lemma. ■

We are going to apply the following discrete Granwall lemma (see [24]).

Lemma 2.9 (Discrete Gronwall lemma.) *Assume that $(k_n)_{n\in\mathbb{N}}$ is a non-negative sequence and that the sequence ϕ_n satisfies :*

$$\phi_0 \le g_0 \ \ \textit{and} \ \ \phi_n \le g_0 + \sum_{s=0}^{n-1} p_s + \sum_{s=0}^{n-1} k_s\phi_s, \ \ \forall\, n\ge 1. \tag{2.23}$$

Then ϕ_n satisfies

$$\phi_0 \le g_0(1+k_0)+p_0 \ \ \textit{and} \ \ \phi_n \le g_0\prod_{s=0}^{n-1}(1+k_s)+\sum_{s=0}^{n-2}p_s\prod_{r=s+1}^{n-1}(1+k_r)+p_{n-1},\ \forall\, n\ge 2. \tag{2.24}$$

Moreover, if $g_0 \ge 0$ and $p_n \ge 0$ for $n \ge 0$, it follows

$$\phi_n \le \Big(g_0+\sum_{s=0}^{n-1}p_s\Big)\exp\Big(\sum_{s=0}^{n-1}k_s\Big), \ \ n\ge 1. \tag{2.25}$$

Proof. (Theorem 1.) From (2.20), using the estimations obtained in the above lemmas, we have:

$$\begin{aligned}&\rho^F\|\mathbf{v}^{n+1}\|^2_{L^2(\Omega^F_{n+1})} - \rho^F\|\mathbf{v}^{n}\|^2_{L^2(\Omega^F_{n})} + 2\mu^F\Delta t\|\epsilon_{\widehat{\mathbf{x}}}(\widehat{\mathbf{v}}^{n+1})\|^2_{L^2(\Omega^F_n)}\\ &+\rho^S\Big\|\frac{\mathbf{u}^{n+1}-\mathbf{u}^n}{\Delta t}\Big\|^2_{L^2(\Omega^S)} - \rho^S\Big\|\frac{\mathbf{u}^{n}-\mathbf{u}^{n-1}}{\Delta t}\Big\|^2_{L^2(\Omega^S)} + X^{n+1}-X^n\\ &\le C_2\Delta t\|\widehat{\mathbf{f}}^{n+1}\|^2_{L^2(\Omega^F_n)} + \frac{\Delta t}{\rho^S}\|\bar{\mathbf{g}}^{n+1}\|^2_{L^2(\Omega^S)}\\ &+\Delta t C'\Big(\|\mathbf{h}^{n+1}_{in}\|^2_{L^2(\Sigma_1)} + \|\mathbf{h}^{n+1}_{out}\|^2_{L^2(\Sigma_3)}\Big) + 2\mu^F\Delta t\|\epsilon_{\widehat{\mathbf{x}}}(\widehat{\mathbf{v}}^{n})\|^2_{L^2(\Omega^F_{n-1})}\\ &+\frac{\rho^S\Delta t}{2}\Big\|\frac{\mathbf{u}^{n+1}-\mathbf{u}^n}{\Delta t}\Big\|^2_{L^2(\Omega^S)} + \frac{\rho^S\Delta t}{2}\Big\|\frac{\mathbf{u}^{n}-\mathbf{u}^{n-1}}{\Delta t}\Big\|^2_{L^2(\Omega^S)}.\end{aligned}$$

Writing now, this inequality for all $k = 1, \ldots, n$ and taking the sum over k, we get

$$\begin{aligned}
&\rho^F \|\mathbf{v}^{n+1}\|^2_{L^2(\Omega^F_{n+1})} + 2\mu^F \Delta t \|\epsilon_{\widehat{\mathbf{x}}}(\widehat{\mathbf{v}}^{n+1})\|^2_{L^2(\Omega^F_n)} + \rho^S \Big\| \frac{\mathbf{u}^{n+1} - \mathbf{u}^n}{\Delta t} \Big\|^2_{L^2(\Omega^S)} \\
&+X^{n+1} \leq \rho^F \|\mathbf{v}^1\|^2_{L^2(\Omega^F_1)} + 2\mu^F \Delta t \|\epsilon_{\widehat{\mathbf{x}}}(\mathbf{v}^1)\|^2_{L^2(\Omega^F_0)} + \rho^S \Big\| \frac{\mathbf{u}^1 - \mathbf{u}^0}{\Delta t} \Big\|^2_{L^2(\Omega^S)} \\
&+X^1 + C_2 \Delta t \sum_{k=1}^n \|\widehat{\mathbf{f}}^{k+1}\|^2_{L^2(\Omega^F_k)} + \sum_{k=1}^n \frac{\Delta t}{\rho^S} \|\bar{\mathbf{g}}^{k+1}\|^2_{L^2(\Omega^S)} \\
&+\Delta t C' \Big(\sum_{k=1}^n \|\mathbf{h}^{k+1}_{in}\|^2_{L^2(\Sigma_1)} + \sum_{k=1}^n \|\mathbf{h}^{k+1}_{out}\|^2_{L^2(\Sigma_3)} \Big) + \frac{\rho^S \Delta t}{2} \Big\| \frac{\mathbf{u}^1 - \mathbf{u}^0}{\Delta t} \Big\|^2_{L^2(\Omega^S)} \\
&+\sum_{k=1}^{n-1} \rho^S \Delta t \Big\| \frac{\mathbf{u}^{k+1} - \mathbf{u}^k}{\Delta t} \Big\|^2_{L^2(\Omega^S)} + \frac{\rho^S \Delta t}{2} \Big\| \frac{\mathbf{u}^{n+1} - \mathbf{u}^n}{\Delta t} \Big\|^2_{L^2(\Omega^S)}. \qquad (2.26)
\end{aligned}$$

On the other hand, we have:

$$\begin{aligned}
&C_2 \Delta t \sum_{k=1}^n \|\widehat{\mathbf{f}}^{k+1}\|^2_{L^2(\Omega^F_k)} + \sum_{k=1}^n \frac{\Delta t}{\rho^S} \|\bar{\mathbf{g}}^{k+1}\|^2_{L^2(\Omega^S)} \\
&+\Delta t C' \Big(\sum_{k=1}^n \|\widehat{\mathbf{h}}^{k+1}_{in}\|^2_{L^2(\Sigma_1)} + \sum_{k=1}^n \|\widehat{\mathbf{h}}^{k+1}_{out}\|^2_{L^2(\Sigma_3)} \Big) \\
&\leq \Delta t \Big(n C_2 \max_{t\in[0,T]} \|\mathbf{f}^F(t)\|^2_{L^2(\Omega^F_t)} + \frac{n}{\rho^S} \max_{t\in[0,T]} \|\mathbf{f}^S(t)\|^2_{L^2(\Omega^S)} \\
&+n C' \max_{t\in[0,T]} \|\mathbf{h}_{in}(t)\|^2_{L^2(\Sigma_1)} + n C' \max_{t\in[0,T]} \|\mathbf{h}_{out}(t)\|^2_{L^2(\Sigma_3)} \Big)
\end{aligned}$$

and by using the fact that $n\Delta t < T$, we get

$$\begin{aligned}
&C_2 \Delta t \sum_{k=1}^n \|\widehat{\mathbf{f}}^{k+1}\|^2_{L^2(\Omega^F_k)} + \sum_{k=1}^n \frac{\Delta t}{\rho^S} \|\bar{\mathbf{g}}^{k+1}\|^2_{L^2(\Omega^S)} \\
&+\Delta t C' \Big(\sum_{k=1}^n \|\mathbf{h}^{k+1}_{in}\|^2_{L^2(\Sigma_1)} + \sum_{k=1}^n \|\mathbf{h}^{k+1}_{out}\|^2_{L^2(\Sigma_3)} \Big) \\
&\leq T \Big(C_2 \max_{t\in[0,T]} \|\mathbf{f}^F(t)\|^2_{L^2(\Omega^F_t)} + \frac{1}{\rho^S} \max_{t\in[0,T]} \|\mathbf{f}^S(t)\|^2_{L^2(\Omega^S)} \\
&+C' \max_{t\in[0,T]} \|\mathbf{h}_{in}(t)\|^2_{L^2(\Sigma_1)} + C' \max_{t\in[0,T]} \|\mathbf{h}_{out}(t)\|^2_{L^2(\Sigma_3)} \Big).
\end{aligned}$$

In this way, we have obtained an upper bound of the terms depending on $\mathbf{f}^F$, $\mathbf{f}^S$, $\mathbf{h}_{in}$, $\mathbf{h}_{out}$ which appear in the right-hand side of (2.26).

Now, let us set

$$\phi_n = \rho^F \|\mathbf{v}^{n+1}\|^2_{L^2(\Omega^F_{n+1})} + 2\mu^F \Delta t \|\epsilon_{\widehat{\mathbf{x}}}(\widehat{\mathbf{v}}^{n+1})\|^2_{L^2(\Omega^F_n)}$$
$$+\rho^S \Big\|\frac{\mathbf{u}^{n+1}-\mathbf{u}^n}{\Delta t}\Big\|^2_{L^2(\Omega^S)} + X^{n+1}.$$

and let us remark that X^{n+1} can be written in the following form:

$$\begin{aligned} X^{n+1} &= \Big(\frac{4\theta-1}{2}\Big)\Big[a_s(\mathbf{u}^{n+1},\mathbf{u}^{n+1}) + a_S(\mathbf{u}^n,\mathbf{u}^n)\Big] \\ &+ \Big(\frac{1-2\theta}{2}\Big) a_S(\mathbf{u}^{n+1}+\mathbf{u}^n, \mathbf{u}^{n+1}+\mathbf{u}^n). \end{aligned} \tag{2.27}$$

In fact, the form $a_S(\cdot,\cdot)$ is bilinear and symmetric, so by developing the last term in (2.27), we get the exact definition of X^{n+1}.
Using the fact that $\theta \in \Big[\frac{1}{4},\frac{1}{2}\Big]$, we have $X^n \geq 0$ for any n. Therefore X^{n+1} is positive.

On the one hand, we have the sum of the last three terms in (2.26) is dominated by:

$$\frac{\rho^S \Delta t}{2}\Big\|\frac{\mathbf{u}^1-\mathbf{u}^0}{\Delta t}\Big\|^2_{L^2(\Omega^S)} + \sum_{k=1}^{n-1} \rho^S \Delta t \Big\|\frac{\mathbf{u}^{k+1}-\mathbf{u}^k}{\Delta t}\Big\|^2_{L^2(\Omega^S)}$$
$$+\frac{\rho^S \Delta t}{2}\Big\|\frac{\mathbf{u}^{n+1}-\mathbf{u}^n}{\Delta t}\Big\|^2_{L^2(\Omega^S)} \leq \sum_{k=0}^{n} \rho^S \Delta t \Big\|\frac{\mathbf{u}^{k+1}-\mathbf{u}^k}{\Delta t}\Big\|^2_{L^2(\Omega^S)}$$
$$\leq \Delta t(\phi_0 + \cdots + \phi_n).$$

and on the other hand, setting

$$g_0 = \rho^F \|\mathbf{v}^1\|^2_{L^2(\Omega^F_1)} + 2\mu^F \Delta t \|\epsilon_{\widehat{\mathbf{x}}}(\widehat{\mathbf{v}}^1)\|^2_{L^2(\Omega^F_0)} + \frac{\rho^S}{2}\Big\|\frac{\mathbf{u}^1-\mathbf{u}^0}{\Delta t}\Big\|^2_{L^2(\Omega^S)} + X^1$$
$$+T\Big(C_2 \max_{t\in[0,T]} \|\mathbf{f}^F\|^2_{L^2(\Omega^F_t)} + \frac{1}{\rho^S}\max_{t\in[0,T]} \|\mathbf{f}^S\|^2_{L^2(\Omega^S)}$$
$$+C' \max_{t\in[0,T]} \|\mathbf{h}_{in}\|^2_{L^2(\Sigma_1)} + C' \max_{t\in[0,T]} \|\mathbf{h}_{out}\|^2_{L^2(\Sigma_3)}\Big),$$

we have $\phi_0 \leq g_0$.

In order to be in the Gronwall lemma assumptions, let us take $p_s = 0$ and $k_s = \Delta t$. Now applying the last result in the Gronwall lemma (with sum from 0 to n) and using the fact that $\displaystyle\sum_{s=0}^{n} k_s = (n+1)\Delta t \leq T$, we get:

$$\begin{aligned}
&\rho^F \|\mathbf{v}^{n+1}\|^2_{L^2(\Omega^F_{n+1})} + 2\mu^F \Delta t \|\epsilon_{\widehat{\mathbf{x}}}(\widehat{\mathbf{v}}^{n+1})\|^2_{L^2(\Omega^F_n)} + \rho^S \left\| \frac{\mathbf{u}^{n+1} - \mathbf{u}^n}{\Delta t} \right\|^2_{L^2(\Omega^S)} \\
&+X^{n+1} \leq \Big[\rho^F \|\mathbf{v}^1\|^2_{L^2(\Omega^F_1)} + 2\mu^F \Delta t \|\epsilon(\widehat{\mathbf{v}}^1)\|^2_{L^2(\Omega^F_0)} + \rho^S \left\| \frac{\mathbf{u}^1 - \mathbf{u}^0}{\Delta t} \right\|^2_{L^2(\Omega^S)} \\
&+X^1 + T\Big(C_2 \max_{t\in[0,T]} \|\mathbf{f}^F(t)\|^2_{L^2(\Omega^F_t)} + \frac{1}{\rho^S} \max_{t\in[0,T]} \|\mathbf{f}^S(t)\|^2_{L^2(\Omega^S)} \\
&+C' \max_{t\in[0,T]} \|\mathbf{h}_{in}(t)\|^2_{L^2(\Sigma_1)} + C' \max_{t\in[0,T]} \|\mathbf{h}_{out}(t)\|^2_{L^2(\Sigma_3)} \Big) \Big] \exp(T). \qquad (2.28)
\end{aligned}$$

We obtain the expected inequality by setting $C = T\max(C_2, C', \frac{1}{\rho^S})$.

Furthermore, because X^{n+1} is positive, we can conclude from (2.28) that

$$\rho^F \|\mathbf{v}^{n+1}\|^2_{L^2(\Omega^F_{n+1})},\ 2\mu^F \Delta t \|\epsilon(\widehat{\mathbf{v}}^{n+1}),\ \|^2_{L^2(\Omega^F_n)},\ \frac{\rho^S}{2} \left\| \frac{\mathbf{u}^{n+1} - \mathbf{u}^n}{\Delta t} \right\|^2_{L^2(\Omega^S)},\ \text{and } X^{n+1}$$

are bounded. ■

2.2.5 Algorithm implementation

The monolithic linear system (2.20) can be solved by finite element method and the continuity of the velocity at the interface must be satisfied as an essential boundary condition. The fluid test functions must coincide with the structure test functions at the interface, implying some constraints for triangulation of the fluid and structure domains as well as in the choice of the finite elements. In [20], a related problem has been solved, using the Augmented Lagrangian Method where the continuity of the velocity was treated by a Lagrange multiplier. The numerical results presented in [20] show that the continuity of the velocity is not very well respected since the error in the L^2 norm between the fluid and structure velocity at the interface is 0.45.

The method that we use here to solve the coupled problem is based on partitioned procedure (the fluid and structure equations are solved separately), which is very often used to solve fluid-structure interaction problem. At each time step, an optimization problem in the form

$$\inf_{\boldsymbol{\alpha}\in\mathbb{R}^m} J(\boldsymbol{\alpha})$$

has to be solved, where $\sum_{i=1}^{m} \alpha_i \boldsymbol{\phi}^i$ is an approximation of the stress at the fluid-structure interface. The shape functions $\boldsymbol{\phi}^i$, $i = 1, \ldots, m$ defined at the interface are orthonormal with respect to the scalar product in L^2. This technique was successfully employed in

[19], [17], where implicit algorithms are presented. We will use the same least square method based on the Broyden, Fletcher, Goldford, Shano (BFGS) method in order to identify the stress at the interface.

We present below the implicit algorithm. More details can be found in [19].

Implicit algorithm

Step 1 Solve by BFGS the optimization problem

$$\boldsymbol{\alpha}^{n+1} \in \arg\min_{\boldsymbol{\alpha}\in\mathbb{R}^m} J(\boldsymbol{\alpha}),$$

where the cost function is computed as follows:

- Let $\sum_{i=1}^m \alpha_i \boldsymbol{\phi}^i$ be a guess of the stress at the fluid-structure interface.
- Solve the structure problem under the load $\sum_{i=1}^m \alpha_i \boldsymbol{\phi}^i$ at the interface to get the displacement $\mathbf{u}$.
- Build a fluid mesh $\mathcal{T}$ depending on the displacement $\mathbf{u}$.
- Solve the fluid problem on the mesh $\mathcal{T}$ under prescribed velocity at the fluid-structure interface in order to get the fluid velocity $\mathbf{v}$ and pressure p.
- Compute $\beta_i = -\displaystyle\int_{\Gamma_0} \left(\sigma^F(\mathbf{v},p)\,\mathbf{n}^F\right)\cdot\boldsymbol{\phi}^i(\mathbf{X})\,\omega(\mathbf{X},t)\,d\mathbf{X}, \quad \forall\, i=1,\ldots,m.$
- Set the cost function
$$J(\boldsymbol{\alpha}) = \frac{1}{2}\|\boldsymbol{\alpha}-\boldsymbol{\beta}\|^2_{\mathbb{R}^m}.$$

Step 2 Save the mesh $\mathcal{T}^{n+1}$, the structure displacement $\mathbf{u}^{n+1}$, the fluid velocity $\mathbf{v}^{n+1}$, the fluid pressure p^{n+1} obtained at the last iteration of the BFGS algorithm at **Step 1**.

Remark 2.5 *We emphasize that in the implicit strategy, the fluid mesh changes at each call of the cost function during the minimization process.*

Semi-implicit algorithm

Step 1 Compute the mesh velocity $\boldsymbol{\vartheta}^n$ from (2.18)

Step 2 Assembling the finite element matrix of fluid problem (2.14) using the mesh $\mathcal{T}^n$ obtained at the previous time step. Get a LU factorization of the matrix.

Step 3 Solve by BFGS the optimization problem using the fluid frozen mesh $\mathcal{T}^n$

$$\boldsymbol{\alpha}^{n+1} \in \arg\min_{\boldsymbol{\alpha}\in\mathbb{R}^m} J(\boldsymbol{\alpha}),$$

where the cost function is computed as follows:

- Let $\sum_{i=1}^m \alpha_i \boldsymbol{\phi}^i$ be a guess of the stress at the fluid-structure interface.
- Solve the structure problem under the load $\sum_{i=1}^m \alpha_i \boldsymbol{\phi}^i$ at the interface to get the displacement $\mathbf{u}$.
- Solve the fluid problem on the mesh $\mathcal{T}^n$ under prescribed velocity at the fluid-structure interface in order to get the fluid velocity $\mathbf{v}$ and pressure p.
- Compute $\beta_i = -\displaystyle\int_{\Gamma_0} \left(\sigma^F(\mathbf{v},p)\,\mathbf{n}^F\right)\cdot\boldsymbol{\phi}^i(\mathbf{X})\,\omega(\mathbf{X},t)d\mathbf{X}, \quad \forall\, i=1,\ldots,m.$
- Set the cost function
$$J(\boldsymbol{\alpha}) = \frac{1}{2}\|\boldsymbol{\alpha}-\boldsymbol{\beta}\|^2_{\mathbb{R}^m}.$$

Step 4 Build mesh $\mathcal{T}^{n+1}$, as the image of $\mathcal{T}^n$ by the map $\widehat{x} \mapsto \widehat{x} + \Delta t \boldsymbol{\vartheta}^n(\widehat{x})$ and save the mesh $\mathcal{T}^{n+1}$, the fluid velocity $\mathbf{v}^{n+1}(\mathbf{x}) = \widehat{\mathbf{v}}^{n+1}(\widehat{\mathbf{x}})$, etc.

Remark 2.6 *Contrary to the implicit strategy, the semi-implicit one use a fixed fluid mesh during the iterative method for solving the optimization problem, which reduces considerably the computational time.*

The BFGS is a gradient like algorithm for solving unconstrained optimization problems. We approximate the gradient of the cost function by a first order finite difference scheme which requires $m+1$ evaluations of the cost function. We recall that m is the number of the shape functions used to compute the stress at the fluid-structure interface. Therefore, it is important to work with small values of m. The shape functions $\boldsymbol{\phi}^i$ are not necessary compatible with the structure or fluid finite element functions. Possible choices for $\boldsymbol{\phi}^i$ are polynomial functions [18], finite element like functions, eigenfunctions associated to the structure equations [19], [17]. In the case where the $\boldsymbol{\phi}^i$ are not orthonormal for the scalar product of L^2 at the interface, the cost function has the form

$$J(\boldsymbol{\alpha}) = \frac{1}{2}\int_{\Gamma_0}\left(\sum_{i=1}^m \alpha_i\boldsymbol{\phi}^i(\mathbf{X}) - \sigma^F(\mathbf{v},p)\,\mathbf{n}^F\,\omega(\mathbf{X},t)\right)^2 d\mathbf{X}.$$

In this chapter, we have chosen $\boldsymbol{\phi}^i$ as the eigenfunctions associated to the structure equations. Since the eigenfunctions are orthonormal, the cost function has the form

$$J(\boldsymbol{\alpha}) = \frac{1}{2}\|\boldsymbol{\alpha}-\boldsymbol{\beta}\|^2_{\mathbb{R}^m},$$

where

$$\beta_i = -\int_{\Gamma_0} \left(\sigma^F(\mathbf{v}, p)\,\mathbf{n}^F\right) \cdot \boldsymbol{\phi}^i(\mathbf{X})\,\omega(\mathbf{X}, t)\,d\mathbf{X}.$$

In this chapter, for convenience, the structure problem (15) is solved numerically by modal decomposition. We set $\mathbf{u}(\mathbf{X}, t) = \sum_{i\geq 1} q_i(t)\boldsymbol{\phi}^i(\mathbf{X})$. The structure problem is: find q_i^{n+1} such that

$$\frac{q_i^{n+1} - 2q_i^n + q_i^{n-1}}{(\Delta t)^2} + \lambda_i(\theta q_i^{n+1} + (1-2\theta)q_i^n + \theta q_i^{n-1}) = \theta\alpha_i^{n+1} + (1-2\theta)\alpha_i^n + \theta\alpha_i^{n-1},$$

where λ_i is the eigenvalue associated to the eigenfunction $\boldsymbol{\phi}^i$ and

$$\alpha_i^{n+1} = \alpha_i(t_{n+1}) = \int_{\Gamma_0} (\sigma^S\mathbf{n}^S)\boldsymbol{\phi}^i(\mathbf{X})\,d\mathbf{X}.$$

We have assumed that $\mathbf{f}^S = (0,\, 0)$. The modal decomposition is efficient only in the context of linear model for the structure. For a non-linear model, the structure problem could be solved by an appropriate finite element method, independent of choice of the shape functions used to approach the stress at the fluid-structure interface. We will study this aspect in a future work.

2.3 Numerical results

2.3.1 Flow in a flexible straight tube

Physical parameters

We consider the following data for the computation: the length of the fluid domain is L= 6 cm and its height is $H = 1\ cm$. The viscosity of the fluid was fixed to be $\mu = 0.035\ \frac{g}{cm\cdot s}$, its density $\rho^F = 1\ \frac{g}{cm^3}$ and the volume force in fluid is $\mathbf{f}^F = (0,\, 0)^T$. The prescribed boundary stress at the outflow is $\mathbf{h}_{out}(x,t) = (0,\, 0)^T$ and at the inflow is

$$\mathbf{h}_{in}(x,t) = \begin{cases} (10^3(1-\cos(2\pi t/0.025)),\, 0)^T, & x \in \Sigma_1, 0 \leq t \leq 0.025 \\ (0,\, 0)^T, & x \in \Sigma_1, 0.025 \leq t \leq T. \end{cases}$$

The thickness of the elastic wall is $h^S = 0.1\ cm$, the Young modulus $E = 3 \cdot 10^6\ \frac{g}{cm\cdot s^2}$, the Poisson ratio $\nu = 0.3$, the mass density $\rho^S = 1.1\frac{g}{cm^3}$ and the volume forces are $\mathbf{f}^S = (0,\, 0)^T$. The Lamé's coefficients are computed by the formulas:

$$\lambda^S = \frac{\nu^S E}{(1-2\nu^S)(1+\nu^S)}, \qquad \mu^S = \frac{E}{2(1+\nu^S)}.$$

The structure is supposed to be fixed at the left and at the right sides.

Numerical parameters

The numerical tests have been performed using FreeFem++ (see [15]). We have used for the structure a reference mesh of 60 triangles and 62 vertices and for the fluid a reference mesh of 1250 triangles and 696 vertices. The meshes are not necessary compatible at the interface (see Figure 2.2).

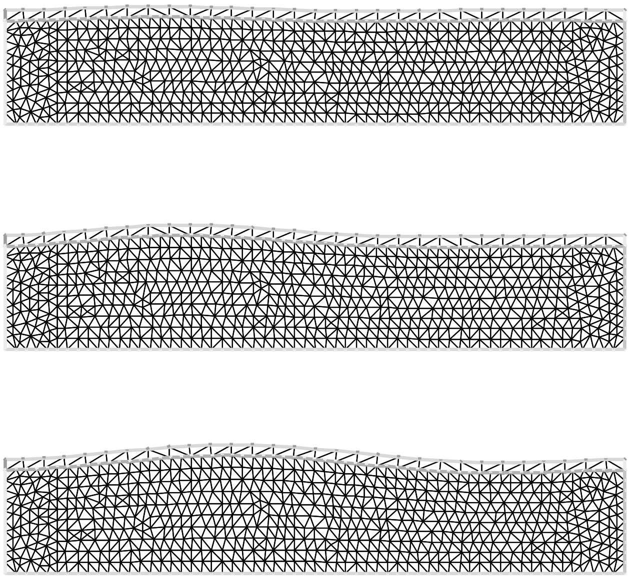

Figure 2.2: Fluid and structure meshes at time instant $t = 0.015$ (top), $t = 0.025$ (middle), $t = 0.035$ (bottom).

For the approximation of the fluid velocity and pressure, we have employed the triangular finite element $\mathbb{P}_1 + bubble$ and $\mathbb{P}_1$ respectively. The finite element $\mathbb{P}_1$ was used in order to solve the eigenproblem of the structure. Only the first $m = 3$ modes have been considered. The first eigenvalues are $\lambda_{1,h} = 7018.91$, $\lambda_{2,h} = 50500$ and $\lambda_{3,h} = 193418$. The real parameter in the θ-centered scheme was chosen to be $\theta = 0.3$.

Stopping criteria

At each time step, the optimization problem have been solved by the BFGS algorithm. We have used the FreeFem++ implementation of the BFGS algorithm which use the stopping criteria: $\|\nabla J\| \leq \epsilon$ or the number of iterations reaches a maximal value *nbiter*. We have performed the computation with $\epsilon = 10^{-4}$ and $nbiter = 10$. We set to 5 maximal number of the iterations for the line search. The final values of the cost function are less than 6.10^{-12}. In other words, the continuity of the velocity at the interface holds at every time step, while the error between the fluid and structure stress at the interface is less than 6.10^{-12}. This implies that $\|\Delta q_i^{n+1}\|$ is less than 10^{-13}.

Behavior of the computed solution

We have performed the simulation for a time duration $T = 0.1\ s$, with time step $\Delta t = 0.001$ and number of iterations in time $N = 100$. We have compared the vertical displacements of three points at the interface between the semi-implicit and the implicit algorithm. Figure 2.3 shows that the solution computed by the semi-implicit algorithm is similar to the one obtained by the implicit algorithm.

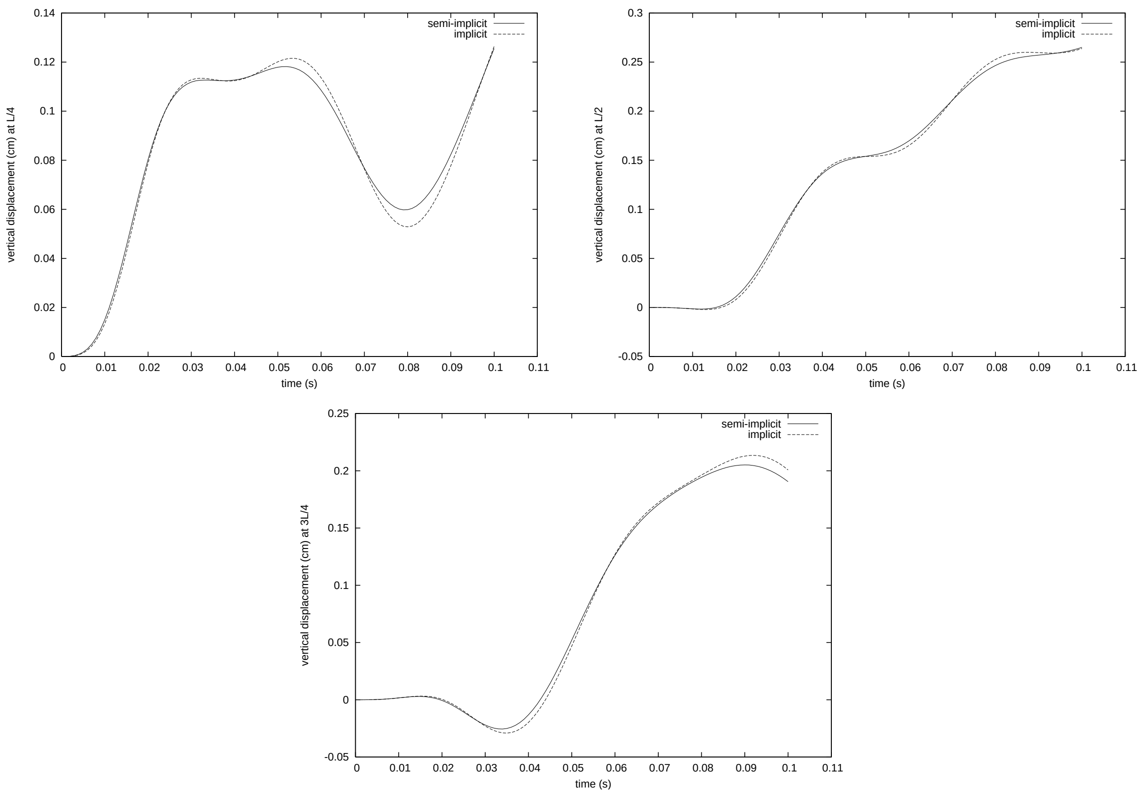

Figure 2.3: Vertical displacement when $\Delta t = 0.001s$ of three points at the interface of horizontal coordinates $x_1 = \dfrac{L}{4}$, (top, left) $x_2 = \dfrac{L}{2}$, (top, right), $x_3 = \dfrac{3L}{4}$ (bottom) for the semi-implicit case and the implicit case.

We have proved that the time stability of the algorithm does not depend on the time step. The vertical displacements of three points at the interface for time steps $\Delta t = 0.001\ s$, $\Delta t = 0.0005\ s$ and $\Delta t = 0.0025\ s$ are presented in Figure 2.4.

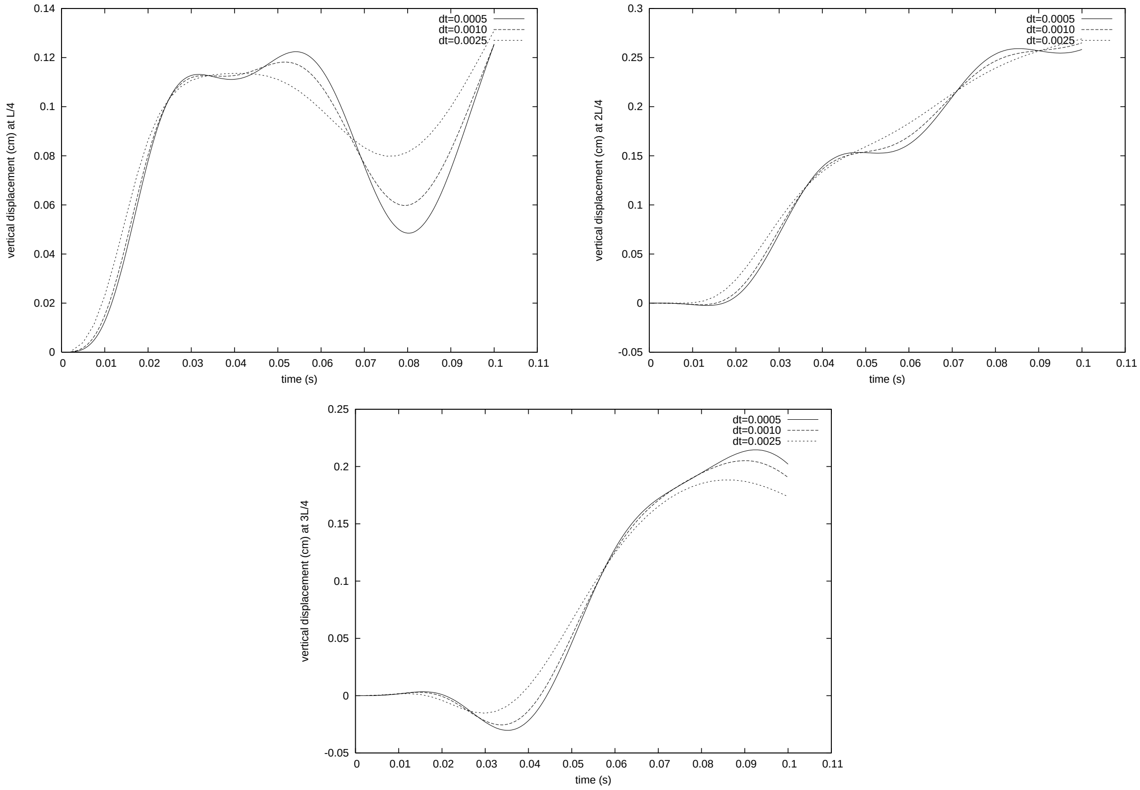

Figure 2.4: Vertical displacement when $\Delta t = 0.001s$, $\Delta t = 0.0005s$, $\Delta t = 0.0025s$ of three points at the interface of horizontal coordinates $x_1 = \frac{L}{4}$ (top, left), $x_2 = \frac{L}{2}$ (top, right), $x_3 = \frac{3L}{4}$ (bottom).

We observe that the vertical displacements are less than 0.3 cm. For $\Delta t = 0.001\ s$, the fluid pressure and velocity at different time instants are plotted in Figures 2.5 and 2.6.

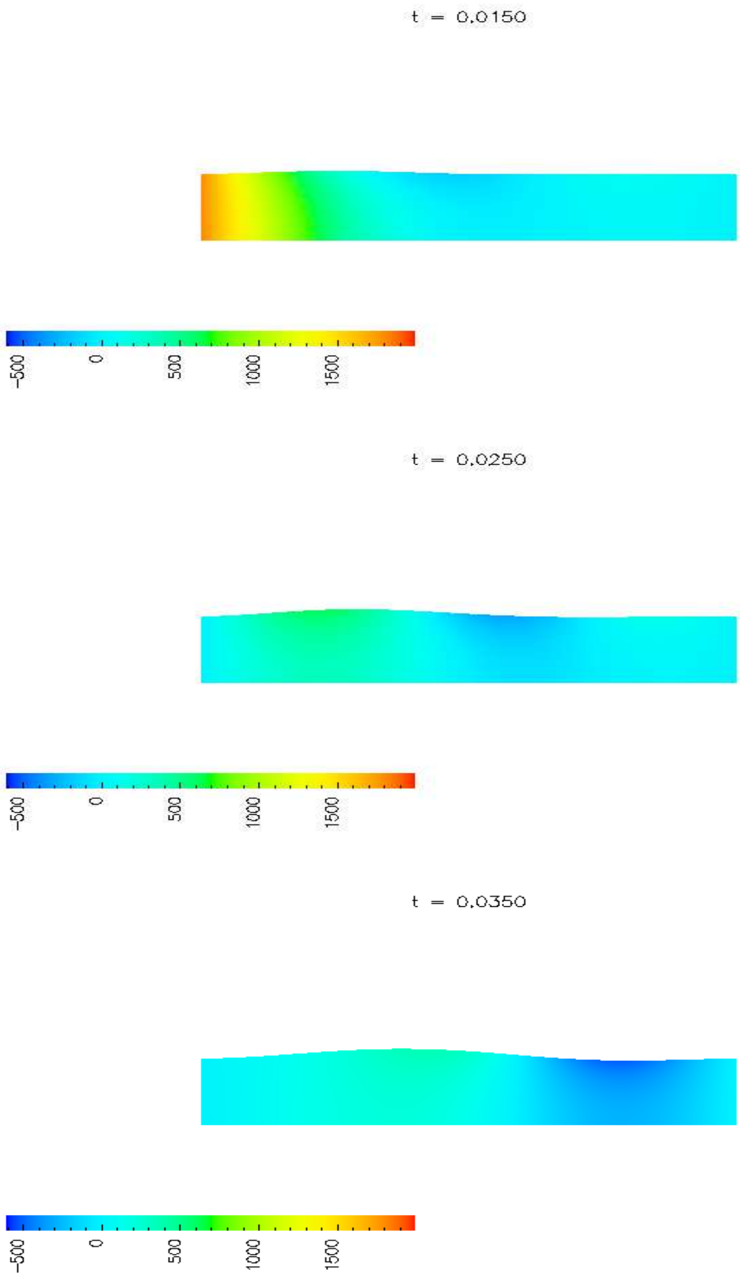

Figure 2.5: Fluid pressure $[\frac{dynes}{cm^2}]$ at time instant $t = 0.015$ (top), $t = 0.025$ (middle), $t = 0.035$ (bottom).

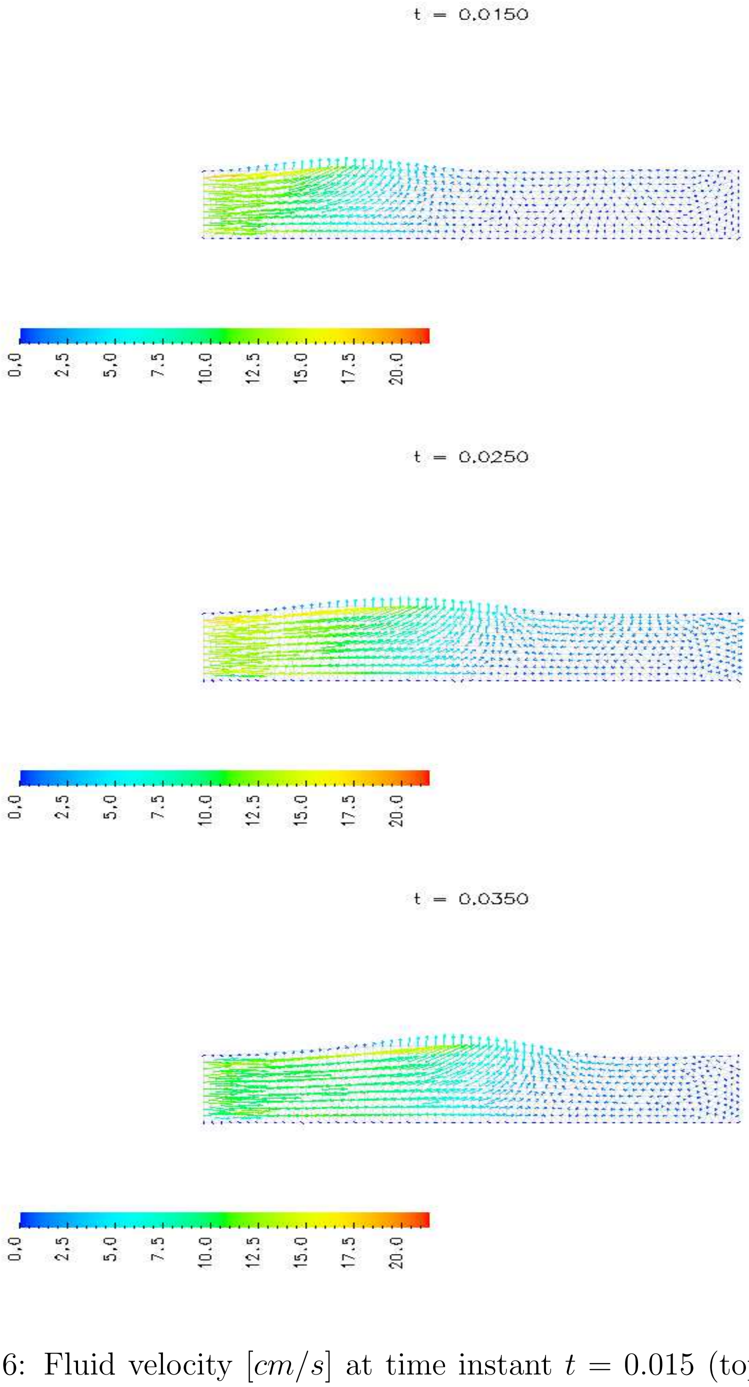

Figure 2.6: Fluid velocity $[cm/s]$ at time instant $t = 0.015$ (top), $t = 0.025$ (middle), $t = 0.035$ (bottom).

CPU time

Here, we will compare the CPU time obtained using the semi-implicit time strategy algorithm proposed in this chapter with the CPU time obtained by the implicit time advancing algorithm. The computation has been made on a computer with one processor of 1.66 GHz frequency and 2 Gb RAM. To compare the computational time between implicit and semi-implicit strategies is mandatory to use the same algorithm for solving the fluid-structure coupled problem at every time step. We emphasize that in the case of implicit strategy the coupled fluid-structure problem is non-linear due to the moving domain, contrary to the semi-implicit strategy, where the coupled problem (20) is linear.

We denote by m the number of eigenfunctions in the modal decomposition of the structure problem and h the mesh seize, nv the number of vertices, nt the number of triangles of the fluid domain.

1. The CPU time in function of m, when the time step is $\Delta t = 0.001s$, the number of steps is $N = 100$, the mesh parameters of fluid are $nv = 696$ and $nt = 1250$ triangles:

m	CPU-semi-implicit	CPU-implicit	$\frac{CPU-implicit}{CPU-semi}$
3	8 mn 30 s	92 mn 30 s	11.12
7	21 mn 44 s	227 mn 53 s	10.62
10	29 mn 54 s	304 mn 22 s	10.30

2. The CPU time in function of fluid mesh size, when $\Delta t = 0.001$, $N = 100$ and $m = 3$:

nv	nt	h	CPU-semi-implicit	CPU-implicit	$\frac{CPU-implicit}{CPU-semi}$
696	1250	0.16	8 mn 30 s	92 mn 30 s	11.12
1632	3052	0.11	19mn 48 s	226 mn 42 s	11.62
2664	5046	0.08	33 mn 50 s	415 mn 23 s	12.39

3. The CPU time in function of Δt, when $m = 3$, $nv = 696$ and $nt = 1250$:

Δt	N	CPU-semi-implicit	CPU-implicit	$\frac{CPU-implicit}{CPU-semi}$
0.0005	200	14 mn 48 s	187 mn 47 s	12.95
0.0010	100	8 mn 30 s	92 mn 30 s	11.12
0.0025	40	3 mn 27 s	36 mn 24 s	11.08

The mean number of cost function calls by time step

At each time step, the BFGS performs on average 5.47 iterations in the semi-implicit case and 6.93 iterations in the implicit case. At each BFGS iteration, 2.68 evaluations of the cost function are necessary on average for the line search in the semi-implicit case and 2.60 iterations in the implicit case. One call of the gradient is necessary at each BFGS iteration for the both semi-implicit and implicit strategies. We compute the gradient $\nabla J(\boldsymbol{\alpha})$ by finite difference scheme:

$$\frac{\partial J}{\partial \alpha_k}(\boldsymbol{\alpha}) = \frac{J(\boldsymbol{\alpha} + \Delta\alpha_k e_k) - J(\boldsymbol{\alpha})}{\Delta\alpha_k}$$

where e_k is the k-th vector of the canonical base of $\mathbb{R}^m$ and $\Delta\alpha_k = 10^{-6}$ is the grid spacing. Thus, $m + 1 = 4$ calls of the cost function are needed to compute the gradient. To sum up, at each time step, the BFGS performs in average 36.59 evaluations of the cost function in the semi-implicit case and 45.80 iterations in the implicit case. We recall that, contrary to the implicit strategy, the semi-implicit one uses a fixed fluid mesh for all calls of the cost function at a time instant, which explains the reduction of the computational time.

2.3.2 Flow in a flexible curved tube

Geometry

The bottom of the fluid domain is Σ_2 the horizontal $[-1, 7] \times \{0\}$. The inflow $\Sigma_1 = \{-1\} \times [0, 1]$ and outflow $\Sigma_3 = \{7\} \times [0, 1]$ sections are vertical segments of length 1 cm. The top boundary Γ_0 of the undeformed fluid domain is composed by three curves: at the left

$$\left\{x_1 = \xi,\ x_2 = 0.1\xi^3 + 0.4\xi^2 + 0.5\xi + 1,\ \xi \in [-1, 0]\right\}$$

in the middle

$$\left\{(x_1, x_2) \in \mathbb{R}^2;\ x_1 = \xi,\ x_2 = -5 + \sqrt{45 - (\xi - 3)^2},\ \xi \in [0, L]\right\}$$

where $L = 6$ and at the right

$$\left\{x_1 = \xi,\ x_2 = -0.1\xi^3 + 2.2\xi^2 - 16.1\xi + 40,\ \xi \in [6, 7]\right\}.$$

As in the previous test, the top boundary is flexible. The initial geometrical configuration is presented in Figure 2.7.

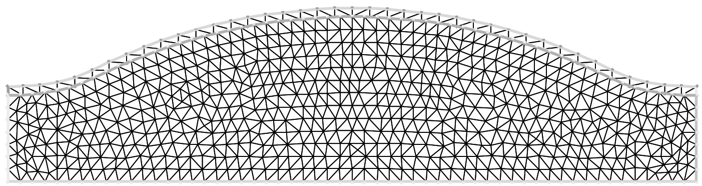

Figure 2.7: Initial fluid and structure meshes.

Physical and numerical parameters

The thickness of the elastic wall is $h^S = 0.1\ cm$ and the left and the right sides are fixed. We have used for the structure a reference mesh of 80 triangles and 82 vertices and for the fluid a reference mesh of 1216 triangles and 672 vertices. The meshes are not necessary compatible at the interface.

We have performed the simulation using the time step $\Delta t = 0.001$ and $N = 120$ time increments. The others physical and numerical parameters are the same as in the previous test.

The fluid velocity computed by the semi-implicit algorithm at different time instants is plotted in Figures 2.8.

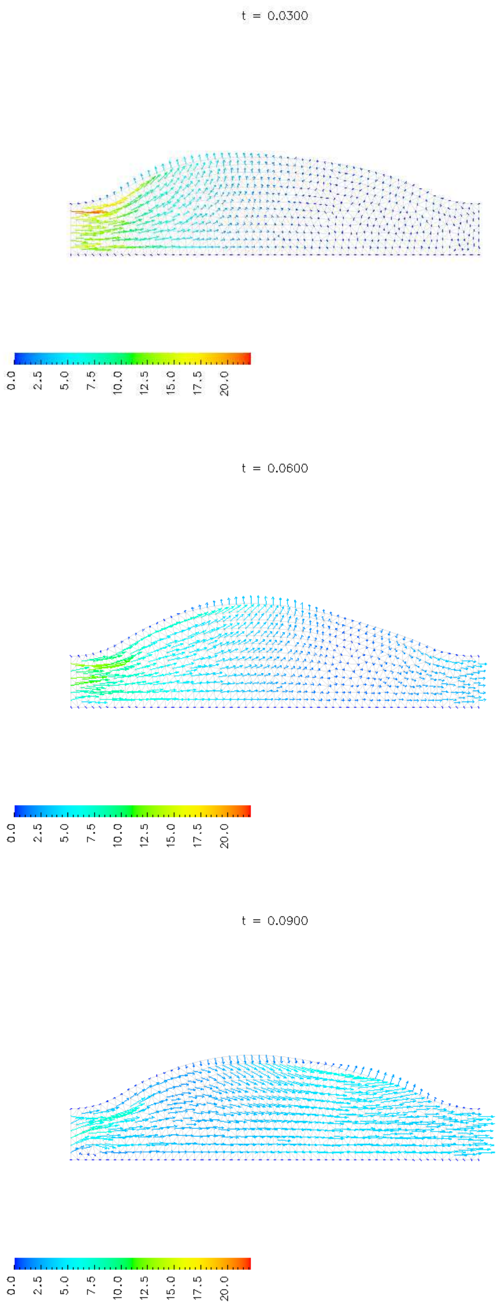

Figure 2.8: Fluid velocity $[cm/s]$ at time instant $t = 0.030$ (top), $t = 0.060$ (middle), $t = 0.090$ (bottom).

The vertical displacement of three points at the interface of horizontal coordinates $x_1 = 1.5$, $x_1 = 3$, $x_1 = 4.5$, respectively, are presented in Figure 2.9.

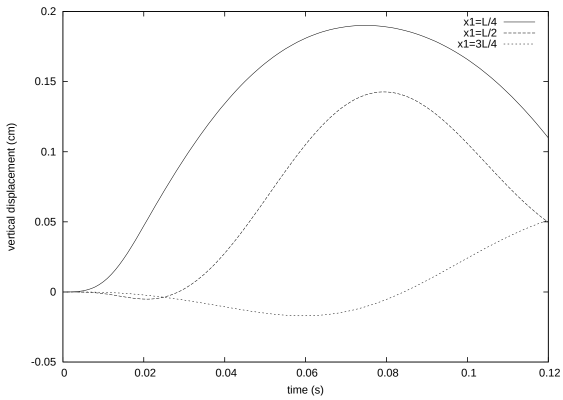

Figure 2.9: Vertical displacement of three points at the interface of horizontal coordinates $x_1 = 1.5$, $x_1 = 3$, $x_1 = 4.5$. The left and right sides of the fluid domain have horizontal coordinates $x_1 = -1$ and $x_1 = 7$.

We recall that the left and right sides of the fluid domain are vertical segments of horizontal coordinates $x_1 = -1$ and $x_1 = 7$, respectively. We observe that the vertical displacements are less than 0.2 cm.

CPU time for small time step

In addition, we have performed the simulation for a small time step $\Delta t = 10^{-6}$. In this case, the BFGS algorithm finds the solution after 2.68 iterations in average, while for a medium time step $\Delta t = 10^{-3}$ the mean number of BFGS iterations was 5.47. The above results have been obtained using the semi-implicit strategy. The mean number of cost function calls at a time instant is 17.74 for $\Delta t = 10^{-6}$, while for $\Delta t = 10^{-3}$, the number of cost function calls was 36.59. When the time step is small, the starting point for the optimization problem is close to the solution, which explains the reduction of the cost function calls. The CPU time for $N = 50$ time iterations and $\Delta t = 10^{-6}$ is 152s when the semi-implicit strategy is used and 689s in the implicit case. The reduction factor of CPU time is 4.53.

2.4 Future works

We intend to apply the semi-implicit algorithm presented in this chapter to realistic applications in haemodynamics and actually we are looking for a three-dimensional computational environment. The partitioned procedures technique employed to solve the coupled fluid-structure problem allows us to employ existing solvers for each sub-problem. We need a structure solver, a solver for Navier-Stokes equations in moving domains and an optimization module. Let us remark that, once the fluid domain is computed by extrapolation, then the structure and the fluid sub-problems could be solved in parallel. We intent to replace the linear model for the structure by a non-linear one which handles large displacements.

2.5 Conclusion

A semi-implicit time advancing scheme for transient fluid-structure interaction problem was presented. For the fluid equations, we consider an implicit Euler scheme for the time derivative and the convection term was linearized. For the structure, we employ a θ-centered scheme of second-order in time. At every time step, a least squares problem is solved by partitioned procedures, such that the continuity of the velocity as well as the continuity of the stress hold at the interface. During the iterative method for solving the optimization problem, the fluid mesh does not move, which reduces the computational effort. The unconditional stability with respect to the time of the algorithm was proved. The numerical results presented in this chapter show that the computed solution is similar to the one obtained by the implicit algorithm, but the computational time is reduced.

Bibliography

[1] K.J. Bathe, H. Zhang, *Finite element developments for general fluid flows with structural interactions*, Int. J. Numer. Meth. Engng. **60** (2004) 213–232.

[2] L. Baffico, *A characteristic-ALE formulation for a fluid-membrane interaction problem*, Comm. Numer. Methods Engrg. **21** (2005) 723–734.

[3] Z.X. Cai, X.Y. Luo, *A fluid-beam model for flow in collapsible channel*, Journal of Fluids and Structures, **17** (2003) 125–146.

[4] P. Causin, J.F. Gerbeau, F. Nobile, *Added-mass effect in the design of partitioned algorithms for fluid-structure problems*, Comput. Methods Appl. Mech. Engrg. **194** (2005) 4506–4527.

[5] S. Deparis, M. Discacciati, A. Quarteroni, *Fluid-structure algorithms based on Steklov-Poincaré operators*, Comput. Methods Appl. Mech. Engrg. **195** (2006) 5797–5812.

[6] W. Dettmer, D. Perić, *A computational framework for fluid-structure interaction: Finite element formulation and applications*, Comput. Methods Appl. Mech. Engrg. **195** (2006) 5754-5779.

[7] G. Duvaut, *Mécanique des milieux continus*, Masson, Paris, 1990.

[8] C. Farhat, M. Lesoinne, *Two efficient staggered algorithms for the serial and parallel solution of three-dimensional nonlinear transient aeroelastic problems*, Comput. Methods Appl. Mech. Engrg. **182** (2000) 499–515.

[9] M.A. Fernàndez, M. Moubachir, *A Newton method using exact jacobians for solving fluid-structure coupling*, Comput. & Structures, **83** (2005) 127-142.

[10] M.A. Fernàndez, J.-F. Gerbeau, C. Grandmont, *A projection semi-implicit scheme for the coupling of an elastic structure with an incompressible fluid*, Internat. J. Numer. Methods Engrg. **69** (2007) no. 4, 794–821.

[11] L. Formaggia, G.F. Gerbeau, F. Nobile, A. Quarteroni, *On the coupling of 3D and 1D Navier-Stokes equations for flow problems in compliant vessels*, Comput. Methods Appl. Mech. Engrg. **191** (2001) 561–582.

[12] C. Forster, W.A. Wall, E. Ramm, *Artificial added mass instabilities in sequential staggered coupling of nonlinear structures and incompressible viscous flows*, Comput. Methods Appl. Mech. Engrg. **196** (2007) 1278–1293.

[13] C. Grandmont, V. Guimet, Y. Maday, *Numerical analysis of some decoupling techniques for the approximation of the unsteady fluid structure interaction*, Math. Models Methods Appl. Sci. **11** (2001), no. 8, 1349–1377.

[14] G.F. Gerbeau, M. Vidrascu, *A quasi-Newton algorithm on a reduced model for fluid-structure interaction problems in blood flows*, Math. Model. Num. Anal., **37** (2003) 631-648.

[15] F. Hecht, O. Pironneau, A. Le Hyaric, K. Ohtsuka, *FreeFem++*: http://www.freefem++.org/ff++.

[16] P. Le Tallec, J. Mouro, *Fluid-structure interaction with large structural displacements*, Comput. Methods Appl. Mech. Engrg. **190** (2001) 3039–3067.

[17] I. Mbaye, C.M. Murea, *Numerical procedure with analytic derivative for unsteady fluid-structure interaction*, Commun. Numer. Meth. Engng. Published Online: July 13, 2007, DOI: 10.1002/cnm.1031

[18] C.M. Murea, *The BFGS algorithm for a nonlinear least squares problem arising from blood flow in arteries*, Comput. Math. Appl., **49** (2005) 171–186.

[19] C.M. Murea, *Numerical simulation of a pulsatile flow through a flexible channel*, ESAIM: Math. Model. Numer. Anal., **40** (2006) 1101–1125.

[20] C.M. Murea, *A semi-implicit algorithm based on the Augmented Lagragian Method for fluid-structure interface*, in: K. Kunish, G. Of, O. Steinbach (eds.) Numerical Mathematics and Advanced Applications, Proceedings of ENUMAT 2007, the 7th Euopean Conference on Numerical Mathematics and Advanced Applications, Graz, Austria, Steptember 2007. Springer, pp. 555-562.

[21] F. Nobile, *Numerical approximation of fluid-structure interaction problems with application to haemodynamics*, Ph.D. Thesis, EPFL, Switzerland, 2001.

[22] F. Nobile, C. Vergara, *An effective fluid-structure interaction formulation for vascular dynamics by generalized Robin conditions*, MOX Report 01/2007.

[23] A. Quarteroni, L. Formaggia, *Mathematical modelling and numerical simulation of the cardiovascular system*, in P.G. Ciarlet (Ed.), Handbook of numerical analysis, Vol. XII, North-Holland, Amsterdam, 2004, 3–127.

[24] A. Quarteroni, A. Valli, *Numerical approximation of PDE*, Springer, Berlin, New York, 1997.

[25] J. Steindorf, H.B. Matthies, *Partioned but strongly coupled iteration schemes for nonlinear fluid-structure interaction*, Comput. & Structures, **80** (2003) 1991–1999.

[26] E.W. Swim, P. Seshaiyer, *A nonconforming finite element method for fluid-structure interaction problems*, Comput. Methods Appl. Mech. Engrg. **195** (2006) 2088–2099.

[27] T.E. Tezduyar, S. Sathe, R. Keedy, K. Stein, *Space-time finite element techniques for computation of fluid-structure interactions*, Comp. Meth. Appl. Mech. Engng, 195 (2006) 2002–2027.

2.6 Application to cerebral aneurysm

Abstract. This section deals with numerical results when the algorithm presented in the chapter II with a nonlinear St-Venant Kirchhoff model for the structure is used to simulate the behaviors of fluid-structure interaction in cerebral aneurysm. At each time step, an optimization problem is solved by partitioned procedure method based in BFGS (Broyden, Fletcher, Goldford, Shano) algorithm in order to get the continuity of stress as well as the continuity of velocity at the interface. The numerical results are presented.

2.6.1 Introduction

The cerebral aneurysm is an abnormal dilation of a blood vessel wall under divers factors, like excess of tobacco and alcohol. It creates therefore a pocket where the blood piles up. The intercranial aneurysm is observed in the outer wall of curved vessel, it is found in the internal carotid artery near the apex of bifurcated vessels including the anterior communicating artery (see [1]). The discovery of cerebral aneurysm holds frequently between 35 years old to 60 years old (2% to 4% of the population and 3 women over 2 men). The unruptured aneurysms have been reported occur in up to 6% of the population and the aneurysm rupture causes over 90% of subarachnoid haemorrhages, which is associated to a high mortality rate (see [3]).

There are some papers dealing with fluid-structure interaction between the blood and the wall aneurysm, for more informations, see ([8] and [9]). In [9], the authors, describe the flow dynamics and arterial wall interaction of a terminal aneurysm of simplified basilar artery and they compute its wall shear stress, pressure, effective stress and wall deformation. In [8], the fluid-structure interaction of a patient specific cerebral aneurysm located in the left middle cerebral bifurcation for high blood pressure is studied.

The geometry configuration of cerebral aneurysm considered here is similar to one used in the article [7].

The aim of this section is to apply the semi-implicit algorithm developed in the paper [6] by replacing the linear elasticity model by nonlinear Saint-Venant Kirchhoff model, in order to simulate the behaviors of fluid-structure interaction arising in cerebral aneurysm. The fluid is governed by Navier Stokes equations and the structure by nonlinear Saint-Venant Kirchhoff model. We follow for the numerical implementation the semi-implicit algorithm developed in [6], where the structure problem is solved by Newton method as in [5].

2.6.2 Setting problem

The fluid and the structure models are setting in two dimensional spaces. We are interested by numerical simulation of fluid-structure interaction problem arising in cerebral aneurysm. Let us denote by Ω^S the undeformed structure domain bounded by: the rigid section Γ_0, the exterior section Γ_1 and the interior section Σ_0. We also denote by Ω_0^F the initial fluid domain bounded by: the rigid section Σ_2, the inflow section Σ_1, the outflow section Σ_3 and the exterior boundary Σ_0, (see Figure 2.10). The boundary Σ_0 is common of both domains and it represents the fluid-structure interface. Under the action of the fluid stress, the structure will be deformed. At the time instant t, the fluid occupies the domain Ω_t^F bounded by the moving interface Σ_t and the rigid boundary $\Sigma_1 \cup \Sigma_2 \cup \Sigma_3$.

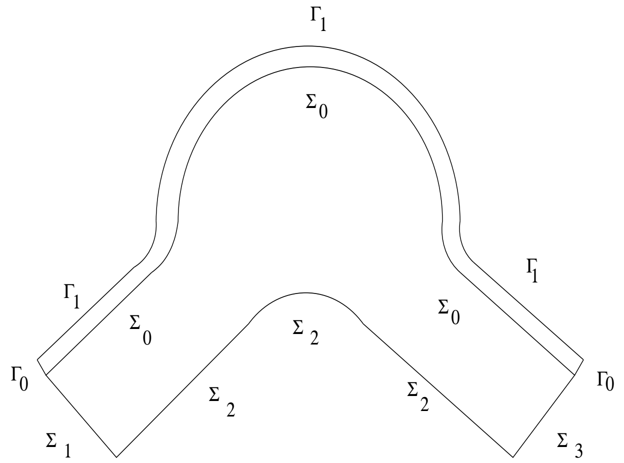

Figure 2.10: Initial geometrical configuration.

2.6.3 Numerical results

Physical parameters

We consider the following data for the numerical computation:
For the fluid: the lengths of the inflow section Σ_1 and of the outflow section Σ_3 are equal to 3mm. The rigid section Σ_2 is is composed of two segments of 5mm length and an arc of circle of 3 mm diameter. The interface Σ_0 is composed of two segments of 5mm length, an arc of circle of 6 mm diameter and two small arcs. The lengths of the small arcs can be computed from Maple. The viscosity of the fluid was fixed to be $\mu = 0.003\ \frac{g}{cm \cdot s}$, its density $\rho^F = 1\ \frac{g}{cm^3}$ and the volume forces in the fluid are $\mathbf{f}^F = (0,\, 0)^T$. The prescribe boundary stress on Σ_3 is $\mathbf{h}_{out}(x,t) = (0,\, 0)^T$ and on Σ_1 is

$$\mathbf{h}_{in}(x,t) = \begin{cases} (10^3(1-\cos(2\pi t/0.025)),\, 0)^T, & x \in \Sigma_2, 0 \le t \le 0.025 \\ (0,\, 0)^T, & x \in \Sigma_2, 0.025 \le t \le T. \end{cases}$$

For the structure: the length of the boundary Γ_1 of the elastic wall is computed in the same way as Σ_0 and the rigid section Γ_0 is composed of two segments of 0.3 mm length. The Young modulus $E = 3 \cdot 10^6 \frac{g}{cm \cdot s^2}$, the Poisson ratio $\nu = 0.3$, the mass density $\rho^S = 1.1 \frac{g}{cm^3}$ and the volume force is $\mathbf{f}^S = (0,\, 0)^T$. The Lamé's coefficients are computed by the formulas:

$$\lambda^S = \frac{\nu^S E}{(1 - 2\nu^S)(1 + \nu^S)}, \qquad \mu^S = \frac{E}{2(1 + \nu^S)}.$$

Numerical parameters

The numerical tests have been performed using FreeFem++ (see [2]). We have used for the structure a reference mesh of 60 triangles and 62 vertices and for the fluid a reference mesh of 1615 triangles and 881 vertices. The compatibility of meshes are not necessary verified at the interface (see Figure 2.11).

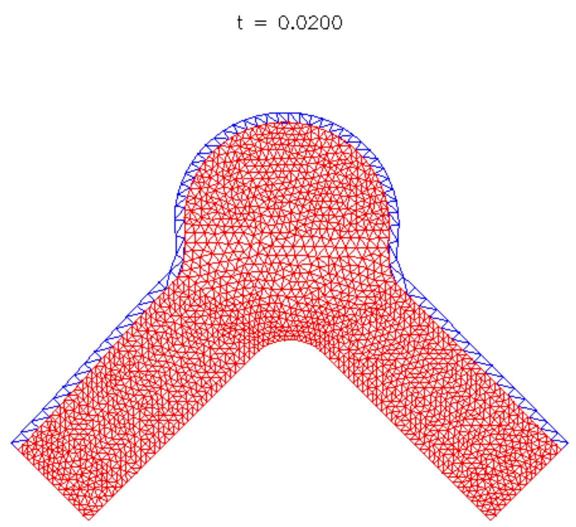

Figure 2.11: Fluid-structure mesh.

For the space approximation of the fluid velocity and pressure, we have used the triangular finite element $\mathbb{P}_1$ + *bubble* and $\mathbb{P}_1$ respectively. The finite element $\mathbb{P}_1$ was employed for the structure displacements. The real parameter in the θ-centered scheme was chosen to be $\theta = 0.3$.

Stopping criteria

At each time step, the optimization problem have been solved by the BFGS. The final values of the cost function are less than $6 \cdot 10^{-10}$. In other words, the continuity of the velocity at the interface holds at every time step, while the error between the fluid and structure stress is less than $6 \cdot 10^{-10}$. In [4], the fluid-structure coupled problem is solved by the Augmented Lagrangian Method and at every time step the continuity of the stress at the interface holds, while the error in the L^2 norm between the fluid and structure velocity at the interface is less than 0.45. Consequently, the boundary conditions at the interface are verified more precisely when we solve by the BFGS algorithm. We have employed as in [5] the FreeFem++ implementation of the BFGS algorithm, which use the stopping criteria: $\|\nabla J\| \leq \epsilon$ or the number of iterations reaches a maximal value *nbiter*. We have performed the computation with $\epsilon = 10^{-4}$ and $nbiter = 10$. We set to 5 maximal number of the iterations for the line search. We compute $\nabla J(\boldsymbol{\alpha})$ by finite difference scheme:

$$\frac{\partial J}{\partial \alpha_k}(\boldsymbol{\alpha}) = \frac{J(\boldsymbol{\alpha} + \Delta\alpha_k e_k) - J(\boldsymbol{\alpha})}{\Delta\alpha_k}$$

where e_k is the k-th vector of the canonical base of $\mathbb{R}^m$. Thus, $m + 1 = 4$ calls of the cost function are needed to compute the gradient.

Behavior of the computed solution

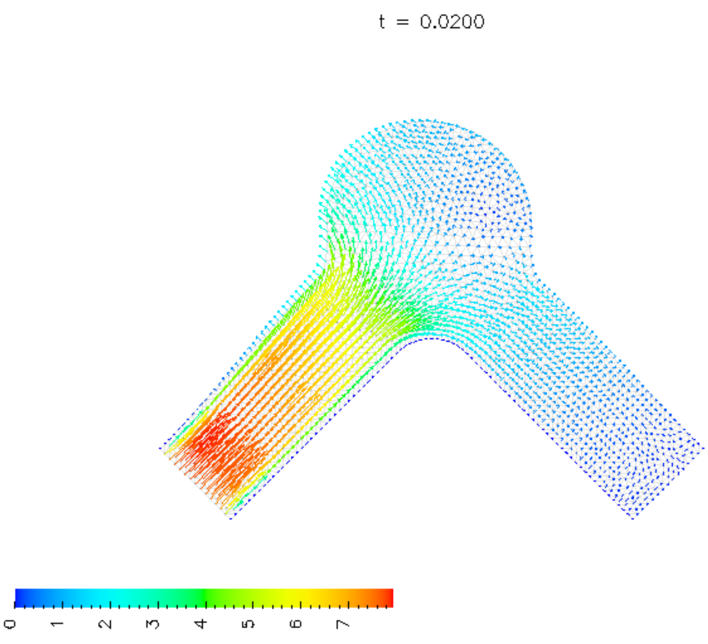

Figure 2.12: Fluid velocities at time instant $t = 0.0200\,s$ in cerebral aneurysm.

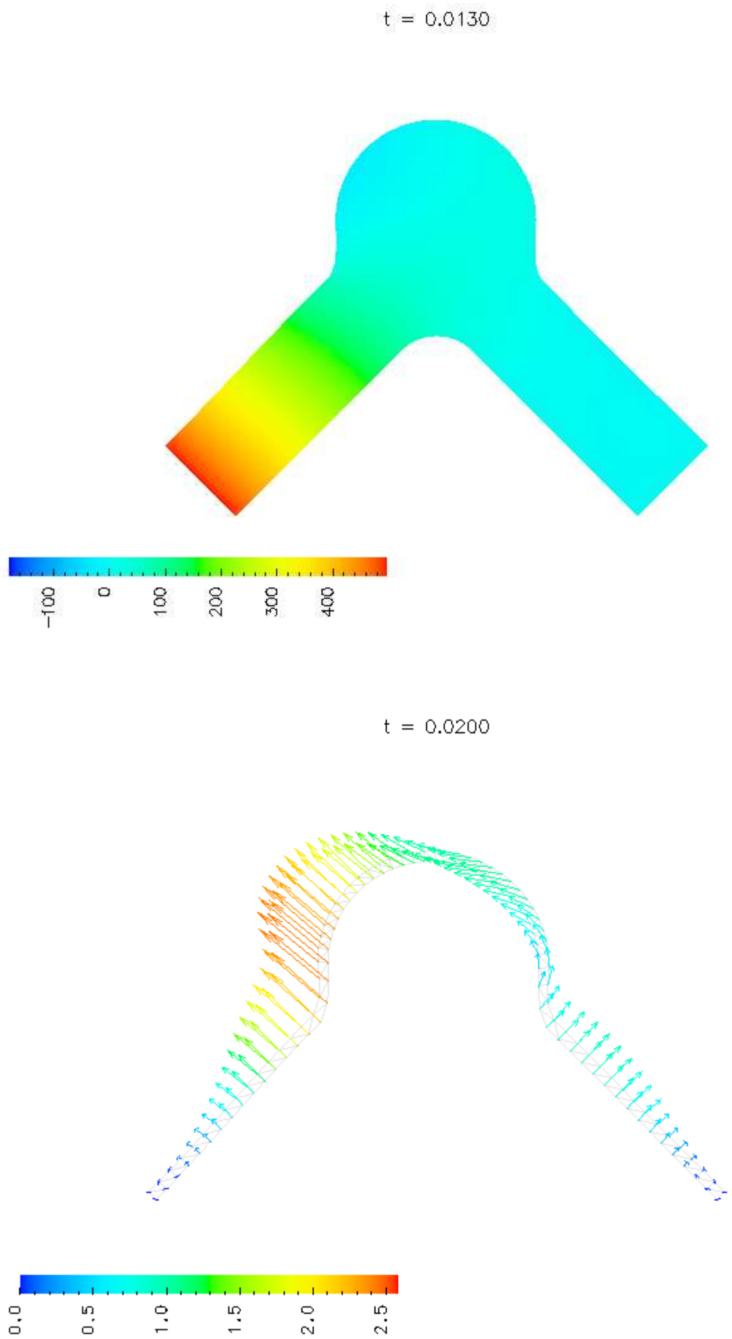

Figure 2.13: Fluid pressure (at the top) at time instant $t = 0.0130\,s$ and structure velocities (at the bottom) at time instant $t = 0.0200\,s$ in cerebral aneurysm.

2.6.4 Conclusion and future works

In this part, a semi-implicit algorithm obtained from the algorithm developed in [6] with nonlinear Saint-Venant Kirchhoff model for the structure has been applied in order to understand some behaviors of fluid-structure interaction in cerebral aneurysm. The Newton method was used to solve the structure problem and at each time step, an optimization problem is solved by partitioned procedure based in BFGS algorithm, in order to get the continuity of velocity as well as the continuity of the stress at the interface.

It is in our intention, to compute the wall shear stress of cerebral aneurysm from this algorithm. In fact, it is known that the wall shear stress are in general responsible for aneurysm rupture.

Bibliography

[1] S. Ahmed, I. D. Sutalo, H. Kavnoudias and A. Madan, *Fluid-structure interaction modelling of a patient specific cerebral aneurysm: ffect of hypertension and modulus of elasticity.* 16^{th} Australasian Fluid Mechanics Conference, Crown Plaza, Gold Coast Australia, 2-7 December 2007.

[2] F. Hecht, O. Pironneau, A. Le Hyaric, K. Ohtsuka, *FreeFem++: http://www.freefem++.org/ff++.*

[3] F. H. Linn, G. J. Rinkel, A. Algra, and J. Van Gijn, *Influence of subarachnoid haemorrhage: role of region, year and rate of computed tomography: a metaanalysis*, *Stokes*, **27** (4):625-629, 1996.

[4] C. M. Murea, *A semi-implicit algorithm based on the Augmented Lagragian Method for fluid-structure interface*, in K. Kunish, G. Of, O. Steinbach (eds.) Numerical Mathematics and Advanced Applications, Proceedings of ENUMAT 2007, the 7th Euopean Conference on Numerical Mathematics and Advanced Applications, Graz, Austria, Steptember 2007. Springer, pp. 555-562.

[5] C. M. Murea, S. Sy, *A fast method for solving fluid-structure interaction problem numerically*, Int. J. Numer. Meth. Fluids, DOI: 10.1002/fld.1931, publisheb online: October, 23, 2008.

[6] S. Sy, C.M. Murea, *A stable time advcing scheme for solving fluid-structure interaction problem at small structural displacements*, Comput. Meth. App. Mech. Eng. **198**, (2008), pp 210-222, DOI: 10.1016/j.cma. 2008. 07. 010.

[7] T. E. Tezduyar, S. Sathe, T. Cragin, B. Nanna, Brian S. Conklin, J. Pausewang and M. Schwaab, *Modelling of fluid-structure interactions with the space-time finite elements: Arterial fluid mechanics*, Int. J. Numer. Meth. Fluids, **54**: 901-922, 2007.

[8] R. Torii, M. Oshima, T. Kobayashi, K. Takagi and E.T. Tezduyar, *Fluid-structure interaction modeling of aneurysmal condition with high and normal blood pressure*, J. Mech, **38**: 482-490, 2006.

[9] A. Valencia, and F. Solis, *Blood flow dynamics and arterial wall interaction in a saccular aneurysm model of the basilar artery*, Comput. Struct, **84**: 1326-1337, 2006.

Chapter 3

A monolithic semi-implicit algorithm for fluid-structure interaction problem at small structural displacements

Abstract. We present a monolithic semi-implicit algorithm for solving fluid-structure interaction problem at small structural displacements. The algorithm uses one global mesh for the fluid-structure domain obtained by gluing the fluid and structure meshes which are matching on the interface. The continuity of velocity at the interface is automatically satisfied and the continuity of stress does not appear explicitly in the global weak form due to the action and reaction principle. At each time step, we have to solve a monolithic system of unknowns velocity and pressure defined on the global fluid-structure domain. Numerical results are presented.

3.1 Introduction

We propose in this chapter a monolithic semi-implicit algorithm to solve fluid-structure interaction problem at small structural displacements. The fluid is assumed to be governed by Navier-Stokes equations and the structure is governed by linear elasticity equations. Usually, the structure equations are written using Lagrangian coordinates and the fluid equations are written in the Eulerian framework. But the boundary conditions at the fluid-structure interface are easily implemented when the structure equations as well as the fluid equations are written in the Eulerian domain. We have introduced a global fluid-structure mesh obtained by gluing the fluid and structure meshes which are matching on the interface. An approach using a global fluid-structure mesh has been presented in [3] for immersed interface problems, but the global mesh is fixed and the position of the fluid-structure interface is determined at each time by the level set method.

We have defined the fluid-structure pressure by extending the fluid pressure to be zero on the structure domain. At each time step, we have to solve a linear system of unknowns velocity and pressure defined on the global fluid-structure domain. We point out that the global mesh is moving in time contrary to [3]. Since the velocity is continuous all over the global domain, the continuity of the velocity at the interface is automatically satisfied. Moreover, the test functions are globally continuous and using the action and reaction principle, the continuity of stress at the interface does not appear explicitly in the global weak formulation.

Monolithic implicit algorithms for solving nonlinear fluid-structure interaction were introduced in [6], [7], [8]. In [6], the algorithm use the same time discretization scheme for the fluid and structure equations where the global nonlinear algebraic system was solved by Newton method and in [7] the author has compared the CPU time between a monolithic algorithm and an implicit partitioned procedures one. The paper [8] deals with space-time finite elements for solving the monolithic algorithm. Space-time finite element techniques for fluid-structure interactions problems are presented in [12].

The term "semi-implicit" used here means that the interface between the fluid and the structure is computed in explicit way while the fluid-structure velocity and pressure in implicit way. Semi-implicit algorithm based on Chorin-Temam projection method was introduced in [4], where the main idea was to decouple the fluid velocity computation from the strong coupled fluid-structure system which involves only the pressure and the structure velocity as unknowns. Other semi-implicit partitioned procedures algorithms have been used in [1], [2], [9], [10], [11], [13] for fluid-structure interaction problem. The advantage in general to use the semi-implicit algorithm instead of the implicit one is that, with the semi-implicit algorithm, the geometric non-linearity disappears. Semi-implicit monolithic algorithms based on algebraic approaches can be found in [1], [2], [13].

The method that we use in this chapter is different from the methods proposed in the papers cited before:
- the continuity of stress is canceled from weak formulation of the coupling system and the continuity of velocity is automatically satisfied, contrary to [1], [2], [13] where the lood from the fluid acting on the structure have to be computed;
- the characteristic functions used here give the freedom to choose the fluid and structure time discretization schemes independently, contrary to [6] where the same time discretization schemes is employed all over the domain;
- the fluid-structure interface is computed in explicit way allows to know at each time step the position of the interface, contrary to [3] where the position of the interface is determined by the level set method.

3.2 Problem setting

We are interested by fluid-structure interaction problem in two dimensions. Let us denote by Ω_0^S the undeformed structure domain and we suppose that its boundary $\partial\Omega_0^S$ admits decomposition $\partial\Omega_0^S = \Gamma_D \cup \Gamma_N \cup \Gamma_0$, with $\Gamma_D = [AB] \cup [CD]$ and $\Gamma_N = [AD]$ (see Figure 3.1 at the left). We denote by Ω_0^F the initial fluid domain bounded by: Σ_1 the inflow section, Σ_2 the bottom boundary, Σ_3 the outflow section and Γ_0 the top boundary. The boundary Γ_0 is common of both domains and it represents the fluid-structure interface. We have assumed that Ω_0^F and Ω_0^S are opened sets and we denote by $\Omega_0 = \Omega_0^S \cup \Omega_0^F \cup \Gamma_0$ the initial fluid-structure domain. We have added Γ_0 in order to get Ω_0 a connected domain.

Under the action of the fluid stress, the structure will be deformed. At the time instant t, the fluid occupies the domain Ω_t^F bounded by the moving interface Γ_t and the rigid boundary $\Sigma = \Sigma_1 \cup \Sigma_2 \cup \Sigma_3$ and the structure occupies the domain Ω_t^S bounded by fluid-structure interface Γ_t, the rigid boundary Γ_D and the top boundary Γ_N (see Figure 3.1 at the right). The fluid-structure domain at time instant t will be denoted by $\Omega_t = \Omega_t^S \cup \Omega_t^F \cup \Gamma_t$.

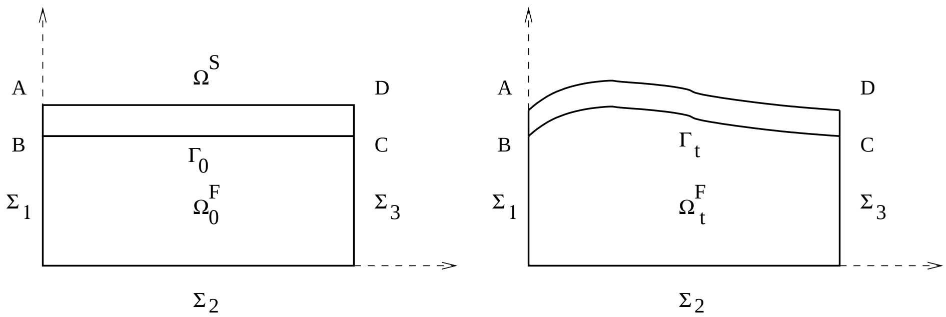

Figure 3.1: Initial (left) and intermediate (right) geometrical configuration.

We suppose that the fluid is governed by Navier-Stokes equations and the structure is governed by linear elasticity equations. The coupling between the fluid and the structure is realized through two boundary conditions at the interface, namely, the continuity of the velocity and the equality of the stress. At each time $t \in [0, T]$, we are interested to know: the fluid velocity $\mathbf{v}^F(t) = (v_1^F(t), v_2^F(t))^T : \Omega_t^F \to \mathbb{R}^2$, the fluid pressure $p^F(t) : \Omega_t^F \to \mathbb{R}$ and the structure displacement $\mathbf{u}^S(t) = (u_1^S(t), u_2^S(t))^T : \Omega_0^S \to \mathbb{R}^2$.

The Arbitrary Eulerian Lagrangian (ALE) transformation is well adopted to solve fluid equations in moving domain (see [14]). Let $\widehat{\Omega}^F$ be a reference fluid domain and let $\mathcal{A}_t, t \in [0, T]$ be a family of transformations such that: $\mathcal{A}_t(\widehat{\mathbf{x}}) = \widehat{\mathbf{x}}$ for all $\widehat{\mathbf{x}} \in \Sigma_1 \cup \Sigma_2 \cup \Sigma_3$ and $\mathcal{A}_t(\widehat{\Omega}^F) = \Omega_t^F$, where $\widehat{\mathbf{x}} = (\widehat{x}_1, \widehat{x}_2)^T \in \widehat{\Omega}^F$ are the ALE coordinates and $\mathbf{x} = (x_1, x_2)^T = \mathcal{A}_t(\widehat{\mathbf{x}})$ the Eulerian coordinates.

Let $\mathbf{v}^F$ be the fluid velocity in the Eulerian coordinates. We denote by $\widehat{\mathbf{v}}^F : \widehat{\Omega}^F \longrightarrow \mathbb{R}^2$ the corresponding function in the ALE coordinates, which is defined by:

$$\widehat{\mathbf{v}}^F(\widehat{\mathbf{x}}, t) = \mathbf{v}^F(\mathcal{A}_t(\widehat{\mathbf{x}}), t) = \mathbf{v}^F(\mathbf{x}, t).$$

We denote the mesh velocity by:

$$\boldsymbol{\vartheta}(\mathbf{x}, t) = \frac{\partial \mathcal{A}_t}{\partial t}(\widehat{\mathbf{x}}) = \frac{\partial \mathcal{A}_t}{\partial t}(\mathcal{A}_t^{-1}(\mathbf{x}))$$

and the ALE time derivative of the fluid velocity by:

$$\left.\frac{\partial \mathbf{v}^F}{\partial t}\right|_{\widehat{\mathbf{x}}}(\mathbf{x}, t) = \frac{\partial \widehat{\mathbf{v}}^F}{\partial t}(\widehat{\mathbf{x}}, t).$$

We assume that the fluid-structure interaction is governed by the following equations:

Navier Stokes equations

$$\begin{aligned}
&\rho^F \left(\left.\frac{\partial \mathbf{v}^F}{\partial t}\right|_{\widehat{\mathbf{x}}} + \left(\left(\mathbf{v}^F - \boldsymbol{\vartheta}\right) \cdot \nabla\right) \mathbf{v}^F \right) - 2\mu^F \nabla \cdot \epsilon\left(\mathbf{v}^F\right) \\
&+\nabla p^F = \mathbf{f}^F, \text{ in } \Omega_t^F \times (0, T] && (3.1)\\
&\nabla \cdot \mathbf{v}^F = 0, \quad \text{in } \Omega_t^F \times (0, T] && (3.2)\\
&\sigma^F(\mathbf{v}^F, p^F) \cdot \mathbf{n}^F = \mathbf{h}_{in}, \quad \text{on } \Sigma_1 \times (0, T] && (3.3)\\
&\sigma^F(\mathbf{v}^F, p^F) \cdot \mathbf{n}^F = \mathbf{h}_{out}, \quad \text{on } \Sigma_3 \times (0, T] && (3.4)\\
&\mathbf{v}^F = 0, \quad \text{on } \Sigma_2 \times (0, T] && (3.5)\\
&\mathbf{v}^F(\mathbf{X}, 0) = \mathbf{v}^0(\mathbf{X}), \quad \text{in } \Omega_0^F. && (3.6)
\end{aligned}$$

Linear elasticity equations

$$\begin{aligned}
&\rho^S \frac{\partial^2 \mathbf{u}^S}{\partial t^2} - \nabla \cdot \sigma^S(\mathbf{u}^S) = \mathbf{f}^S, \quad \text{in } \Omega_0^S \times (0, T] && (3.7)\\
&\mathbf{u}^S = 0, \quad \text{on } \Gamma_D \times (0, T] && (3.8)\\
&\sigma^S(\mathbf{u}^S)\mathbf{n}^S = 0, \quad \text{on } \Gamma_N \times (0, T] && (3.9)\\
&\mathbf{u}^S(\mathbf{X}, 0) = \mathbf{u}^0(\mathbf{X}), \quad \text{in } \Omega_0^S. && (3.10)
\end{aligned}$$

Coupling conditions

$$\begin{aligned}
&\mathbf{v}^F(\mathbf{X} + \mathbf{u}^S(\mathbf{X}, t), t) = \frac{\partial \mathbf{u}^S}{\partial t}(\mathbf{X}, t), \quad \text{on } \Gamma_0 \times (0, T] && (3.11)\\
&(\sigma^F \mathbf{n}^F)_{(\mathbf{X} + \mathbf{u}^S(\mathbf{X}, t), t)} = -(\sigma^S \mathbf{n}^S)_{(\mathbf{X}, t)}, \quad \text{on } \Gamma_0 \times (0, T], && (3.12)
\end{aligned}$$

where the strain tensor is $\epsilon(\mathbf{v}) = \dfrac{1}{2}\Big(\nabla\mathbf{v} + (\nabla\mathbf{v})^T\Big)$ and the stress tensors are

$$\sigma^F(\mathbf{v}^F, p^F) = -p^F\mathbb{I}_2 + 2\mu^F\epsilon(\mathbf{v}^F), \quad \sigma^S(\mathbf{u}^S) = \lambda^S(\nabla\cdot\mathbf{u}^S)\mathbb{I}_2 + 2\mu^S\epsilon(\mathbf{u}^S).$$

Moreover, $\rho^F > 0$ is the mass density of the fluid (respectively $\rho^S > 0$ the density mass of the structure), μ^F is the viscosity of the fluid (respectively μ^S, and λ^S are the Lamé's coefficients), $\mathbf{f}^F = (f_1^F, f_2^F)$ are the applied volume forces of the fluid, in general the gravity forces, (respectively $\mathbf{f}^S = (f_1^S, f_2^S)$ the applied volume forces on the structure), $\mathbf{h}_{in}$ (respectively $\mathbf{h}_{out}$) is the prescribed boundary stress on Σ_1 (respectively on Σ_3), $\mathbf{n}^S = (n_1^S, n_2^S)$ is the structure unit outward normal to Γ_0, $\mathbf{n}^F = (n_1^F, n_2^F)$ is the fluid unit outward normal to Γ_t, $\mathbb{I}_2$ is the unitary matrix of dimension two.

Without risk of confusion, we use the same notation ∇ for the gradient operator with respect to Lagrangian coordinates $\mathbf{X}$ or Eulerian coordinates $\mathbf{x}$. We use the same convention for the divergence and Laplacian operators.

3.3 Time discretization

The time discretization of the fluid equations is based on the backward Euler scheme and a linearization of the convective term. We use a Newmark scheme of second order for the time approximation of the structure equations. Let N be the number of time step and $\Delta t = \frac{T}{N}$ the time step. We set $t_n = n\Delta t$ for all $n = 0, \cdots, N$ the subdivision points of $[0, T]$. We denote by $\mathbf{u}^{S,n}$, $\dot{\mathbf{u}}^{S,n}$, $\ddot{\mathbf{u}}^{S,n}$ the approximations of $\mathbf{u}^S(t_n)$, $\dfrac{\partial\mathbf{u}^S}{\partial t}(t_n)$, $\dfrac{\partial^2\mathbf{u}^S}{\partial t^2}(t_n)$ respectively, and $\mathbf{v}^{F,n}$, $p^{F,n}$ the approximations of $\mathbf{v}^F(t_n)$, $p^F(t_n)$, respectively.

We define $\boldsymbol{\vartheta}^n = (\vartheta_1^n, \vartheta_2^n)^T$ the velocity of the fluid domain as solution of:

$$\left\{\begin{array}{lll} \Delta\boldsymbol{\vartheta}^n & = & 0, \quad \Omega_n^F \\ \boldsymbol{\vartheta}^n & = & 0, \quad \partial\Omega_n^F \setminus \Gamma_n \\ \boldsymbol{\vartheta}^n & = & \mathbf{v}^{F,n}, \quad \Gamma_n. \end{array}\right. \tag{3.13}$$

For the ALE domain, we set $\widehat{\Omega}^F = \Omega_n^F$ and for all $n = 0, \cdots, N-1$, we denote by $\mathcal{A}_{t_{n+1}}$ the map from $\overline{\Omega}_n^F$ to $\mathbb{R}^2$ defined by:

$$\mathcal{A}_{t_{n+1}}(\widehat{x}_1, \widehat{x}_2) = (\widehat{x}_1 + \Delta t\vartheta_1^n, \widehat{x}_2 + \Delta t\vartheta_2^n).$$

We set $\Omega_{n+1}^F = \mathcal{A}_{t_{n+1}}(\Omega_n^F)$ and we define the map:

$$\mathbb{T} = \mathcal{A}_{t_n} \circ \mathcal{A}_{t_{n-1}} \cdots \circ \mathcal{A}_{t_1}$$

then, we may observe that

$$\Gamma_n = \mathbb{T}(\Gamma_0).$$

We define the fluid velocity $\widehat{\mathbf{v}}^{F,n+1} : \Omega_n^F \to \mathbb{R}^2$ (respectively the fluid pressure $\widehat{p}^{F,n+1} : \Omega_n^F \to \mathbb{R}$) at time instant t_{n+1} on Ω_n^F by:

$$
\begin{aligned}
&\widehat{\mathbf{v}}^{F,n+1}(\widehat{\mathbf{x}}) = \mathbf{v}^{F,n+1}(\mathbf{x}), \quad \widehat{p}^{F,n+1}(\widehat{\mathbf{x}}) = p^{F,n+1}(\mathbf{x}),\\
&\forall\, \widehat{\mathbf{x}} \in \Omega_n^F,\ \mathbf{x} = \mathcal{A}_{t_{n+1}}(\widehat{\mathbf{x}}) \in \Omega_{n+1}^F.
\end{aligned}
$$

Discrete fluid equations

Find $\widehat{\mathbf{v}}^{F,n+1} : \Omega_n^F \to \mathbb{R}^2$ and $\widehat{p}^{F,n+1} : \Omega_n^F \to \mathbb{R}$ such that:

$$
\begin{aligned}
&\rho^F \left(\frac{\widehat{\mathbf{v}}^{F,n+1} - \mathbf{v}^{F,n}}{\Delta t} + \left(\left(\mathbf{v}^{F,n} - \boldsymbol{\vartheta}^n \right) \cdot \nabla \right) \widehat{\mathbf{v}}^{F,n+1} \right)\\
&-2\mu^F \nabla \cdot \epsilon \left(\widehat{\mathbf{v}}^{F,n+1} \right) + \nabla \widehat{p}^{F,n+1} = \widehat{\mathbf{f}}^{F,n+1}, \ \text{in } \Omega_n^F && (3.14)\\
&\nabla \cdot \widehat{\mathbf{v}}^{F,n+1} = 0, \ \text{in } \Omega_n^F && (3.15)\\
&\sigma^F(\widehat{\mathbf{v}}^{F,n+1}, \widehat{p}^{F,n+1}) \cdot \mathbf{n}^F = \mathbf{h}_{in}^{n+1}, \ \text{on } \Sigma_1 && (3.16)\\
&\sigma^F(\widehat{\mathbf{v}}^{F,n+1}, \widehat{p}^{F,n+1}) \cdot \mathbf{n}^F = \mathbf{h}_{out}^{n+1}, \ \text{on } \Sigma_3 && (3.17)\\
&\widehat{\mathbf{v}}^{F,n+1} = 0, \ \text{on } \Sigma_2 && (3.18)\\
&\mathbf{v}^F(\mathbf{X}, 0) = \mathbf{v}^0(\mathbf{X}), \ \text{in } \Omega_0^F. && (3.19)
\end{aligned}
$$

Discrete structure equations

Find $\mathbf{u}^{S,n+1}$, $\dot{\mathbf{u}}^{S,n+1}$, $\ddot{\mathbf{u}}^{S,n+1}$: $\Omega_0^S \to \mathbb{R}^2$ such that:

$$
\begin{aligned}
&\rho^S \ddot{\mathbf{u}}^{S,n+1} - \nabla \cdot \sigma^S(\mathbf{u}^{S,n+1}) = \mathbf{f}^{S,n+1}, \quad \text{in } \Omega_0^S && (3.20)\\
&\mathbf{u}^{S,n+1} = 0, \quad \text{on } \Gamma_D && (3.21)\\
&\sigma^S(\mathbf{u}^{S,n+1})\mathbf{n}^S = 0, \quad \text{on } \Gamma_N && (3.22)\\
&\mathbf{u}^S(\mathbf{X}, 0) = \mathbf{u}^0(\mathbf{X}), \quad \text{in } \Omega_0^S && (3.23)
\end{aligned}
$$

$$
\begin{aligned}
\dot{\mathbf{u}}^{S,n+1} &= \dot{\mathbf{u}}^{S,n} + \Delta t \Big[(1-\delta)\ddot{\mathbf{u}}^{S,n} + \delta \ddot{\mathbf{u}}^{S,n+1} \Big] && (3.24)\\
\mathbf{u}^{S,n+1} &= \mathbf{u}^n + \Delta t \dot{\mathbf{u}}^{S,n}\\
&\quad + (\Delta t)^2 \Big[\Big(\frac{1}{2} - \theta \Big) \ddot{\mathbf{u}}^{S,n} + \theta \ddot{\mathbf{u}}^{n+1} \Big]. && (3.25)
\end{aligned}
$$

For $\delta = \dfrac{1}{2}$, the Newmark scheme is of second order in time.

Coupling conditions

$$
\begin{aligned}
&\widehat{\mathbf{v}}^{F,n+1} \circ \mathbb{T} = \dot{\mathbf{u}}^{S,n+1}, \quad \text{on } \Gamma_0 \times (0, T] && (3.26)\\
&(\sigma^F(\widehat{\mathbf{v}}^{F,n+1}, \widehat{p}^{F,n+1})\mathbf{n}^F) \circ \mathbb{T} = -\sigma^S(\mathbf{u}^{S,n+1})\mathbf{n}^S, \quad \text{on } \Gamma_0 \times (0, T]. && (3.27)
\end{aligned}
$$

3.4 Weak formulation of the time discrete equations

We define the spaces of test functions $\widehat{W}_n^F$ for the fluid velocity and $\widehat{Q}_n^F$ for the fluid pressure as following:

$$\widehat{W}_n^F = \left\{ \widehat{\mathbf{w}}^F \in (H^1(\Omega_n^F))^2; \;\; \widehat{\mathbf{w}}^F = 0 \;\text{ on }\; \Sigma_2 \right\},$$
$$\widehat{Q}_n^F = L^2(\Omega_n^F).$$

We multiply the equations (3.14) by a test function $\widehat{\mathbf{w}}^F \in \widehat{W}_n^F$ and the equation (3.15) by a test function $\widehat{q} \in \widehat{Q}_n^F$, after integrating them over the domain Ω_n^F by part, and using the corresponding boundary conditions, we get the following discrete weak form:

Find $\widehat{\mathbf{v}}^{F,n+1} \in \widehat{W}_n^F$ and $\widehat{p}^{F,n+1} \in \widehat{Q}_n^F$ such that:

$$\begin{aligned}
&\int_{\Omega_n^F} \rho^F \frac{\widehat{\mathbf{v}}^{F,n+1}}{\Delta t} \cdot \widehat{\mathbf{w}}^F + \int_{\Omega_n^F} \rho^F \left(\left(\left(\mathbf{v}^{F,n} - \boldsymbol{\vartheta}^n \right) \cdot \nabla \right) \widehat{\mathbf{v}}^{F,n+1} \right) \cdot \widehat{\mathbf{w}}^F \\
&- \int_{\Omega_n^F} \left(\nabla \cdot \widehat{\mathbf{w}}^F \right) \widehat{p}^{F,n+1} + \int_{\Omega_n^F} 2\mu^F \epsilon\left(\widehat{\mathbf{v}}^{F,n+1} \right) : \epsilon\left(\widehat{\mathbf{w}}^F \right) \\
&- \int_{\Gamma_n} \left(\sigma^F \mathbf{n}^F \right) \cdot \widehat{\mathbf{w}}^F = \mathcal{L}_F(\widehat{\mathbf{w}}^F), \quad \forall \widehat{\mathbf{w}}^F \in \widehat{W}_n^F
\end{aligned} \tag{3.28}$$

$$\int_{\Omega_n^F} \widehat{q}(\nabla \cdot \widehat{\mathbf{v}}^{F,n+1}) = 0, \quad \forall \widehat{q} \in \widehat{Q}_n^F \tag{3.29}$$

where

$$\mathcal{L}_F(\widehat{\mathbf{w}}^F) = \int_{\Omega_n^F} \rho^F \frac{\widehat{\mathbf{v}}^{F,n}}{\Delta t} \cdot \widehat{\mathbf{w}}^F + \int_{\Omega_n^F} \widehat{\mathbf{f}}^{n+1,F} \cdot \widehat{\mathbf{w}}^F + \int_{\Sigma_1} \widehat{\mathbf{h}}_{in}^{n+1} \cdot \widehat{\mathbf{w}}^F + \int_{\Sigma_3} \widehat{\mathbf{h}}_{out}^{n+1} \cdot \widehat{\mathbf{w}}^F.$$

Remark 3.1 *The system (3.20), (3.24), (3.25) is a system of three vectorial unknowns and three vectorial equations, we can reduce it to a system where the only unknown is the structure velocity. For that we have to express the displacement $\mathbf{u}^{S,n+1}$ and the acceleration $\ddot{\mathbf{u}}^{S,n+1}$ in function of the velocity $\dot{\mathbf{u}}^{S,n+1}$ from (3.25) and (3.24), see [9] for the details.*

We now define the space of test functions for the structure velocity

$$W^S = \left\{ \mathbf{w}^S \in (H^1(\Omega_0^S))^2; \;\; \mathbf{w}^S = 0 \;\text{ on }\; \Gamma_D \right\}.$$

Let us multiply the equation (3.20) by a test function $\mathbf{w}^S \in W^S$ and we integrate it over the domain Ω_0^S by part, using the corresponding boundary conditions and following the remark (3.1), we get the following discrete structure weak form:

Find $\dot{\mathbf{u}}^{S,n+1} \in W^S$ such that:

$$\begin{aligned}
&\int_{\Omega_0^S} \frac{2\rho^S}{\Delta t} \dot{\mathbf{u}}^{S,n+1} \cdot \mathbf{w}^S + 2\theta \Delta t a_S(\dot{\mathbf{u}}^{S,n+1}, \mathbf{w}^S) \\
&- \int_{\Gamma_0} (\sigma^S \mathbf{n}^S) \cdot \mathbf{w}^S = \mathcal{L}_S(\mathbf{w}^S), \quad \forall \mathbf{w}^S \in W^S,
\end{aligned} \tag{3.30}$$

where

$$a_S(\mathbf{u}, \mathbf{w}) = \int_{\Omega_0^S} \Big[\lambda^S (\nabla \cdot \mathbf{u})(\nabla \cdot \mathbf{w}) + 2\mu^S \epsilon(\mathbf{u}) : \epsilon(\mathbf{w}) \Big]$$

and

$$\begin{aligned}
\mathcal{L}_S(\mathbf{w}^S) = &\int_{\Omega_0^S} f^S \cdot \mathbf{w}^S + \int_{\Omega_0^S} \frac{2\rho^S}{\Delta t} \dot{\mathbf{u}}^{S,n} \cdot \mathbf{w}^S + \int_{\Omega_0^S} \rho^S \ddot{\mathbf{u}}^{S,n} \cdot \mathbf{w}^S - a_S(\mathbf{u}^{S,n}, \mathbf{w}^S) \\
&- \Delta t (1 - 2\theta) a_S(\dot{\mathbf{u}}^{S,n}, \mathbf{w}^S) - (\Delta t)^2 \Big(\frac{1}{2} - 2\theta \Big) a_S(\ddot{\mathbf{u}}^{S,n}, \mathbf{w}^S).
\end{aligned}$$

3.5 Monolithic formulation for the fluid-structure equations

In this section, we will formulate the fluid-structure interaction problem as a monolithic system, for that we need to define one single vector field for the velocity and to extend the fluid pressure and fluid mesh velocity on the fluid-structure domain $\Omega_t = \Omega_t^F \cup \Omega_t^S \cup \Gamma_t$. We denote the fluid-structure velocity by $\mathbf{v} = (v_1, v_2)^T : \Omega_t \to \mathbb{R}^2$ and we define the time approximation of the fluid-structure velocity, displacement and acceleration by:

$$\mathbf{v}^n : \Omega_n \to \mathbb{R}^2, \quad \mathbf{u}^n : \Omega_n \to \mathbb{R}^2, \quad \ddot{\mathbf{u}}^n : \Omega_n \to \mathbb{R}^2.$$

The characteristic functions related to the fluid domain $\chi_{\Omega_t^F} : \overline{\Omega}_t \to \mathbb{R}$ and structure domain $\chi_{\Omega_t^S} : \overline{\Omega}_t \to \mathbb{R}$ are defined by:

$$\chi_{\Omega_t^S} = \begin{cases} 1, & \text{on } \overline{\Omega}_t^S \\ 0, & \text{otherwise} \end{cases} \qquad \chi_{\Omega_t^F} = 1 - \chi_{\Omega_t^S}.$$

We denote by Ω_n the time approximation space of Ω_t and we define the space of test functions $\widehat{W}_n$ for the fluid-structure velocity by:

$$\widehat{W}_n = \left\{ \widehat{\mathbf{w}} \in (H^1(\Omega_n))^2; \quad \widehat{\mathbf{w}} = 0 \text{ on } \Gamma_D \cup \Sigma_2 \right\}.$$

In order to have the equivalent structure discrete weak formulation on the global fluid-structure domain Ω_n, we recall that we work with the small structural displacements, therefore we can approximate (3.30) by the below equations:

$$\int_{\Omega_n} \chi_{\Omega_n^S} \frac{2\rho^S}{\Delta t} \widehat{\mathbf{v}}^{n+1} \cdot \widehat{\mathbf{w}} + 2\theta \Delta t \tilde{a}_S(\widehat{\mathbf{v}}^{n+1}, \widehat{\mathbf{w}})$$
$$- \int_{\Gamma_n} (\sigma^S \mathbf{n}^S) \cdot \widehat{\mathbf{w}} = \tilde{\mathcal{L}}_S(\widehat{\mathbf{w}}), \quad \forall \widehat{\mathbf{w}} \in \widehat{W}_n, \tag{3.31}$$

where

$$\tilde{a}_S(\mathbf{u}, \mathbf{w}) = \int_{\Omega_n} \chi_{\Omega_n^S} \Big[\lambda^S (\nabla \cdot \mathbf{u})(\nabla \cdot \mathbf{w}) + 2\mu^S \epsilon(\mathbf{u}) : \epsilon(\mathbf{w}) \Big]$$

and

$$\tilde{\mathcal{L}}_S(\widehat{\mathbf{w}}) = \int_{\Omega_n} \chi_{\Omega_n^S} f^S \cdot \widehat{\mathbf{w}} + \int_{\Omega_n} \chi_{\Omega_n} \frac{2\rho^S}{\Delta t} \mathbf{v}^n \cdot \widehat{\mathbf{w}} + \int_{\Omega_n} \chi_{\Omega_n^S} \rho^S \ddot{\mathbf{u}}^n \cdot \widehat{\mathbf{w}}$$
$$- \tilde{a}_S(\mathbf{u}^n, \widehat{\mathbf{w}}) - \Delta t (1 - 2\theta) \tilde{a}_S(\mathbf{v}^n, \widehat{\mathbf{w}}) - (\Delta t)^2 \Big(\frac{1}{2} - 2\theta \Big) \tilde{a}_S(\ddot{\mathbf{u}}^n, \widehat{\mathbf{w}}).$$

The fluid-structure mesh velocity $\tilde{\boldsymbol{\vartheta}}^n = (\tilde{\vartheta}_1^n, \tilde{\vartheta}_2^n)$ is obtained as the extention of the fluid mesh velocity on whole domain Ω_n:

$$\begin{cases} -\triangle \tilde{\boldsymbol{\vartheta}}^n &= 0, \quad \text{on } \Omega_n \\ \tilde{\boldsymbol{\vartheta}}^n &= 0 \quad \text{on } \partial\Omega_n \\ \tilde{\boldsymbol{\vartheta}}^n &= \mathbf{v}^n, \quad \text{on } \Gamma_n. \end{cases} \tag{3.32}$$

Remark 3.2 *We can notice that Γ_n is a curve which separates Ω_n^F and Ω_n^S, therefore the problem (3.32) is well posed.*

We introduce a global pressure $p : \Omega_t \longrightarrow \mathbb{R}$, which coincides with the fluid pressure p^F on the fluid domain Ω_t^F. The value of p on the structure domain Ω_t^S has no physical signification. We will return to this point later. We denote by $\widehat{p}^{n+1} : \Omega_n \rightarrow \mathbb{R}$ the time approximation of p at t_{n+1}. The space of test function for the pressure is denoted by $\widehat{Q}_n = L^2(\Omega_n)$.

From (3.27), we have

$$\int_{\Gamma_n} (\sigma^S \mathbf{n}^S) \cdot \widehat{\mathbf{w}} + \int_{\Gamma_n} \big(\sigma^F \mathbf{n}^F \big) \cdot \widehat{\mathbf{w}} = 0, \quad \forall \widehat{\mathbf{w}} \in \widehat{W}_n. \tag{3.33}$$

Using the fluid characteristic function, we can replace (3.28) and (3.29) by:

Find $\widehat{\mathbf{v}}^{F,n+1} \in \widehat{W}_n$ and $\widehat{p}^{F,n+1} \in \widehat{Q}_n$ such that:

$$\begin{aligned}
&\int_{\Omega_n} \chi_{\Omega_n^F} \rho^F \frac{\widehat{\mathbf{v}}^{n+1}}{\Delta t} \cdot \widehat{\mathbf{w}} + \int_{\Omega_n} \chi_{\Omega_n^F} \rho^F \left(\left(\left(\mathbf{v}^n - \tilde{\boldsymbol{\vartheta}}^n \right) \cdot \nabla \right) \widehat{\mathbf{v}}^{n+1} \right) \cdot \widehat{\mathbf{w}} \\
&- \int_{\Omega_n} \chi_{\Omega_n^F} \left(\nabla \cdot \widehat{\mathbf{w}} \right) \widehat{p}^{n+1} + \int_{\Omega_n} \chi_{\Omega_n^F} 2\mu^F \epsilon \left(\widehat{\mathbf{v}}^{n+1} \right) : \epsilon \left(\widehat{\mathbf{w}} \right) \\
&- \int_{\Gamma_n} \left(\sigma^F \mathbf{n}^F \right) \cdot \widehat{\mathbf{w}} = \tilde{\mathcal{L}}_F(\widehat{\mathbf{w}}), \quad \forall \widehat{\mathbf{w}} \in \widehat{W}_n \qquad (3.34) \\
&\int_{\Omega_n} \chi_{\Omega_n^F} \widehat{q}(\nabla \cdot \widehat{\mathbf{v}}^{n+1}) = 0, \quad \forall \widehat{q} \in \widehat{Q}_n, \qquad (3.35)
\end{aligned}$$

where

$$\tilde{\mathcal{L}}_F(\widehat{\mathbf{w}}) = \int_{\Omega_n} \chi_{\Omega_n^F} \rho^F \frac{\mathbf{v}^n}{\Delta t} \cdot \widehat{\mathbf{w}} + \int_{\Omega_n} \chi_{\Omega_n^F} \widehat{\mathbf{f}}^{n+1,F} \cdot \widehat{\mathbf{w}} + \int_{\Sigma_1} \widehat{\mathbf{h}}_{in}^{n+1} \cdot \widehat{\mathbf{w}} + \int_{\Sigma_3} \widehat{\mathbf{h}}_{out}^{n+1} \cdot \widehat{\mathbf{w}}.$$

Now using the identity (3.33) and summing up the equations (3.31), (3.34), we get after adding the equation (3.35) the following fluid-structure weak formulation:

Find $(\widehat{\mathbf{v}}^{n+1}, \widehat{p}^{n+1}) \in \widehat{W}_n \times \widehat{Q}_n$ such that:

$$\begin{aligned}
&\int_{\Omega_n} \chi_{\Omega_n^F} \rho^F \frac{\widehat{\mathbf{v}}^{n+1}}{\Delta t} \cdot \widehat{\mathbf{w}} + \int_{\Omega_n} \chi_{\Omega_n^F} \rho^F \left(\left(\left(\mathbf{v}^n - \tilde{\boldsymbol{\vartheta}}^n \right) \cdot \nabla \right) \widehat{\mathbf{v}}^{n+1} \right) \cdot \widehat{\mathbf{w}} \\
&- \int_{\Omega_n} \chi_{\Omega_n^F} \left(\nabla \cdot \widehat{\mathbf{w}} \right) \widehat{p}^{n+1} + \int_{\Omega_n} \chi_{\Omega_n^F} 2\mu^F \epsilon \left(\widehat{\mathbf{v}}^{n+1} \right) : \epsilon \left(\widehat{\mathbf{w}} \right) \\
&+ \int_{\Omega_n} \chi_{\Omega_n^S} \frac{2\rho^S}{\Delta t} \widehat{\mathbf{v}}^{n+1} \cdot \widehat{\mathbf{w}} + 2\theta \Delta t \tilde{a}_S(\widehat{\mathbf{v}}^{n+1}, \widehat{\mathbf{w}}) \\
&= \tilde{\mathcal{L}}_F(\widehat{\mathbf{w}}) + \tilde{\mathcal{L}}_S(\widehat{\mathbf{w}}), \quad \forall \widehat{\mathbf{w}} \in \widehat{W}_n \qquad (3.36) \\
&\int_{\Omega_n} \chi_{\Omega_n^F} \widehat{q}(\nabla \cdot \widehat{\mathbf{v}}^{n+1}) = 0, \quad \forall \widehat{q} \in \widehat{Q}_n. \qquad (3.37)
\end{aligned}$$

The fluid-structure displacement at time instant t_{n+1} on Ω_n: $\widehat{\mathbf{u}}^{n+1} : \Omega_n \to \mathbb{R}^2$ can be computed from (3.24), (3.25) and from the remark (3.1), as following:

$$\widehat{\mathbf{u}}^{n+1} = \mathbf{u}^n + (\Delta t)^2 \Big(\frac{1}{2} - 2\theta \Big) \ddot{\mathbf{u}}^n + \Delta t (1 - 2\theta) \mathbf{v}^n + 2\theta \Delta t \, \widehat{\mathbf{v}}^{n+1}. \qquad (3.38)$$

The fluid-structure acceleration $\widehat{\ddot{\mathbf{u}}}^{n+1} : \Omega_n \to \mathbb{R}^2$ is obtained by combining (3.24), (3.25):

$$\widehat{\ddot{\mathbf{u}}}^{n+1} = \frac{2}{\Delta t} \Big(\widehat{\mathbf{v}}^{n+1} - \mathbf{v}^n \Big) - \ddot{\mathbf{u}}^n. \qquad (3.39)$$

We define the map $\mathbb{T}_n : \overline{\Omega}_n \to \mathbb{R}^2$ by:

$$\mathbb{T}_n(\widehat{\mathbf{x}}) = \widehat{\mathbf{x}} + \Delta t \tilde{\boldsymbol{\vartheta}}^n(\widehat{\mathbf{x}}) \chi_{\Omega_n^F}(\widehat{\mathbf{x}}) + (\widehat{\mathbf{u}}^{n+1}(\widehat{\mathbf{x}}) - \mathbf{u}^n(\widehat{\mathbf{x}})) \chi_{\Omega_n^S}(\widehat{\mathbf{x}}). \qquad (3.40)$$

We set

$$\Omega_{n+1} = \mathbb{T}_n(\Omega_n)$$

and we can observe that:

$$\Gamma_{n+1} = \mathbb{T}_n(\Gamma_n).$$

We now define the fluid-structure velocity and pressure defined on the current time domain, $\mathbf{v}^{n+1} : \Omega_{n+1} \to \mathbb{R}^2$ and $p^{n+1} : \Omega_{n+1} \to \mathbb{R}^2$ by:

$$\mathbf{v}^{n+1}(\mathbf{x}) = \widehat{\mathbf{v}}^{n+1}(\widehat{\mathbf{x}}), \quad p^{n+1}(\mathbf{x}) = \widehat{p}^{n+1}(\widehat{\mathbf{x}}), \quad \forall\, \widehat{\mathbf{x}} \in \Omega_n \text{ and } \mathbf{x} = \mathbb{T}_n(\widehat{\mathbf{x}}).$$

In the similar way, we define the fluid-structure displacements and acceleration at time instant t_{n+1} on Ω_{n+1}: $\mathbf{u}^{n+1} : \Omega_{n+1} \to \mathbb{R}^2$, and $\ddot{\mathbf{u}}^{n+1} : \Omega_{n+1} \to \mathbb{R}^2$ by:

$$\mathbf{u}^{n+1}(\mathbf{x}) = \widehat{\mathbf{v}}^{n+1}(\widehat{\mathbf{x}}), \quad \ddot{\mathbf{u}}^{n+1}(\mathbf{x}) = \widehat{\ddot{\mathbf{u}}}^{n+1}(\widehat{\mathbf{x}}), \quad \forall\, \widehat{\mathbf{x}} \in \Omega_n \text{ and } \mathbf{x} = \mathbb{T}_n(\widehat{\mathbf{x}}).$$

The system (3.36), (3.37) is a linear system of unknowns fluid-structure velocity and pressure with a regular matrix. For the numerical implementation, we have used the GMRES algorithm.

The system (3.36), (3.37) can be written in the following matrix form:

$$\begin{bmatrix} A & B^T & 0 \\ B & 0 & 0 \\ 0 & 0 & 0 \end{bmatrix} \begin{bmatrix} \mathbf{v} \\ p^F \\ p^S \end{bmatrix} = \begin{bmatrix} \mathcal{L} \\ 0 \\ 0 \end{bmatrix}, \tag{3.41}$$

where $\mathbf{v}$ is the velocity field, p^F (respectively p^S) the fluid pressure (respectively the structure pressure),
$\mathcal{L} = \tilde{\mathcal{L}}_F(\phi_i) + \tilde{\mathcal{L}}_S(\phi_i)$ and the matrices given by:

$$\begin{aligned} A_{i,j} = & \int_{\Omega_n} \chi_{\Omega_n^F}\, \rho^F \frac{\phi_j}{\Delta t} \cdot \phi_i + \int_{\Omega_n} \chi_{\Omega_n^F}\, \rho^F \left(\left(\left(\mathbf{v}^n - \tilde{\boldsymbol{\vartheta}}^n \right) \cdot \nabla \right) \phi_j \right) \cdot \phi_i \\ & + \int_{\Omega_n} \chi_{\Omega_n^F}\, 2\mu^F \epsilon\left(\phi_j\right) : \epsilon\left(\phi_i\right) + \int_{\Omega_n} \chi_{\Omega_n^S} \frac{2\rho^S}{\Delta t} \phi_j \cdot \phi_i + 2\theta \Delta t\, \tilde{a}_S(\phi_j, \phi_i) \end{aligned}$$

and

$$B_{i,j} = -\int_{\Omega_n} \chi_{\Omega_n^F} \left(\nabla \cdot \phi_j\right) \pi_i,$$

with ϕ_i (respectively π_i) the velocity (respectively the pressure) finite element shape functions.

We can remark that this system has non unique solution, because the pressure p^S can take any value. To get round this difficulty we have added to the system (3.36), (3.37) the term $\epsilon \displaystyle\int_{\Omega_n} \widehat{p}^{n+1}\widehat{q}$ to get a zero value of p^S on Ω_n^S and the global matrix becomes:

$$\begin{bmatrix} A & B^T & 0 \\ B & \epsilon M^F & 0 \\ 0 & 0 & \epsilon M^S \end{bmatrix} \begin{bmatrix} \mathbf{v} \\ p^F \\ p^S \end{bmatrix} = \begin{bmatrix} \mathcal{L} \\ 0 \\ 0 \end{bmatrix}, \tag{3.42}$$

where $\epsilon = 10^{-6}$ and

$$\begin{bmatrix} \epsilon M^F & 0 \\ 0 & \epsilon M^S \end{bmatrix} = \left(\epsilon \int_{\Omega_n} \pi_j \pi_i\right)_{1\le i,j\le nv},$$

with nv the number of vertices of the fluid-structure mesh.

Remark 3.3 *If we approach the global pressure by finite element functions, which are globally continuous, we obtain on the vertices of the triangles of* $\Omega_t^S \setminus \Gamma_t$ *the pressure* $p^S = 0$ *and on the domain* $\Omega_t^F \cup \Gamma_t$ *the fluid pressure* p^F*.*

Algorithm

We have employed the algorithm presented below to implement numerically the linear system (3.36), (3.37).

We assume that we know Ω_n, $\mathbf{v}^n$, $\mathbf{u}^n$, $\ddot{\mathbf{u}}^n$.

Step 1: Compute $\tilde{\boldsymbol{\vartheta}}^n$ from (3.32).

Step 2: Solve the linear system (3.36), (3.37) by GMRES on the mesh $\mathcal{T}_n$ of Ω_n. Get the fluid-structure velocity $\widehat{\mathbf{v}}^{n+1}$ and pressure $\widehat{p}^{n+1}$.

Step 3: Compute the fluid-structure displacement $\widehat{\mathbf{u}}^{n+1}$ from (3.38) and acceleration $\widehat{\ddot{\mathbf{u}}}^{n+1}$ from (3.39).

Step 4: Build mesh $\mathcal{T}_{n+1}$ as image of $\mathcal{T}_n$ by the map (3.40) and save the mesh $\mathcal{T}_{n+1}$, the velocity $\mathbf{v}^{n+1}$, the pressure p^{n+1}, the displacement $\mathbf{u}^{n+1}$ and the acceleration $\ddot{\mathbf{u}}^{n+1}$.

3.6 Numerical results

We are motivated by fluid-structure interaction problems with application to haemodynamics. The fluid is the blood and the structure represents the artery. But before simulating real three dimensional applications, it is important to test our method on an academic case.

Physical parameters

We consider the following data for the numerical computations: the length of the fluid domain is L= 6 *cm* and its height $H = 1$ *cm*. The viscosity of the fluid was fixed to be $\mu = 0.035\ \frac{g}{cm\cdot s}$, its density $\rho^F = 1\ \frac{g}{cm^3}$ and the volume force in fluid is $\mathbf{f}^F = (0,\ 0)^T$. The prescribed boundary stress at the outflow is $\mathbf{h}_{out}(x,t) = (0,\ 0)^T$ and at the inflow is:

$$\mathbf{h}_{in}(x,t) = \begin{cases} (10^3(1-\cos(2\pi t/0.025)),\ 0)^T, & \text{if} \quad x \in \Sigma_1, 0 \leq t \leq 0.025 \\ (0,\ 0)^T, \quad \text{if} \quad x \in \Sigma_1, 0.025 \leq t \leq T. \end{cases}$$

The thickness of the elastic wall is $h^S = 0.1\ cm$, the Young modulus $E = 3\cdot 10^6\ \frac{g}{cm\cdot s^2}$, the Poisson ratio $\nu = 0.3$, the mass density $\rho^S = 1.1\frac{g}{cm^3}$ and the volume force is $\mathbf{f}^S = (0,\ 0)^T$. The Lamé's coefficients are computed by the formulas:

$$\lambda^S = \frac{\nu^S E}{(1-2\nu^S)(1+\nu^S)}, \qquad \mu^S = \frac{E}{2(1+\nu^S)}.$$

Numerical parameters

The computation has been made on a computer with two processors of 3.6 GHz frequency. The numerical tests have been performed using FreeFem++ (see [5]). We have chosen the following parameters: $\delta = 0.5$ and $\theta = 0.3$ for the Newmark scheme, $\Delta t = 0.001s$ the time step and $N = 100$ the number of time step. We denote by m the number of eigenfunctions when the structure problem is solved by modal decomposition method in the case of partitioned procedures algorithm.

CPU time for monolithic algorithm

The number of segments on the fluid-structure interface is denoted by $nsFS$. We have used for the fluid-structure a reference mesh of number of triangles $nt = 2426$ and number of vertices $nv = 1305$. For the finite element approximation of the fluid-structure velocity, we have used the triangular finite element $\mathbb{P}_1 + bubble$ and we have employed for the pressure the finite element $\mathbb{P}_1$. For the characteristic functions, the triangular finite element $\mathbb{P}_0$ was used on each triangle. The linear fluid-structure system is solved by GMRES algorithm where the continuity of velocity is automatically satisfied and the continuity of stress does not appear in the global weak form. We have summarized in the Table 3.1 the CPU time for monolithic algorithm when different values of segments on the interface have been considered: $nsFS = 80$, $nsFS = 100$ and $nsFS = 120$. The degree of freedoms computed in the Table 3.1 are obtained from the formulas: $Dof = 2(nv + nt) + nv = 3nv + 2nt$, where $2(nv + nt)$ is considered for velocity and nv for the pressure.

$nsFS$	nt	nv	global Dof	CPU_{mono}
80	2426	1305	8767	5 mn 25 s
100	3916	2070	14042	7 mn 18 s
120	5039	2649	18016	11 mn 34 s

Table 3.1: Monolithic (mono) algorithm for three different values of $nsFS$.

CPU time for semi-implicit partitioned procedures algorithm

In the semi-implicit partitioned procedures algorithm, some iterations are necessary for solving the optimization problem (see [11]) in order satisfy the continuity conditions at the interface. During these iterations, the fluid matrix is factorized one time by LU solver and the structure problem is solved by modal decomposition at the beginning of the algorithm. We denote by ntF (respectively ntS) the number of triangles in the fluid mesh (respectively in the structure mesh) and nvF (respectively nvS) the number of vertices in the fluid mesh (respectively in the structure mesh). For the finite element approximation, we have used, $\mathbb{P}1 + bubble$ for the fluid velocity, $\mathbb{P}1$ for the pressure and $\mathbb{P}1$ for the structure displacements. The degree of freedoms of the fluid is obtained from: $DofF = 3nvF + 2ntF$, where $2(nvF + ntF)$ is considered for velocity and nvF for the pressure and the degree of freedoms of the structure is obtained from: $DofS = 2\,nvS$.

$nsSF$	ntF	nvF	ntS	nvS	DofF	DofS	CPU_{pp}	$\frac{CPU_{pp}}{CPU_{mono}}$
80	2106	1144	320	242	7644	484	10 mn 49 s	1.99
100	3538	1880	378	291	12716	582	15 mn 57 s	2.18
120	4582	2422	452	348	16430	696	21 mn 06 s	1.82

Table 3.2: Semi-implicit partitioned procedures (pp) algorithm for $m = 3$.

To show that, when we increase the number m in structure problem, the CPU time in the semi-implicit partitioned procedures increases, we computed the CPU time for different values of m. We have also computed the CPU times ratio between the partitioned procedures algorithm and the monolithic one. We can conclude from the last column of the Tables 3.2 and 3.3 that the monolithic algorithm is faster than the partitioned procedures one.

m	CPU_{pp}	$\dfrac{CPU_{pp}}{CPU_{mono}}$
3	10 m 49 s	1.99
7	27 m 47 s	5.12
10	41 m 07 s	7.59

Table 3.3: CPU time ratio for $nsFS = 80$ and for different values of m.

Fluid-structure mesh

The system (3.36), (3.37) is a linear system of unknowns velocity and pressure defined on the whole fluid-structure domain. The mesh $\mathcal{T}_n$ of the fluid-structure domain Ω_n is obtained by gluing the fluid and structure meshes which are compatible at the interface. This compatibility at the interface can also be checked from the formula:

$$nv = nvF + nvS - (nsFS + 1) \quad nt = ntF + ntS.$$

We plotted the global fluid-structure mesh and separately the fluid and structure meshes, see Figure 3.2.

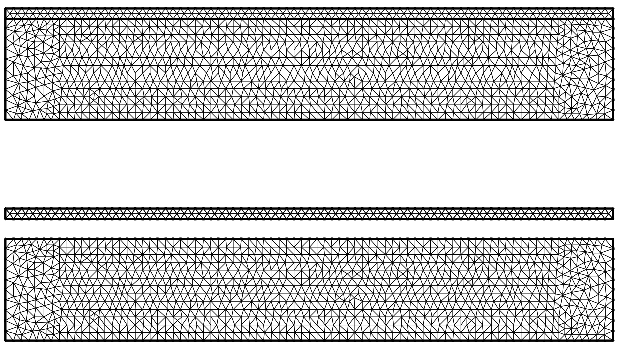

Figure 3.2: Global fluid-structure mesh (top), the structure and fluid meshes (bottom).

Behavior of the solutions

The behaviors of fluid-structure velocity and pressure at three different time instants are plotted in Figures 3.3 and 3.4. We have also plotted the vertical displacements of three different points at the fluid-structure interface for the monolithic and partitioned procedures algorithms, in order to compare the behaviors of the solutions, see Figure 3.5 at the left for the monolithic case and at the right for the partitioned procedures case.

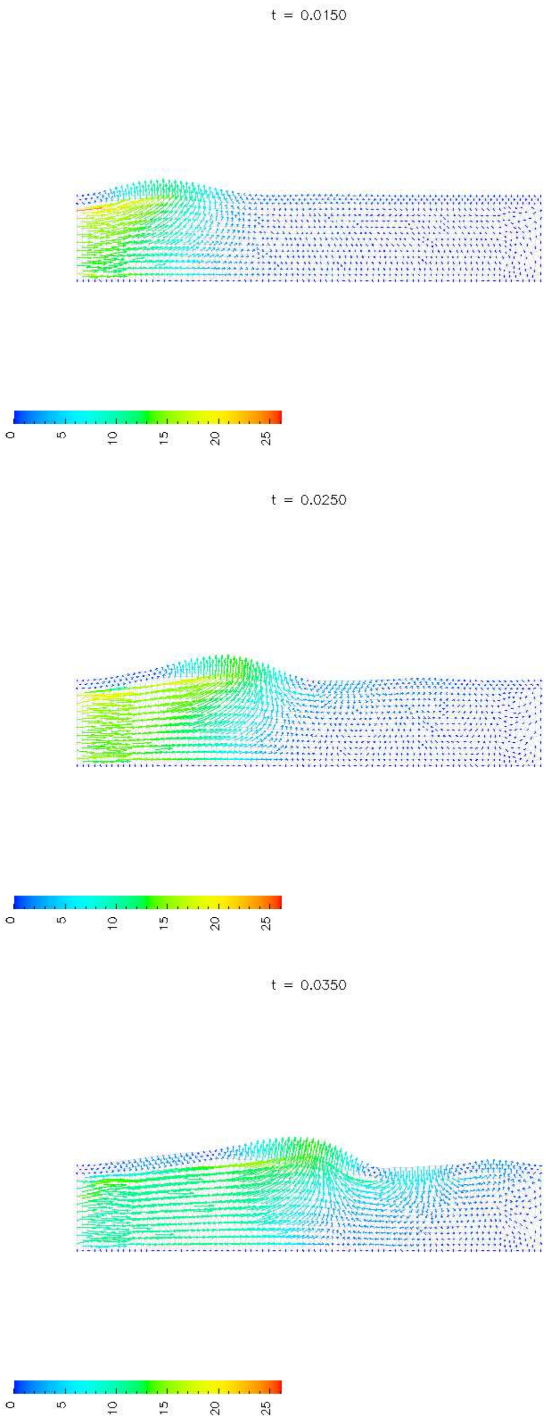

Figure 3.3: Fluid-structure velocities $[cm/s]$ at time instant $t = 0.015$ (top) , $t = 0.025$ (middle), $t = 0.035$ (bottom).

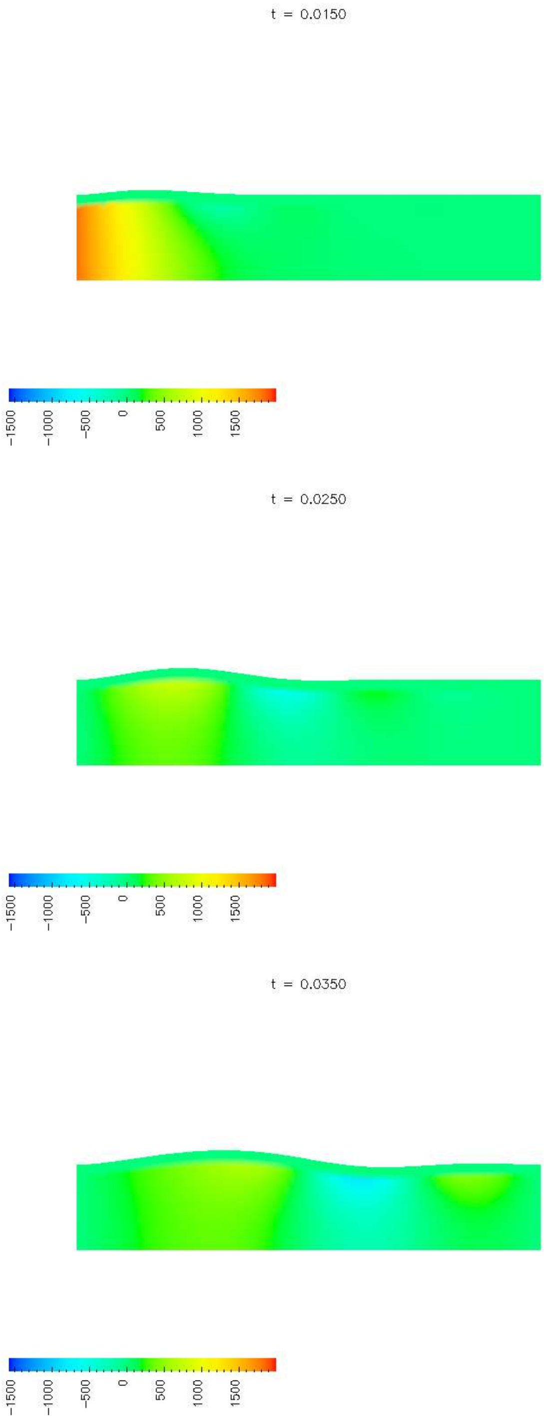

Figure 3.4: Fluid-structure pressure $[dynes/s^2]$ at time instant $t = 0.015$ (top), $t = 0.025$ (middle), $t = 0.035$ (bottom).

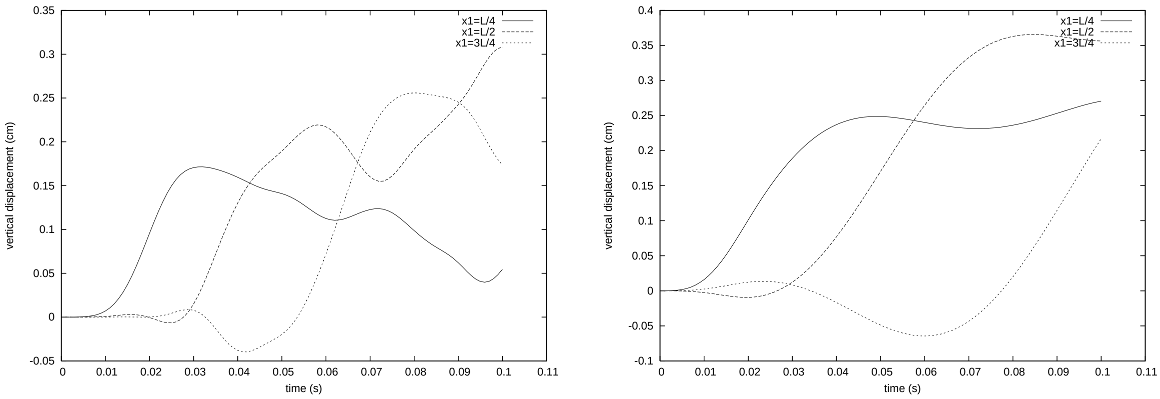

Figure 3.5: Vertical displacements of three points at the interface of horizontal coordinates $x_1 = \dfrac{L}{4}$, $x_2 = \dfrac{L}{2}$ and $x_3 = \dfrac{3L}{4}$, in the monolithic case (at the left) and in partitioned procedures case (at the right).

Remark 3.4 *We can observe from the Figure 3.5, that the vertical displacements obtained by monolithic and partitioned procedures algorithms are different. These differences can be explained by the fact that the structure problem is formulated in Lagrangian framework in the partitioned procedures case and in Eulerian framework in the monolithic case. In addition these differences can also be explained by the fact that the structure problem is solved by modal decomposition method in the partitioned procedures case.*

3.7 Conclusion and future works

A monolithic semi-implicit algorithm for fluid-structure interaction problem at small structural displacement was presented. This algorithm use a global fluid-structure mesh obtained by gluing the fluid and structure meshes which are matching at the interface. The characteristic functions were introduced in order to be able to choose independently the time discretization schemes of the fluid and structure. The continuity of velocity at the interface is automatically satisfied by using one velocity vector field and the continuity of stress is canceled from the weak form. Therefore the fluid-structure problem was written as a linear system of unknowns velocity and pressure. We choose the GMRES algorithm to solve numerically the system. When the monolithic approach is used, the CPU time is reduced compared to a particular partitioned procedures strategy.

In the future works, we will replace the linear structure model by the nonlinear Saint-Venant Kirchhoff model.

Bibliography

[1] S. Badia, A. Quaini, A. Quarteroni, *Splitting methods based on algebraic factorization for fluid-structure interaction.* SIAM J. Sci. Comput. **30** (2008), no. 4, 1778–1805.

[2] S. Badia, A. Quaini, A. Quarteroni, *Modular vs. non-modular preconditioners for fluid-structure systems with large added-mass effect.* Comput. Methods Appl. Mech. Engrg. **197** (2008), no. 49-50, 4216–4232.

[3] T. Dunne, *An Eulerian approach to fluid-structure interaction and goal-oriented mesh adaptation.* Inter. J. Num. Meth. Fluids, **51** (2006), pp. 1017-1039.

[4] M. A. Fernàndez, J.-F. Gerbeau, C. Grandmont, *A projection semi-implicit scheme for the coupling of an elastic structure with an incompressible fluid.* Internat. J. Numer. Methods Engrg. **69** (2007), no. 4, 794–821.

[5] F. Hecht, O. Pironneau, A. Le Hyaric, K. Ohtsuka, *FreeFem++:* http://www.freefem++.org/ff++.

[6] J. Hron, S. Turek, *A monolithic FEM/multigrid solver for an ALE formulation of fluid-structure interaction with application in biomechanics.* In Fluid-Structure Interaction, pp. 146–170, Lect. Notes. Comput. Sci. Eng. **53**, Springer, Berlin, 2006.

[7] M. Heil, A. L. Hazed, J. Boyle, *Solvers for large-displacement fluid-structure interaction problems: segregated versus monolithic approaches.* Cumput. Mech. **193** (2008), 91-101

[8] B. Hubner, E. Walhorn, D. Dinkler, *A monolithic approach to fluid-structure interaction using space-time finite elements.* Comput. Meth. Appl. Mech. Eng., **193** (2004), pp. 2087-2104

[9] C. M. Murea, *A semi-implicit algorithm based on the Augmented Lagrangian Method for fluid-structure interaction,* Num. Math. Adv. App, Proceedings of ENUMATH 2007, the 7th European Conference on Numerical Mathematics and Advanced Applications, Graz, Austria, September 2007. Springer, 2008, pp. 555-562.

[10] C. M. Murea, S. Sy, *A fast method for solving fluid-structure interaction problem numerically.* Int. J. Numer. Meth. Fluids DOI: 10.1002/fld.1931.

[11] S. Sy, C. M. Murea, *A stable time advancing scheme for solving fluid-structure interaction problem at small structural displacements.* Comput. Meth. Appl. Mech. Eng. **198** (2008), pp. 210-222.

[12] TE. Tezduyar, S. Sathe, R. Keedy, K. Stein, *Space-time finite element techniques for computation of fluid-structure interactions.* Comput. Meth. Appl. Mech. Eng. **195** (2006), pp. 2002–2027.

[13] A. Quaini, A. Quarteroni, *A semi-implicit approach for fluid-structure interaction based on an algebraic fractional step method.* Math. Models Methods Appl. Sci. **17** (2007), no. 6, 957–983.

[14] A. Quarteroni, L. Formaggia, *Mathematical modelling and numerical simulation of the cardiovascular system,* P.G. Ciarlet (ED.),Handbook of numerical analysis, vol. XII, North-Holland, Amsterdam, 2004, 3-127.